
Dynamics of Auxin Sensing
by SCF^{TIR1/AFB}-AUX/IAA Co-Receptor Complexes
in Arabidopsis

Dissertation

zur Erlangung des

Doktorgrades der Naturwissenschaften (Dr. rer. nat.)

der

Naturwissenschaftlichen Fakultät I – Biowissenschaften –

der Martin-Luther-Universität

Halle-Wittenberg,

vorgelegt

von Frau Diplom-Biochemikerin

Antje Hellmuth

geb. am 28.02.1986 in Havelberg

Gutachter:

Prof. Dr. Steffen Abel

Prof. Dr. Ingo Heilmann

Prof. Dr. Claus Schwechheimer

Day of defense: Halle (Saale), 13.06.2017

Wonderful are Your works;
My soul knows it very well.

Psalm 139:14

Table of Contents

Table of Contents	i
Abbreviations and Symbols	iv
1 Introduction	1
1.1 The phytohormone auxin.....	1
1.2 Auxin perception and signaling.....	3
1.2.1 The Ubiquitin Proteasome System (UPS) in Auxin Signaling	4
1.2.2 Molecular mechanism of auxin perception.....	14
1.2.3 Emerging concepts and questions in auxin perception mechanism	17
1.3 Hypothesis and objectives	23
2 Results	25
2.1 Auxin co-receptor complexes undergo multifaceted assembly.....	25
2.1.1 Different residues in loop-12 might contribute to functional differences between TIR1, AFB1, AFB2 and AFB3.....	25
2.1.2 Combinatorial events and auxin dependency of auxin co-receptor assembly.....	27
2.1.3 Characterization of auxin co-receptors TIR1-IAA1, TIR1-IAA2, AFB2-IAA1 and AFB2-IAA2 ...	33
2.2 Redefining the degron	67
2.2.1 The influence of degron-flanking regions on auxin-dependent TIR1/AFB-AUX/IAA interaction is highly interconnected.....	70
2.2.2 The degron-tail (DT) is required for AUX/IAA destabilization <i>in vivo</i>	73
3 Discussion	76
3.1 Combinatorial events in auxin co-receptor assembly.....	76
3.2 Auxin co-receptors might differentially assemble based on variable loop regions in TIR1, AFB1, AFB2 and AFB3	78
3.3 Sister pair genes <i>IAA1</i> and <i>IAA2</i> show evidence for purifying selection, possibly hinting at conserved, crucial function	79
3.4 TIR1-IAA1 and TIR1-IAA2 auxin co-receptors.....	81
3.5 Differential effects downstream of co-receptor formation	84
3.6 <i>In vivo</i> studies of <i>IAA1</i> and <i>IAA2</i> in auxin receptor formation	87
3.7 Redefining the degron	89
3.8 Co-receptors perceiving auxins other than IAA	94
3.9 Challenging the co-receptor model – auxin as an orthosteric regulator of target-recognition by SCF ^{TIR1}	96
3.10 Concluding remarks	100
4 Summary	101
5 Zusammenfassung	102
6 Material and Methods	104
6.1 Material.....	104
6.1.1 Chemicals and supplies	104
6.1.2 Bacterial and yeast strains, insect cell culture, and plasmid vectors	104
6.2 Media	105
6.3 Plant material and cultivation.....	106

6.3.1 Plant lines	106
6.3.2 Plant cultivation under sterile conditions	106
6.3.3 Plant cultivation on soil	107
6.3.4 Floral-dip transformation of Arabidopsis	107
6.4 Bacterial and yeast general procedures.....	108
6.4.1 <i>Escherichia coli</i> and <i>Agrobacterium tumefaciens</i> cultivation	108
6.4.2 <i>Escherichia coli</i> and <i>Agrobacterium tumefaciens</i> transformation	108
6.4.3 <i>Saccharomyces cerevisiae</i> cultivation	109
6.4.4 <i>Saccharomyces cerevisiae</i> transformation with LexA Y2H plasmid vectors	109
6.5 Insect cell and Baculovirus general procedures.....	110
6.5.1 Cultivation of Sf9 cells	110
6.5.2 Freezing, storage and thawing of Sf9 cell stocks	111
6.5.3 Baculovirus amplification and storage	111
6.6 Molecular biology methods	111
6.6.1 Polymerase chain reaction (PCR).....	111
6.6.2 Overlap extension PCRs.....	113
6.6.3 Site-directed mutagenesis of plasmids	114
6.6.4 Agarose gel electrophoresis	114
6.6.5 DNA extraction from agarose gel after electrophoretic separation.....	114
6.6.6 DNA isolation.....	114
6.6.7 Gateway cloning.....	115
6.6.8 Golden Gate modular cloning (MoClo) assembly of chimeras	117
6.6.9 Analysis of transcript levels from Arabidopsis seedlings.....	118
6.7 Biochemical methods.....	121
6.7.1 Protein quantitation	121
6.7.2 SDS-PAGE.....	121
6.7.3 Immunoblotting (Western Blot)	123
6.7.4 Recombinant protein expression	124
6.7.5 Protein extraction from <i>E. coli</i> and Sf9 cells.....	125
6.7.6 Protein purification	125
6.7.7 General protein handling procedures	127
6.7.8 Yeast protein extraction and expression analysis	127
6.7.9 Plant protein extraction	128
6.7.10 <i>In vitro</i> ubiquitination assays.....	129
6.8 Protein-Protein Interaction analyses	130
6.8.1 Yeast Two Hybrid Assay.....	130
6.8.2 Radioligand Binding Assays	131
6.9 Protoplast-based stability assays	133
6.9.1 Plasmid construction	133
6.9.2 Plant material	133
6.9.3 Protoplast isolation, transformation and auxin treatment	133
6.9.4 Inducers.....	134
6.9.5 Luminescence analysis	134
6.9.6 Statistical analysis.....	134
6.10 Physiological assays	134
6.10.1 Root elongation assay	134
6.10.2 Temperature-induced hypocotyl elongation	134
6.10.3 Measurements and data analyses.....	134
6.11 <i>In silico</i> analyses.....	135
6.11.1 Homology modeling of auxin receptor complexes.....	135
6.11.2 Gene expression data analysis	135
6.11.3 Sequence divergence between <i>A. thaliana</i> and <i>A. lyrata</i>	135

7	References	136
8	Appendix	152
	8.1 List of Publications	152
	8.2 List of Figures	153
	8.3 List of Tables	154
	8.4 List of Supplementary Figures.....	154
	8.5 List of Supplementary Tables	156
	8.6 Supplementary Figures and Tables	157
	Acknowledgements	8
	Curriculum vitae	10
	Statutory declaration	11

Abbreviations and Symbols

B_{\max}	maximum binding
IC50	half-maximal inhibitory concentration
K_D	(equilibrium) dissociation constant
K_i	(equilibrium) inhibitory constant
k_{off}	dissociation rate constant
k_{on}	association rate constant
2,4,5-T	2,4,5-trichlorophenoxyacetic acid
2,4-D	2,4-dichlorophenoxyacetic acid
35S	Cauliflower mosaic virus 35S promoter
^3H -IAA	tritium-labeled indole-3-acetic acid [$5\text{-}^3\text{H}$]
4-Cl-IAA	4-chloroindole-3-acetic acid
<i>A. lyrata</i>	<i>Arabidopsis lyrata</i>
<i>A. thaliana</i>	<i>Arabidopsis thaliana</i>
AD	activation domain
AFB	AUXIN SIGNALING F-BOX
ANOVA	analysis of variance
ARF	AUXIN RESPONSE FACTOR
ASK	ARABIDOPSIS S-PHASE KINASE ASSOCIATED PROTEIN
At[<i>gene name</i>]	<i>Arabidopsis thaliana</i> [<i>gene name</i>]
ATP	adenosine triphosphate
AUX/IAA	AUXIN/INDOLE-3-ACETIC ACID INDUCIBLE
<i>AuxRE</i>	auxin-responsive element
AXR	AUXIN RESISTANT
B3	B3 deoxyribonucleic acid binding domain
BDL	BODENLOS (IAA12)
BM3	triple basic patch mutant
bp	base pairs
BSA	bovine serum albumin
<i>C. elegans</i>	<i>Caenorhabditis elegans</i>
cDNA	complementary deoxyribonucleic acid
COI1	CORONATINE INSENSITIVE 1
Col-0	Columbia-0
Ct	cycle threshold
C-terminal	carboxyterminal
CUL1	CULLIN 1
Da	Dalton
DBD	deoxyribonucleic acid binding domain
DD	dimerization domain
DI	domain I
dN/dS	nonsynonymous/synonymous substitution rate
DNA	deoxyribonucleic acid
DT	degron-tail
DTT	dithiothreitol
DUB	deubiquitinating enzyme
<i>E. coli</i>	<i>Escherichia coli</i>
e.g.	<i>exempli gratia</i> – for example
E1	E1 ubiquitin-activating enzyme
E2	E2 ubiquitin-conjugating enzyme
E3	E3 ubiquitin ligase
EAR	ethylene response factor-associated amphiphilic repression

EDTA	ethylenediaminetetraacetic acid
EMS	Ethyl methanesulfonate
<i>et al.</i>	<i>et alii</i> – and others
FBP	F-box protein
FF	firefly luciferase
FW	forward primer
GFP	green fluorescent protein
GH3	GRETCHEN HAGEN3
gof	gain-of-function
GST	glutathione S-transferase
HDAC	histone deacetylase
Hs[<i>gene name</i>]	<i>Homo sapiens</i> [<i>gene name</i>]
HSP90	HEAT SHOCK FACTOR 90
i.e.	<i>id est</i> – that is
IAA	indole-3-acetic acid
IB	immunoblot
IBA	indole-3-butyric acid
IP	immunoprecipitation
IP6	myo-inositol-1,2,3,4,5,6-hexakisphosphate
ITC	Isothermal Titration Calorimetry
IVU	<i>in vitro</i> ubiquitination
JA	jasmonic acid/jasmonate
JA-Ile	(3 <i>R</i> ,7 <i>S</i>)-jasmonoyl-L-isoleucine
JAZ	JASMONATE-ZIM-DOMAIN PROTEIN
lof	loss-of-function
LRR	leucine-rich repeat
LRT2	LATERAL ROOTLESS 2
LUC	luciferase
M	molar
MCPA	2-methyl-4-chlorophenoxyacetic acid
min	minutes
Mm[<i>gene name</i>]	<i>Mus musculus</i> [<i>gene name</i>]
MP	MONOPTEROS (ARF5)
MR	middle region
MSG2	MASSUGU2 (IAA19)
<i>N. benthamiana</i>	<i>Nicotiana benthamiana</i>
NAA	1-Naphtaleneacetic acid
NPA	1- <i>N</i> -Naphthylphthalamic acid
NPH4	NON-PHOTOTROPIC HYPOCOTYL4 (ARF7)
N-terminal	aminoterminal
OD ₆₀₀	optical density at 600 nm wavelength
OPCA	octicosapeptide repeat, p40phox, Cdc24p, atypical PKC interaction domain
Os[<i>gene name</i>]	<i>Oryza sativa</i> [<i>gene name</i>]
<i>p</i>	probability value
PAA	phenylacetic acid
PB1	Phox/Bem1p
PBS(-T)	phosphate buffered saline (with Tween-20)
PCR	polymerase chain reaction
PDB	protein data bank
PP2A	SERINE/THREONINE PROTEIN PHOSPHATASE 2A
PPI	protein-protein interaction
Ps[<i>gene name</i>]	<i>Pisum sativum</i> [<i>gene name</i>]

qPCR	quantitative real-time polymerase chain reaction
RBX1	RING-BOX PROTEIN 1
REN	renilla luciferase
RING	REALLY INTERESTING NEW GENE
RNA	ribonucleic acid
RT	room temperature
RT-qPCR	reverse transcription quantitative real-time polymerase chain reaction
RUB1/Nedd8	RELATED TO UBIQUITIN1/Neural Precursor Cell Expressed, Developmentally Down-Regulated 8
RV	reverse primer
<i>S. cerevisiae</i>	<i>Saccharomyces cerevisiae</i>
SAUR	SMALL AUXIN UPREGULATED RNA
SCF	SKP1-CULLIN1-F-BOX PROTEIN
SD	synthetic defined
SDS	sodium dodecyl sulfate
SDS-PAGE	sodium dodecyl sulfate polyacrylamide gel electrophoresis
SEM	standard error of the means
<i>Sf9</i>	<i>Spodoptera frugiperda</i> clone 9 cell line
SGT1	SUPPRESSOR OF G2 ALLELE SKP1
SHY	SUPPRESSOR OF HY2 MUTATION
SKP1	S-PHASE KINASE ASSOCIATED PROTEIN 1
SLR	SOLITARY ROOT (IAA14)
SPR	surface plasmon resonance
TBS(-T)	tris-buffered saline (with Tween-20)
T-DNA	transfer deoxyribonucleic acid
TIR1	TRANSPORT INHIBITOR RESPONSE 1
TPD	TOPLESS domain
TPL	TOPLESS
TPR	TOPLESS-RELATED
Tris	tris(hydroxymethyl)aminomethane
Ub	ubiquitin
Uba1	Ubiquitin-activating enzyme 1
Ubc8	Ubiquitin-conjugating enzyme 8
UPS	ubiquitin proteasome system
v/v	volume per volume
w/v	weight per volume
Y2H	yeast-2-hybrid
YFP	yellow fluorescent protein
β-Gal	β-Galactosidase

Throughout this thesis, the 1-letter code for amino acids is used (IUPAC-IUB, 1968).

Non-covalent protein-protein interactions (PPIs) or protein-ligand interactions are signified with a colon (e.g. TIR1:auxin:IAA1). Covalent bonds between molecules are signified with a hyphen (e.g. translational fusions like YFP-IAA1, protein-protein conjugates like IAA1-Ub_n), or a swung hyphen to point out the high energy covalent bond (e.g. thioester bond between E2 enzyme and ubiquitin denoted as E2~Ub). Note, that co-receptor pairs are written with a

hyphen when the pairing of components and not the physical interaction is in focus (e.g. TIR1-
IAA1).

1 Introduction

1.1 The phytohormone auxin

In the late 19th century, in their work *The power of movements in plants*, Charles and Francis Darwin evidenced long distance communication in plant cells. They showed that a stimulus, such as directional light, is perceived at the plant tip, whereas the triggered response, i.e. bending towards the light, occurs in the stem. This observation led them to postulate that “some influence is transmitted” from the tip downward towards the place where the response is needed (Darwin and Darwin, 1881). What the Darwins called “influence” added to the increasing proof of the existence of a group of chemically and structurally related phytohormones called auxins. The Greek “αυξανω” means “to grow” (Kögl and Haagen-Smit, 1931), and nowadays auxin is undoubtedly considered a key growth regulator and morphogen in plants (Perrot-Rechenmann, 2010). Thus, other hormone signaling pathways either converge on or crosstalk with auxin.

The most prominent, natural auxin is indole-3-acetic acid (IAA; **Figure 1-1**) – a small tryptophane-derived molecule. It is present in cells at picogram per milligram fresh weight concentrations down to below the current technical detection limit (Ljung *et al.*, 2002; Sugawara *et al.*, 2015). Besides IAA, various related compounds have been reported to have auxinic activities (De Rybel *et al.*, 2009; Simon and Petrasek, 2011). Naturally occurring (or endogenous) auxins include 4-chloroindole-3-acetic acid (4-Cl-IAA), indole-3-butyric acid (IBA) and phenylacetic acid (PAA; **Figure 1-1**) (Schneider *et al.*, 1985; Ludwig-Müller and Cohen, 2002; Simon and Petrasek, 2011). 4-Cl-IAA is a potent auxin when exogenously applied (Reinecke, 1999; Katayama, 2000; Karcz and Burdach, 2002). It stimulates the growth of deseeded pea pericarp, and therefore has been suggested to play a role in pea fruit development (Ngo *et al.*, 2002; Ozga *et al.*, 2009). This role is distinct from IAA, as only 4-Cl-IAA but not IAA stimulates pea pericarp growth (Reinecke *et al.*, 1995). Interestingly, occurrence of endogenous 4-Cl-IAA seems to be restricted to the *Fabaceae* family (Lam *et al.*, 2015). Unlike 4-Cl-IAA, IBA has been detected in various plant species (Ludwig-Müller, 2000) and occurs mostly at lower levels than IAA in plants (Epstein and Ludwig-Müller, 1993). IBA is well known for its high activity in stimulating lateral and adventitious root formation, and is widely used as rooting agent (Nordstrom *et al.*, 1991; Chhun *et al.*, 2004; Ludwig-Müller *et al.*, 2005; Schlicht *et al.*, 2013; Márquez *et al.*, 2016). It has been postulated IBA transporters mobilize IBA from the vacuole to facilitate its contribution to the active auxin pool driving root architecture (unpublished, Lucia C. Strader, personal communication). Plants convert IBA to IAA via peroxisomal β -oxidation (Strader *et al.*, 2010), and at least in *Arabidopsis thaliana*,

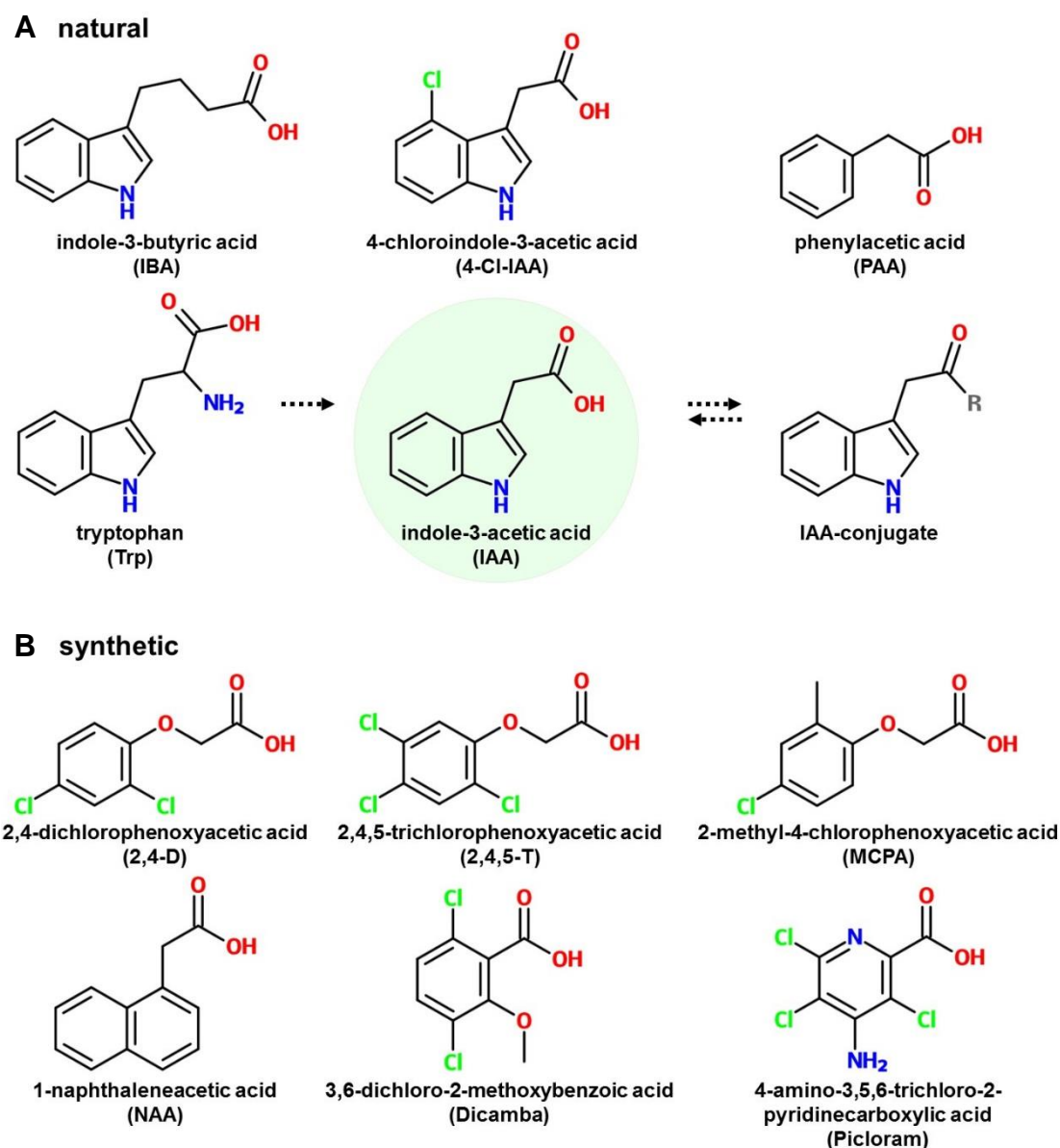


Figure 1-1: Structures of auxins

The structural formulas and names of (A) the known natural auxins IAA, IBA, 4-Cl-IAA and PAA, as well as the related compound tryptophan and a general IAA-conjugate, and (B) of a selection of synthetic auxinic compounds are shown. The most prominent, naturally occurring auxin indole-3-acetic acid (IAA) is highlighted with a green circle. Plants mainly synthesize IAA from tryptophan (signified by dashed arrow) (Zhao, 2014). Auxin metabolism and homeostasis greatly relies on conjugation and deconjugation of IAA (double dashed arrows), and likely other natural auxins, to sugars, amino acids or small proteins (R) by ester or amide bonds, respectively (Ludwig-Müller, 2011). Common abbreviations or common names are written in brackets. Heteroatoms are color-coded for better visualization of the functional groups: nitrogen in blue, oxygen in red, chlorine in green. Note the shared structural features. All auxins are based upon an aryl ring structure and a carboxyl functional group. Three out of the four natural auxins share an indole ring structure. Many synthetic auxins are chlorinated phenoxyacids, e.g. 2,4-D, 2,4,5-T, and MCPA depicted here. Picloram is shown as a representative for the large group of picolinate auxin herbicides.

genetic evidence suggests that auxin activity of IBA is entirely dependent on this conversion to IAA (Zolman *et al.*, 2000; Strader and Bartel, 2011). Therefore, IBA is considered a storage form or precursor of IAA (Korasick *et al.*, 2013), but its IAA-independent role as an active auxin in other plant species has also been proposed (Poupart and Waddell, 2000; Chhun *et al.*,

2004). The natural auxin PAA is also widely distributed in both vascular and non-vascular plants. It often occurs at higher concentrations than IAA, albeit with varying concentrations in different tissues (Wightman and Lighty, 1982; Sugawara *et al.*, 2015). Various studies suggest that PAA, as well as IBA rely on different transport mechanisms throughout the plant in comparison to IAA. This could hint at distinct roles for these natural auxins (Rashotte *et al.*, 2003; Sumimoto *et al.*, 2007; Strader and Bartel, 2011).

Among the most characteristic physiological effects of exogenous auxin application – at concentrations below cellular toxicity – are growth promotion in shoots, growth inhibition in roots, and induction of adventitious and lateral roots (Woodward and Bartel, 2005). IAA, for example, causes approximately 50 percent root growth inhibition in *Arabidopsis* seedlings at 3×10^{-8} M when exogenously applied (Wilson *et al.*, 1990). Besides their physiological effects, these auxins have common features on the structural level. They all share a carboxyl group and some form of an aryl ring structure. These structural features are also found in a number of synthetic auxins such as 2,4-dichlorophenoxyacetic acid (2,4-D) and naphthalene acetic acid (NAA). These compounds, as well as manifold derivatives, e.g. 2,4,5-trichlorophenoxyacetic acid (2,4,5-T), 2-methyl-4-chlorophenoxyacetic acid (MCPA), dicamba, and picloram (**Figure 1-1**) have been extensively used as herbicides. Auxinic herbicides elicit the same type of plant responses as IAA, but with a long-lasting and stronger intensity of action, particularly owing to their higher stability in the plant. Not least, because natural auxins like IAA are subject to rapid inactivation through conjugation and degradation by multiple pathways in the plant. (Grossmann, 2010). Although IAA, 2,4-D, NAA, and other auxinic compounds can cause similar physiological responses, the molecules cause distinct but overlapping changes in gene expression (Pufky *et al.*, 2003), likely reflecting differences in metabolism, transport, or interaction with the signaling machinery (Woodward and Bartel, 2005; De Rybel *et al.*, 2009).

1.2 Auxin perception and signaling

In plants, auxin biosynthesis, transport, conjugation and degradation contribute to a cell-specific auxin level (Michniewicz *et al.*, 2007; Normanly, 2010; Ludwig-Müller, 2011). The establishment of auxin gradients throughout the plant controls cell elongation, cell division and cell differentiation. Thus, key processes including tropic responses to light and gravity (Friml *et al.*, 2002b; Abas *et al.*, 2006), embryo and vascular patterning (Weijers *et al.*, 2006; Möller and Weijers, 2009; Scarpella *et al.*, 2010), organ initiation (Benkova *et al.*, 2003), root and shoot elongation (Perrot-Rechenmann, 2010), as well as apical dominance (McSteen and Leyser, 2005), and even defense and various stress responses (Kazan and Manners, 2009) are

regulated by auxin. Rapid changes in gene expression within minutes underlie these responses, indicating a short and immediate signal perception and transduction from outside the cell to the nucleus. Indeed, once inside the cell either by passive diffusion or active uptake, IAA is small enough to enter the nucleus through its pores (Keminer and Peters, 1999), obviating the need for a long signal relay cascade from cell membrane to transcriptional control. Once inside the nucleus, auxin acts on the ubiquitin-proteasome system (UPS) which links auxin perception and rapid auxin transcriptional response (**Figure 1-3**).

1.2.1 The Ubiquitin Proteasome System (UPS) in Auxin Signaling

The UPS comprises the machinery that orchestrates the posttranslational protein modification known as ubiquitination (or ubiquitylation). Ubiquitination marks a specific target protein with ubiquitin (Ub) moieties for degradation by the 26S proteasome (**Figure 1-2 A**) (Smalle and Vierstra, 2004). Specifically, Ub is covalently attached to a target protein. The ubiquitination cascade involves E1 Ub-activating, E2 Ub-conjugating and E3 Ub-ligase enzymes (Hershko and Ciechanover, 1998). In an ATP-dependent manner, E1 Ub-activating enzyme activates Ub by linking its terminal carboxyl group via a thioester bond to the catalytic cysteine of E1. In the following step, Ub is transferred from the E1~Ub complex to the sulfhydryl group of a specific cysteine of an E2 Ub-conjugating enzyme via trans-thioesterification. Subsequently, an E3 Ub-ligase facilitates the transfer of activated Ub from E2 to a lysine ϵ -amino group of its substrate or target protein. Hence, Ub is attached to the target protein by an isopeptide bond (**Figure 1-2 B**) (Weissman, 2001; Voet and Voet, 2004). In successive rounds of Ub transfer, the carboxyl group of the C-terminal glycine of another Ub can be linked to a different lysine residue of the target protein, or to one of the seven exposed lysine residues (K6, K11, K27, K29, K33, K48, K63) or the N-terminus (M1) of the previously transferred Ub. Consequently, besides monoubiquitination, many different covalent concatenations are possible including multimonoubiquitination, homotypic chains like K48- or K63-linked polyubiquitination, branched chains, or mixed, heterotypic chains depending on the specificity of the E2 or E3 (Komander and Rape, 2012). Extensive studies on K48- and K63-ubiquitination have established essential roles for these modifications in proteasomal degradation and in cell signaling, respectively (Chen and Sun, 2009; Komander and Rape, 2012; Kulathu and Komander, 2012). K48-, K11-linked, and mixed polyubiquitination is recognized by the 26S proteasome and leads to ATP-dependent proteasomal unfolding and degradation of the target protein (Thrower *et al.*, 2000; Komander and Rape, 2012) (**Figure 1-2 A**).

1.2.1.1 SCF^{TIR1/AFBs} recognize AUX/IAA repressors for degradation

Specific recognition of various target proteins is facilitated by numerous E3 ligases differing in subunit composition and mechanism of action (Vierstra, 2009). Plant E3 ligases are estimated to range above 1000, allowing precise cellular responses to environmental cues (Chen and Hellmann, 2013). Among the various types of E3 ligases that specifically recognize targets for Ub transfer are the SKP1-CULLIN1-F-BOX PROTEIN (SCF) E3 ligase complexes (**Figure 1-2 B**). SCFs are multiprotein complexes consisting of CULLIN1 (CUL1), RING BOX1 (RBX1), S-PHASE KINASE ASSOCIATED PROTEIN1 (SKP1) and an interchangeable F-box protein (FBP; Skowyra *et al.*, 1997; Zheng *et al.*, 2002). CUL1 serves as a scaffold protein or docking platform for RBX1 at its C-terminal, and for SKP1-FBP heteromer recruitment at its N-terminal end (Patton *et al.*, 1998). In Arabidopsis, any of the 21 SKP1 homologs, called ARABIDOPSIS SKP1-LIKE (ASK) proteins act as adaptor proteins that link an FBP through its eponymous N-terminal F-box domain to the SCF (Bai *et al.*, 1996; Marrocco *et al.*, 2003; Kuroda *et al.*, 2012). A protein family of >700 Arabidopsis FBPs confers target specificity to SCF complexes (Gagne *et al.*, 2002; Xu *et al.*, 2009). While all FBPs share an F-box domain for ASK interaction, they vary vastly in their specific target recognition domain (Gagne *et al.*, 2002).

TRANSPORT INHIBITOR RESPONSE 1 (TIR1) and its five close homologs AUXIN SIGNALING F-BOX 1-5 (AFB1-5) are Arabidopsis FBPs that are soluble, nuclear-localized 60-70 kDa proteins that recruit target proteins in auxin signaling (**Figure 1-5 C**) (Ruegger *et al.*, 1998; Gray *et al.*, 2001; Dharmasiri *et al.*, 2003; Dharmasiri *et al.*, 2005b; Parry *et al.*, 2009; Prigge *et al.*, 2016). Through their N-terminal F-box domain, TIR1/AFBs interact with ASKs and thereby assemble into an SCF complex (**Figure 1-2 C**) (Gray *et al.*, 1999; Dharmasiri *et al.*, 2005b). This interaction is essential for TIR1/AFB function, and auxin signaling (Calderón Villalobos *et al.*, 2012; Yu *et al.*, 2015). The TIR1/AFB C-terminal domain for specific target recognition consists of 18 leucine-rich repeats (LRRs; Ruegger *et al.*, 1998; Gagne *et al.*, 2002; Tan *et al.*, 2007). Through their LRR domain, and in auxin-dependent manner TIR1/AFBs recognize AUXIN/INDOLE-3-ACETIC ACID INDUCIBLE (AUX/IAA) short-lived transcriptional repressors for proteasomal degradation (Gray *et al.*, 2001). Auxin enhances this FBP:target interaction at nanomolar concentrations (Gray *et al.*, 2001; Dharmasiri *et al.*, 2003). Subsequently, degradation of AUX/IAA repressors leads to derepression and AUXIN RESPONSE FACTOR (ARF)-dependent transcription of auxin-response genes (see **Section 1.2.2**, **Figure 1-2 C** and **Figure 1-3 B**).

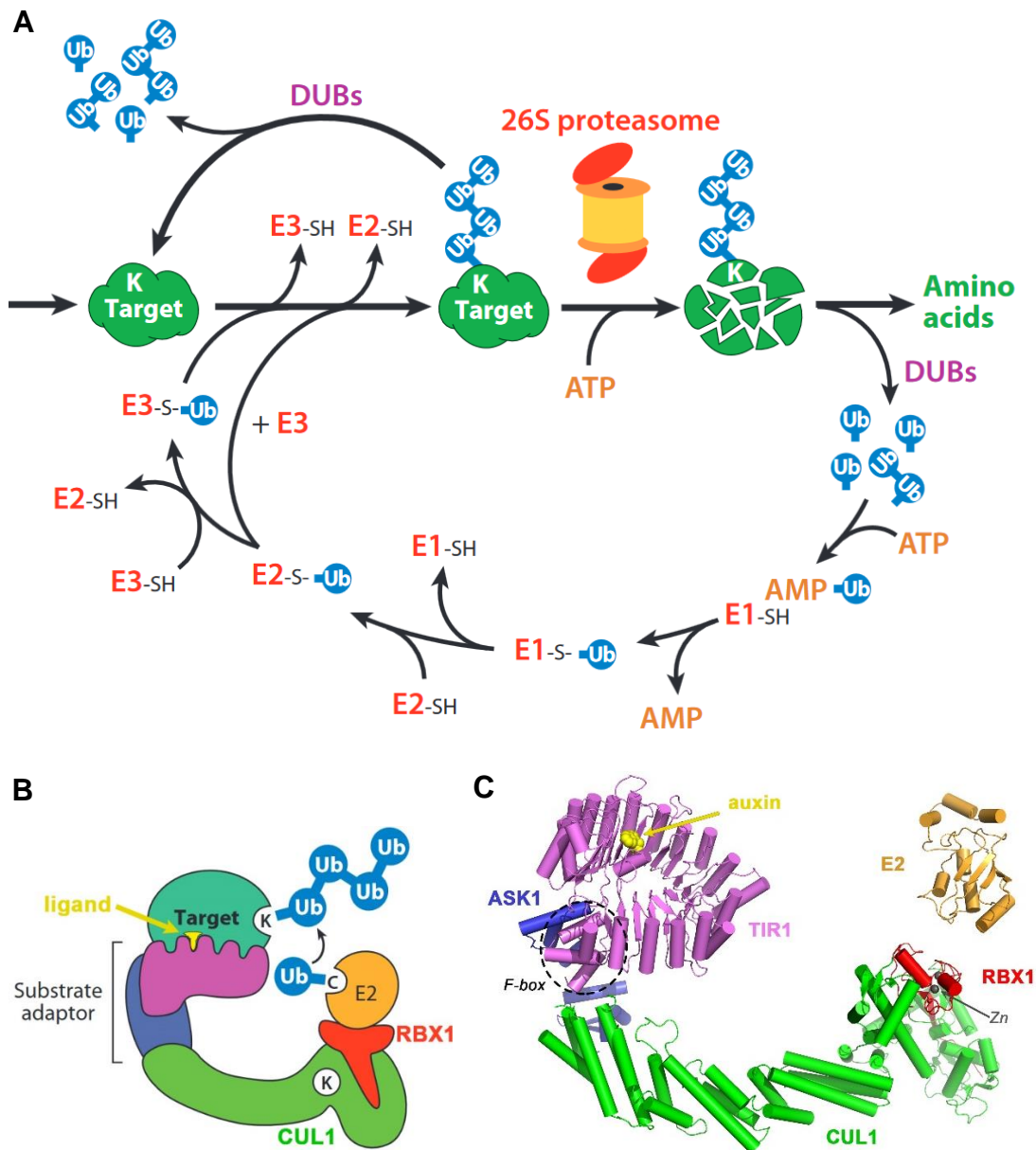


Figure 1-2: Ubiquitin proteasome system (UPS) and small-molecule mediated target recognition by SCF E3 Ub-ligases

A. The UPS pathway begins with E1 Ub-activating enzyme ATP-dependently activating Ub. Next, Ub is transferred from the E1~Ub complex to the sulfhydryl group of a specific cysteine of an E2 Ub-conjugating enzyme, and finally attached to the target with the help of an E3 Ub-ligase. The resulting product is a Ub-protein conjugate where the C-terminal carboxyl group of Ub is linked through an isopeptide bond to a lysine ϵ -amino group in the target or in another Ub, if poly-Ub chains are added. After iterative assembly, the Ub-protein conjugate can be disassembled by deubiquitylating enzymes (DUBs) to release the target protein and Ubs intact, or the target can be broken down by the 26S proteasome, with the concomitant release of the bound Ub molecules by DUBs. **B.** Subunit organization of SCF complexes with ligand-mediated target recognition. The CUL1 scaffold binds a substrate adaptor (or target receptor) at the N-terminus and a RBX1 protein for E2 association on the C-terminus. Target recognition is enhanced by a ligand at the interface of receptor and target. The K in the target and the CUL1 are the acceptor sites for Ub and RUB1/Nedd8, respectively. The C in the E2 locates the active-site cysteine that binds activated Ub. **C.** Structural ribbon model of SCF^{TIR1} in complex with auxin. ASK1 and FBP TIR1 associate through the F-box domain (black dashed circle) of TIR1 to form the substrate adaptor which is linked by CUL1 to the RBX1 platform for E2 binding. The C-terminal LRR domain of TIR1 serves for specific substrate or target recognition. Auxin binds in a pocket on the surface of the solenoid-formed TIR1-LRRs and thereby enhances the ability of TIR1 to physical interact with its targets, the AUX/IAAs (not shown). Grey spheres in RBX1 indicate zinc atoms. ASK1 of TIR1-ASK1 structure (PDB code: 2P1Q; Tan *et al.*, 2007) was structurally aligned with SKP1 of HsSCF^{SKP2} structure (PDB code: 1LDK/1LDJ; Zheng *et al.*, 2002) to give SCF^{TIR1} complex. RING domain CBL of CBL-HsUbcH7 complex (1FBV; Zheng

et al., 2000) was structurally aligned with RBX1 of SCF^{SKP2} to show an exemplary E2 oriented towards the SCF (Zheng *et al.*, 2002). Modified from Hua and Vierstra (2011).

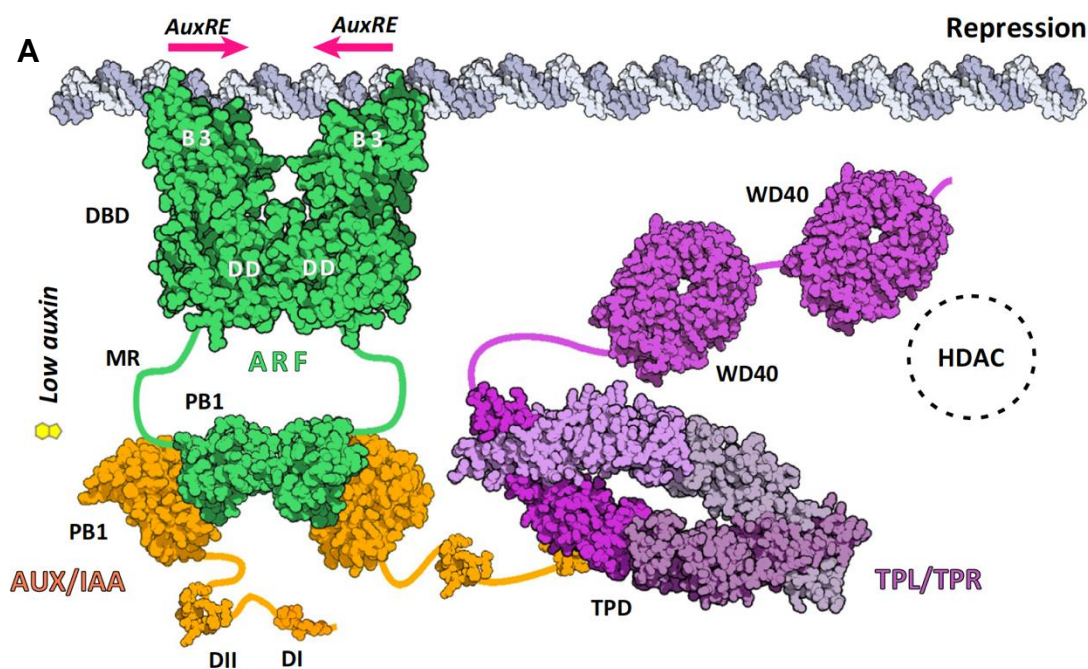
1.2.1.2 AUX/IAAs are negative regulators of auxin response

AUX/IAA transcriptional regulators are small (18-36 kDa) proteins, which upon translation rapidly localize to the nucleus due to two conserved nuclear localization signals: one in the C-terminus and a polymorphic, bipartite signal in the N-terminus (Abel and Theologis, 1995). In Arabidopsis, a family of 29 genes encodes for AUX/IAAs (**Figure 1-5 B**) (Abel *et al.*, 1995; Remington *et al.*, 2004; Overvoorde *et al.*, 2005). The Arabidopsis AUX/IAA gene family has expanded due to gene and genome duplication events (**Figure 1-5 A**) (Vision *et al.*, 2000; Simillion *et al.*, 2002; Blanc *et al.*, 2003; Remington *et al.*, 2004). Often, the duplicate gene copies (or ohnologs) which arise from those events serve as basis for evolutionary innovation as they undergo neo- or sub-functionalization, or pseudogenization and eventually gene loss (Prince and Pickett, 2002). The Arabidopsis AUX/IAA family has nine such ohnolog pairs (Remington *et al.*, 2004). Amino acid identity among AUX/IAAs ranges from 83 % to 10 % (Overvoorde *et al.*, 2005). 23 of the 29 members of the AUX/IAA family are considered canonical, because they share four regions of highly conserved sequence, initially named domain I, II, III, and IV (**Figure 1-3 A**) (Oeller *et al.*, 1993; Abel *et al.*, 1995).

AUX/IAAs confer transcriptional repression through a conserved ethylene response factor-associated amphiphilic repression (EAR) motif hallmarked by the consensus LxLxL located in the N-terminal region referred to as domain I (DI) (Ulmasov *et al.*, 1997b; Tiwari *et al.*, 2001; Tiwari *et al.*, 2004; Kagale *et al.*, 2010). Through the EAR motif, AUX/IAAs bind to TOPLESS (TPL) and TOPLESS-RELATED 1-4 (TPR1-4) co-repressors (Szemenyei *et al.*, 2008; Causier *et al.*, 2012a; Causier *et al.*, 2012b). These are a family of global co-repressors involved in regulating various transcriptional responses in plants, including e.g. jasmonate, gibberellin, and brassinosteroid signaling (Pauwels *et al.*, 2010; Krogan *et al.*, 2012b; Oh *et al.*, 2014; Fukazawa *et al.*, 2015). TPL/TPRs recruit histone deacetylases (HDACs) which modify chromatin to be transcriptionally inactive (**Figure 1-3 A**) (Long *et al.*, 2006; Causier *et al.*, 2012a; Krogan *et al.*, 2012b). TPL/TPR proteins form tetramers and interact with EAR motifs, including those of AUX/IAAs, through a conserved binding mode (Ke *et al.*, 2015). Three conserved leucine residues undergo hydrophobic interactions with hydrophobic and positively charged residues along a groove in each TPL/TPR monomer (Ke *et al.*, 2015). Recent findings also suggested that the EAR-flanking, largely charged residues, might contribute to different affinities in TPL/TPR:AUX/IAA binding (Ke *et al.*, 2015). While it has been proposed that a single AUX/IAA monomer is sufficient to repress ARF activity (Pierre-Jerome *et al.*, 2016), multivalent interactions between oligomeric AUX/IAA repressors and the tetrameric TPR/TPL might

stabilize the repressor:co-repressor complex (Ke *et al.*, 2015). Mutational analyses of the EAR motif showed contrasting effects on auxin signaling in different AUX/IAAs, pointing to intrinsic differences in AUX/IAA repression domains (Li *et al.*, 2011)(Figure 1-3 A).

AUX/IAAs classify as primary auxin-responsive genes, as their expression rapidly rises within minutes of auxin application independently of *de novo* protein synthesis, indicating direct gene activation (Theologis *et al.*, 1985; Abel and Theologis, 1996). Since AUX/IAAs themselves are early auxin response genes, degradation of AUX/IAAs and thus derepression of these genes allows for a rapid termination of the auxin response by replenishing the AUX/IAA repressor pool (Abel and Theologis, 1996; Benjamins and Scheres, 2008). This allows a fast and tightly controlled auxin response gene activation. Yet, not all AUX/IAAs show a strong auxin induction. Indeed, induction kinetics range from few minutes after auxin application for e.g. IAA1 to IAA6 to half an hour for e.g. IAA9 and IAA10. Expression of IAA7 and IAA8 depends on *de novo* protein synthesis. Thus, they belong to genes which are expressed in a secondary wave of auxin response (Abel *et al.*, 1995). Overall, AUX/IAAs differ not only in their auxin-induced, but also in their basal expression profile, indicating distinct functions of their gene products. In fact, the distinct expression patterns of AUX/IAAs and ARFs – the two key transcriptional regulators in auxin signaling – have been proposed to guide specific auxin-mediated growth and developmental responses in plants (Paponov *et al.*, 2008).



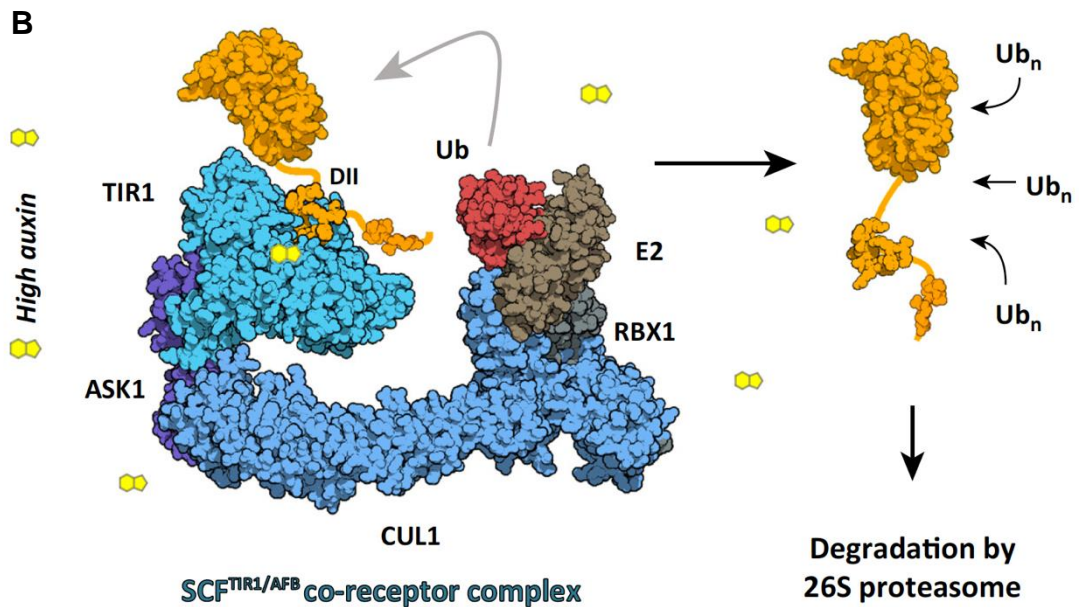


Figure 1-3: Classical model of auxin signaling

The composite model is exemplarily showing the structures of ARF5 (green) for ARF activators, IAA17 PB1 domain, IAA7 degron peptide, and IAA1 EAR motif (orange) for AUX/IAA repressors, OsTPR2 (purple) for TPL/TPR co-repressors, SCF^{TIR1} (shades of cyan/blue) for SCF^{TIR1/AFBs}. Auxin is represented by a simplified bicyclic structure (yellow). **A.** Under low-auxin conditions, transcription of primary auxin genes is actively repressed by inactivation of promoter-bound ARF activators. The ARF dimer binds two everted *AuxRE* motifs via its B3-type subdomains. Dimerization of the N-terminal ARF DNA-binding domain (DBD) is mediated by the dimerization subdomain (DD), and the C-terminal ARF PB1 domain may further stabilize ARF dimerization. The structure of the ARF middle region (MR) remains to be determined (green line). ARFs and AUX/IAA repressors interact via their PB1 domain. The structures of the connecting loops in AUX/IAAs are unknown (orange lines). The EAR motif in DI of AUX/IAAs interacts with TPL/TPR co-repressors via their N-terminal TOPLESS domain (TPD), which tetramerizes. Thus, four AUX/IAA EAR motifs may cooperate in the recruitment of TPL/TPR co-repressor tetramers (only one TPL/TPR monomer is depicted). The C-terminal WD40 repeat domains of TPL/TPR co-repressors sequester chromatin-modifying enzymes such as the histone deacetylase complex (HDAC, broken circle), leading to transcriptional repression. **B.** Under high-auxin conditions, ARF derepression and transcriptional activation is triggered by sequestering AUX/IAAs via their degron peptide (DII) to the SCF^{TIR1} E3 Ub-ligase complex, which comprises the TIR1 F-box protein (marine blue), the ASK1 adapter (dark blue), the CUL1 scaffold (light blue), the RING finger protein RBX1 (grey). The SCF^{TIR1} complex interacts with an E2 ubiquitin-conjugating enzyme (brown), which presents an activated ubiquitin (Ub, red). Polyubiquitination (Ub_n) of AUX/IAAs leads to subsequent degradation via the 26S proteasome. Modified from Dinesh *et al.* (2016).

1.2.1.3 AUX/IAAs repress AUXIN RESPONSE FACTORS (ARFs)

ARFs resemble very much truncated AUX/IAA proteins as they share a highly similar C-terminus but lack AUX/IAA N-termini. The C-terminal domain of AUX/IAAs, formerly referred to as domain III and IV, adopts a globular ubiquitin-like β -grasp fold with secondary structure homology to the type I/II Phox/Bem1p (PB1) domain (Han *et al.*, 2014; Dinesh *et al.*, 2015). Henceforth, domain III/IV of AUX/IAAs is referred to as *PB1 domain*. Type I/II PB1 domains contain both an acidic octicosapeptide repeat, p40phox, Cdc24p, atypical PKC interaction domain (OPCA) motif and a basic surface patch that mediate electrostatic interactions leading to front-to-back oligomerization (Sumimoto *et al.*, 2007). AUX/IAAs share the PB1 domain with ARF transcription factors (Ulmasov *et al.*, 1999a; Tiwari *et al.*, 2003). Through their highly homologous PB1 domain, ARFs and AUX/IAAs undergo homo- and heterotypic interactions

(Kim *et al.*, 1997; Vernoux *et al.*, 2011; Han *et al.*, 2014; Korasick *et al.*, 2014; Nanao *et al.*, 2014; Dinesh *et al.*, 2015; Korasick *et al.*, 2015), which are crucial in the relay of the nuclear auxin signal (**Figure 1-3 A**)(Tiwari *et al.*, 2003; Lau *et al.*, 2011; Krogan *et al.*, 2012a).

ARFs are encoded by a family of 23 genes in Arabidopsis (**Figure 1-5 A**)(Guilfoyle and Hagen, 2007; Finet *et al.*, 2013). ARF transcription factors bind to *cis* regulatory elements, the auxin-responsive elements (*AuxREs*) to activate or repress transcription of downstream genes. *AuxREs*, with their TGTCNN (most frequently TGTCTC) consensus sequence, lie in the upstream promoter region of auxin response genes (Ballas *et al.*, 1993; Oeller *et al.*, 1993; Ulmasov *et al.*, 1995; Mironova *et al.*, 2014). These genes include members of the *AUX/IAA*, *GRETCHEN HAGEN3 (GH3)*, and *SMALL AUXIN UPREGULATED RNA (SAUR)* gene families, which are involved in auxin homeostasis and response (Hagen and Guilfoyle, 2002; Chapman and Estelle, 2009). Only recently, the specific mode of ARF binding to *AuxREs* has been elucidated via structural studies (Boer *et al.*, 2014; Dinesh *et al.*, 2016). ARFs contain an N-terminal B3-type DNA-binding domain (DBD) for *AuxRE* binding (Ulmasov *et al.*, 1997a, 1999b). The ARF DBD consists of three distinct structural domains: a dimerization domain (DD), the B3 domain for DNA-binding (B3) and an ancillary domain (Boer *et al.*, 2014). Furthermore, ARFs consist of a middle region (MR) with characteristic amino acid bias, through which ARFs can act either as transcriptional activators or repressors (Ulmasov *et al.*, 1999a; Tiwari *et al.*, 2003; Guilfoyle and Hagen, 2007). A glutamine-rich MR as found in ARF5 to ARF8 and ARF19 turns these to transcriptional activators. The other ARFs with proline-, serine-, and threonine-rich MRs act as repressors (Guilfoyle and Hagen, 2007; Chandler, 2016)(**Figure 1-3 A**).

By recruiting TPL/TPR co-repressors and thereby chromatin-modifying factors to the DNA, *AUX/IAAs* interact with and thereby exert their repressor activity on ARF activators directly on auxin-response genes (Long *et al.*, 2006; Li *et al.*, 2009; Kagale and Rozwadowski, 2011; Krogan *et al.*, 2012b; Wang *et al.*, 2013a)(**Figure 1-3 A**). Genetic studies – not least guided by the similarity between *AUX/IAA* gain-of-function (*gof*) and ARF loss-of-function (*lof*) mutant phenotypes – have identified specific ARF:*AUX/IAA* pairs that direct growth and development in different tissues. For example, ARF7/MONOPTEROS (MP) promotes embryonic root formation and is regulated by IAA12/BODENLOS (BDL) and IAA13 (Hamann *et al.*, 1999; Hamann *et al.*, 2002; Weijers *et al.*, 2005). IAA3/SUPPRESSOR OF HY2 MUTATION2 (SHY2) inhibits ARF7/NON-PHOTOTROPIC HYPOCOTYL4 (NPH4) and ARF19 in regulating seedling root response to auxin (Weijers *et al.*, 2005). IAA19/MASSUGU2(MSG2) and ARF7/NPH4 co-function in tropic responses in hypocotyls (Tatematsu *et al.*, 2004), whereas ARF7:IAA14,

ARF19:IAA14, ARF7:IAA28, and ARF19:IAA28 co-function in roots (Fukaki et al., 2005; De Rybel et al., 2010; De Smet et al., 2010; Goh et al., 2012; Piya et al., 2014). Indeed, mainly ARF activators physically interact with AUX/IAAs. This supports the classical model of auxin signaling, where ARF activators that control auxin response genes are repressed by AUX/IAAs (Vernoux *et al.*, 2011; Piya *et al.*, 2014). A few scenarios have been proposed for the yet unclear role of ARF repressors. They might act as competitors of DNA-binding for ARF activators, or repress auxin response genes *AuxRE*-independently (Guilfoyle and Hagen, 2007; Chapman and Estelle, 2009). Interestingly, ARF repressors have been shown to preferentially interact with non-canonical IAA32 and IAA34 (Piya *et al.*, 2014). Also, it has been described for ARF5 and ARF7 that they can activate auxin-response independently of a PB1 domain (Wang *et al.*, 2013b). These findings suggest that the classical model (**Figure 1-3**) does not fully explain all aspects of ARF-AUX/IAA-mediated auxin signaling yet.

1.2.1.4 Auxin-response relies on rapid AUX/IAA degradation

The key to rapid AUX/IAA degradation, and to regulation of the transcriptional response by auxin lies in an AUX/IAA primary degron, formerly referred to as domain II. Through their degron, AUX/IAAs are auxin-dependently recognized for degradation by the SCF^{TIR1/AFB} E3 ligase (**Figure 1-3 B**)(Gray *et al.*, 2001). The degron comprises a highly conserved consensus sequence QVVGWPPVRSYRK, including invariant amino acids VGWPP at the core (Ramos *et al.*, 2001)(**Figure 1-4 A**). It represents a transferable and specifically auxin-responsive degradation signal (Worley *et al.*, 2000; Zenser *et al.*, 2001; Zenser *et al.*, 2003). This degron has nowadays even been utilized to drive degradation of proteins in non-plant systems such as yeast, mammalian cells, and *C. elegans* (Nishimura *et al.*, 2009; Kanke *et al.*, 2011; Holland *et al.*, 2012; Zhang *et al.*, 2015). Precisely, it has been shown that 13 amino acids of the degron are necessary and sufficient for degradation. Thus, naturally occurring variations from the consensus degron sequence do not affect degradation, and this degradation is unmistakably proteasome-dependent (Gray *et al.*, 2001; Ramos *et al.*, 2001; Zenser *et al.*, 2001). If the degron is compromised, for instance by individual amino acid substitutions due to mutations, AUX/IAA proteins are stabilized and their accumulation causes constitutive repression of auxin signaling. This then results in auxin-resistant phenotypes, aberrant plant growth and development, and in the most severe cases serious impairment of embryo development (Hamann *et al.*, 1999; Worley *et al.*, 2000; Gray *et al.*, 2001; Ouellet *et al.*, 2001). Over the years, dominant negative *gof* mutant alleles containing single amino acid exchanges in the highly conserved residues of the AUX/IAA degron have been isolated (Wilson *et al.*, 1990; Leyser *et al.*, 1996). For example, EMS mutagenesis lead to identifying *auxin-resistant (axr)* mutants *axr2-1 (iaa7)*, *axr3-1 (iaa17)* and *axr5-1 (iaa1)*, which carry non-conservative

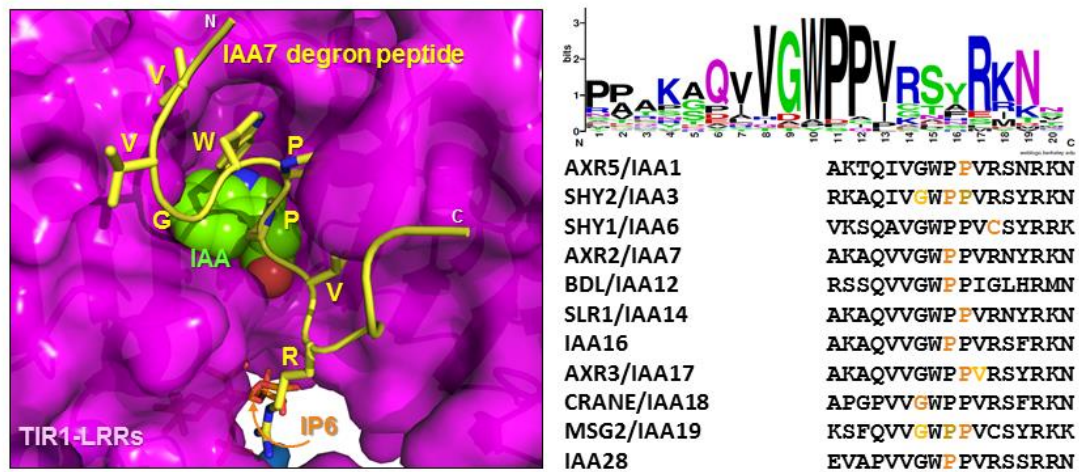
exchanges in the first or second proline (P87S, P88L, P61S, respectively) of the invariant degron core (Timppte *et al.*, 1994; Leyser *et al.*, 1996; Rouse *et al.*, 1998; Nagpal *et al.*, 2000; Yang *et al.*, 2004)(**Figure 1-4 A**). Roots of *axr* mutant seedlings are resistant to growth inhibition caused by exogenous auxin applications. Furthermore, these mutants exhibit stunted overall growth, small and curled leaves, strongly reduced etiolation response in the dark, agravitropism of shoots and roots, and lack of root hairs (**Figure 1-4 B**)(Timppte *et al.*, 1992; Nagpal *et al.*, 2000; Yang *et al.*, 2004). In addition, other eight AUX/IAA *gof* mutants were characterized in the past. These include *suppressor of hy2 mutation 2 (shy2/iaa3)* (Kim *et al.*, 1996; Tian and Reed, 1999; Tian *et al.*, 2002), *suppressor of hy2 mutation 1 (shy1/iaa6)* (Kim *et al.*, 1996), *bodenlos (bdl/iaa12)* (Hamann *et al.*, 1999), *solitary root 1 (slr1/iaa14)* (Fukaki *et al.*, 2002), *iaa16* (Rinaldi *et al.*, 2012), *crane/iaa18* (Uehara *et al.*, 2008) and *iaa18-1* (Ploense *et al.*, 2009), *massugu 2 (msg2/iaa19)* (Tatematsu *et al.*, 2004), and *iaa28-1* (Rogg *et al.*, 2001)(**Figure 1-4 A, B**). All of these AUX/IAA *gof* mutants contain single amino acid exchanges in the primary degron.

Degrone mutations not only impair the basal destabilization of AUX/IAAs, but also compromise degradation rates in response to auxin (Gray *et al.*, 2001; Zenser *et al.*, 2001). While overall canonical AUX/IAAs exhibit basal half-lives from 6 to 80 minutes (min) and auxin-sensitivities from 2- to 5-fold half-life reduction upon auxin treatment, *aux/iaa* *gofs* are stable (Abel *et al.*, 1994; Gray *et al.*, 2001; Ouellet *et al.*, 2001; Ramos *et al.*, 2001; Dreher *et al.*, 2006; Havens *et al.*, 2012)(For detailed discussion of AUX/IAA degradation rates see **Section 1.2.3.3**). Moreover, AUX/IAAs that lack or only partially share the conserved degron occur naturally. These include IAA20, IAA30, IAA31, IAA32, IAA33, and IAA34, which are considered non-canonical AUX/IAAs (Overvoorde *et al.*, 2005). Accordingly, degron-less IAA20 exhibits an extended half-life and is not auxin-dependently destabilized (Dreher *et al.*, 2006). It has been proposed stable AUX/IAAs function in dampening and thus reducing fluctuations in auxin signaling by sequestering ARFs (Sato and Yamamoto, 2008a, b). Thus, AUX/IAAs, in few cases, might occupy TIR1-independent roles in auxin signaling.

A recent study in rice has shown, that LATERAL ROOTLESS 2 (LRT2), a cyclophilin for peptidyl-prolyl *cis/trans* isomerization, acts on rice AUX/IAA proteins (Jing *et al.*, 2015). LRT2 catalyzes isomerization of the tandem proline residues of the AUX/IAA GWPPV core, so that the first W-P bond is in *cis*, and the P-P bond in *trans*, which is the conformation necessary for recognition by OsTIR1 (Jing *et al.*, 2015). Also, the study showed that association of LRT2 with the OsTIR1:OsIAA11 complex is enhanced by auxin, and required for efficient degradation of AUX/IAAs (Jing *et al.*, 2015). This suggests that additional factors regulate AUX/IAA function.

Furthermore, one study showed that the AUX/IAA N-terminal part encompassing DI and the degron can be phosphorylated *in vitro* by phytochromes. Yet, the *in vivo* implications of this remain elusive (Colon-Carmona *et al.*, 2000).

A



B

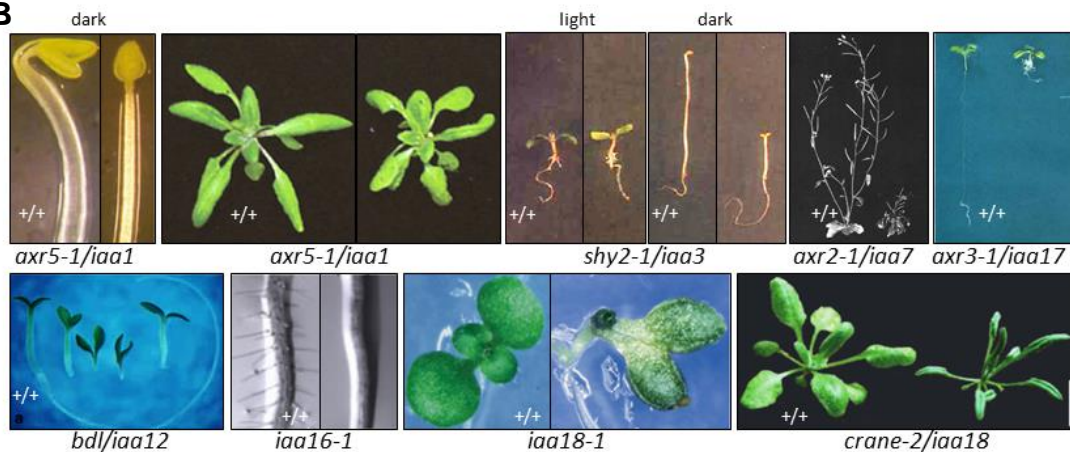


Figure 1-4: Point mutations in AUX/IAA degrons cause grave phenotypes by interfering with their recognition by SCF^{TIR1}-type E3 ligases

A. Crystal structure of the AUX/IAA degron peptide (yellow) how it is bound on top of the IAA molecule (green) sitting in the auxin-binding pocket formed by TIR1-LRRs (magenta) and IP6 (orange) binding site lying beneath (left panel; PDB code: 2P1Q, Tan *et al.*, 2007). Thus, auxin enhances the recognition of AUX/IAA by the SCF^{TIR1} ligase for ubiquitination and subsequent proteasomal degradation. A sequence logo comprising 20 residues of the primary degron from all Arabidopsis AUX/IAs is shown in the upper right panel (via <http://weblogo.berkeley.edu/>; Crooks *et al.*, 2004). It clearly depicts the highly conserved core degron sequence VGWPP, which is essential for the interaction as seen in the structural representation. For eleven AUX/IAs, mutant alleles carrying single amino acid substitutions in their degron sequence have been isolated (lower right panel; residues affected by substitutions are marked in shades of orange representing different mutant alleles). Through these gain-of-function (gof) mutations, AUX/IAs become stabilized and accumulate causing auxin-related phenotypes. **B.** A selection of *aux/iaa* gof mutants showing typical phenotypes are depicted including de-etiolated seedlings (*axr5-1*, *shy2-1*), stunted growth (*axr2-1*), abnormal embryonic patterning (*bdl*, *iaa18-1*), affected leaf size and shape (*axr5-1*, *crane-2*), impaired seedling root growth (*axr3-1*, *bdl*), as well as lack of root hairs and lateral roots (*iaa16-1*). Note that most *aux/iaa* gof mutants exhibit several of these phenotypes (e.g. *axr5-1*) but not all are depicted here. Wild-type plants are denoted with +/+. Reproduced and modified from following references: *axr5-1* de-etiolation and rosette phenotype (Yang *et al.*, 2004), *shy2-1* de-etiolation (Kim *et al.*, 1996), *axr2-1* dwarf phenotype (Timpte *et al.*, 1992), *axr3-1* seedling root phenotype (Leyser *et al.*, 1996), *bdl* seedling root phenotype (Hamann *et al.*, 1999), *iaa16-1* seedling root hair phenotype (Rinaldi *et al.*, 2012), *iaa18-1* seedling phenotype of severe class (Ploense *et al.*, 2009), *crane-2* leaf phenotype (Uehara *et al.*, 2008).

1.2.2 Molecular mechanism of auxin perception

Auxin enhances recognition of AUX/IAAs via their degrons by SCF^{TIR1/AFB} E3 ligases. This effect has been shown to be independent of additional factors or post-translational modifications, as TIR1 is capable to bind auxin directly *in vitro* (Dharmasiri *et al.*, 2005a; Kepinski and Leyser, 2005). Thus, TIR1 was initially considered to constitute the sole receptor for auxin. However, the manner in which auxin stimulates the interaction between SCF^{TIR1} and its targets, the AUX/IAAs, remained elusive until structural studies followed. Tan *et al.* (2007) elucidated the crystal structure of a TIR1:ASK1 heterodimer alone and in complex with either IAA, NAA, or 2,4-D, and a 17-amino acid degron peptide of IAA7 (**Figure 1-4 A**). Their study revealed that the TIR1:ASK1 complex folds into a mushroom-like structure, with the TIR1 F-box domain bound to ASK1 forming the 'stem' and the 18 LRRs (LRR-1 to -18) forming the 'cap' of the mushroom. The LRRs fold into a twisted horseshoe-shaped solenoid, on the top of which the auxin and the AUX/IAA target bind (**Figure 1-2 C**). Especially, few long intra-repeat loops on the top surface of the solenoid, together with the proximal concave surface of the LRR fold form the auxin- and AUX/IAA-binding pocket (Tan *et al.*, 2007). The carboxyl group of IAA, NAA or 2,4-D is anchored via a salt bridge and hydrogen bonds, in particular through the highly selective residues R403 and S438 at the bottom of the auxin-binding pocket. The aromatic ring of auxin undergoes hydrophobic and van-der-Waals interactions with the sides of the pocket, which provide less selective interactions, thus creating a partially promiscuous auxin binding site. In contrast to NAA and 2,4-D, only IAA additionally forms a hydrogen bond between the amine group of the indole ring and a carbonyl group in the TIR1 pocket (Tan *et al.*, 2007). *In silico* data suggests that different residues at the rim and sides of the auxin binding pocket contribute to TIR1 ligand selectivity as an auxinic molecule descends into the pocket (Uzunova *et al.*, 2016).

Furthermore, the crystal structure studies showed, that a synthetic IAA7 degron peptide binds atop the auxin-bound TIR1 pocket through extensive hydrophobic interactions. The residues of the invariant degron core (GWPPV) provide the hydrophobic interacting residues that stack on top of auxin and interact with surrounding TIR1 residues. The conserved glycine provides the flexibility for the degron to obtain a coiled conformation that dips into the TIR1 pocket (**Figure 1-4 A**). Based on these findings auxin was proposed to act as “molecular glue” enhancing the interaction between target receptor TIR1 and AUX/IAA targets (Tan *et al.*, 2007). Moreover, crystal structure elucidation revealed a myo-inositol-1,2,3,4,5,6-hexakisphosphate (IP6) molecule that co-purified with the TIR1-ASK1 protein complex from insect cells. IP6 positioning is tightly coordinated by positively charged residues directly underneath the bottom of the auxin binding pocket. Mutations in these residues abrogate

auxin-dependent AUX/IAA as well as ASK1 binding, suggesting IP6 is an essential structural cofactor of TIR1 (**Figure 1-4 A**)(Tan *et al.*, 2007; Calderón Villalobos *et al.*, 2012).

1.2.2.1 TIR1/AFBs are crucial players in auxin perception, that are regulated on multiple levels

TIR1/AFBs are required for full auxin sensitivity in plants, and although partially redundant, they are also implicated in distinct functions in plant growth and development (Dharmasiri *et al.*, 2005b; Mockaitis and Estelle, 2008; Parry *et al.*, 2009). Similar to the *aux/iaa* *gof* mutants, the *lof* mutant *tir1-1* is resistant to the auxins IAA and 2,4-D and the auxin transport inhibitor 1-*N*-Naphthylphthalamic acid (NPA), and shows reduced typical auxin responses (Ruegger *et al.*, 1998). Such responses include inhibition of root growth and lateral root formation upon exogenous auxin application, as well as reduced auxin response gene expression (Dharmasiri *et al.*, 2005b). Still, the *tir1-1* mutant exhibits residual auxin response, because the closely related AFB1-5 share TIR1- like molecular functions (Dharmasiri *et al.*, 2005b; Prigge *et al.*, 2016). Single *afb1*, *afb2*, and *afb3* *lof* mutants exhibit no or only mild auxin-resistance (Dharmasiri *et al.*, 2005b; Parry *et al.*, 2009). However, the contribution of AFB1, AFB2, and AFB3 to auxin responses becomes evident when combined with the *tir1-1* mutation in higher order mutants (Dharmasiri *et al.*, 2005b; Parry *et al.*, 2009). In particular, genetic analyses indicated the most predominant role in auxin response for *TIR1*, followed by *AFB2*. *AFB1* and *AFB3* also contribute to auxin response albeit to a lesser extent (Dharmasiri *et al.*, 2005b; Parry *et al.*, 2009). Promoter-swap experiments revealed that AFB1 and AFB2 cannot complement for TIR1 function in *tir1-1* mutants (Parry *et al.*, 2009). AFB4 and AFB5 have diverged more from the rest of the TIR1/AFB family, as they carry an additional N-terminal extension (Prigge *et al.*, 2016). Interestingly, *afb4* and *afb5* mutant plants show resistance to picloram, and consistently, AFB4 and AFB5 exhibit preferential binding affinity for the auxinic herbicide picloram and other auxinic compounds from the picolinate class (**Figure 1-5 C**)(Walsh *et al.*, 2006; Calderón Villalobos *et al.*, 2012; Lee *et al.*, 2014; Prigge *et al.*, 2016).

Auxin sensitivity is linked to TIR1/AFB abundance (Gray *et al.*, 1999; dos Santos Maraschin *et al.*, 2009) as seen in haploinsufficiency of *TIR1* and additive effects of mutations in *TIR1/AFBs* (Ruegger *et al.*, 1998; Dharmasiri *et al.*, 2005b). Therefore, to control auxin responses, tight regulation of TIR1/AFB levels is essential. While *TIR1/AFB1-3* are ubiquitously expressed (Dharmasiri *et al.*, 2005b; Parry *et al.*, 2009), *TIR1*, *AFB2* and *AFB3* undergo posttranscriptional regulation (Parry *et al.*, 2009). Micro RNA *miR393* specifically restricts the expression domain of *TIR1*, *AFB2* and *AFB3* (Navarro *et al.*, 2006). Also, *miR393* specifically acts through *AFB3* to regulate root system architecture in response to nitrogen availability (Vidal *et al.*, 2010).

Furthermore, *miR393* is involved in down-regulating *TIR1* and *AFB2* levels, and thus, auxin signaling, in response to salinity stress (Iglesias *et al.*, 2014). Besides the posttranscriptional regulation, SCF^{TIR1} activity is posttranslationally regulated. TIR1 has been shown to undergo ubiquitination and proteasomal degradation (Stuttman *et al.*, 2009). Mutations that result in amino acid substitutions in the N-terminal H1 helix of the TIR1 F-box domain abolish interaction of the TIR1:ASK1 complex with CUL1. This results in stabilization of TIR1, suggesting TIR1 undergoes autoubiquitination when assembled into an SCF complex (Yu *et al.*, 2015). Naturally occurring variations in the H1 helix of AFB1 might render it a poorer interactor with the SCF. This is consistent with AFB1 being more stable than TIR1 (Yu *et al.*, 2015). While autocatalytic processing might impact TIR1/AFB abundance, additional layers of regulation appear to influence their function. The chaperone HEAT SHOCK FACTOR 90 (HSP90) and co-chaperone SUPPRESSOR OF G2 ALLELE SKP1 (SGT1) stabilize TIR1 and AFB2 at elevated temperatures. This enhances auxin signaling, and hence causes the typical temperature-response of increased seedling growth (Wang *et al.*, 2016). Furthermore, HSP90 has been proposed to function in keeping TIR1 nuclear-localized and buffering the defects of the *tir1-1* mutation (Watanabe *et al.*, 2016). Moreover, posttranslational modification of TIR1 through S-nitrosylation on C140 has been proposed to increase TIR1:AUX/IAA interaction facilitating thereby AUX/IAA degradation, and subsequently promoting activation of gene expression (Terrile *et al.*, 2012). Also, a recent study proposed TIR1 oligomerization through a set of spatially clustered residues around TIR1 LRR 3, 4, and 5 is essential for AUX/IAA interaction and degradation (Dezfulian *et al.*, 2016). In addition, Yeast-Two-Hybrid (Y2H) screens have been performed in search for TIR1 mutations with altered AUX/IAA interaction. In that way, single amino acid substitutions D170E and M473L have been found to enhance interaction with the degron motif of AUX/IAAs (Yu *et al.*, 2013). This indicates that residues D170 and M473, which are located in the TIR1-LRRs away from the auxin binding site, play a role in AUX/IAA binding. Accordingly, this effect was partially independent of auxin. The precise interacting AUX/IAA residues, however, are yet unknown (Yu *et al.*, 2013).

1.2.2.2 FBP TIR1 and AUX/IAA target form a co-receptor complex for auxin sensing and UPS target recognition

Crystal structure studies on TIR1:ASK1 postulated that the optimal binding site for auxin is cooperatively formed by the AUX/IAA degron peptide and TIR1 (Tan *et al.*, 2007). Indeed, experimental evidence substantiated that TIR1 and AUX/IAA together form a *co-receptor system* for auxin sensing (Calderón Villalobos *et al.*, 2012). TIR1 alone, IAA7 alone, or an IAA7 degron peptide alone are not able to bind auxin in radioligand binding assays. Instead, TIR1

together with the IAA7 degron peptide exhibit auxin binding with low affinity [$K_D \geq 200$ nM and $K_D \approx 5$ μ M as determined by Calderón Villalobos *et al.* (2012) and Lee *et al.* (2014), respectively]. In contrast, only TIR1 combined with full-length IAA7 shows substantial auxin binding with high affinity ($K_D \approx 18$ nM). Thus, similar experiments showed that TIR1 combined with a gof mutant version of the IAA7 protein were not able to bind auxin, suggesting that both TIR1 and AUX/IAA are necessary and sufficient for auxin binding (Calderón Villalobos *et al.*, 2012).

1.2.3 Emerging concepts and questions in auxin perception mechanism

1.2.3.1 The auxin co-receptor system offers variable affinity and selectivity

The combinatorial potential for auxin co-receptors is large considering the six-membered TIR1/AFB and 29-membered AUX/IAA gene family in Arabidopsis (**Figure 1-5 B, C**), although not all AUX/IAAs might assemble into co-receptors due to lack of a degron. Indeed, combinations of different TIR1/AFBs and AUX/IAAs interact at various auxin concentrations with different strength in a Y2H system, and exhibit different nanomolar affinities for auxin in *in vitro* binding assays. High affinity TIR1-IAA7 and low affinity TIR1-IAA12 ($K_D \approx 17$ and 270 nM, respectively) are exemplary of the auxin co-receptor affinity range presently known (Calderón Villalobos *et al.*, 2012). Several more co-receptor affinities were determined to lie in that nanomolar range (TIR1-IAA1, TIR1-IAA3, TIR1-IAA14, TIR1-IAA17, TIR1-IAA28, AFB5-IAA7) (Calderón Villalobos *et al.*, 2012). This is biochemical evidence that different combinations of TIR1/AFBs and AUX/IAAs constitute co-receptor pairs with specific sensing capabilities (Calderón Villalobos *et al.*, 2012). Recently, two studies examined the auxin effect on TIR1/AFB:AUX/IAA interaction in yeast-based assays. By using AUX/IAA degradation as an indirect read-out of auxin co-receptor formation, the researchers demonstrated differential auxin sensitivities of various TIR1/AFB:AUX/IAA combinations (Havens *et al.*, 2012; Shimizu-Mitao and Kakimoto, 2014). Presumably, the different auxin affinities are due to different dissociation rates of the co-receptor complex, which seem to be determined by both the AUX/IAA and the TIR1/AFB5 partner in the co-receptor pair (Calderón Villalobos *et al.*, 2012; Lee *et al.*, 2014).

With regard to the contribution by TIR1/AFBs to the auxin co-receptor system, it has been proposed they provide ligand selectivity (Calderón Villalobos *et al.*, 2012). The TIR1 auxin-binding pocket has been shown to be partially promiscuous, as it can accommodate IAA, NAA and 2,4-D (Tan *et al.*, 2007). Interestingly, more distantly related AFB5 and AFB4 appear to preferably bind the synthetic auxin picloram, indicating that the TIR1/AFB family has diversified with regard to auxin selectivity (Calderón Villalobos *et al.*, 2012; Prigge *et al.*,

2016). However, besides TIR1, only AFB5 has been studied in more detail with regard to its binding affinities and structural features so far. Considering there is a variety of natural and synthetic auxinic compounds, a number of key questions emerge. Such as, how are those ligands perceived, and do they employ the TIR1/AFB-AUX/IAA receptor module? What are the affinities for complex formation with auxins other than IAA? Are there co-receptor combinations that preferably assemble with specific auxinic compounds?

Interestingly, intracellular auxin concentrations vary, and asymmetric auxin distribution and auxin gradients across tissues are essential in auxin responses (Friml, 2003). The spectrum of tissue- and cell-specific auxin concentrations might be specifically sensed by differently composed co-receptors with distinct affinities, thus allowing auxin concentration-dependent transcriptional outputs (Calderón Villalobos *et al.*, 2012; Rosquete *et al.*, 2012; Vanneste and Friml, 2012). Accordingly, auxin has been suggested to act as a threshold-specific trigger of transcriptional responses (Lau *et al.*, 2011; Rosquete *et al.*, 2012). Such differential auxin sensing capabilities would have implications in various biological responses, as auxin gradients guide basal-apical axis formation in embryo development (Friml *et al.*, 2003), as well as root patterning and polarity, and lateral root initiation (Sabatini *et al.*, 1999; Friml *et al.*, 2002a; Dubrovsky *et al.*, 2011). Furthermore, high IAA levels are strongly correlated with high rates of cell division in *Arabidopsis* leaves (Ljung *et al.*, 2001), and laterally asymmetric auxin concentrations in shoots and roots mediate differential growth during tropisms (Friml *et al.*, 2002b).

1.2.3.2 Redefining the AUX/IAA degron

AUX/IAAs carry intrinsic differences that contribute to different affinities in auxin co-receptor assembly as well as different degradation rates. The same high auxin affinity of a TIR1-IAA7 co-receptor ($K_D \approx 17$ nM) is also exhibited by a co-receptor consisting of TIR1 and the N-terminal part of IAA7 lacking the PB1 domain, but not by a co-receptor consisting of TIR1 and a 17-amino acid degron peptide ($K_D \geq 200$ nM) (Calderón Villalobos *et al.*, 2012). This indicates that residues outside the conserved degron located N-terminally of PB1 domain contribute to complex formation. IAA12 constitutes a low affinity auxin co-receptor with TIR1 ($K_D \approx 270$ nM). Exchanging the core degron residues of IAA12 co-receptor for those of IAA7 (GWPPIG to GWPPVR) increases the affinity but not to the same level of a TIR1-IAA7 co-receptor (Calderón Villalobos *et al.*, 2012). These findings on the level of co-receptor assembly also reflect in AUX/IAA stability. A 13-amino acid degron cannot confer the same short half-life to LUC fusions as full-length AUX/IAAs (Ramos *et al.*, 2001). Thus some AUX/IAAs, although equipped with the same consensus core degron, can have different degradation rates (Dreher

et al., 2006; Havens *et al.*, 2012; Gilkerson *et al.*, 2015). This suggests that regions outside the degron also affect AUX/IAA degradation rate. Also, a conserved KR duplet located between EAR-motif and primary degron, likely plays a role in destabilization of AUX/IAAs under basal auxin levels (Dreher *et al.*, 2006). Since the KR duplet has been proposed to play a role in nuclear localization (Abel and Theologis, 1995), it is conceivable that nuclear import of short-lived AUX/IAAs is required for AUX/IAA destabilization and proper auxin-responsiveness (Padmanabhan *et al.*, 2006; Herud *et al.*, 2016). However, mutations in the N-terminal, conserved KR residues diminished auxin-binding in a TIR1-IAA7 co-receptor (Calderón Villalobos *et al.*, 2012), and decreased the basal, but not auxin-induced degradation rates of IAA17 (Dreher *et al.*, 2006), suggesting a role of these residues in AUX/IAA target recognition. Moreover, regions flanking the conserved degron are highly variable in length and amino acid content among AUX/IAAs, and thus might influence the co-receptor assembly. These indications that regions flanking the primary degron affect complex formation as well as AUX/IAA stability, make it necessary to redefine the degron from the perspective of FBP-target complex formation, i.e. auxin co-receptor assembly, as well as AUX/IAA target stability.

1.2.3.3 Auxin co-receptor assembly directing AUX/IAA ubiquitination and destabilization

Auxin co-receptor complex formation represents an interval in which AUX/IAAs are ubiquitinated and subsequently subjected to proteasomal degradation (dos Santos Maraschin *et al.*, 2009). Characterization of TIR1:auxin:AUX/IAA co-receptor complex formation has suggested that auxin affinity inversely correlates with AUX/IAA stability (Calderón Villalobos *et al.*, 2012). For instance, co-receptor TIR1-IAA7 assembles with a K_D of 17 nM and exhibits a short half-life of approximately 10 min. In contrast, a rather stable AUX/IAA, IAA31, interacts poorly in a co-receptor complex (Gray *et al.*, 2001; Dreher *et al.*, 2006; Calderón Villalobos *et al.*, 2012). Studies in the heterologous system yeast suggest that co-receptor assembly, auxin sensitivities of AUX/IAA degradation and AUX/IAA half-lives might be intricately correlated (Havens *et al.*, 2012; Shimizu-Mitao and Kakimoto, 2014). However, a detailed study of the sequential events auxin-mediated co-receptor assembly, ubiquitination and degradation, and their correlation is missing so far. Some studies have covered the determination of basal and auxin-induced half-lives of selected AUX/IAAs *in planta* (Abel *et al.*, 1994; Gray *et al.*, 2001; Ouellet *et al.*, 2001; Ramos *et al.*, 2001; Dreher *et al.*, 2006; Gilkerson *et al.*, 2015) or the half-lives of most AUX/IAAs in a heterologous yeast system (Havens *et al.*, 2012). Yet, the dynamics of AUX/IAA ubiquitination, and how it relates to their degradation is largely uninvestigated to date. IAA1, IAA3 and IAA12 have actually been the sole AUX/IAAs ever to be published in

single studies addressing AUX/IAA ubiquitination (dos Santos Maraschin *et al.*, 2009; Gilkerson *et al.*, 2015). One study demonstrated the auxin-dependent ubiquitination of IAA3 and IAA12 in Arabidopsis protoplasts, that increased upon co-transfection of TIR1, indicating that levels of SCF^{TIR1} closely influence AUX/IAA ubiquitination (dos Santos Maraschin *et al.*, 2009). In another study, IAA1 basal half-life has been determined to be 8-12 min by tracking degradation of IAA1-LUC fusions through cycloheximide chase assays in transgenic seedlings. Upon auxin treatment, IAA1-LUC degradation accelerates about two-fold (Ramos *et al.*, 2001; Zenser *et al.*, 2001; Dreher *et al.*, 2006). Consequently, IAA1 classifies as a very rapidly degraded AUX/IAA according to the classification recently proposed by Gilkerson *et al.* (2015), with IAA6, IAA7 and IAA17 classified likewise as very rapidly, IAA8, IAA9 and IAA10 as rapidly, and IAA28 as slowly degraded (Dreher *et al.*, 2006; Gilkerson *et al.*, 2015). Furthermore, the researchers aimed to map lysine residues in IAA1 that are targets for ubiquitination and thus critical for *in vivo* protein destabilization. Surprisingly, even upon conservative mutation of all 16 K residues in IAA1, the protein is still very rapidly degraded *in vivo*. Thus, it has been proposed that non-lysine residues are targeted for oxyester-linked ubiquitination in the K-less mutant protein (Gilkerson *et al.*, 2015). Apart from these studies, the SCF^{TIR1/AFB}-mediated ubiquitination of AUX/IAAs, and comparative analysis of not only half-lives, but also of ubiquitination of different AUX/IAAs is a desideratum of auxin research.

To date, AUX/IAA half-lives have been investigated only in a wild-type background, solely focusing on its role as transcriptional repressor. However, to understand the underlying basis of auxin responses it would be also important to see AUX/IAAs in their role as part of the co-receptor for auxin sensing. Therefore, an approach assessing AUX/IAA stability not only in wild-type but also in different TIR1/AFB-deficient mutant backgrounds would be informative to assess *in vivo* formation of auxin co-receptors and the dynamics of auxin sensing.

1.2.3.4 AUX/IAA diversity adds to the combinatorial auxin co-receptor system

As mentioned above (see **Section 1.2.1.2**), the expanded AUX/IAA family has retained many ohnologs, also called *sister pairs* (**Figure 1-5 B**). Among the canonical AUX/IAAs, IAA1 and IAA2, IAA3 and IAA4, IAA6 and IAA19, as well as IAA12 and IAA13 represent sister pairs that share high similarity in their coding sequences, as well as in their upstream flanking regions (Remington *et al.*, 2004). It is important to establish why AUX/IAAs have been retained after radiation of the family in Arabidopsis. Possibly, AUX/IAAs have undergone functional diversification. Hence, they might have become co-receptor components that provide different auxin affinities for example.

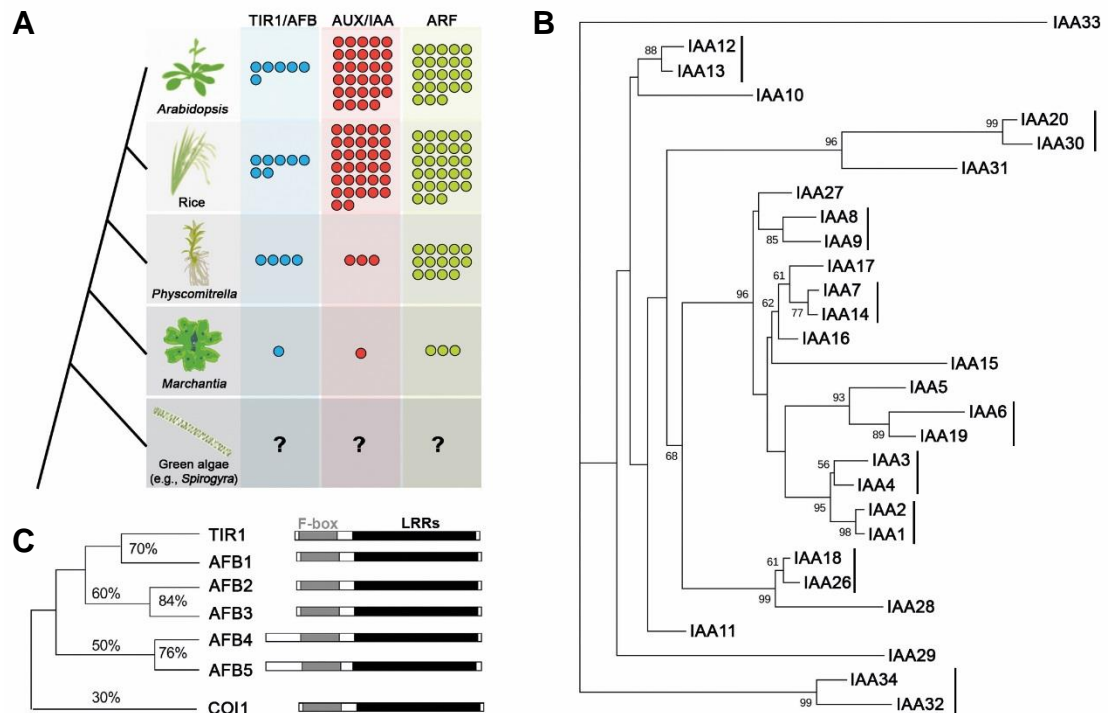


Figure 1-5: The gene families involved in auxin signaling have expanded and diversified during plant evolution
A. Number of TIR1/AFB, AUX/IAA, and ARF proteins in published plant genomes for several plant species. Species represent eudicots (Arabidopsis), monocots (rice), mosses (Physcomitrella), liverworts (Marchantia), and green algae (Spirogyra, as an example of charophytes). The tree on the left-hand side indicates the divergence order but is not drawn to scale. Reproduced from Weijers and Wagner (2016). **B.** Phylogenetic tree of Arabidopsis AUX/IAA family created based on maximum likelihood with bootstrap-values >50% shown at the corresponding node. Vertical black bars denote the AUX/IAA sister pairs (ohnologs). Reproduced and modified from Winkler *et al.* (under review). **C.** Phylogenetic tree of Arabidopsis TIR1/AFB family. Values represent % identical amino acids. Schematic representation of protein domain organization on the right. Note that AFB4 and AFB5 carry additional N-terminal residues. The most distantly related protein in this subclade is COI1, the FBP in the jasmonic acid-isooleucin co-receptor. Reproduced and modified from Dharmasiri *et al.* (2005b).

1.2.3.4.1 IAA1 and IAA2 – an exemplary AUX/IAA sister pair

An example of AUX/IAAs ohnologs are *IAA1* and *IAA2*. These two AUX/IAAs are among the first identified early auxin-inducible transcripts of *PsIAA4/5*-like homologous genes in Arabidopsis (Abel *et al.*, 1994), indicating they are key players in the early auxin response. They are canonical members of the AUX/IAA family with regard to their sequences and domain organization (Abel *et al.*, 1994; Abel *et al.*, 1995; Overvoorde *et al.*, 2005). Since *IAA1* and *IAA2* proteins share 75% sequence identity and 81.25% sequence similarity, it is likely that they function at least partially redundant. A *gof* mutant allele of *IAA1*, namely *axr5-1*, showing a number of auxin-related phenotypes has been previously characterized (Yang *et al.*, 2004). *Axr5-1* mutant plants are smaller than wild-type, with smaller rosette leaves and shorter petioles. They produce more siliques, yet with overall smaller seed yield (Yang *et al.*, 2004). The mutant seedlings exhibit resistance to exogenously applied auxin in root elongation, dark-grown hypocotyl elongation, as well as lateral root formation (Yang *et al.*,

2004). Auxin induction of early auxin response genes *IAA1* and *IAA5*, but not *IAA2*, is reduced in *axr5-1* seedlings, and auxin response reporter expression is reduced in mutant roots (Yang *et al.*, 2004). Furthermore, *axr5-1* seedlings show a decrease in tropism responses (Yang *et al.*, 2004). These mutant phenotypes indicate a pivotal role of *IAA1* in auxin signaling and thus plant growth and development. The *axr5-1* mutant expresses a stabilized version of IAA1 due to a P61S point mutation in the core degron sequence, and IAA1 wild-type protein was shown to be a target of SCF^{TIR1} (Yang *et al.*, 2004; Calderón Villalobos *et al.*, 2012). IAA1-LUC fusions have been instrumental in studying rapid basal and auxin-induced AUX/IAA degradation *in vivo* (Ramos *et al.*, 2001; Zenser *et al.*, 2001; Dreher *et al.*, 2006)(also see **Section 1.2.3.3**). Furthermore, a transgenic line conditionally overexpressing IAA1 with a stabilizing P60L mutation in the core degron, has been extensively studied with regard to auxin signaling (Park *et al.*, 2002). Plants expressing stabilized IAA1 revealed loss of gravitropism and phototropism, reduction in number of lateral roots, inhibited hypocotyl and stem elongation, and altered leaf expansion. This further corroborated *IAA1*'s key role in auxin-mediated growth responses (Park *et al.*, 2002). In contrast, no *gof* mutant has been isolated for the ohnolog *IAA2* so far, nor have lines been studied that conditionally express stabilized IAA2 in analogy to the study from Park *et al.* (2002) about IAA1. Therefore, IAA1 and IAA2 could serve as important representatives of AUX/IAAs, yielding hints for features that might be common to all canonical AUX/IAAs. Additionally, pinning down distinct features of each individual ohnolog could help understand their diversification and justify their retention after expansion.

1.3 Hypothesis and objectives

A great overarching question in auxin biology has been how a small and seemingly inconspicuous molecule like IAA can elicit such a vast range of growth and developmental responses. For decades, studies have aimed at answering this question. By analyzing auxin signal transduction and transcriptional responses, approximations have been made to understand auxin morphogen activity. Despite of such genetic and gene expression analyses, early events of nuclear auxin sensing and the subsequent impact on AUX/IAA regulation are poorly understood. Auxin is perceived by a co-receptor system formed by a TIR1/AFB F-box protein and an AUX/IAA transcriptional repressor. TIR1/AFBs act as target receptors of SCF-type E3 Ub-ligases, which recognize the degron of AUX/IAAs mediating their ubiquitination and subsequent turnover by the proteasome. Thus, derepression of auxin response genes takes place. The present work addresses auxin perception and its contribution to the biochemical and transcriptional output specifically by providing biochemical insights into receptor complex formation. Given the diversity of AUX/IAA, and TIR1/AFB protein families numerous co-receptor combinations are possible. We hypothesize that this array of receptor combinations offers a spectrum of auxin sensing capabilities. Differential auxin sensing might concomitantly influence AUX/IAA ubiquitination and degradation dynamics. The display of sensors would thus provide the system with plasticity in transcriptional regulation of growth and developmental responses. A number of questions arise from the current knowledge, which are the focus of this study:

- What are specific biochemical properties and functions of TIR1/AFB-AUX/IAA receptor complexes?
- How does the combinatorial potential provided by the expanded TIR1/AFB and AUX/IAA families influence the auxin receptor properties? Particularly, as 29 members of AUX/IAAs coexist in Arabidopsis, why have these genes been retained?
- What are the sequence and structural features in TIR1/AFBs and AUX/IAAs underlying specificities of auxin sensing?
- How do biochemical properties of auxin receptors instruct downstream events like AUX/IAA ubiquitination, TIR1/AFB-dependent AUX/IAA turnover and ultimately, specific physiological responses?

In order to answer these questions, in this doctoral thesis, I pursue the following goals:

- Exploration of the array of putative auxin co-receptor combinations and their auxin sensing capabilities by comprehensively analyzing auxin-dependent TIR1/AFB:AUX/IAA interactions in yeast.

- Implementation of a homology modeling approach, to obtain structural information on AFB1, AFB2, and AFB3 architecture in comparison to TIR1.
- Identification of sequence and structural features in AUX/IAAs that cause distinct auxin affinities in a co-receptor complex, by employing an AUX/IAA chimera approach.
- Detailed biochemical and specific functional characterization of SCF^{TIR1}:IAA1 and SCF^{TIR1}:IAA2 receptor complexes, including determination of affinities and auxin selectivity for auxin co-receptors.
- Assessment of the impact of auxin sensing on AUX/IAA ubiquitination by SCF^{TIR1} via an *in vitro* enzymatic assay.
- Establishment of transgenic lines to address co-receptor formation and AUX/IAA stability *in vivo*.

This work will significantly broaden our understanding of the mechanism of auxin perception. Correlating the biochemical insights on auxin receptors with *in vivo* auxin responses will then yield important insight on differential auxin-sensing and auxin-dependent proteostasis for plant fitness.

2 Results

2.1 Auxin co-receptor complexes undergo multifaceted assembly

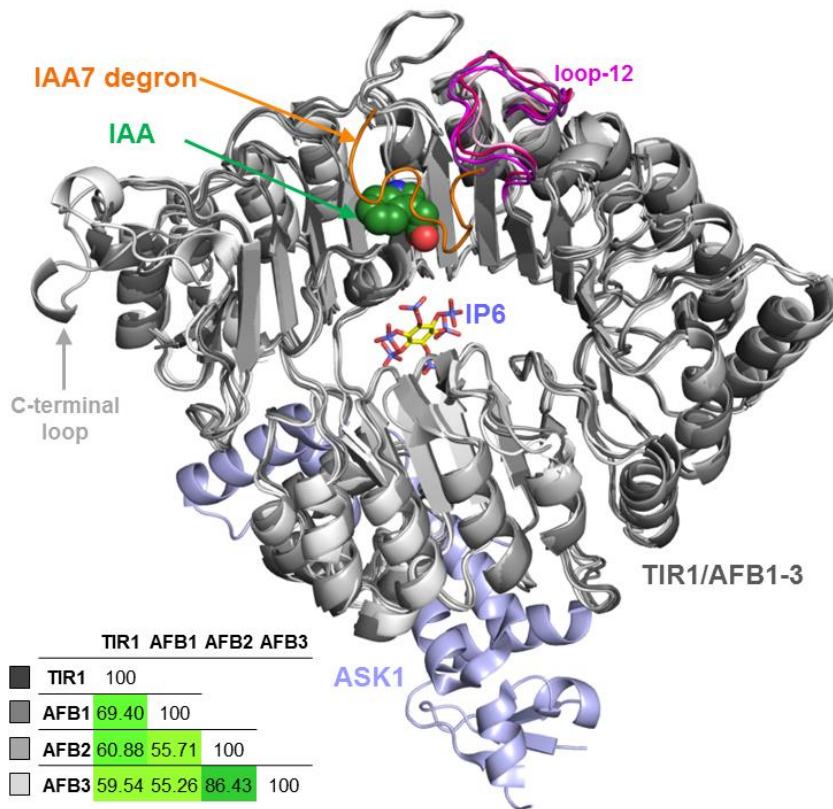
The first part of this thesis focuses on the biochemical characterization of the three-part (or ternary) complex for auxin perception. In order to identify and describe functional differences in the auxin co-receptor system, its components – TIR1/AFBs, AUX/IAAs and auxins –, their features, and their interactions were examined.

2.1.1 Different residues in loop-12 might contribute to functional differences between TIR1, AFB1, AFB2 and AFB3

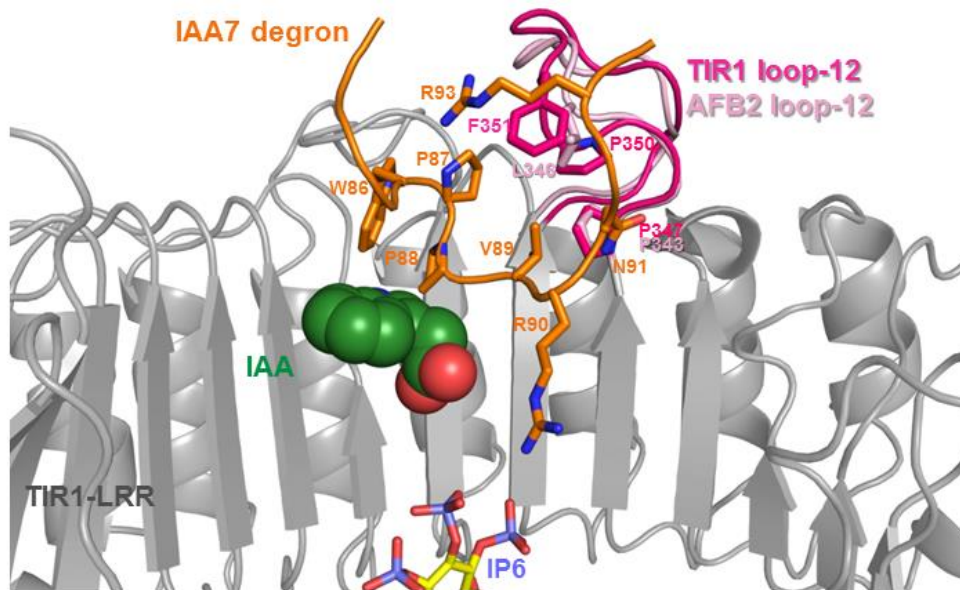
Crystal structure studies revealed how auxin and AUX/IAA degron are bound to the TIR1 (Tan *et al.*, 2007). Functional differences among TIR1 and AFB1, AFB2, AFB3 have been hypothesized to be caused by non-conservative substitutions in AFB1-3 within loop-12, which contributes to AUX/IAA degron binding (Parry *et al.*, 2009). Also, crucial roles in AUX/IAA binding have been attributed to TIR1-residues F82 (located in loop-2) and F351 (located in loop-12) which are not strictly conserved in AFB1-3 (Hao and Yang, 2010). Yet, to date, no detailed structural analyses of AFB1, AFB2, or AFB3 have been performed. In order to identify structural features in AFB1, AFB2, and AFB3 in comparison to TIR1 that could possibly underlie differences in interaction with AUX/IAAs, we carried out homology modeling (in collaboration with Richard Bartelt and Wolfgang Brandt, Department of Bioorganic Chemistry, Leibniz Institute of Plant Biochemistry). This approach might also allow inferring other functional features, e.g. auxin binding preferences. The closest TIR1 homologs, AFB1-3 are suitable for such approach as they share 60-70% amino acid identity with TIR1 (**Figure 2-1 A** inset). To build structural models of AFB1, AFB2, and AFB3, homology modeling has been performed using YASARA software (Krieger *et al.*, 2009) with the TIR1 crystal structure including co-crystallized ligands and IAA7 degron (PDB codes: 2P1N, 2P1O, 2P1Q; Tan *et al.*, 2007) as a template. A short molecular dynamics simulation using the force field YASARA2 was employed for structural refinement (Krieger *et al.*, 2002). After validation with Procheck (Laskowski *et al.*, 1993), ProSA2 (Sippl, 1993) and Qmean (Benkert *et al.*, 2008), we obtained final structural models of AFB1, AFB2, and AFB3 (**Figure 2-1**).

Comparison of TIR1 crystal structure and AFB1-3 homology models revealed high similarity in overall architecture (**Figure 2-1 A**). Key residues R403, H78, R436, and S438 involved in formation of the TIR1 auxin binding pocket and auxin binding, are conserved and positionally overlapping in AFB1, AFB2 and AFB3 model (**Supplementary Table 1**). This suggests that AFB1, AFB2, and AFB3 bind auxin and AUX/IAA degrons in a fashion highly similar to TIR1. LRRs of AFB1, AFB2 and AFB3 largely overlap with TIR1 LRRs. However, few structural differences

A



B



C

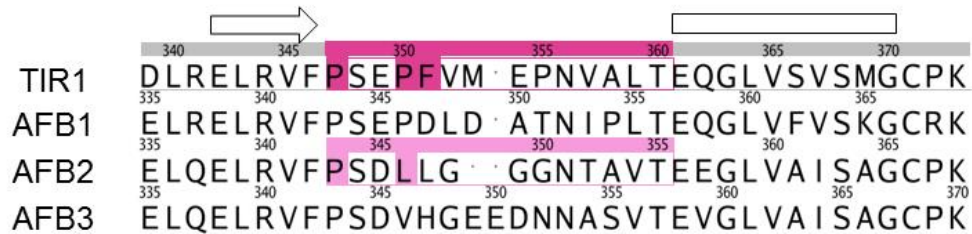


Figure 2-1: Homology models of AFB1-3 superimposed on TIR1 crystal structure

A. TIR1 and AFB1-3 share highly similar structures. Overall representation of AFB1-3 models (shades of gray) in superimposition on TIR1 structure (dark gray, PDB code: 2P1Q) shown in complex with ASK1 (light blue), IAA7 degron peptide (orange), indole-3-acetic acid (IAA; green and red spheres), and IP6 (yellow, red and blue sticks). Loop-12 is highlighted in pink shades. Inset: Identity matrix shows percent identity in amino acid composition of

TIR1 and AFB1-3. **B.** Close-up view of loop-12 of TIR1 (magenta) and AFB2 (light pink) with key residue side chains in stick representation. A shorter and more flexible loop-12 in AFB2 might exert less steric obstruction upon degron binding. Apart from loop-12, only TIR1-LRR structure is shown (gray). Auxin, IP6 and IAA7 degron as in A. **C.** Alignment of loop 12 and surrounding residues based on structure superimposition of homology models. Coloring as in B. TIR1 and AFB2 residues directly compared with stick representation in B are highlighted in respective coloring in the alignment. Arrow and bar atop the alignment designate α -helix and β -sheet secondary structure of LRRs, respectively.

stood out when comparing the AFB1, AFB2, and AFB3 model with the TIR1 crystal structure. The C-terminal loop between the third and second to last β -sheet is shortened by one residue in AFB1 and four residues longer in AFB2 and AFB3 compared to TIR1 (**Figure 2-1 A**). It remains to be determined whether this difference might have an impact on AFB1, AFB2, and AFB3 architecture, and hence function. Furthermore, we observed changes in loop-12 of AFB1 and AFB3 – specifically, F351 is replaced by aspartate and histidine, respectively (**Figure 2-1**). This variation might contribute to differential AUX/IAA binding. Interestingly, in AFB2, loop-12 is shortened by one residue in comparison to TIR1. In addition, AFB2 loop-12 shows an amino acid composition of less rigid and less bulky (compare P343, L346 in AFB2 with P346, P350, F351 in TIR1), as well as more flexible (G348, G349, G350 in AFB2) residues compared to TIR1 (**Figure 2-1 B, C, Supplementary Table 1**). TIR1 loop-12 contributes to AUX/IAA degron binding with residues F351, F380, P347 and P350 (Tan et al., 2007; Hao and Yang, 2010; Calderón Villalobos et al., 2012). While still providing hydrophobic interactions, the shorter and more flexible loop-12 in AFB2 might exert less steric obstruction upon degron binding. This could mean that the AFB2 auxin-binding site is better accessible for AUX/IAA degron recruitment. This, in turn, would be consistent with the observation of AFB2 exhibiting strong auxin-dependent interaction with IAA3 and IAA7 in in vitro pull-down experiments (Parry et al., 2009) and with most AUX/IAAs in yeast (Calderón Villalobos et al., 2012)(**Section 2.1.2**).

2.1.2 Combinatorial events and auxin dependency of auxin co-receptor assembly

Based on the differences we observed at the structural level, it is possible that among TIR1/AFBs, particularly AFB2 shows preferential auxin-dependent interaction patterns with AUX/IAAs. Apart from the contribution to co-receptor formation by the TIR1/AFB target receptors, also the expanded family of AUX/IAA proteins enables a plethora of combinations in co-receptor assembly. Previously, a Y2H approach for nine representatives from distinct subclades of the AUX/IAAs revealed that co-receptors assemble at different auxin concentrations, and that TIR1/AFBs have target preferences (Calderón Villalobos *et al.*, 2012). We decided then to expand those Y2H analyses to systematically assess the combinatorial possibilities and relative strength of auxin-mediated TIR1/AFB:AUX/IAA interactions corresponding to putative auxin receptors by performing quantitative LexA Y2H assays. For that, previously described LexA DNA-binding domain (DBD)-TIR1/AFB1/AFB2 fusions were

used (Calderón Villalobos *et al.*, 2012). Unfortunately, a DBD-AFB3 fusion was not available and despite repeated attempts, *AFB3* could not be amplified from *Arabidopsis* seedling cDNA. LexA activation domain (AD)-AUX/IAA fusions were generated by cloning *AUX/IAA* coding sequences via Gateway technology. Thus, all AD fusion proteins are equipped with 21- or 34-amino acid linkers between AD tag and *AUX/IAA* coding sequence. Only *IAA15*, for which no amplicon could be obtained from seedling cDNA (as also reported by Overvoorde *et al.*, 2005), and *IAA29*, for which no functional AD-fusion protein could be confirmed, are exempt from this analysis. The LexA-based Y2H approach utilized here, is suitable for this analysis for several reasons: (1) It is convenient for a systematic high-throughput analyses, since β -Galactosidase (β -Gal) serves as reporter output for protein-protein interaction (PPI). After yeast is grown in liquid cultures and subjected to cell lysis, reporter expression can be quantified by adding chromogenic β -Gal substrate followed by absorbance measurement in a plate-based format. (2) A Y2H assay allows the detection of interaction types ranging from weak and transient to strong and comparably stable contact (as discussed in Ding *et al.*, 2009) – as one would expect for TIR1/AFBs and AUX/IAAs in the absence and presence of auxin. (3) The LexA Y2H approach has been successfully utilized to assess hormone-dependent PPIs in previous studies (Thines *et al.*, 2007; Prigge *et al.*, 2010; Calderón Villalobos *et al.*, 2012). Also, this assay has proven robust in testing interactions with transcriptional repressors such as AUX/IAAs, as no artefacts have emerged from such a transcription-based reporter system.

To test auxin-dependent co-receptor formation in yeast, diploid yeast expressing a combination of DBD-TIR1, -AFB1, or -AFB2 and an AD-AUX/IAA were generated, and cultivated in triplicate samples in liquid selective induction medium. To test auxin-mediated interaction of TIR1/AFBs with AUX/IAAs, the medium was supplied with 25 μ M IAA, since auxin concentration in the 10^{-5} M range typically produced a suitable dynamic range of reporter output in plate-based LexA Y2H assays (Calderón Villalobos *et al.*, 2012 and data not shown). For assessing auxin-independent interactions, the medium was supplied with mock (solvent only). The culture density (OD_{600}) was recorded, before cells were lysed and extracts tested for β -Gal reporter activity. The turnover of chromogenic substrate by β -Gal was quantified after a fixed time-point for all samples by absorbance measurement, and the obtained values were normalized against culture density to compensate for different amount of starting cell material. When a total protein quantitation of the cell lysates via Bradford assay was used for normalization, it yielded similar results (data not shown) indicating uniform cell lysis.

The resulting data was processed for visualization as a heatmap in R (R Development Core Team, 2012; <http://cran.r-project.org>). On the one hand, average values of triplicate samples were calculated and graphed to highlight the range of absolute strengths of TIR1/AFB:AUX/IAA interactions in the absence and presence of auxin (**Figure 2-2 A**). Low and high normalized reporter outputs corresponding to weaker and stronger interactions are represented by yellow and red heatmap coloring, respectively. On the other hand, relative interaction responses were assessed based on calculated t -values from auxin-treated versus mock-treated samples (**Figure 2-2 B**). Low and high t -values are represented by yellow and red heatmap coloring, respectively. T -values measure the size of the difference between two values relative to the variation in the respective sample data. Simplified, the t -value expresses the change in values in units of the standard error. Thus, the analysis based on t -values is superior to the use of averages as it incorporates the information on variances among biological replicates into the analyses. Furthermore, to visualize similarities of interaction strength in auxin co-receptors (**Figure 2-2 A**), and to identify subgroups of TIR1/AFB-AUX/IAA combinations based on their auxin-induced interaction response (**Figure 2-2 B**), hierarchical cluster analysis was applied to AUX/IAA and TIR1/AFBs in the matrix and additionally visualized with dendrograms next to the heatmaps.

The physical interactions between DBD-TIR1/AFBs and AD-AUX/IAs detected in the Y2H assay could be dictated by the expression levels of these proteins in yeast. Therefore, DBD-TIR1/AFB and AD-AUX/IAA protein levels were analyzed by immunoblotting via their tag fusions, and were found not to correlate with reporter output (**Supplementary Figure 7**)(Calderón Villalobos *et al.*, 2012). Combinations of DBD-TIR1/AFBs and AD-empty vector (expressing only AD), or AD-AUX/IAs and DBD-empty vector (expressing only DBD) were employed as negative controls and showed no or very low reporter activity (**Figure 2-2 A**). In the absence of auxin, reporter activity for several TIR1/AFB1/AFB2:AUX/IAA combinations was similar as in negative controls, indicating no interaction (**Figure 2-2 A**). The remaining TIR1/AFB1/AFB2:AUX/IAA interactions in the absence or presence of auxin ranged from strong, to intermediate, to weak. Reporter outputs close to the maximum, which was exhibited by TIR1:IAA1 in the presence of auxin in quantitative assays, were defined as strong interactions. Intermediate strength of interaction was defined when reporter outputs were around half of the maximum. When reporter output was just above the negative control, it was interpreted as weak interaction (**Figure 2-2 A**).

In quantitative Y2H assays, IAA1, IAA2, IAA3, IAA4, IAA9 and IAA10 interacted strongly with TIR1 and AFB2 and to a lesser extent with AFB1 in the presence of auxin. IAA14 and IAA19

interacted strongly with TIR1 and to a lesser extent with AFB1 and AFB2. Most of the remaining canonical AUX/IAAs, IAA18, IAA26, IAA28, IAA11, IAA12, and IAA13, showed intermediate auxin-mediated interaction with TIR1 and AFB2 and weaker or no interaction with AFB1 (**Figure 2-2 A**). This is consistent with genetic studies, that reveal TIR1 and AFB2 as major members of the family in auxin signaling and as the strongest auxin-dependent AUX/IAA interactors in *in vitro* pull-down experiments (Parry *et al.*, 2009). TIR1 and AFB2 cluster together as they similarly and strongly interact with AUX/IAAs, whereas AFB1 shows a distinct and weaker pattern for most AUX/IAA interactions (**Figure 2-2 A**). Few canonical AUX/IAAs, however, namely IAA5, IAA6, IAA8, IAA27, IAA17, do not show such a clear preference for auxin-dependent TIR1- and AFB2-interaction, but interact with AFB1 with the same strength as with TIR1 or even more strongly (**Figure 2-2 A**). IAA31, which carries a degenerate degron sequence interacted weakly with TIR1 and AFB2 in the presence of auxin. As expected, non-canonical IAA30, IAA32, IAA33, IAA34 which lack the canonical degron (**Supplementary Figure 1**) did not show any auxin-dependent interaction with TIR1/AFB1/AFB2 (**Figure 2-2 A**). A number of AUX/IAAs (IAA9, IAA1, IAA14, IAA17, IAA19, and IAA27) exhibited weak to intermediate auxin-independent (basal) interaction with TIR1/AFB1/AFB2 (**Figure 2-2 A**), indicating that auxin is dispensable for some AUX/IAAs to interact, albeit weakly, with their target receptors. IAA7, IAA16 and IAA20 did not give consistent results in independent Y2H experiments. AD-IAA7 used here in its Gateway-cloned form behaved as a much weaker TIR1/AFB1/AFB2 interactor than the previously reported fusion construct (Calderón Villalobos *et al.*, 2012)(also see **Supplementary Figure 38**). IAA16, although carrying a canonical degron and being highly expressed (**Supplementary Figure 7**), did not interact with TIR1/AFBs in most Y2H assays (**Figure 2-2** and data not shown). IAA20 lacking a degron interacted poorly with TIR1/AFBs in the quantitative Y2H assay (**Figure 2-2**), but as expected, did not interact with TIR1/AFBs in a plate-based Y2H assay (data not shown). Mostly, phylogenetically related AUX/IAAs also fall into similar clusters of interaction behavior, as for example the two neighboring branches of sister pairs IAA1, IAA2, IAA3, and IAA4, or IAA6 and its second closest relative IAA5 (**Figure 1-5 B** and **Figure 2-2 A**). This suggests that their primary amino acid structure is the main determinant of interaction properties with TIR1/AFBs. However, there are also closely related AUX/IAAs that show rather different interaction behavior, such as the sister pair IAA6 and IAA19 (**Figure 1-5 B** and **Figure 2-2 A**), indicating that also subtle sequence differences can underlie functional diversity. AUX/IAAs can be clustered into the following subgroups that share a specific auxin-dependent TIR1/AFB interaction behavior: (1) strong auxin-dependent interaction with AFB2 and/or TIR1 and weaker interaction with AFB1, (2) intermediate auxin-dependent interaction with TIR1/AFB2

and weaker interaction with AFB1, (3) auxin-dependent interaction with TIR1 and/or AFB2 that is weaker than interaction with AFB1, (4) weak or no interaction with TIR1/AFB1/AFB2 (mostly non-canonical AUX/IAAs), and (5) basal auxin-independent interaction with TIR1/AFB1/AFB2 (**Figure 2-2 A**).

To assess the relative interaction responses upon auxin responses, the auxin-independent interaction between TIR1/AFB1/AFB2 and ASK1 was used as a negative control. As expected, *t*-values adopt values around zero, indicative of no interaction change upon addition of auxin (**Figure 2-2 B**). The same is true for the interaction response of non-canonical IAA30, IAA32, IAA33 and IAA34 with TIR1/AFB1/AFB2 (**Figure 2-2 B**), since these did not interact in absence nor in the presence of auxin (**Figure 2-2 A**). IAA1, IAA6, IAA7, IAA8, IAA9, IAA16 and IAA17, show a strong interaction response upon addition of auxin with AFB1 but to a lesser extent with TIR1 and AFB2. These AUX/IAAs cluster together as a subgroup exhibiting this distinct behavior (**Figure 2-2 B**). Furthermore, IAA2, IAA5, IAA10 and IAA27 show a high induction of interaction with AFB2 upon auxin addition, while the interaction response with TIR1 and AFB1 is induced to a lesser extent (**Figure 2-2 B**). IAA27 is an exception from this cluster as it also shows induced interaction with AFB1. This suggests that these co-receptor pairs might be most responsive to an auxin surge. Canonical AUX/IAAs, IAA1, IAA2, IAA3, IAA4, IAA5, IAA6, IAA9, IAA10, IAA11, IAA18, IAA26, IAA27, and IAA28 show intermediate interaction responses upon auxin treatment mostly with TIR1. Fewer AUX/IAAs show intermediate responses with AFB1, namely IAA2, IAA3, IAA5, IAA7, IAA10, IAA13, IAA26, and IAA28, and with AFB2, namely IAA1, IAA3, IAA4, IAA6, IAA11, IAA12, and IAA28 (**Figure 2-2 B**). As a consequence, the most auxin-responsive co-receptor combinations are constituted of AUX/IAAs and TIR1/AFB1. Therefore, AFB2, although showing strong absolute interaction with AUX/IAAs in the presence of auxin (**Figure 2-2 A**), might play a lesser role in exhibiting a clear relative response upon an auxin surge. Interestingly, AUX/IAAs similarly behaving with regard to relative TIR1/AFB1/AFB2 interaction responses, represent distinct phylogenetic branches of canonical AUX/IAAs. This could mean that the auxin effect on interaction with TIR1/AFB1/AFB2 is mediated by distinct residues or sequence motifs in AUX/IAAs. One would expect that AUX/IAAs that exhibit basal interaction with TIR1/AFBs, do not show a pronounced relative interaction response. Indeed, this is largely the case for most basally interacting pairs, such as AFB2:IAA9 or TIR1:IAA1 (compare cluster of basally interacting TIR1/AFB:AUX/IAA pairs in **Figure 2-2 A** with their relative interaction response in **Figure 2-2 B**).

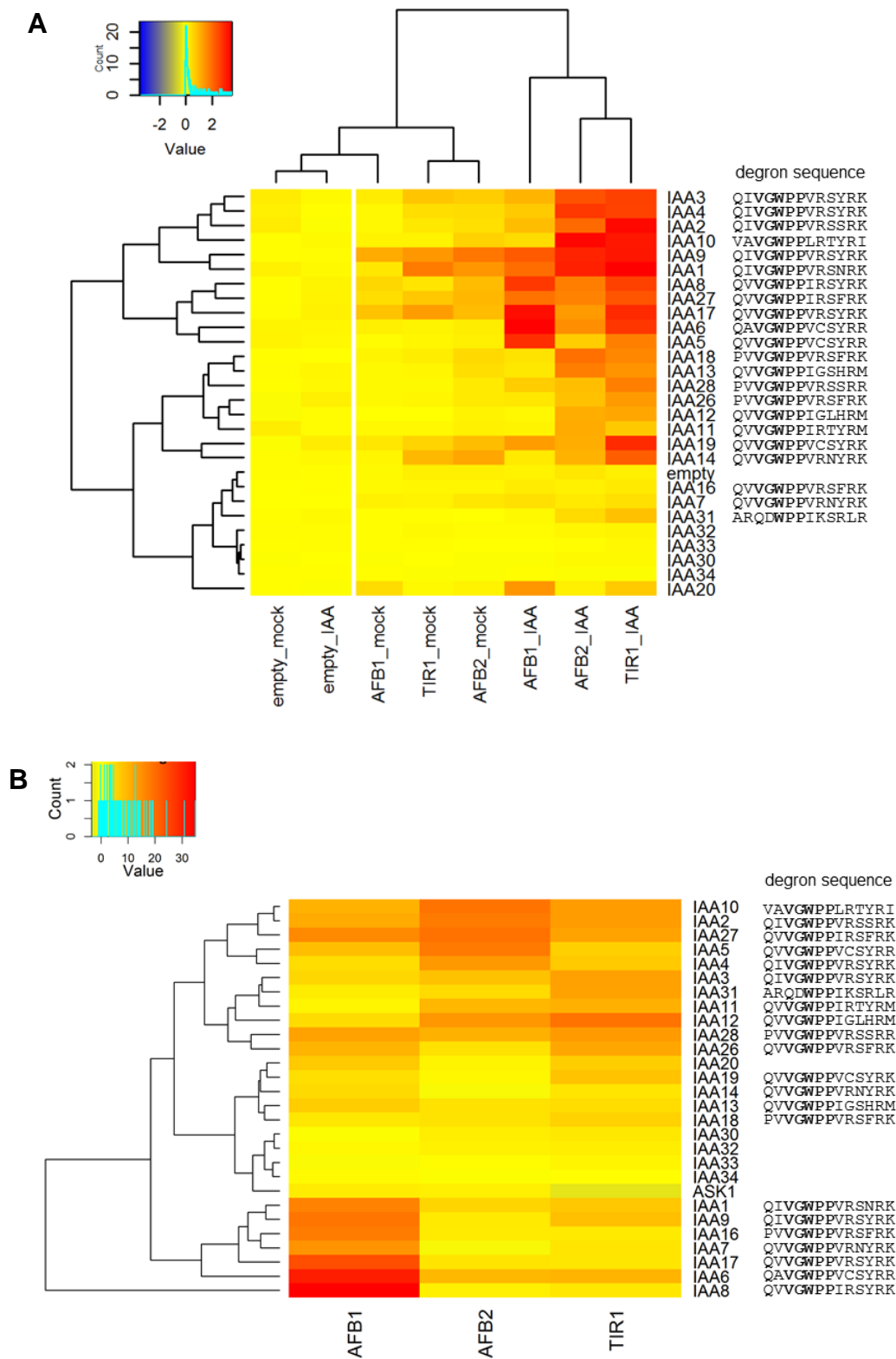


Figure 2-2: Quantitative assessment of TIR1/AFB1/AFB2:AUX/IAA interactions in yeast

β -Galactosidase (β -Gal) activity reflecting protein-protein interaction in the LexA Y2H between DBD-TIR1/AFB1/AFB2 and AD-AUX/IAAs was assessed after cultivation of yeast liquid cultures in the absence (mock) or presence of 25 μ M IAA (IAA). β -Gal activity was normalized against culture OD_{600} . Empty: DBD-/AD-empty vector controls. Samples in triplicates. Two different representations are shown (A and B). **A.** Absolute strengths of interaction and auxin-mediated stabilization effect on interaction between TIR1/AFBs and AUX/IAAs. Heatmap depicting average values of three biological replicates ($n=3$) of normalized β -Gal activity. Yellow and red shades represent low and high β -Gal activity values, respectively. **B.** Relative interaction responses of TIR1/AFB-AUX/IAA co-receptor pairs upon auxin treatment. Heatmap depicts t -value s from normalized β -Gal activity of auxin-treated

versus mock-treated samples. Yellow and red shades represent low and high *t*-values, respectively. Heatmaps and clustering was performed in R (R Development Core Team, 2012) using `heatmap.2` function of the `gplots` package. Dendrograms depicted are generated by hierarchical clustering according to complete linkage method with Euclidean distance measure.

All in all, this data indicates a multifaceted assembly of auxin co-receptors through a wide range of potentially possible combinations that exhibit different interaction preferences and auxin sensitivities depending on the AUX/IAA and the TIR1/AFB involved.

2.1.3 Characterization of auxin co-receptors TIR1-IAA1, TIR1-IAA2, AFB2-IAA1 and AFB2-IAA2

The broad assessment of auxin co-receptor formation in yeast provides a starting point for detailed co-receptor analyses. Although detailed identification of differences between all possible auxin sensors is desirable, this study for practical reasons focuses on few representatives of the AUX/IAA family together with TIR1. This allows a more detailed study of AUX/IAA sequence and structural features contributing to co-receptor assembly on the one hand (see **Section 2.2**). On the other hand, it allows to specifically concentrate on AUX/IAA ohnologs and also explore functional diversification (this section).

As expounded in the introduction (see **Section 1.2.3.4.1**), IAA1 and IAA2 are prominent examples of canonical AUX/IAAs suitable for further biochemical studies. IAA1 and IAA2 ohnologs fall into a larger subgroup of AUX/IAAs exhibiting strong auxin-inducible TIR1 and AFB2 interaction in our Y2H analyses (see **Section 2.1.2**), suggesting that both function similarly in auxin co-receptor formation. *IAA1* function has been thoroughly characterized through analysis of its *gof* mutant *axr5-1* (Yang *et al.*, 2004) and a transgenic line expressing a stabilized version of IAA1 protein (Park *et al.*, 2002). No *lof* mutant of *IAA1* or *IAA2* has been characterized to date, and mostly AUX/IAA *lof* mutants do not exhibit phenotypes likely due to redundancy within the gene family and the unstable nature of their gene products (Overvoorde *et al.*, 2005). Given that no mutant expressing a stabilized version of IAA2 has been identified so far, a possibly more crucial role of IAA2 in plant growth and development is conceivable. To broaden the understanding of *IAA1* and *IAA2* functional diversification and to elucidate what kind of diversification in *IAA1* and *IAA2* caused retention of these duplicates, we first mined publicly available expression data and applied sequence-based analyses.

2.1.3.1 Purifying selection acts on *IAA1* and *IAA2* and other factors might justify their coexistence

There are different mechanisms of how natural selection can act on duplicate genes leading to their retention. Mutations can directly impart new functions (neofunctionalization), ancestral functions can be subdivided among duplicates (sub-functionalization) and selection

for changes in gene dosage can occur (Conant and Wolfe, 2008). Duplicated genes diverge most commonly in their regulation (Prince and Pickett, 2002; Conant and Wolfe, 2008), therefore comparison of *IAA1* and *IAA2* expression patterns and levels may yield useful insight into their regulatory diversification, and, in case of *IAA2*, into gene function. We compared *IAA1* and *IAA2* transcript levels across various tissues, developmental stages and Arabidopsis ecotypes by drawing upon publicly available Arabidopsis expression data (in collaboration with Philipp Janitza and Marcel Quint, Department of Crop Physiology, University of Halle; **Figure 2-3**; see Materials and Methods **Section 6.11.2** for detailed references).

In all three analyzed datasets, *IAA2* transcripts were significantly more abundant – albeit with a broad variance in transcript levels – than *IAA1* transcripts (**Figure 2-3 A**). Also, a more detailed look at the individual expression levels underlying each dataset shows that this is an overall tendency (**Supplementary Figure 4** to **Supplementary Figure 6**). This result indicates that *IAA1* and *IAA2* have diverged in their regulatory regions. While Remington *et al.* (2004) report that *IAA1* and *IAA2* are highly similar in stretches of their upstream flanking regions, a prediction of transcription factor binding sites revealed shared as well as unique features for *IAA1* and *IAA2* (**Supplementary Table 4** and **Supplementary Table 5**), which likely control differential expression.

To analyze functional divergence, we studied the selective pressure acting on protein-coding regions of *IAA1* and *IAA2*. To this end, we determined the nonsynonymous/synonymous substitution rate (dN/dS) ratio across 80 *A. thaliana* ecotypes and *A. lyrata* (in collaboration with Philipp Janitza and Marcel Quint; affiliation as stated above). The dN/dS ratio measures the nonsynonymous substitutions (i.e. nucleotide substitutions that result in an amino acid substitution) per synonymous substitutions (i.e. nucleotide substitutions causing no changes on the amino acid level). This measure can be used to infer the direction and strength of natural selection. If no selection is acting, dN/dS should equal 1. A dN/dS value smaller than 1 indicates an under-representation of nonsynonymous substitutions, which can be interpreted as the preferential elimination of deleterious mutations by purifying selection. If dN/dS is larger than 1, it indicates an overrepresentation of nonsynonymous substitutions, which can be interpreted as positive selection on new variants, also called diversifying selection (Fischer *et al.*, 2014b). Classical models predict that one duplicate is kept under purifying selection to provide the function of the ancestral gene, while the other duplicate is free to accumulate changes in the regulatory or coding regions (Prince and Pickett, 2002). We applied a sliding window approach, which allows mapping of selection signatures at specific regions across the coding sequence of the *IAA1/IAA2* sister pair. We observed that both *IAA1*

and *IAA2* show a dN/dS ratio less than 1 across the whole coding sequence (**Figure 2-3 B**), indicating a purifying selection acting on both genes. The selective constraint throughout the coding sequences of *IAA1* and *IAA2* suggests these duplicates are both well conserved and therefore may be essential players in auxin signaling. Thus, their coexistence might be justified by their regulatory diversification suggested by their different expression levels, or by diversification at the functional level. For example, *IAA1* and *IAA2* might occupy strictly conserved roles in specific multiprotein complexes.

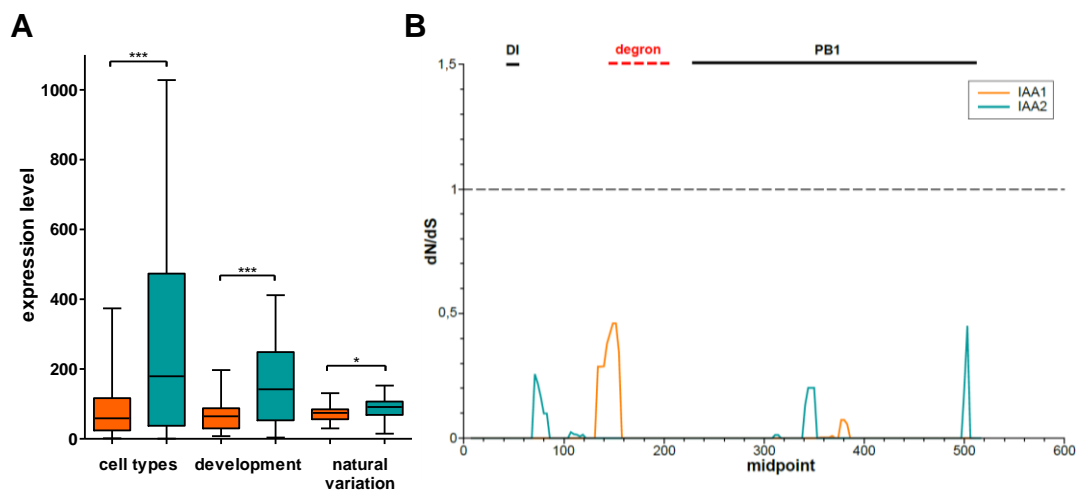


Figure 2-3: Expression and nucleotide diversity of *IAA1* and *IAA2* ohnologs

A. *IAA1* (orange) and *IAA2* (teal) expression levels for three different publicly available AtGenExpress datasets: cell types (cell-type-specific expression), development (developmental-stages-specific expression), and natural variation (Expression in different *A. thaliana* ecotypes). See **Section 6.11.2** for detailed dataset references. Mann-Whitney statistical testing for differences between *IAA1* and *IAA2* expression for each dataset was performed (* $p \leq 0.05$; ** $p \leq 0.01$; *** $p \leq 0.001$). Detailed plots of expression levels for each dataset are shown in **Supplementary Figure 4** to **Supplementary Figure 6**. **B.** Sliding window plots of nucleotide sequence divergence for *IAA1* (orange), *IAA2* (teal) in 80 *A. thaliana* ecotypes and *A. lyrata*. dN/dS ratios of pairwise comparisons between each *A. thaliana* ecotype and *A. lyrata* were calculated and average dN/dS ratios, indicating selective pressure acting on *AUX/IAA* protein-coding genes, plotted against the midpoint position of each 15 bp window. Lines at the top of the plot display the positions of the different protein domains: EAR motif in domain I (DI), degron (red dashed line) and PB1 domain. Grey dashed line at $dN/dS = 1$ delimiting positive and negative selection is shown for reference.

2.1.3.2 *AUX/IAA* homomerization does not seem to affect auxin receptor complex formation

Besides auxin-triggered complex formation with TIR1, *IAA1* and *IAA2* seemingly undergo heterotypic interactions with ARFs and TPL/TPR proteins and homotypic oligomerization. These interactions could potentially compete with SCF^{TIR1} :auxin:*AUX/IAA* complex formation through steric hindrance. Also, some binding partners might require the same *AUX/IAA* residues and hence are mutually exclusive. While structural information on *AUX/IAA* contribution to interaction with TIR1 from the study by Tan *et al.* (2007) is restricted to a 17-residues degron peptide from *IAA7*, nothing is known about how the interactions of flanking domains of *AUX/IAAs* affect co-receptor assembly. Since *AUX/IAAs* undergo

considerable oligomerization in a front-to-back fashion through acidic and basic patches on opposite faces of their C-terminal PB1 domain (Han *et al.*, 2014; Nanao *et al.*, 2014; Dinesh *et al.*, 2015), co-receptor formation could likely interfere with homooligomerization or vice versa. Whereas the C-terminal PB1 domain of AUX/IAAs adopts a globular β -grasp fold, the N-terminal part, including the conserved EAR motif and primary degron, is predicted to be intrinsically disordered (**Supplementary Figure 17**), thus allowing for high flexibility of the degron flanking regions. To evaluate an interplay between IAA1/IAA2 homotypic oligomerization and auxin-mediated co-receptor formation with TIR1, the Y2H interaction assay and *in vitro* radioligand binding approaches were implemented.

The *axr5-1* mutant gene product carries a P to S substitution in the second proline of its AUX/IAA core degron sequence, and pull-down experiments indicated that this substitution prevents the interaction between IAA1 and the SCF (Yang *et al.*, 2004). In analogy, a P61S mutant version of AD-IAA1 was generated, corresponding to AD-IAA1^{P61S/axr5-1}. As expected, this mutant protein did not show any TIR1/AFB1/AFB2 interaction in yeast (**Figure 2-4** and **Figure 2-9**). In addition, to test whether the IAA2 core degron functions alike in auxin-dependent TIR1/AFB interaction, an IAA2 mutant version was generated, referred to as AD-IAA2^{P66S}, that mimics the *axr5-1* mutation in the second proline of the core degron. In the Y2H assay, this substitution in IAA2 was also sufficient to abolish all interactions with the tested TIR1/AFBs (**Figure 2-4** and **Figure 2-9**). This indicates that, for both IAA1 and IAA2, the core degron plays the same crucial role in auxin-dependent interactions with TIR1/AFBs, and the second proline is a crucial residue of this core degron. Furthermore, based on studies on the PB1 domain of pea IAA4 (PsIAA4), an exchange of three highly conserved residues in the basic patch can abolish homotypic interaction (Dinesh *et al.*, 2015). Therefore, we substituted the three corresponding basic residues K77, R88, and K89 to alanines in Arabidopsis IAA1 to generate the basic patch mutant IAA1^{BM3}. First, we tested the wild-type and different mutant IAA1 and IAA2 proteins for their ability to interact with one another in a LexA Y2H approach.

DBD and AD fusions of wild-type IAA1 and IAA2, as well as mutants IAA1^{P61S/axr5-1} and IAA2^{P66S} interacted strongly in yeast, indicating that a dysfunctional core degron does not influence oligomerization (**Figure 2-4**). IAA1^{BM3} mutant protein interacted with wild-type or degron mutant IAA1 and IAA2 in both AD- and DBD-directions (**Figure 2-4**), indicating that IAA1^{BM3} can still undergo homo- or heterotypic interactions with intact IAA1 and IAA2 through its unaltered acidic PB1 interface. Only when AD-IAA1^{BM3} and DBD-IAA1^{BM3} are combined, homotypic interaction of IAA1^{BM3} is reduced (**Figure 2-4**). This indicates that, as expected, homomerization of IAA1 relies on these highly conserved basic residues. But does

oligomerization state influence auxin-mediated recognition of IAA1 and IAA2 degrons by TIR1? To address this question, the auxin-dependent interaction of AD-IAA1^{BM3} with DBD-TIR1 was initially assessed in yeast, and it was indistinguishable from auxin-dependent interaction of wild-type AD-IAA1 with DBD-TIR1. Assuming that through overexpression intracellular protein levels of wild-type AD-IAA1 and -IAA2 are high enough to yield a substantial fraction of homotypic oligomers in yeast cells, and that this fraction is reduced when yeast cells express AD-IAA1^{BM3} instead, this result suggests that TIR1 interacts with IAA1 independently of its oligomerization state.

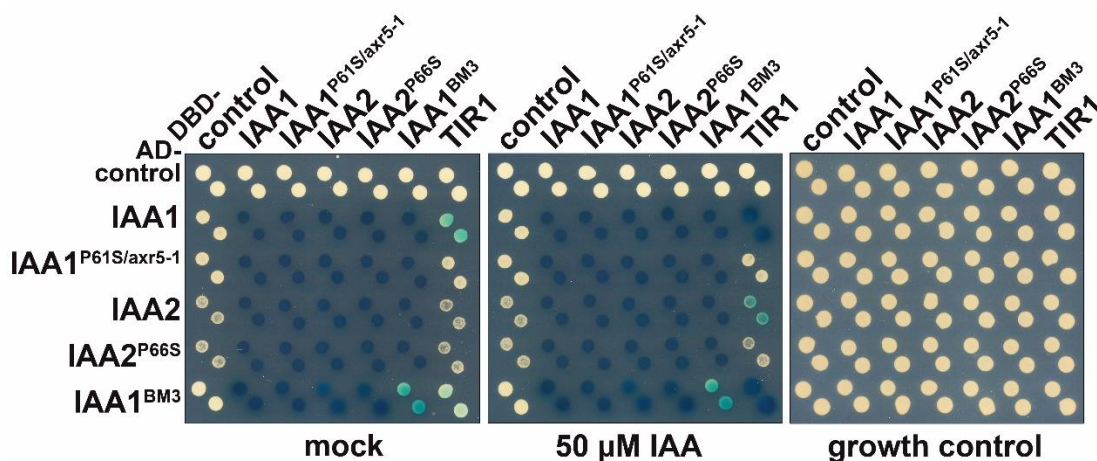


Figure 2-4: PB1 basic patch mutant IAA1^{BM3} shows reduced homotypic interaction

Diploid yeast co-expressing AD- and DBD-IAA1/-IAA2 wild-type or mutant forms or DBD-TIR1 were tested for β -Gal reporter activity on selective induction medium without or with addition of 50 μ M IAA. IAA1 and IAA2 mutants include such with dysfunctional degron (IAA1^{P61S/axr5-1}, IAA2^{P66S}) or impaired basic patch in PB1 domain (IAA1^{BM3}). Impaired degrons do not affect IAA1 or IAA2 homotypic interaction. PB1 basic patch mutant IAA1^{BM3} shows reduced homotypic interaction, but still interacts with TIR1 in an auxin-dependent manner. Yeast cell dispersions of a similar OD₆₀₀ were spotted on selective induction medium plates and pictures taken after three days of growth at 30°C. Control yeast are carrying an AD- or DBD-empty vector plasmid.

To further corroborate the finding, this question was also addressed in an *in vitro* radioligand binding assay. Affinities of homotypic dimer formation have been determined to be K_D 6.4 μ M and 6.6 μ M for PsIAA4 and IAA17, respectively (Han *et al.*, 2014; Dinesh *et al.*, 2015), and evidence for the same K_D representing association events during IAA17 oligomerization was provided (Han *et al.*, 2014). Also, based on measuring oligomer formation at different protein concentrations and applying equilibrium models, it was predicted that IAA17 is largely monomeric at concentrations below 1 μ M and oligomers of varying sizes increase at higher concentrations (Han *et al.*, 2014).

Based on the assumption that IAA1 and IAA2 behave similarly and that the formation of oligomers is at equilibrium in a radioligand binding reaction, the following experimental setup was designed. Wild-type IAA1 or IAA2 protein were used at a constant concentration, where a fraction of AUX/IAAs should be monomeric and a fraction assembles to different-sized

homomers. By adding increasing amounts of mutant AUX/IAA with a dysfunctional degnon, the equilibrium of monomers and oligomers will form accordingly since the PB1 domain is functional. However, overall the concentration of intact degrons per monomer as well as the concentration of intact degrons per oligomer available for co-receptor assembly will become reduced, because oligomers will be consisting of a mix of wild-type and degnon mutant proteins (**Figure 2-5 A**). If the accessibility of the degnon for auxin-dependent interaction with TIR1 is positively or negatively affected by AUX/IAA oligomerization state, it should become detectable with an increasing ratio of degnon mutant to wild-type in a mixed monomer/oligomer equilibrium (**Figure 2-5 A**).

To test this, we recombinantly expressed and purified TIR1:ASK1 as previously described (Tan *et al.*, 2007; Calderón Villalobos *et al.*, 2012), and established optimized *E. coli* expression and purification protocols for identically Gateway-cloned GST-IAA1 and -IAA2 (**Supplementary Figure 9**), as well as GST-IAA1^{P61S/axr5-1} and GST-IAA2^{P66S} degnon mutant proteins. These mutant proteins are unable to undergo auxin-mediated interaction with TIR1 in yeast and *in vitro* binding assays (**Figure 2-5 B** and **Figure 2-9**), but still have the capacity to oligomerize in yeast (**Figure 2-4**). Using a radioligand binding approach, we tested samples with constant amounts of TIR1:ASK1, tritium-labeled indole-3-acetic acid [5-³H] (³H-IAA) and wild-type IAA1 or IAA2, and added increasing amounts of mutant IAA1^{P61S/axr5-1} or IAA2^{P66S}, respectively. The auxin-binding capability of a co-receptor consisting of TIR1 and wild-type IAA1 or IAA2 was neither impaired nor ameliorated by increasing amounts of the corresponding degnon mutant added to the reaction (**Figure 2-5 B**). This result indicates that AUX/IAA homomerization status is likely irrelevant to complex formation with auxin and TIR1.

Additionally, to further test the influence of IAA1 oligomerization status on recognition by TIR1, we recombinantly expressed the basic patch mutant GST-IAA1^{BM3} that exhibits strongly reduced homotypic interaction in yeast (**Figure 2-4**). Notably, compared to the wild-type GST-IAA1, the recombinant, purified GST-IAA1^{BM3} was much more stable when stored, subjected to freezing and thawing, and concentrated. When tested in the radioligand binding assay with the same constant amounts of TIR1:ASK1 and ³H-IAA as above, the GST-IAA^{BM3} was capable to form a complex with TIR1 and auxin, suggesting that the monomeric state is not disadvantaged in co-receptor complex formation. Note that a reliable quantitative comparison of binding capacity between wild-type IAA1 and IAA1^{BM3} mutant is not possible from this experiment, since the concentration of active protein in samples cannot be determined with absolute certainty, especially with regard to the observed enhanced stability of GST-IAA^{BM3} mutant protein in comparison to the wild-type protein. Taken together, these

results strengthen our view of AUX/IAAs as modular proteins, in which individual domains provide independently functioning PPI interfaces.

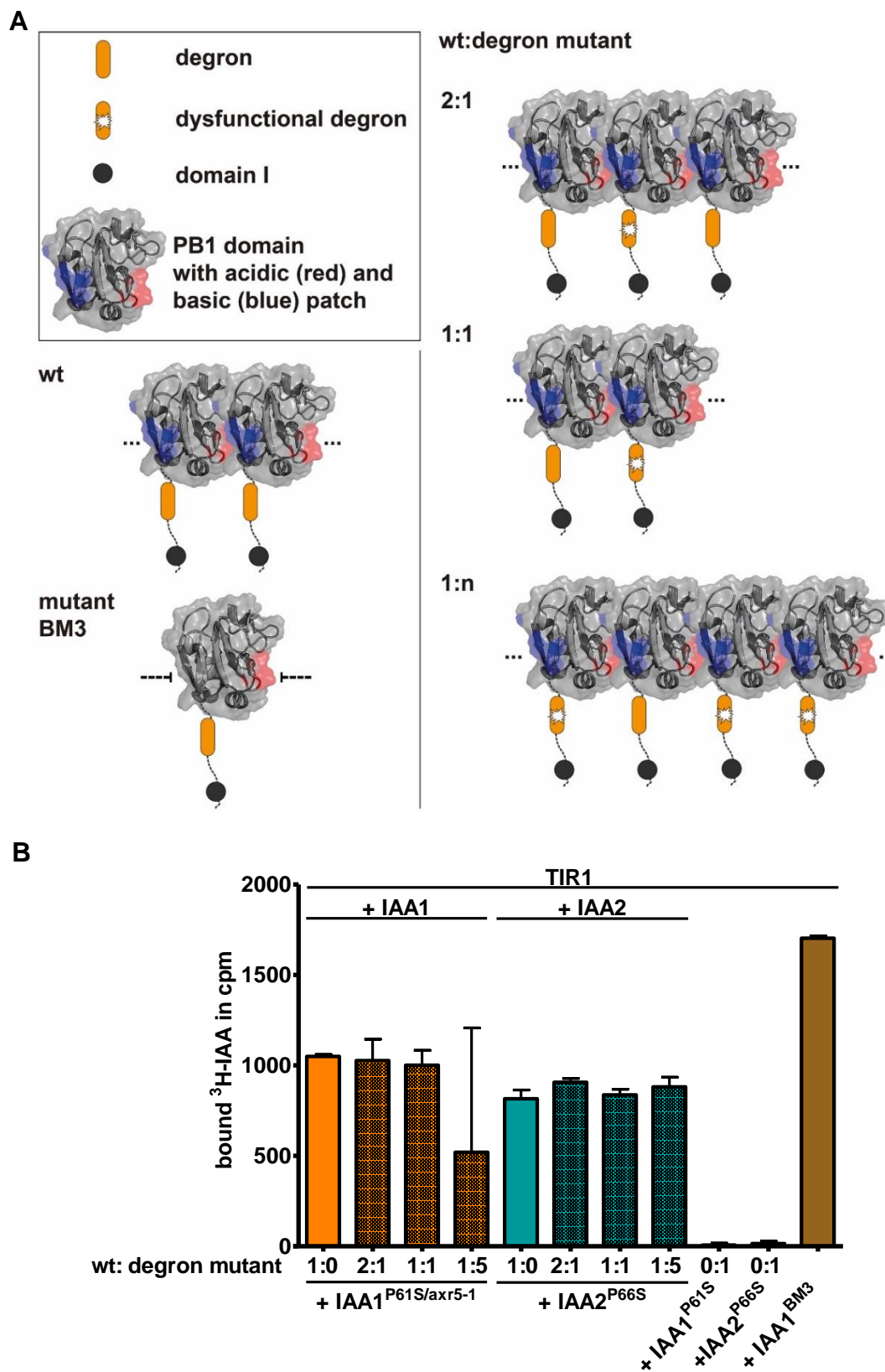


Figure 2-5: AUX/IAA oligomerization does not affect co-receptor complex formation

A. The scheme visualizes the protein variants and ratios used in **B**. Wild-type (wt) AUX/IAAs carrying both acidic and basic patches in their PB1 domain are able to oligomerize (signified by several side by side proteins followed by ellipsis). The BM3 mutant lacks the basic patch and therefore its monomeric form prevails. AUX/IAAs with a

degron can partake in auxin co-receptor formation, whereas those with a dysfunctional degron cannot. The mixing ratios of wild-type and degron-mutated AUX/IAA variants (wt:degron mutant) are expected to be reflected in oligomer formation. The higher the wt:degron mutant ratio (1:n), the less functional degrons are available per AUX/IAA oligomer for auxin co-receptor formation. **B.** Fixed concentrations of recombinant, pure TIR1:ASK1 (8 nM), wild-type (wt) GST-tagged AUX/IAA (2 μ M) were incubated with 75 nM 3 H-IAA. Additionally, degron mutants GST-IAA1^{P61S/axr5-1} and GST-IAA2^{P66S} were included in the reaction at indicated ratios. Samples for total and non-specific binding in duplicates. Specific binding as difference of total and non-specific binding is shown. One representative experiment out of two experiments is shown. Error bars denote standard deviation.

2.1.3.3 Assessing functional diversification in IAA1- and IAA2-containing auxin co-receptors

In order to assess whether IAA1 and IAA2 have diversified on the functional level, we aimed at determining the auxin sensing capabilities of TIR1-IAA1 and TIR1-IAA2 co-receptors. For that purpose, radioligand binding assays were implemented as they provide a quantitative measure of binding by yielding a dissociation constant for the binding event (Calderón Villalobos *et al.*, 2012; Hellmuth and Calderón Villalobos, 2016). Previously, a number of AUX/IAAs have been shown to equip auxin co-receptors with a range of sensing capabilities (Calderón Villalobos *et al.*, 2012). To determine whether IAA1 and IAA2 contribute to formation of specific auxin sensors, a reliable quantitative assessment of co-receptor complex formation is imperative, as the Y2H approach serves mainly as an estimation of auxin co-receptor formation. Furthermore, this *in vitro* approach allows a reductionist view onto auxin co-receptor complex assembly without additional, influencing PPIs. While typical hormone binding reactions simply comprise a one-site binding between a receptor protein and a ligand, the auxin co-receptor system involves two proteins, TIR1/AFBs and AUX/IAAs, and the auxin ligand.

The nature of the auxin binding pocket in TIR1, where auxin is anchored at the bottom of the pocket and sandwiched by the AUX/IAA degron binding atop TIR1 and auxin (Tan *et al.*, 2007), suggests a hierarchy of two putative, reversible binding events constituting ternary complex formation as follows. First, auxin binds to TIR1 with K_D^{auxin} to yield a TIR1:auxin complex (**Figure 2-6 (1)**). Subsequently, AUX/IAA binds to TIR1:auxin with $K_D^{\text{AUX/IAA}}$, resulting in TIR1:auxin:AUX/IAA complex (**Figure 2-6 (2)**). In radioligand binding assays using 3 H-IAA, it has not been possible so far to determine the K_D^{auxin} for the first binding reaction, suggesting a highly dynamic reaction with high dissociation rate of the TIR1:auxin complex. Nevertheless, in saturation binding experiments using both TIR1, excess amounts of AUX/IAA protein, and varying concentrations of 3 H-IAA, the apparent dissociation constant K'_D for ternary complex formation (**Figure 2-6 (3)**) could be assessed in previous studies (Calderón Villalobos *et al.*, 2012). Such include studies of the analogous co-receptor system for the phytohormone (3R,7S)-jasmonoyl-L-isoleucine (JA-Ile), consisting of the FBP CORONATINE INSENSITIVE1

(COI1) and its targets, the JASMONATE-ZIM-DOMAIN PROTEIN (JAZ) repressors (Sheard *et al.*, 2010). As this approach empirically describes co-receptor assembly, it allows comparison of apparent affinity values. Hereafter, the apparent dissociation constant K'_D is referred to as K_D .



Figure 2-6: Hypothesized TIR1:auxin:AUX/IAA ternary complex formation

Ternary complex formation likely consists of two hierarchical, reversible binding reactions. First, TIR1 and auxin form a TIR1:auxin complex (1). The equilibrium dissociation constant K_D^{auxin} describes this partial reaction. Next, the TIR1:auxin complex binds the AUX/IAA with $K_D^{\text{AUX/IAA}}$ (2). In radioligand binding assays, neither dissociation constant of the partial reactions is assessable, but the apparent dissociation constant K'_D for ternary complex formation from the three reactants, i.e. the net binding reaction (3), can be determined. In this scheme, TIR1 is shown as exemplary case for TIR1/AFBs.

2.1.3.3.1 IAA1 and IAA2 provide TIR1-containing co-receptors with similar high affinities for the auxin indole-3-acetic acid

For a quantitative comparison of apparent dissociation constants for TIR1:auxin:IAA1 and TIR1:auxin:IAA2 complexes, we combined recombinantly expressed and purified TIR1:ASK1 and GST-IAA1 and -IAA2 in saturation binding experiments with different concentrations of ^3H -IAA (Hellmuth and Calderón Villalobos, 2016). The concentrations were chosen to lie around the K_D , which was expected to adopt a value similar to previously characterized auxin co-receptors between 10^{-8} and 2×10^{-7} M (Calderón Villalobos *et al.*, 2012). ^3H -IAA concentrations up to ca. 10-fold K_D were chosen to approximate maximum, or saturated, binding. TIR1 occupancy ranged between 4 and 10 % at maximum binding (**Supplementary Figure 12**), indicating low but sufficient activity of the protein preparation. After complex-bound radioligand at equilibrium was quantified and plotted against concentrations c , a one-site binding was assumed based on crystal structure information (Tan *et al.*, 2007). Thus, the data was fitted to a hyperbolic binding curve, from which the apparent dissociation constant K_D could be obtained (see **Section 6.8.2** for details on radioligand binding experiments). An exemplary saturation binding experiment for co-receptors TIR1-IAA1 and -IAA2 is shown in **Figure 2-7 A**. Several independent experiments were performed, and mean K_D values,

resulting from individual curve fittings, were calculated (**Figure 2-7 B** and **Supplementary Figure 12**). Both TIR1:auxin:IAA1 and TIR1:auxin:IAA2 complexes assembled with a similar mean K_D value of 55 nM and 69 nM, respectively (**Figure 2-7 B** and **Supplementary Table 6 A**). This indicates that, at least *in vitro*, the highly similar ohnologs IAA1 and IAA2 confer the same auxin binding capabilities to a TIR1-containing co-receptor system.

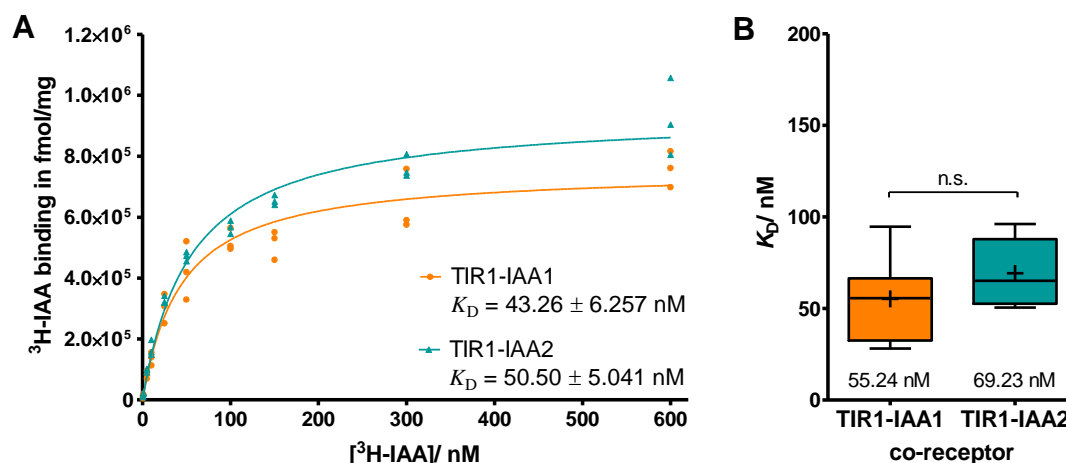


Figure 2-7: TIR1:auxin:IAA1 and TIR1:auxin:IAA2 complexes can be reconstituted *in vivo* and bind IAA with similar high affinity

A. In an exemplary saturation binding experiment for co-receptors TIR1-IAA1 and -IAA2, fixed concentrations of recombinant, highly pure TIR1:ASK1 (8 nM) and GST-AUX/IAA (2 μ M) were incubated with varying concentrations of radiolabeled IAA (³H-IAA). Samples containing co-receptor and radioligand for total binding, as well as identical samples with excess of unlabeled IAA (1 mM) for non-specific binding were measured. Specific binding was calculated by subtracting non-specific from total binding, subsequently converted to binding sites in fmol per TIR1 amount in mg, and plotted against radioligand concentration. At 600 nM ³H-IAA, TIR1 occupancy in IAA1- and IAA2-containing co-receptor complexes was 8 and 10%, respectively (see **Supplementary Figure 12**). Data points were fitted and K_D values obtained, using non-linear regression for a one-site, hyperbolic binding curve. Samples for total and non-specific binding in triplicates. **B.** K_D values from seven (TIR1-IAA1) and five (TIR1-IAA2) independent saturation binding experiments performed similarly as in A, but with varying concentrations of TIR1 and AUX/IAA and ³H-IAA (see **Supplementary Figure 11** and **Supplementary Figure 12**). K_D values are depicted as a box plot with whiskers denoting minimum and maximum values. Horizontal line denotes median. Cross and values underneath box denote mean. Mann-Whitney test shows that K_D values of both co-receptors do not differ significantly ($p > 0.05$; **Supplementary Table 6 A**).

2.1.3.3.2 Exchanging TIR1 for AFB2 in IAA1- and IAA2-containing co-receptors does not alter affinities for auxin *in vitro*

Based on our structural modeling data, which revealed a shorter and more flexible loop-12 in AFB2, it is possible that in AFB2, binding of the core degron might be favored in comparison to TIR1 (**Figure 2-1**). In order to test binding properties of AFB2-IAA1 and AFB2-IAA2 co-receptor complexes, GST-AFB2 was recombinantly expressed in insect cells and used in radioligand binding assays with ³H-IAA and IAA1 or IAA2 as above. However, TIR1/AFB2 recombinant expression is challenging, and despite several attempts, only two batches of few microgram of GST-AFB2 protein could be obtained. Therefore, we refrained from cleaving the GST-tag and performing additional purification steps after affinity chromatography. Thus, a

first assessment of saturation binding was implemented for AFB2-IAA1 and AFB2-IAA2 auxin receptors. The K_D values obtained for these auxin co-receptor pairs were in a similar range as for the TIR1-IAA1 and -IAA2 co-receptors, namely around 50-80 nM – albeit with a high variance for K_D values determined for AFB2-IAA1 (**Figure 2-8** and **Table 2-1**, also see **Supplementary Table 6 B**). **Table 2-1** summarizes the curve fitting results for radioligand binding data obtained for AFB2-IAA1 and AFB2-IAA2 co-receptor complexes and presents the mean K_D . Consequently, although there is no indication for a favorable complex formation of AFB2 with IAA1 or IAA2 from this *in vitro* binding assay, it remains to be substantiated whether AFB2 exhibits advantageous AUX/IAA degraon recruitment capabilities.

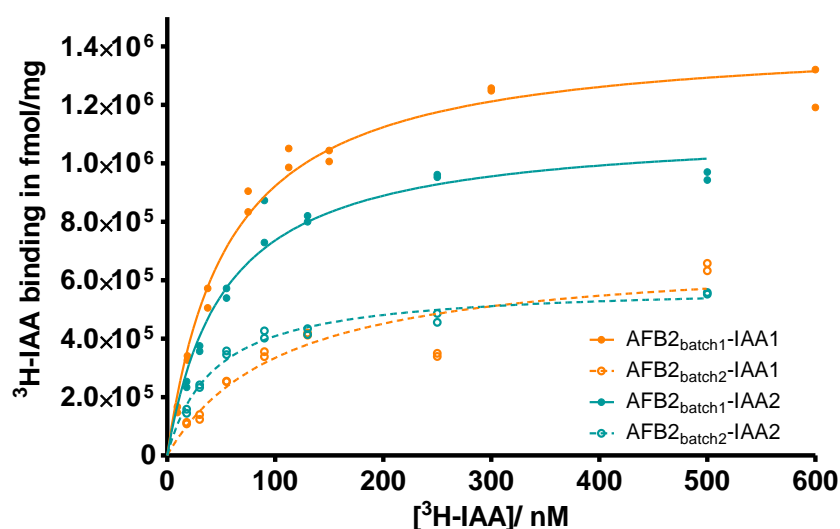


Figure 2-8: AFB2:auxin:IAA1 and AFB2:auxin:IAA2 complexes can be reconstituted *in vitro* and bind IAA with a similar high affinity

Fixed concentrations of recombinant, pure GST-AFB2:ASK1 (6-10 nM) and GST-AUX/IAA (2 μ M) were used in a saturation binding assay with varying concentrations of radiolabeled IAA (3 H-IAA). Specific binding was calculated by subtracting non-specific from total binding, subsequently converted to binding sites in fmol per AFB2 amount in mg, and plotted against radioligand concentration. At maximum 3 H-IAA concentration, AFB2 occupancy in IAA1- and IAA2-containing co-receptor complexes was 5 to 12%, respectively (see **Supplementary Figure 13**). Data points were fitted and K_D values obtained, using non-linear regression for a one-site, hyperbolic binding curve (see **Table 2-1**). Samples for total and non-specific binding were in duplicates. For each co-receptor, two independent experiments from different batches of AFB2 and AUX/IAAs are depicted. Raw data plots are shown in **Supplementary Figure 11**.

Table 2-1: Results from non-linear fit of radioligand binding data obtained for AFB2:auxin:IAA1 and AFB2:auxin:IAA2 complexes

K_D in nM and B_{max} in fmol binding sites/mg protein values were obtained from curve fittings of experiments shown in **Figure 2-8**. All individual K_D values have small, around 10%, standard error of the mean (SEM) values, except for the AFB2_{batch2}-IAA1 co-receptor data, curve fitting yielded a K_D with comparably high SEM. The mean K_D and SEM for both co-receptor pairs are shown in the right column.

	<i>curve fitting</i>		<i>curve fitting</i>		<i>mean</i>	
	K_D / nM		B_{max} / fmol/mg		K_D / nM	
co-receptor	mean	SEM	mean	SEM	mean	SEM
AFB2_{batch1}-IAA1	55.91	5.506	1243	36.81	81.755	25.845
AFB2_{batch2}-IAA1	107.6	31.64	599.9	68.85		
AFB2_{batch1}-IAA2	52.52	7.237	970.9	41.52	47.775	4.745
AFB2_{batch2}-IAA2	43.03	4.177	505.2	14.22		

2.1.3.4 Auxinic compounds differentially influence TIR1-IAA1/TIR1-IAA2 co-receptor assembly

Besides TIR1/AFBs and AUX/IAAs, the hormone auxin itself is a third variable for the events leading to auxin co-receptor formation. Structural analyses have shown that besides the natural auxin IAA, the synthetic auxins 2,4-D and NAA can be accommodated by the TIR1 auxin binding pocket and an IAA7 degron peptide (Tan *et al.*, 2007)(see **Section 1.2.2**). In addition, surface plasmon resonance (SPR) experiments demonstrated binding of various natural and synthetic auxins including aforementioned IAA, 2,4-D, and NAA, as well as several phenylacetic acids, picolinates, and propionic and butyric acids, by a TIR1-IAA7 degron receptor complex (Calderón Villalobos *et al.*, 2012; Lee *et al.*, 2014). Also, Shimizu-Mitao and Kakimoto (2014) showed that 4-Cl-IAA and PAA can trigger AUX/IAA degradation when TIR1/AFB2-AUX/IAA co-receptors are expressed in yeast. This suggests that auxin co-receptors exhibit sensing capabilities for these two natural auxins. Nevertheless, direct biochemical evidence for binding of natural auxins, as well as comparative assessment of binding of different auxins by specific and full-length AUX/IAA-containing co-receptors such as TIR1-IAA1 and TIR1-IAA2 is still missing.

Therefore, we wanted to explore whether and at which concentrations endogenous auxins other than IAA can promote interaction of TIR1/AFBs with IAA1 and IAA2. Furthermore, we aimed at gaining insights into putative selectivity towards different natural and synthetic auxins among these TIR1-IAA1 and TIR1-IAA2 highly similar co-receptors. To that end, and to begin with, we evaluated the two synthetic auxins 2,4-D and NAA, as well as the four natural auxins IAA, 4-Cl-IAA, IBA and PAA for their ability to promote TIR1/AFB1/AFB2:IAA1/IAA2 interaction in LexA Y2H experiments. Since other plant factors are absent, the approach via the yeast system is suitable to assess the question whether the natural auxins are bound by

TIR1/AFB-containing co-receptors. One needs to consider, though, that this is not a quantitative assessment and that false negative results could arise from toxic effects of auxinic compounds or turnover inside and/or efflux from the yeast cells (Prusty *et al.*, 2004; Teixeira *et al.*, 2007).

A strongly interacting AD-IAA7 construct (Calderón Villalobos *et al.*, 2012) was included for comparison and as a positive control, as the promotion of TIR1:IAA7 interaction in Y2H assays by various auxins (IAA, NAA, 2,4-D and picloram) was previously demonstrated (Calderón Villalobos *et al.*, 2012). As negative controls, aforementioned AD-IAA1^{P61S/axr5-1} and AD-IAA2^{P66S} were included (see **Section 2.1.3.2** and **Figure 2-4**). As expected, these mutant AUX/IAAs did not interact with TIR1/AFB1/AFB2 in the presence of any auxin tested (**Figure 2-9**). Similar DBD-TIR1/AFB protein expression levels have been previously shown (Calderón Villalobos *et al.*, 2012), and AD-AUX/IAA protein expression was similar in immunoblot analysis (**Supplementary Figure 14**). The auxin-independent interaction of TIR1/AFBs with ASK1 was included as a control. As expected, none of the auxins affected this interaction (**Figure 2-9**).

We found that IAA, and interestingly, also 4-Cl-IAA, promoted interaction of TIR1/AFB1/AFB2 with wild-type IAA1/IAA2/IAA7 equally and in a concentration-dependent manner in yeast (**Figure 2-9**). This indicates a potential role for 4-Cl-IAA as an auxin perceived by co-receptor pairs containing TIR1/AFB1/AFB2 and IAA1/IAA2/IAA7. The natural auxins IBA and PAA very weakly promoted only TIR1:IAA1 interaction and only at high concentration of 100 μ M (**Figure 2-9**). The synthetic auxin NAA promoted co-receptor interactions in a concentration-dependent manner, albeit to a lesser extent than IAA and 4-Cl-IAA (**Figure 2-9**). Besides the previously shown strong promotion of TIR1:IAA7 interaction by NAA (Calderón Villalobos *et al.*, 2012), the effect was mainly detectable in interactions involving IAA1. Only at high concentrations around 100 μ M, NAA promoted TIR1:IAA2 interaction (**Figure 2-9**). While 2,4-D promoted TIR1:IAA7 interaction as previously shown (Calderón Villalobos *et al.*, 2012), 2,4-D appears to be a poor ligand for the TIR1:IAA1 pair (**Figure 2-9**). According to the AUX/IAA phylogeny in Remington *et al.* (2004), IAA7 belongs to the IAA7-14-16-17 subgroup which clusters basal to the IAA1-2-3-4 subgroup. IAA7 more readily interacted with TIR1/AFBs at lower concentrations of 2,4-D, PAA and IBA in comparison to IAA1 and IAA2. This indicates that AUX/IAAs in the co-receptor likely influence the sensitivity not only for IAA, but also for other auxins. Interestingly, there seems to be no selectivity for a specific auxin among the co-receptors tested (**Figure 2-9** and data not shown). This might indicate that TIR1 and its next closely related homologs AFB1 and AFB2 (**Figure 1-5**) tested here confer a highly similar selectivity to the auxin receptor complex. So far, only the more distantly related AFB4 and

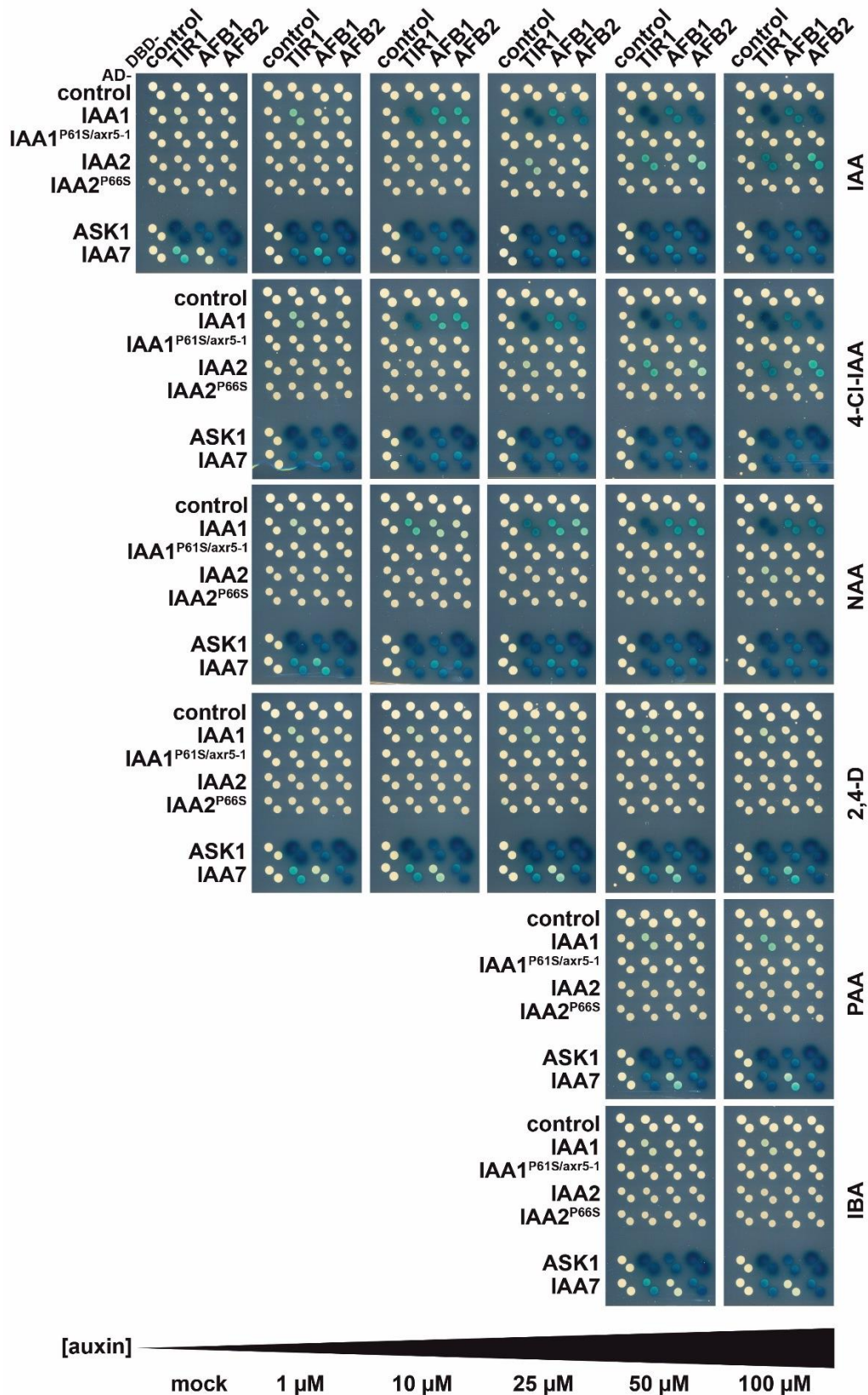


Figure 2-9: Various auxins differentially promote TIR1/AFB:IAA1/IAA2 interaction in yeast

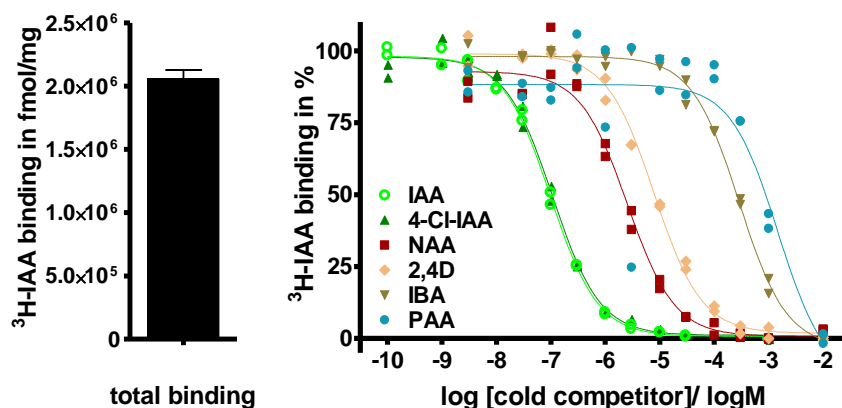
Diploid yeast co-expressing AD-IAA1/-IAA2 variants or AD-IAA7/-ASK1 and DBD-TIR1/-AFB1/-AFB2 were tested for β -Gal reporter activity on selective induction medium supplemented with different concentrations of various natural and synthetic auxins. Yeast cell dispersions of the same OD₆₀₀ were spotted on selective induction medium plates and pictures taken after three days of growth at 30°C. One representative out of three experiments with similar results is depicted.

AFB5 have been reported to exhibit selectivity for picolinate auxins (see **Section 1.2.2**). Thus, the poor effect of IBA, PAA and 2,4-D on co-receptor formation in yeast could indicate that these compounds are less likely to be perceived by these co-receptors. Nevertheless, reduced stability of these compounds in yeast cannot be ruled out at this point.

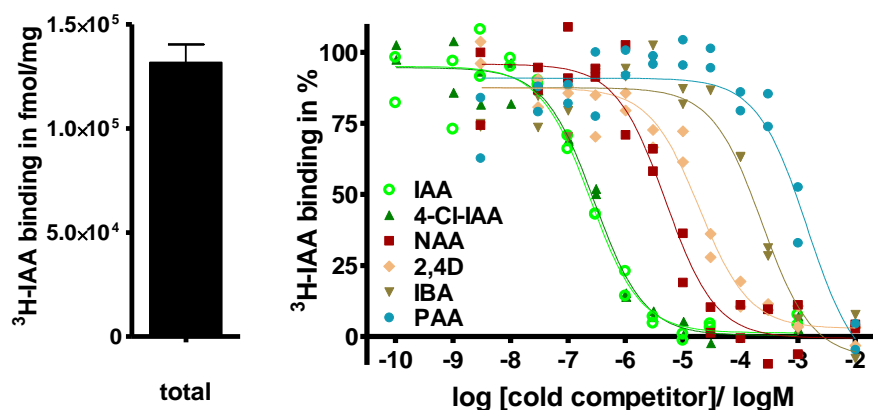
2.1.3.4.1 4-Chloroindole-3-acetic acid (4-Cl-IAA), as IAA, can be a high affinity ligand for TIR1-IAA1 and TIR1-IAA2 co-receptors

In order to quantitatively determine the binding capabilities of TIR1-IAA1 and TIR1-IAA2 co-receptors for natural and synthetic auxins, recombinant, pure TIR1 and GST-IAA1 or GST-IAA2 proteins were used in competition binding assays. Thereby, the ability of unlabeled IAA, 4-Cl-IAA, IBA, PAA, NAA and 2,4-D to outcompete a fixed concentration of ^3H -IAA from the co-receptor complex was assessed. The affinity for the radioligand ^3H -IAA from saturation binding assays (**Figure 2-7**) was used for determination of the inhibitory constant K_i according to Cheng and Prusoff (1973) – a measure of apparent affinity of the competitor compound in complex assembly (Motulsky and Neubig, 2001). Unlike the Y2H assessment of the auxins' effect, in this *in vitro* approach, stability and availability of auxinic compounds remains largely unaffected.

In competition binding, 4-Cl-IAA acted similarly as IAA with regard to binding to TIR1-IAA1 and -IAA2 co-receptors, consistent with Y2H results (**Figure 2-9**). For the TIR1-IAA1, as well as TIR1-IAA2 co-receptor, both IAA and 4-Cl-IAA exhibited K_i values in the nanomolar range (44 to 130 nM)(**Figure 2-10 A and B, Supplementary Figure 15**). The other two natural auxins tested, IBA and PAA, outcompeted ^3H -IAA from the same complex at much higher concentrations, resulting in K_i values in the high micromolar range. The synthetic auxins 2,4-D and NAA exhibited K_i values in the low micromolar range (**Figure 2-10 A and B, Supplementary Figure 15**). While synthetic 2,4-D and NAA can be bound by these auxin co-receptors, their lower affinities suggest that their high potency in causing auxin responses is likely due to their cellular stability and transport characteristics (Woodward and Bartel, 2005). These results further corroborate the possible perception of 4-Cl-IAA by TIR1-IAA1 and TIR1-IAA2 auxin co-receptors, and suggest that natural auxins IBA and PAA are unlikely candidates for perception by these co-receptors.

A TIR1-IAA1

competitor	curve fitting		K_d nM
	Best fit values	SEM	
IAA	-6.999	0.025	44.1
4-CI-IAA	-6.978	0.034	46.3
NAA	-5.597	0.066	1112.9
2,4-D	-5.103	0.036	3471.0
IBA	-3.542	0.034	126314.3
PAA	-2.829	0.253	652308.0

B TIR1-IAA2

competitor	curve fitting		K_d nM
	Best fit values	SEM	
IAA	-6.599	0.083	125.0
4-CI-IAA	-6.552	0.067	139.3
NAA	-5.3	0.162	2487.9
2,4-D	-4.715	0.115	9568.3
IBA	-3.624	0.122	117987.0
PAA	-2.839	0.095	719174.5

Figure 2-10: Various auxins can be bound by TIR1-IAA1 and TIR1-IAA2 co-receptors

Fixed concentrations of recombinant, pure TIR1:ASK1 (11 nM), ^3H -IAA (70 nM), and GST-IAA1 (1 μM) (A) as well as GST-IAA2 (1 μM) (B) were used in a heterologous competition binding assay with varying concentrations of unlabeled auxins. Absolute total binding is shown as a bar graph (left panel; containing no unlabeled competitor). Binding relative to total is plotted against Logarithm of competitor concentration in M, and data points were fitted

and IC_{50} values obtained, using non-linear regression for a one-site binding. Samples in duplicates. One representative experiment out of two to three (depending on the auxinic compound) independent binding experiments is depicted. Tables show $\log IC_{50}$ values and Standard error of the means (SEM) of $\log IC_{50}$ obtained from curve fitting, as well as K_i values. K_i values were calculated according to Cheng and Prusoff (1973) assuming a K_D for the radioligand of 55 and 69 nM for TIR1-IAA1 and TIR1-IAA2, respectively, in accordance with saturation bindings performed previously (Figure 2-7 B). See **Supplementary Figure 15** for a summary of K_i values obtained in independent competition binding experiments.

Taken together, IAA1 and IAA2 behave very similar in *in vitro* co-receptor assembly with regard to auxin affinity in a co-receptor with TIR1 or AFB2, and also exhibit identical preference for auxinic compounds in a co-receptor with TIR1. This indicates that IAA1 and IAA2 ohnologs occupy a conserved function with regard to the auxin sensors they build.

2.1.3.5 Ubiquitination of IAA1 and IAA2 by SCF^{TIR1}

2.1.3.5.1 SCF^{TIR1}-dependent ubiquitination of IAA1 and IAA2 can be reconstituted *in vitro*

TIR1/AFB-AUX/IAA auxin co-receptor assembly coincides with AUX/IAA target recognition for its ubiquitination by SCF^{TIR1/AFBs} E3 ligases. Thus, IAA1 and IAA2 as targets for SCF^{TIR1/AFBs} might exhibit functional diversification with regard to the biochemical output of co-receptor formation. Since AUX/IAA ubiquitination is still underexplored, it is imperative to gain insights into the specific events leading to AUX/IAA processing. To reconstitute AUX/IAA ubiquitination, an *in-vitro*-ubiquitination (IVU) assay was established in our research group (in frame of a Master's thesis; Winkler, 2015; Winkler *et al.*, under review). This IVU allows obtaining hints for possible differences between these closely related targets with regard to auxin responsiveness or processivity of ubiquitination by SCF^{TIR1}.

In brief, to ensure a flexible, amenable assay with a minimum of additional effectors, the reactions were performed with recombinantly expressed and purified components. For activation and E2-conjugation of Ub, E1 and E2 enzymes, as well as wild-type Arabidopsis Ub were preincubated in the presence of ATP. Arabidopsis UBIQUITIN-ACTIVATING ENZYME 1 (Uba1) was used out of the two-membered family of Arabidopsis E1 enzymes, which are functionally redundant (Hatfield *et al.*, 1997). As an E2 enzyme, Arabidopsis UBIQUITIN-CONJUGATING ENZYME 8 (Ubc8) was used, as it has been shown as a reliable, highly active E2 in previous *in vitro* assays (Girod *et al.*, 1993; Bachmair *et al.*, 2001; Kraft *et al.*, 2005). For preassembly of the SCF^{TIR1}:auxin:AUX/IAA complex, E3 components HsCUL1:MmRBX1 and AtASK1:AtTIR1, as well GST-IAA1 or -IAA2 as targets and auxin were incubated. By combining reactions containing ubiquitin charged E2 (E2~Ub) and SCF^{TIR1}:auxin:AUX/IAA complexes, the ubiquitination reactions were initiated. Since only covalently-linked Ub was to be analyzed, thiolester intermediates were reduced using SDS-PAGE loading buffer containing β -

mercaptoethanol. Samples were then separated on gradient SDS-PAGE and immunoblotted. To identify ubiquitinated protein species or unmodified as well as ubiquitinated GST-AUX/IAA target species, α -Ub or α -GST antibody was used in immunodetection, respectively.

First, in order to evaluate the specificity of the ubiquitination reaction on IAA1 and IAA2 targets, and to gauge the signal-to-noise ratio when probing with different antibodies, a control IVU assay was performed (**Figure 2-11**). For that, typical IVU reactions were set up, but one component was excluded each time from the reaction (**Figure 2-11**, upper panel: total protein). When probed with α -GST antibody, all lanes showed the prominent band at >40 kDa corresponding to GST-IAA1 (46.8 kDa) and GST-IAA2 (47.7 kDa), respectively (**Figure 2-11**, middle panel, black triangle, also see **Supplementary Figure 18**). Apart from that, a similar background pattern of GST-signal was detected in all lanes except where AUX/IAA was excluded, indicating that the α -GST immunoblot gives a true reflection of the presence of the GST-AUX/IAA species (**Figure 2-11**, middle panel). In the positive control reaction (“complete” reaction, **Figure 2-11**), between >40 kDa and ca. 110 kDa, a strong increase in GST-signal over the background occurred, indicative of GST-IAA1 and GST-IAA2 that have undergone extensive Ub conjugation (**Figure 2-11**, middle panel). Interestingly, an increase in GST-signal at a lower molecular weight, around 50-70 kDa, was also observed in samples where either TIR1:ASK1 or auxin were omitted. This suggests that GST-AUX/IAAs can, at least in part, become ubiquitinated independent of auxin and SCF^{TIR1} (**Figure 2-11**, middle panel). This unspecific ubiquitination in the lower molecular weight range needs to be considered when interpreting α -GST immunoblot results of IVU assays.

In the α -Ub immunoblot, no ubiquitination signals were detected in samples where Ub, E1, E2 or CUL1:RBX1 were omitted (**Figure 2-11**, bottom panel). This result is consistent with Ub activation and conjugation by E1 and E2, respectively, being indispensable steps in the ubiquitination cascade. Also, this result shows that CUL1:RBX1 is an essential component in the ubiquitination reaction, as it serves as a scaffold that combines E2- and target receptor-binding. Surprisingly, in samples where TIR1:ASK1, or auxin, or even AUX/IAA target was omitted, strong Ub signals over a range of 40-170 kDa, very similar to ubiquitin signals in the positive control, were detected (**Figure 2-11**, bottom panel, also see **Supplementary Figure 18**). This, again, is indicative of TIR1- and auxin-independent ubiquitination of targets to some extent as observed in α -GST immunoblots mentioned above. Curiously, this Ub signal occurs over a wider molecular weight range and even in target-free samples (**Figure 2-11**, bottom panel). Therefore, it hints at extensive ubiquitination of reaction components other than the target, most likely CUL1 (as observed in e.g. Wu *et al.*, 2003; Duda *et al.*, 2008). Although the

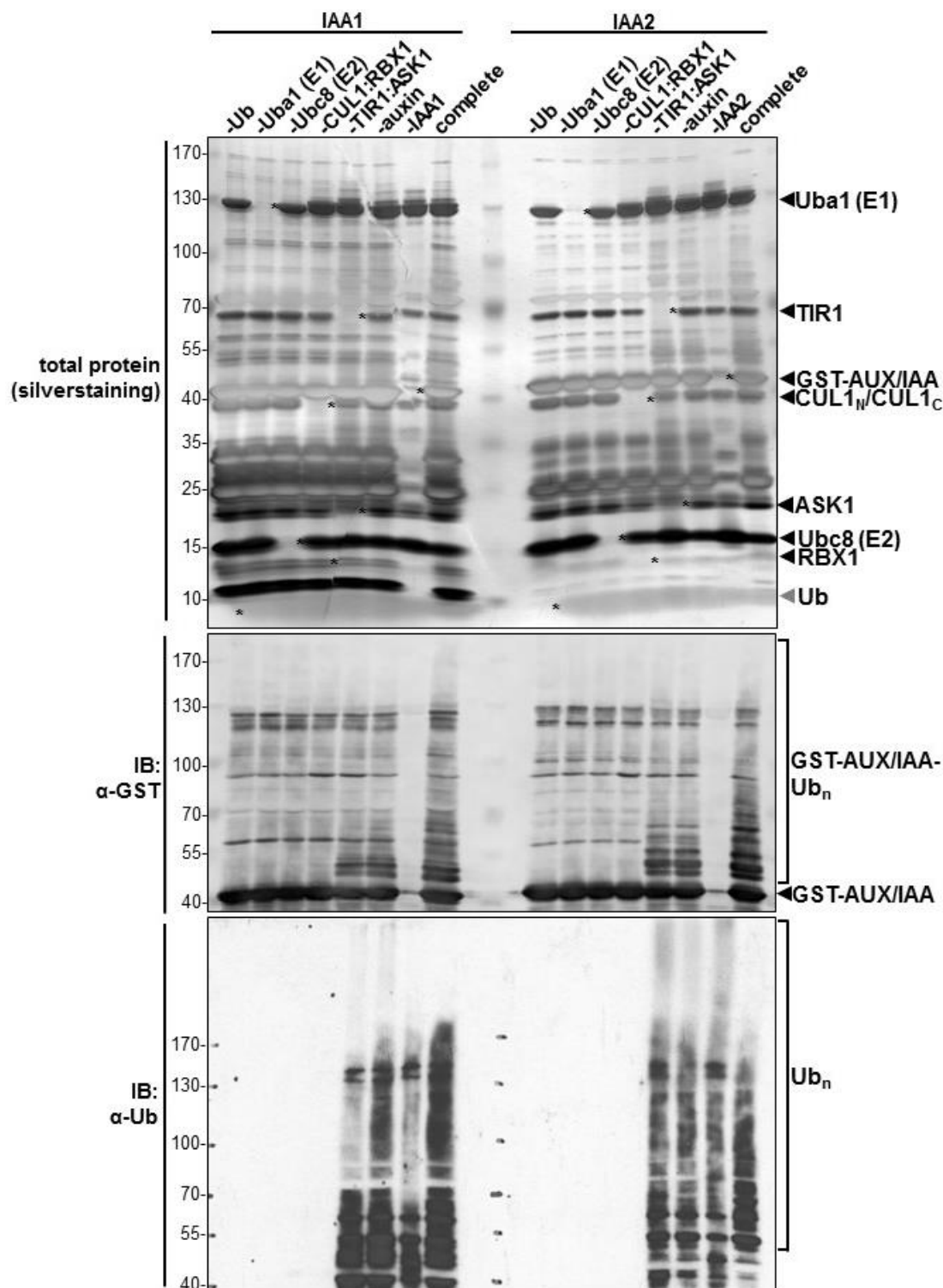


Figure 2-11: Specificity of ubiquitination of IAA1 and IAA2 by Uba1, Ubc8, SCF^{TIR1} and auxin *in vitro*

Ubiquitination reactions were performed leaving out one component at a time as indicated. A reaction including all components (“complete”) was used as positive control. Samples were loaded on 5-15% gradient SDS-PAGE and silver stained for detection of total protein (upper panel), probed with α -GST antibody for detection of the GST-tagged AUX/IAA targets (middle panel), or probed with α -Ubiquitin (α -Ub) antibody for detection of Ub and thus ubiquitinated protein species (bottom panel). In the silver stained SDS-PAGE (upper panel), asterisks denote the missing protein band of the excluded reaction component which is present in all other lanes and specified on the right hand side next to triangle symbols. Since targets GST-IAA1 and -IAA2 have a molecular weight of 46.8 kDa and 47.7 kDa, respectively, the immunoblots are only shown for protein species >40 kDa. Note that unspecific ubiquitination of proteins other than targets (bottom panel; “minus IAA1/IAA2” lanes), as well as TIR1- and auxin-independent ubiquitination of targets or other components (middle and bottom panel; “minus TIR1:ASK1” and

“minus auxin” lanes) were detected. However higher molecular weight ubiquitinated target-specific species are only present in the positive control and especially distinct in α -GST immunoblots. ATP was included in the reaction buffer (see **Section 6.7.10** for IVU details). Auxin concentration was 600 nM IAA and samples were taken after 20 min.

patterns of ubiquitination differ slightly compared with the positive control, the results from α -Ub immunoblots were henceforth treated with caution, and in the following experiments, focus was put on interpretation of the more reliable and consistent results from α -GST immunoblots. The latter admittedly exhibited higher background and also a slight auxin- and TIR1-independent ubiquitination, but can be relied upon with regard to target-specific ubiquitination.

2.1.3.5.2 Ubiquitination of IAA1 and IAA2 requires an intact core degron sequence

The conserved core degron of AUX/IAAs is required for co-receptor complex assembly (**Figure 2-9** and **Figure 2-5 B** for IAA1 and IAA2) and for their destabilization (Worley *et al.*, 2000; Gray *et al.*, 2001; Ramos *et al.*, 2001; Zenser *et al.*, 2001; Zenser *et al.*, 2003; Dreher *et al.*, 2006). Therefore, also ubiquitination should be affected when the core degron is compromised, because the required co-receptor complex cannot assemble. To test this, aforementioned GST-AUX/IAAs with dysfunctional core degrons, IAA1^{P61S/axr5-1} and IAA2^{P66S}, were used in an IVU reaction and compared with the wild-type targets. After 20 min, wild-type IAA1 shows an increase of high-molecular weight species, indicative of strong ubiquitination. No such signals were detected when IAA1^{P61S/axr5-1} was used as a target (**Figure 2-12**). This further demonstrates the specificity of the IVU assay and its dependence on co-receptor complex formation. When comparing wild-type IAA2 and IAA2^{P66S}, ubiquitination was not completely abolished in mutant targets, but strongly reduced, hinting at a possibly less severe effect of the P66S mutation on the IAA2 degron.

Furthermore, auxin should promote co-receptor complex assembly and positively affect ubiquitination. The effect of addition of the auxin IAA was tested in this IVU. The concentration of 600 nM was chosen empirically. In radioligand binding assays, complex formation had usually reached maximum binding at 600 nM ³H-IAA. In IVUs TIR1 concentration is ca. 100-fold above that in binding assays, so we tested whether 600 nM IAA would already suffice to detect an effect on AUX/IAA ubiquitination. Surprisingly, wild-type IAA1 ubiquitination was comparable in samples with and without auxin (**Figure 2-12**). In contrast, IAA2, although exhibiting Ub conjugates in the absence of auxin, these were much more prominent upon addition of auxin – as one would expect. Mutant IAA1^{P61S/axr5-1} was not ubiquitinated either in the presence or absence of auxin. However, addition of auxin led to

slight increase in ubiquitination in mutant IAA2^{P66S}, consistent with residual ubiquitination of this mutant version mentioned above (**Figure 2-12**). This result suggests that although the IAA1- and IAA2-containing auxin co-receptor complexes assembled with similar K_D values in radioligand binding assays, they exhibit differences with regard to ubiquitination dynamics *in vitro*.

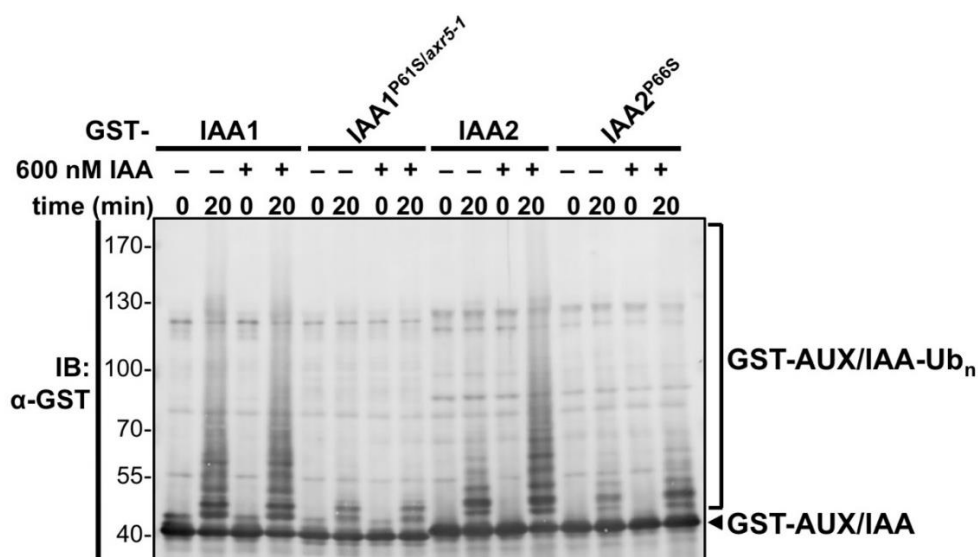


Figure 2-12: Ubiquitination of IAA1 and IAA2 *in vitro* relies on an intact core degron

Ubiquitination reactions were performed with wild-type IAA1 and IAA2 and their corresponding degron mutants IAA1^{P615/axr5-1} and IAA2^{P66S} as targets. Samples were taken at the start of the reaction (0 min) and after the reaction had proceeded for 20 min. Also, reactions were run in the absence or presence of 600 nM IAA. Samples were loaded on 5-15% gradient SDS-PAGE and probed with α -GST antibody for detection of the GST-tagged AUX/IAA targets. Unmodified targets GST-IAA1 and -IAA2 have a molecular weight of 46.8 kDa and 47.7 kDa, respectively, and are denoted with a black triangle ("GST-AUX/IAA"). GST-protein species >40 kDa, which are above GST background signals seen in 0 min timepoints, are therefore indicative of ubiquitinated AUX/IAAs and denoted with a bracket (GST-AUX/IAA-Ub_n). See **Supplementary Figure 19** for loading control.

2.1.3.5.3 Auxin promotes *in vitro* ubiquitination of IAA2, but not IAA1, in a dose-dependent manner

To study the effect of auxin on ubiquitination of IAA1 and IAA2 in more detail, and to test how sensitive the IVU assay is to lower auxin concentrations, a dose response IVU was performed. Here, 0 to 0.6 μ M IAA was added to the IVU reactions and Ub conjugation assessed at the start (0 min) as a control, and after the reaction had proceeded for 30 min. Strikingly, when IAA1 is used as a target, higher molecular weight species that appear after 30 min of reaction are uniform across increasing auxin concentrations (**Figure 2-13**). In a similar independent experiment higher molecular weight species slightly increased with higher auxin concentrations (**Supplementary Figure 20**). This substantiates the previous result of IAA1 ubiquitination being hardly responsive to auxin *in vitro* – at least for the concentrations tested. In contrast, when IAA2 was used as a target, the higher molecular weight species that appeared after 30 min incubation changed with increasing auxin concentration (**Figure 2-13**,

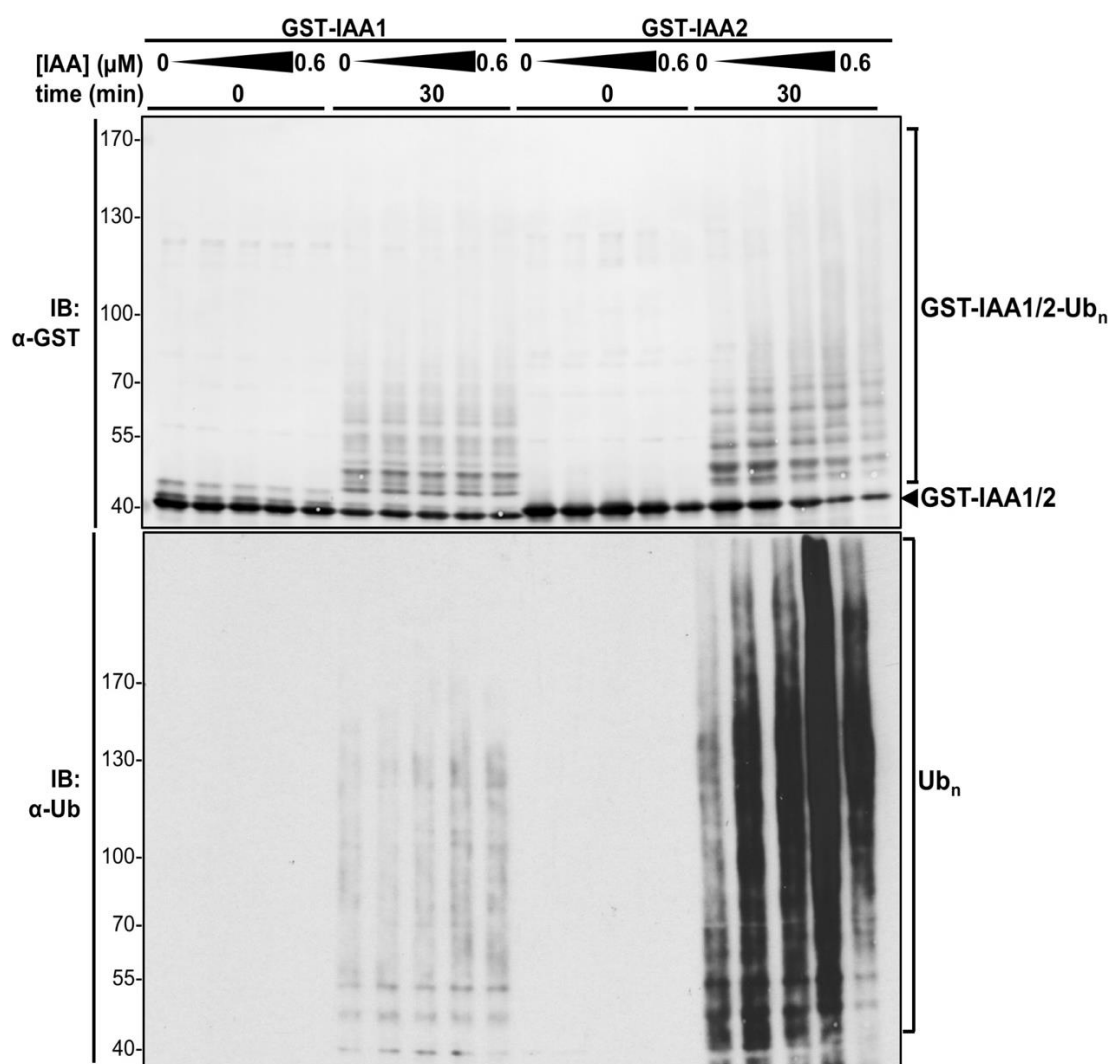


Figure 2-13: Auxin dose response of *in vitro* ubiquitination reaction with targets IAA1 and IAA2

Ubiquitination reactions were performed with wild-type IAA1 and IAA2 as targets and five different auxin concentrations ([IAA]= 0; 0.03; 0.06; 0.24; 0.6 μ M). Samples were taken at the start of the reaction (0 min) and after the reaction had proceeded for 30 min. Samples were loaded on 5-15% gradient SDS-PAGE and probed with α -GST antibody (upper panel) for detection of the GST-tagged AUX/IAA targets, or with α -Ubiquitin (α -Ub; bottom panel) antibody for detection of ubiquitinated protein species (denoted with bracket “(Ub)_n”) which might include ubiquitinated proteins other than AUX/IAA (see **Figure 2-11**). Unmodified targets GST-IAA1 and GST-IAA2 have a molecular weight of 46.8 kDa and 47.7 kDa, respectively, and are denoted with a black triangle (“GST-IAA1/2”). GST-protein species >40 kDa are therefore indicative of ubiquitinated AUX/IAs and denoted with bracket (“GST-IAA1/2-Ub_n”).

Supplementary Figure 20). The immunoblots were detected with antibodies against GST and against Ub. In both immunoblots, the amount of ubiquitinated IAA2 increased upon addition of auxin compared to 0 μ M IAA, and also the ubiquitinated species shifted towards a higher molecular weight with increasing auxin concentration (**Figure 2-13, Supplementary Figure 20**). This indicates that firstly, the IVU is much more sensitive to the addition of low concentrations of auxin when IAA2 is used as a target in contrast to IAA1. Secondly, this result demonstrates that auxin promotes the formation of ubiquitin chains on IAA2 target – poly- and/or multi-ubiquitination – likely due to an increased processivity of the auxin-stabilized

E3:target complex. Although IAA1 and IAA2 have assembled into auxin co-receptor complexes with similar K_D values in radioligand binding assays, it is conceivable that IAA1 and IAA2 exhibit different auxin-responsive behavior in the context of Ub conjugation. Therefore, also the effect of auxin concentrations above 600 nM in IVU reactions has to be tested in the future.

It is possible that the incubation times, which were chosen to analyze the IVU reaction (20 and 30 min in **Figure 2-12** and **Figure 2-13**, respectively), were too long. Thus, detecting an effect of auxin on the ubiquitination of IAA1 could have been masked, because the endpoint of maximum ubiquitination of target was reached in all samples. To better resolve the dynamics of ubiquitination of IAA1 and IAA2, a time course IVU was performed. For that, samples were taken at the start of the reaction (0 min) and after 1, 3, 6, 12, 24 and 36 min, thereby following progression of ubiquitination until the previously assessed end points (**Figure 2-12**, **Figure 2-13**). To get a detailed view on the effect of auxin on Ub conjugation dynamics, samples were prepared without or with 600 nM IAA. Both IAA1 and IAA2 were increasingly ubiquitinated over time. In α -GST-probed immunoblots, ubiquitination was detectable in all samples as early as one minute after the reaction was started (**Figure 2-14**). With progressing reaction time, increasing amounts of high molecular weight conjugates were detected in α -Ub and α -GST immunoblots. This is indicative of increasing ubiquitination over time (**Figure 2-14 A** and **B**). Again, for IAA1, the ubiquitination patterns in both immunoblots are almost identical when comparing mock and auxin-containing samples (**Figure 2-14 A**). This shows, that the ubiquitination of IAA1 indeed seems to proceed with the same rate *in vitro* whether or not 600 nM IAA are added. In contrast, the same concentration of auxin has a clear promoting effect on the IVU of IAA2 (**Figure 2-14 B**). In the absence of auxin, IAA2 is still ubiquitinated indicated by the higher molecular weight species in the α -GST immunoblot. However, the IVU without auxin fails to produce the high molecular weight Ub conjugates >60 kDa, that were clearly detectable in auxin-containing samples in the α -GST immunoblot (**Figure 2-14 B**). Also, despite unspecific background ubiquitination, the α -Ub immunoblot reveals a promoted IVU of IAA2 upon addition of auxin. This further corroborates the observation that IAA1 and IAA2 targets differ with regard to their processing by the SCF^{TIR1} ligase *in vitro*.

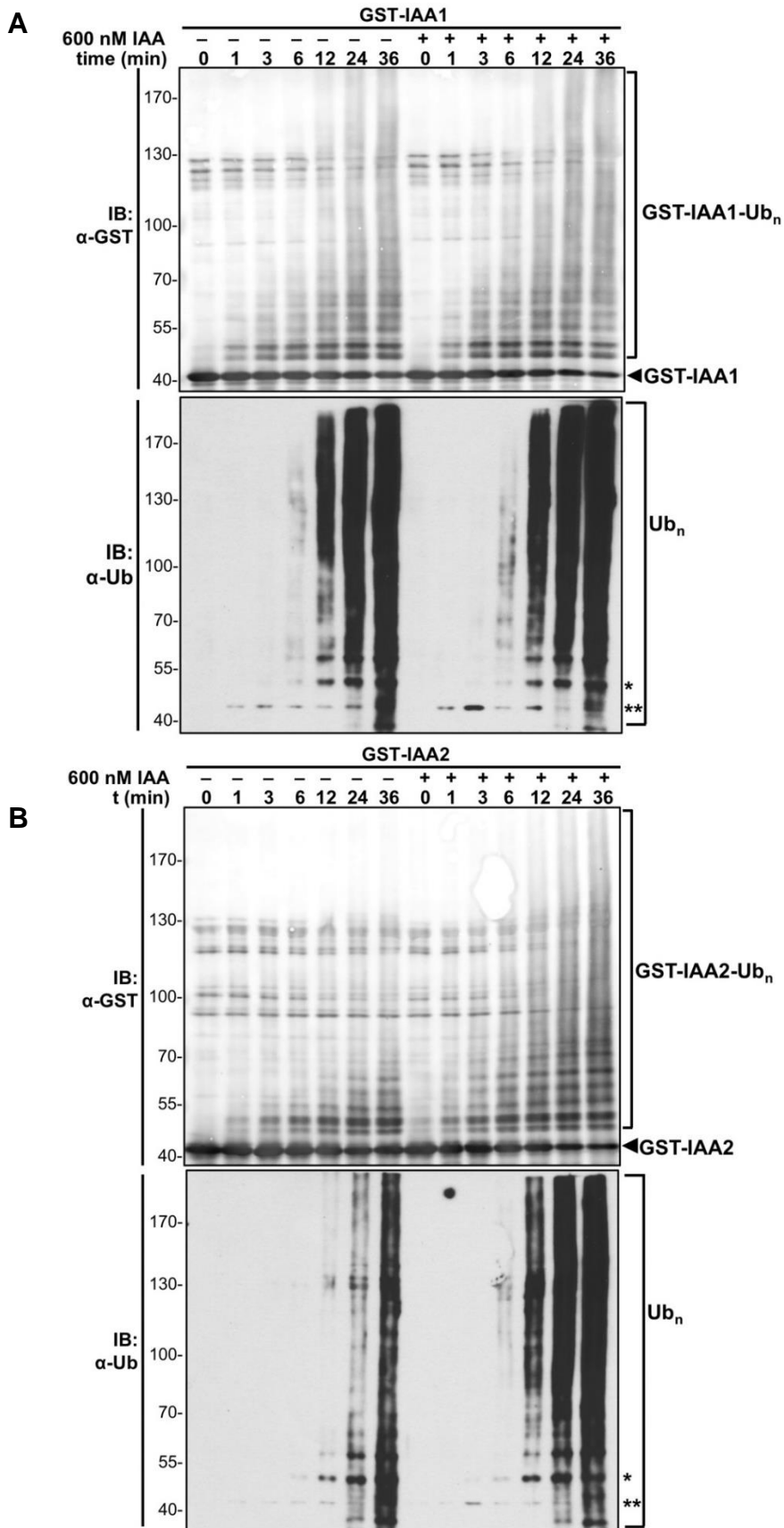


Figure 2-14: Time course of *in vitro* ubiquitination of targets IAA1 and IAA2 in the absence and presence of auxin
 Ubiquitination reactions were performed with wild-type IAA1 (A) and IAA2 (B) as targets in the absence and presence of 0.6 μ M IAA. Samples were taken at the start of the reaction (0 min) and after the reaction had proceeded for the indicated times. Samples were loaded on 5-15% gradient SDS-PAGE and probed with α -GST antibody (upper panel) for detection of the GST-tagged AUX/IAA targets, or with α -Ubiquitin (α -Ub; bottom panel)

antibody for detection of ubiquitinated protein species (denoted with bracket “Ub_n”) which might include ubiquitinated proteins other than AUX/IAA (see **Figure 2-11**). Ubiquitinated protein marked with one asterisk is likely monoubiquitinated target (GST-IAA1/2-Ub₁). Ubiquitinated protein marked by two asterisks is likely monoubiquitinated Cullin1 fragments (CUL1_N-Ub₁; CUL1_C-Ub₁). Unmodified targets GST-IAA1 and GST-IAA2 have a molecular weight of 46.8 kDa and 47.7 kDa, respectively, and are denoted with a black triangle (“GST-IAA1” or “GST-IAA2”) in the α-GST immunoblot. GST-protein species >40 kDa are therefore indicative of ubiquitinated AUX/IAs and denoted with bracket (“GST-IAA1-Ub_n” or “GST-IAA2-Ub_n”).

All in all, the biochemical characterization of IAA1 and IAA2 yielded key information about their contribution to co-receptor affinity and specificity for auxin, as well as their auxin-dependent ubiquitination by SCF^{TIR1}. Both ohnologs form auxin receptors with similar high affinity and preferably bind the auxins IAA and 4-Cl-IAA. In contrast, IAA1 and IAA2 ubiquitination following complex assembly with auxin and SCF^{TIR1} exhibits differences. Most interestingly, IAA2 ubiquitination seems to be highly auxin-responsive in contrast to IAA1.

2.1.3.6 *In vivo* studies on TIR1/AFB-IAA1/IAA2 auxin co-receptors

2.1.3.6.1 *Generation of transgenic lines for TIR1/AFB-IAA1/IAA2 co-receptor analysis*

To further elucidate the function of TIR1/AFB-IAA1 and -IAA2 auxin co-receptors and to complement our biochemical data, *in vivo* analyses of these co-receptors is mandatory. To this end, transgenic plant lines were generated and characterized in a preliminary, overview-like manner. In the future, these lines will serve to address questions regarding *in vivo* TIR1/AFB-IAA1 and -IAA2 co-receptor assembly, AUX/IAA ubiquitination, stability and ultimately auxin responses.

It is important to take into account that in only few cases, lof mutants of *AUX/IAAs* show mild phenotypes (Overvoorde *et al.*, 2005; Arase *et al.*, 2012). In contrast, their often severely and pleiotropically affected *gof* mutants have been key to studying the role of a number of *AUX/IAAs in planta* (Timppte *et al.*, 1994; Tian and Reed, 1999; Rogg *et al.*, 2001; Fukaki *et al.*, 2002; Hamann *et al.*, 2002; Tatematsu *et al.*, 2004; Ploense *et al.*, 2009; Rinaldi *et al.*, 2012). A forward genetic screen for auxin resistant mutants for instance was the platform for the identification of *axr5-1/iaa1* (Yang *et al.*, 2004). Unfortunately, no *gof* mutant is available for *IAA2* so far, which makes it uncharacterized to date. In another approach, a stabilized version of *IAA1* was expressed under an inducible promoter and the effects on auxin signaling were successfully studied (Park *et al.*, 2002). Similar approaches of conditional or constitutive overexpression of wild-type *AUX/IAA* have yielded hints for the physiological responses that specific *AUX/IAAs* are involved in (Worley *et al.*, 2000; Falkenberg *et al.*, 2008; Arase *et al.*, 2012; Yan *et al.*, 2013).

Therefore, here, an approach was chosen that aimed at stabilizing *IAA1* and *IAA2* proteins through overexpression. It is to expect, however, that the SCF^{TIR1/AFB} and UPS machinery is still efficient in degrading the high levels of overexpressed *AUX/IAA* protein. Thus, generating transgenic lines in *TIR1/AFB*-deficient backgrounds would aid to further stabilize overexpressed *IAA1* or *IAA2*. To this effect, both overexpression of *IAA1* or *IAA2* was combined with different *tir1/afb* mutant backgrounds (Dharmasiri *et al.*, 2005b; Parry *et al.*, 2009) in stably transformed lines (**Figure 2-15**). In addition to *AUX/IAA* stabilization, combining overexpression of *IAA1* or *IAA2* in a specific *TIR1/AFB*-deficient mutant will be informative under another aspect: By comparing the differential effects on *AUX/IAA* ubiquitination and stability, as well as auxin responses in different *tir1/afb* mutant backgrounds, combinatorial differences in *TIR1/AFB-IAA1/IAA2* co-receptor assembly could be elucidated (**Figure 2-15**).

Previously, tagged versions of AUX/IAAs have been proven useful for studying degradation and ubiquitination *in vivo* (Worley *et al.*, 2000; Dreher *et al.*, 2006; Gilkerson *et al.*, 2015). Therefore, transgenic plants were generated which overexpress *IAA1* or *IAA2* with an N-terminal *YELLOW FLUORESCENT PROTEIN (YFP)* fusion under the control of the cauliflower mosaic virus *35S* promoter. To focus on the major players among the TIR1/AFBs and to obtain a manageable set of transgenic lines, wild-type Col-0, single mutants *tir1-1*, *afb2-3*, *afb3-4*, and double mutants *tir1-1 afb2-3* and *tir1-1 afb3-4* (Parry *et al.*, 2009) were transformed via floral-dip with the *35S::YFP-IAA1*, *35S::YFP-IAA2* or control *35S::YFP*.

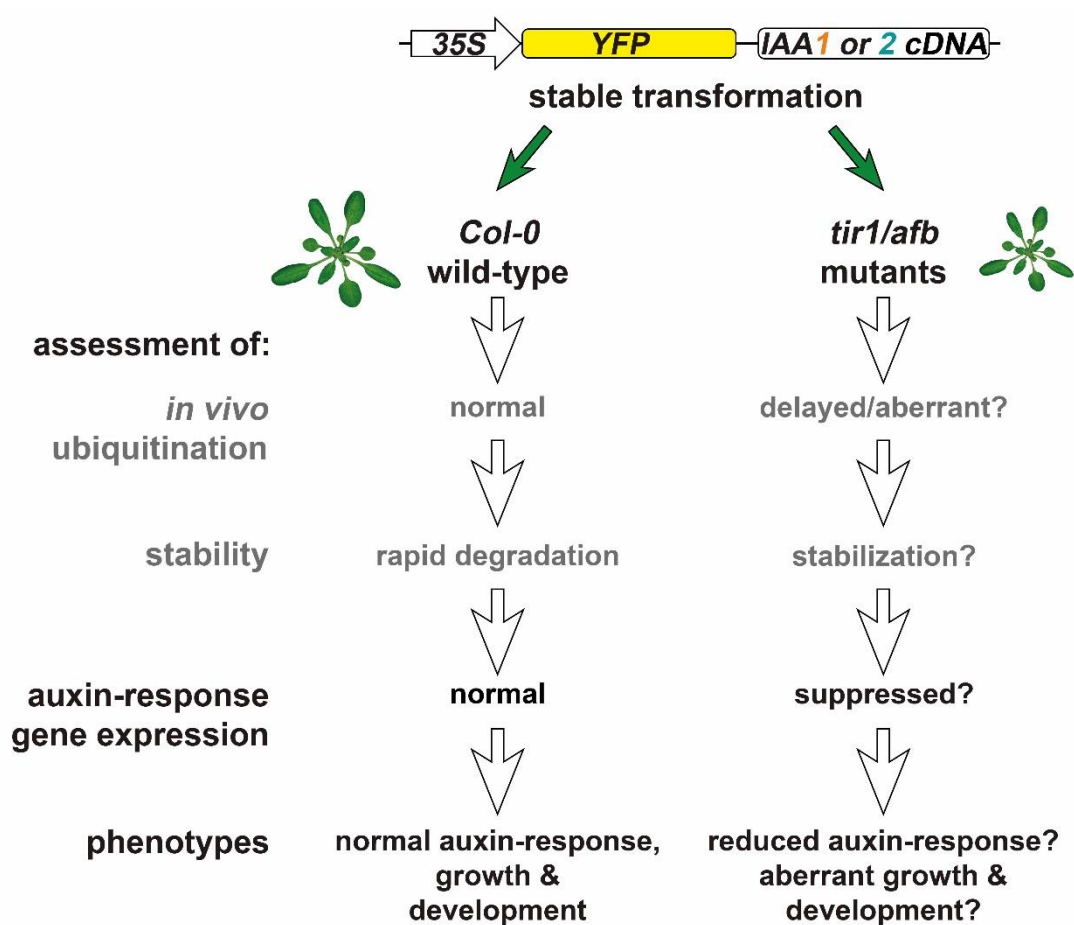


Figure 2-15: Schematic view of *in vivo* strategy to generate plant lines for co-receptor characterization

A. thaliana was stably transformed to overexpress N-terminal YFP fusions of *IAA1* or *IAA2* under a *35S* promoter in different genetic backgrounds. On the one hand, the transgene was expressed in wild-type, where the SCF^{TIR1/AFBs} machinery is fully intact and able to ubiquitinate and thereby destabilize the increased amount of YFP-*IAA1* or YFP-*IAA2* fusion protein (left). On the other hand, the transgene was expressed in different TIR1/AFBs-deficient backgrounds (*tir1/afb* mutants; right) (Dharmasiri *et al.*, 2005b; Parry *et al.*, 2009). Here, the SCF^{TIR1/AFBs} machinery lacks one or two F-Box components for AUX/IAA recognition and the signaling cascade might be impaired due to increased YFP-*IAA1* or -*IAA2* levels. This approach allows comparing differential ubiquitination and degradation of YFP-*IAA1* or YFP-*IAA2* and downstream effects such as auxin response gene expression and ultimately, auxin-related phenotypes between wild-type and mutant backgrounds. Thereby, hints for *in vivo* assembly and function of TIR1/AFB-*IAA1/IAA2* co-receptors can be obtained. Differential ubiquitination and degradation (gray) were not assessed in frame of this thesis, but preliminary data on auxin response gene expression could be obtained, and phenotypic assessment was initiated.

To begin with, a number of independent transformants, which show a range of expression levels, were to be established. These transformants could then be drawn upon for different purposes: For analyses that require high amounts of fusion protein, lines with high overexpression could be chosen. For a comparative analysis of how auxin responses are affected, representative, medium overexpressor lines would serve for generating crosses to obtain all mutant allele combinations with the same transgene insertion. Thus, two to three homozygous transgenic T3 lines from independent T1 individuals were established for each combination of transgene and genetic background (Table 2-2 and **Supplementary Table 7**).

Table 2-2: Selection of transgenic T3 lines

Transgenic Arabidopsis lines were generated that overexpress YFP alone (\emptyset ; empty vector control), or N-terminal YFP fusions of IAA1, IAA2, IAA7, or IAA12 under control of a 35S promoter. Constructs for expression of transgenes with BASTA resistance marker were transformed into wild-type (Col-0) or mutant backgrounds (*tir1-1*, *tir1-1 afb2-3*, *tir1-1 afb3-4*). Seeds from transformed plants were first selected for about ten BASTA resistant T1 individuals, and individual transformants were numbered (#1, #2, #3...). Next, T2 seeds were tested for approximate 3:1 segregation on selection medium to ensure single insertions, and candidate lines were checked for YFP expression in seedlings via fluorescence microscopy. T3 seeds derived from individual candidate T2 lines were numbered with a second numeral (e.g. #4.1, 4.2, 4.3...) and tested for homozygosity on selection medium. Ultimately, several homozygous T3 lines were established for part of the material. Lines in gray were excluded from the following analyses presented in this thesis (partly due to bad germination or ambiguous segregation). A comprehensive listing of transgenic lines can be found in **Supplementary Table 7**.

35S::YFP			
homozygous T3 lines	- \emptyset	-IAA1	-IAA2
<i>Col-0</i>			
<i>tir1-1</i>	- #4.9, #4.5, #4.6, #4.10 - #5.6, #5.7	- #3.5, #3.3 - #7.9 - #8.8, #8.2, #8.6	- #1.1, #1.2, #1.5 - #2.8 - #3.4, #3.9
<i>tir1-1 afb2-3</i>	- #3.1 - #6.10	- #1.10, #1.1, #1.8, #1.9 - #2.10 - #3.1, #3.10	- #1.1, #1.5 - #3.4, #3.2 - #6.1
<i>tir1-1 afb3-4</i>	- #4.7, #4.1 - #6.10	- #4.6 - #7.9 - #10.9	- #4.6, #4.2, #4.8, #4.9 - #5.9, #5.2 - #8.2, #8.4, #8.9

2.1.3.6.2 IAA1 and IAA2 overexpression hints at differential posttranscriptional regulation

Transgene expression among independent transformants can differ greatly depending on the insertion site of the transgene into the genome, depending on the copy number of insertions, or due to silencing effects (Glowacka *et al.*, 2016). To exclude multiple insertions, a segregation analyses for a 3:1 ratio in T2 lines was performed. However, it has been shown that multiple insertions can still occur for example at a single locus that cannot be detected by segregation analysis (Glowacka *et al.*, 2016). The transgene transcript level in 5-day old seedlings of T3 lines was determined through reverse transcription quantitative real-time PCR (RT-qPCR) using primer combinations specifically amplifying only the YFP fusions of IAA1 or

IAA2 and no endogenous transcripts (**Figure 2-16**). In all lines, an overexpression of at least 5-fold up to about 266-fold over the reference gene *PP2A* was detected, except for *YFP-IAA2* in the *tir1-1 afb2-3* background where no transgene transcript was detected (**Figure 2-16**). For *YFP-IAA1* overexpressing lines, a wide range of transcript levels was detected ranging from 22- to 266-fold compared to *PP2A* reference. The *YFP-IAA2* overexpression was clearly lower, ranging from only 5- to 15-fold compared to *PP2A* reference (**Figure 2-16**). This could hint at a posttranscriptional regulation of *IAA2*, which suppresses higher transcript levels, whereas *IAA1* transcript levels do not seem to be affected.

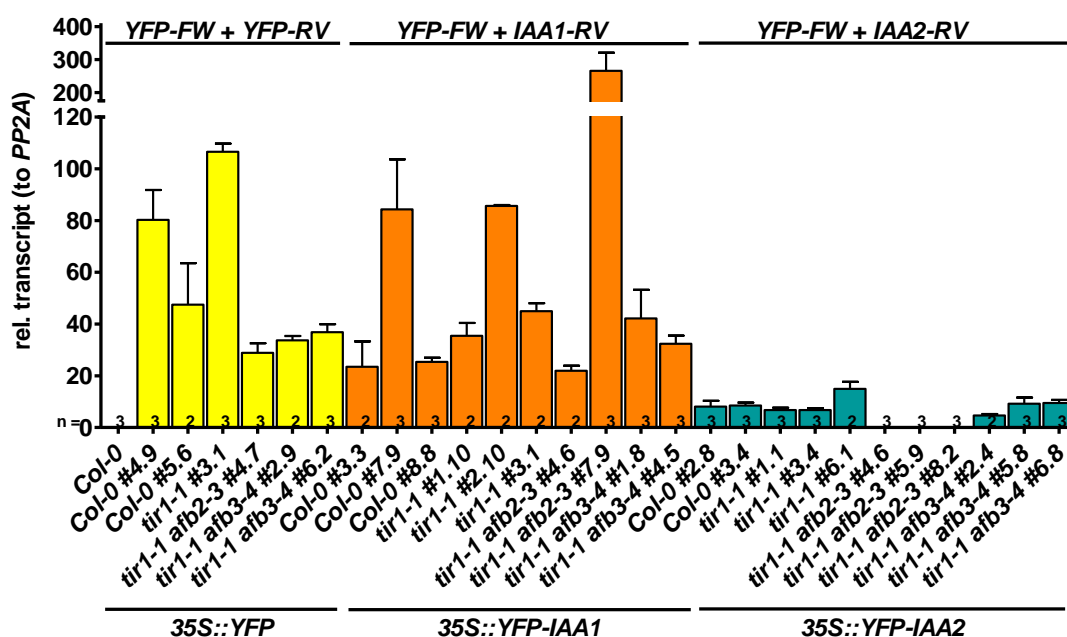


Figure 2-16: Transcript levels of transgenic *YFP-IAA1* and *-IAA2* overexpressor lines

Homozygous T3 lines overexpressing *YFP* (empty vector control; yellow), *YFP-IAA1* (orange) and *YFP-IAA2* (teal) in various genetic backgrounds were derived from independent lines. RNA from 5-day old seedlings was extracted, reverse-transcribed and analyzed for the transgene expression level through RT-qPCR using primers amplifying transcript of *YFP* fusions only (forward primer: *YFP-FW*, reverse primer: *IAA1-RV* or *IAA2-RV*, respectively). Transcript levels are displayed relative to the constitutively expressed reference gene *PP2A* (Czechowski *et al.*, 2005). The number of biological replicates that were analyzed for each sample is given at the bottom of each bar (n=2-3). Error bars denote standard error.

Considering the endogenous transcript levels of *IAA1* and *IAA2* (**Figure 2-3 A** and **Supplementary Figure 4** to **Supplementary Figure 6**), the overexpression of transgene versus endogenous expression levels is highly contrasting between *IAA1* and *IAA2* (**Supplementary Figure 22 B**). Levels of endogenous *IAA1* and *IAA2* transcript in wild-type Col-0 (**Supplementary Figure 22 A**) were drawn upon to roughly estimate a fold-ratio of transgenic expression compared to endogenous levels (**Supplementary Figure 22 B**). While *YFP-IAA1* transcript in transgenic lines is around 11- to 135-fold higher than endogenous *IAA1* transcript in wild-type, *YFP-IAA2* transcript levels in transgenic lines show a 0.6- to 2-fold overexpression

over the endogenous wild-type *IAA2* levels (**Supplementary Figure 22 B**). Again, this hints at a more stringent control of the amount of *IAA2 in planta* at the transcript level.

The independent transformants that were generated yielded a range of overexpression levels for *YFP-IAA1* and *-IAA2*. In order to choose lines suitable for further analyses, an assessment of the frequency distribution of relative transcript levels was performed for each *YFP-IAA1* and *-IAA2* overexpressors (**Figure 2-17** and **Supplementary Table 8**). Lines with transgene levels in the interquartile range were grouped as “medium overexpressors”. These are most representative with regard to overexpression levels and will be suitable for crosses into various backgrounds for subsequent phenotypic analyses. Lines with transgene levels in the upper and lower quartile are grouped as “high” and “low overexpressors”, respectively. These lines are considered outliers with regard to transcript levels (**Figure 2-17** and **Supplementary Table 8**). Nevertheless, high overexpressor lines could potentially be useful for analyses that require high amount of protein for immunoprecipitation-based approaches for instance. When T2 seedlings, which were further propagated to T3 lines listed in **Table 2-2**, were microscopically screened for YFP expression, YFP-expressing control lines showed strong fluorescence signal throughout the whole seedling. In contrast, all *YFP-IAA1* and *YFP-IAA2* overexpressors exhibited weak, diffuse fluorescence signal (data not shown). This suggests that *IAA1* and *IAA2* mediate destabilization of YFP. T2 seedlings showing higher YFP expression were observed as well, but these did not show 3:1 segregation and were therefore disregarded. Interestingly, the *35S::YFP-IAA1 (tir1-1afb2-3)* #7.9 line showed a weak fluorescence signal with distinct punctae of stronger fluorescence (data not shown). This could be indicative of overexpressed *YFP-IAA1* aggregates or strong nuclear expression, which requires further validation in T3 lines.

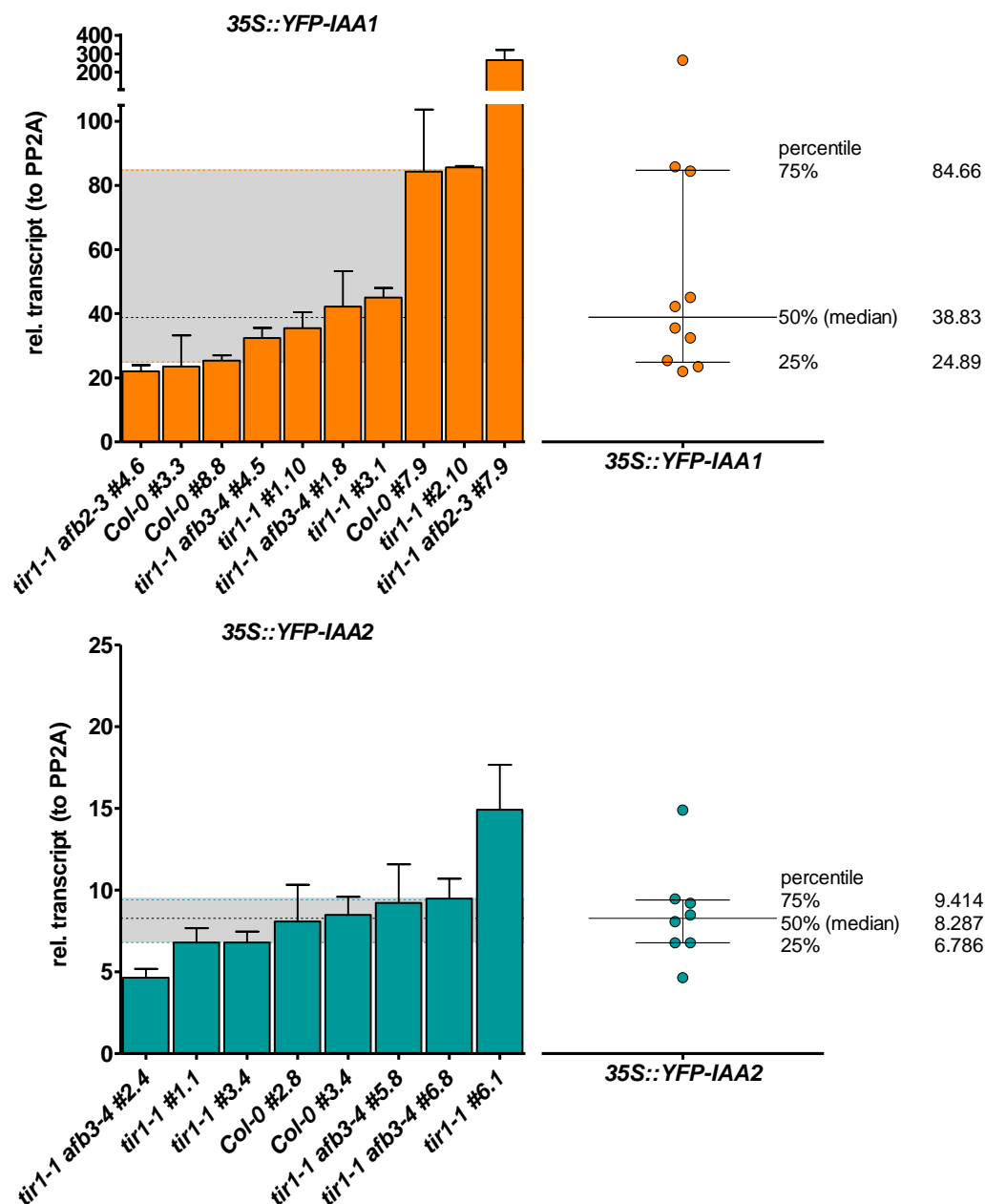


Figure 2-17: Grouping and frequency distribution of expression levels in overexpressor lines

Transcript level data shown in **Figure 2-16** was analyzed with regard to frequency distribution and displayed as a box plot (right) including lines demarking percentiles, and as a bar graph (left) that displays the individual transgenic lines falling into the respective percentiles. While the interquartile range is shadowed in light gray and represents the “medium overexpressor” group, the quartile below was grouped as “low overexpressors” and the quartile above as “high overexpressors”. The lines showing no overexpression of *YFP-IAA2* in the *tir1-1 afb2-3* mutant background were excluded from this analysis. Listing of the lines according to groups shown in **Supplementary Table 8**.

2.1.3.6.3 Overexpressor lines show stabilized *YFP-IAA1* and *YFP-IAA2* protein levels

AUX/IAA protein levels are crucial for the regulation of auxin transcriptional response. When AUX/IAA proteins are stabilized, they suppress normal auxin signaling (Chapman and Estelle,

2009). Therefore, in overexpression lines generated here, after confirming increased *IAA1* and *IAA2* transcript levels, AUX/IAA protein levels needed to be assessed. Since AUX/IAAs are highly unstable proteins, it proved challenging to detect YFP-fusion protein in crude extracts from transgenic seedlings (data not shown). AUX/IAA turnover mediated by the remaining members of TIR1/AFB family seems to be still highly efficient in these lines despite the *IAA1/IAA2* overexpression, the N-terminal YFP-tag, and the partial TIR1/AFB deficiency. Therefore, an α -GFP immunoprecipitation step (GFPtrap) was applied to enrich YFP-fusion protein from crude extract of 7-day old seedlings of transgenic lines. YFP fusion proteins of interest were then detected in immunoblots with α -GFP antibody.

In samples from lines stably transformed with empty vector control which express YFP alone, high amounts of YFP could be successfully recovered (**Figure 2-18 A**). In contrast, in samples from lines overexpressing YFP-*IAA1* or YFP-*IAA2* in different genetic backgrounds, much lower amounts of fusion protein were detected in immunoblots (**Figure 2-18 A**). This is indicative of short-lived *IAA1* and *IAA2* mediating the destabilization of their respective YFP fusions, as shown previously with an *IAA1*-LUC translational fusion (Worley *et al.*, 2000). High amounts of free YFP were detected in YFP-*IAA1* samples, suggesting a significant fraction of fusion protein undergoes cleavage of the tag (**Figure 2-18 A**).

To enhance the detection of highly unstable YFP-*IAA1* and YFP-*IAA2*, seedlings were treated with 50 μ M of proteasome inhibitor MG-132 for 16 hours before harvest. Clearly, YFP-*IAA1* and -*IAA2* fusions were stabilized upon MG-132 treatment, confirming that *IAA1* and *IAA2* destabilization mainly occurs via the UPS (**Figure 2-18 A**). YFP-*IAA2* in wild-type background was not detectable in immunoblots even when treated with MG-132. To detect even small amounts of YFP-*IAA2*, the same immunoprecipitation samples were additionally immunoblotted with adjusted loading (**Figure 2-18 B**), in contrast to equal loading presented in **Figure 2-18 A**.

When comparing different genetic backgrounds, both YFP-*IAA1* and -*IAA2* levels were most destabilized in Col-0 wild-type backgrounds. As expected upon partial TIR1/AFB deficiency, i.e. in *tir1-1*, *tir1-1 afb2-3*, and *tir1-1 afb3-4* mutant backgrounds, YFP-*IAA1* and -*IAA2* became at least partially stabilized (**Figure 2-18 A and B**). The protein levels differed between independent transformants and between single and double mutants (**Figure 2-18 A and B**, **Supplementary Figure 24**), thus preventing a conclusion about the role of a single TIR1/AFB on *IAA1* or *IAA2* degradation.

YFP-IAA2 levels were overall lower than YFP-IAA1 levels (**Figure 2-18**) or even undetectable in some immunoblot analyses (**Supplementary Figure 24**), which is likely due to the limited overexpression of *YFP-IAA2* shown in the transcript analyses (**Figure 2-16**). However, a differential destabilization of IAA1 and IAA2 cannot be ruled out.

Furthermore, high molecular weight species were detected with α -GFP immunodetection in YFP-IAA1 samples from mutant backgrounds (**Figure 2-18 B**). While the bands around 80-90 kDa are likely oligomeric forms of YFP-IAA1, the 50-80 kDa YFP-IAA1 species prompted us to speculate that also ubiquitinated forms of YFP-IAA1 might have been immunoprecipitated. Unfortunately, probing the GFP-trap samples with α -Ub antibody could not confirm this (data not shown).

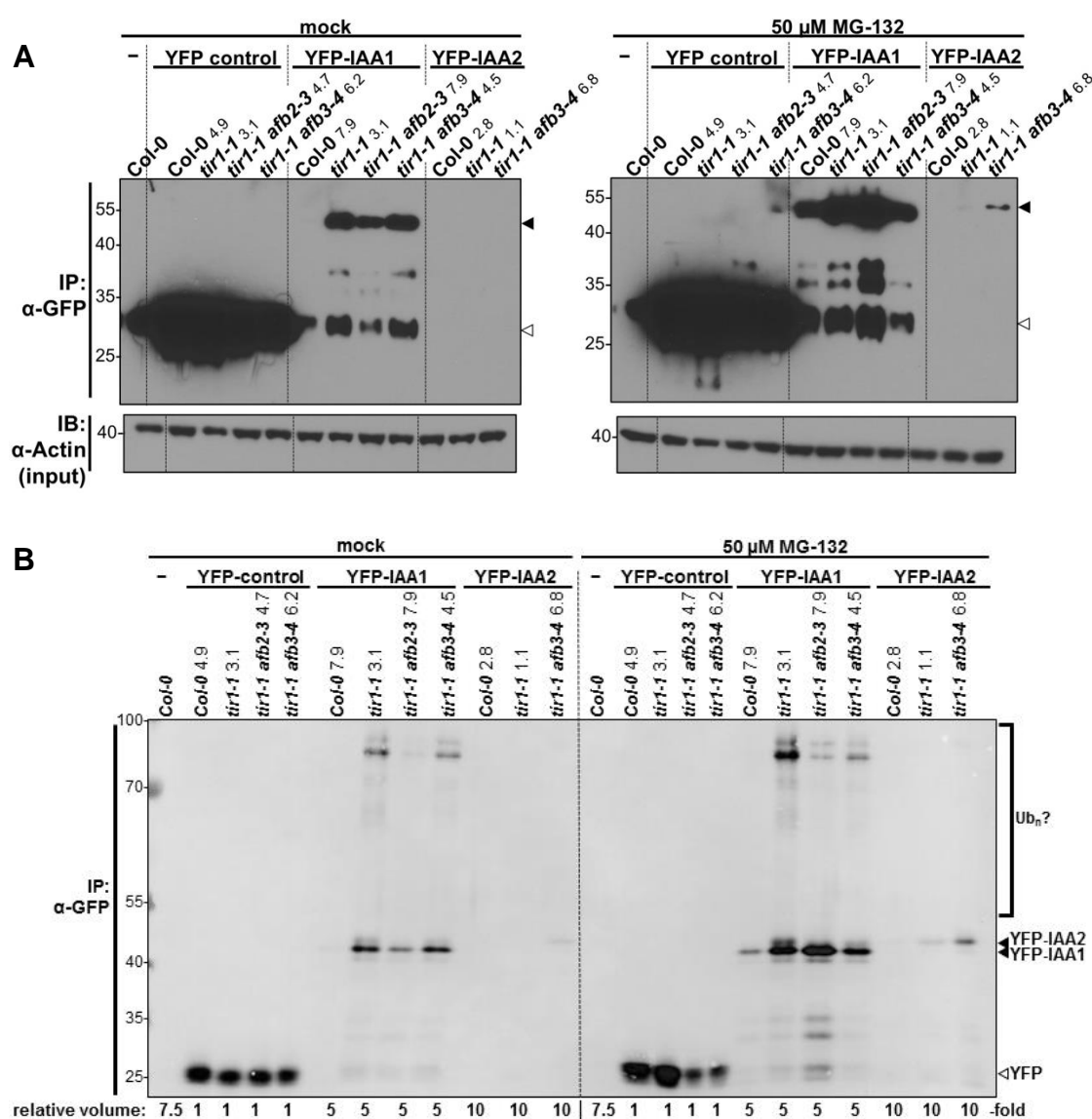


Figure 2-18: Overexpressed YFP-IAA1 or YFP-IAA2 proteins can be recovered from *35S::YFP-IAA1* or *35S::YFP-IAA2* transgenic lines and are stabilized upon MG-132 treatment

7-day old seedlings of T4 transgenic lines were treated with 50 μ M MG-132 (right) or mock (left) for 16 hours, protein extracts were prepared and YFP-IAA1 and YFP-IAA2 fusion protein was enriched by immunoprecipitation

through α -GFP-beads (GFPtrap). Two different immunoblots of the same set of samples are shown. **A.** Equal amounts of GFPtrap samples were loaded and probed with α -GFP antibody to detect YFP fusion proteins. Filled triangles denote YFP-IAA1 (53.7 kDa), open triangles denote YFP (26.6 kDa). For loading control, input protein extract was probed with α -Actin antibody (input). **B.** For more nuanced detection, relative amounts of the same samples as in (A) were loaded as indicated on the bottom of the immunoblot. Thereby, overexposure in YFP control samples could be reduced, and low YFP-IAA2 levels could be detected. Also, high molecular weight species (bracket denoted with "Ub_n?") were detected. Filled triangles denote YFP-IAA1 and -IAA2 (53.7 kDa and 56 kDa, respectively), open triangle denotes YFP (26.6 kDa). Analysis of more lines is shown in **Supplementary Figure 24**.

Taken together, this *in vivo* approach shows that IAA1 and IAA2 proteins can be stabilized through combining transcriptional overexpression, and translational YFP fusion with a TIR1/AFB-deficient mutant background. YFP-AUX/IAA fusions, at least those from YFP-IAA1, can be recovered from plant material, and therefore, serve for further immunoprecipitation-based approaches, such as analysis of *in vivo* AUX/IAA ubiquitination for instance.

2.1.3.6.4 Outlook on future *in vivo* studies

To identify the specific auxin-responses that IAA1 and IAA2 are involved in, phenotypic analyses of the generated transgenic lines that exhibit diminished IAA1 and IAA2 turnover will be informative. IAA1 stabilization causes auxin-related phenotypes, such as resistance in root growth inhibition upon auxin treatment, smaller rosettes in adult plants, reduced hypocotyl elongation in dark-grown seedlings (Park *et al.*, 2002; Yang *et al.*, 2004). Some of the transgenic lines generated in this work exhibited root, hypocotyl, leaf and overall growth phenotypes (**Supplementary Figure 25** and **Supplementary Figure 26**), which, however, could be arbitrary due to transgene insertion affecting unrelated genes. To estimate whether *YFP-IAA1* or *-IAA2* overexpression levels might be the cause for auxin-related phenotypes, we performed a correlation analyses. To this end, a preliminary assessment of auxin-related phenotypes in the T4 generation of *YFP-IAA1* and *YFP-IAA2* transgenic lines was implemented, guided by previously published phenotypes of the *axr5-1* mutant and conditional *IAA1* overexpressor lines (Park *et al.*, 2002; Yang *et al.*, 2004) (**Supplementary Figure 27** to **Supplementary Figure 36**). Following this, Pearson correlation coefficients were determined for *YFP-IAA1* or *YFP-IAA2* transcript levels (as shown in **Figure 2-16**) versus phenotypic data from different experiments assessing phenotypes in the respective lines (see **Supplementary Table 9** and **Supplementary Table 10** for *35S::YFP-IAA1* and *35S::YFP-IAA2* lines). While no correlation was found between *YFP-IAA1* transcript levels and most of the phenotype datasets, there was negative correlation between *YFP-IAA1* transcript levels and hypocotyl elongation in dark grown seedlings (Pearson correlation coefficients: -0.71, -0.79, -0.65; **Supplementary Table 9**). This shows that, at least for this particular auxin-related phenotype, higher amounts of *IAA1* transcript, and therefore, likely stabilized IAA1 protein levels, lead to impairment of auxin response in dark-grown hypocotyls. This is consistent with findings from

Yang *et al.* (2004) and Park *et al.* (2002). For *YFP-IAA2* lines, no conclusive correlations have been found between transcript levels and phenotypic output (**Supplementary Table 10**), which could be in part due to the small sampling size of *YFP-IAA2* lines. Nevertheless, as mentioned above, a uniform transgene insertion is mandatory for future in depth phenotypic analysis. To obtain comparable transgenic lines, *YFP-IAA1* and *YFP-IAA2* medium overexpressor lines will be used for crossing into higher order *tir1/afb* mutant backgrounds (**Supplementary Table 11**).

All in all, a comprehensive array of transgenic *35S::YFP-IAA1* and *35S::YFP-IAA2* lines in different *tir1/afb* mutant backgrounds was generated. These transgenic lines cover a spectrum of transgene overexpression and serve to recover AUX/IAA protein from plants. They represent a toolset for different future *in vivo* analysis, such as analysis of *in vivo* AUX/IAA ubiquitination and turnover, or identification of specific IAA1- or IAA2-mediated responses.

2.2 Redefining the degron

A degradation signal or 'degron', is usually defined as a minimal element within a protein that is sufficient for recognition and degradation by a proteolytic apparatus (Varshavsky, 1991; Ravid and Hochstrasser, 2008). While the GWPPV core sequence is absolutely necessary for AUX/IAA degradation, it is not sufficient, since additional residues flanking this degron core are required for low protein accumulation (Ramos *et al.*, 2001). A number of findings suggest that regions outside the 13-amino acid primary degron contribute to differential co-receptor assembly (Calderón Villalobos *et al.*, 2012) and AUX/IAA destabilization (Worley *et al.*, 2000; Dreher *et al.*, 2006; Havens *et al.*, 2012). This is in line with the concept that a degron does not solely consist of the *primary degron* comprising conserved residues (Guharoy *et al.*, 2016). Several other prerequisites have to be fulfilled for a target to be recognized for degradation by the 26S proteasome. As a *secondary degron*, one or more target lysines providing a ubiquitination zone for attachment of a polyubiquitin tag are required (Thrower *et al.*, 2000; Mattioli and Sixma, 2014). Finally, as a *tertiary degron*, an unstructured region, so called initiation site, is required for efficient engagement by the proteasome (Prakash *et al.*, 2004; Fishbain *et al.*, 2011). Together these constitute the *tripartite degron* (Guharoy *et al.*, 2016). Furthermore, the primary degron is often located within an intrinsically disordered region and the initiation site is often located in proximity to the ubiquitination zone (Guharoy *et al.*, 2016). These requirements seem to apply clearly to AUX/IAAs, since beside a primary degron (Ramos *et al.*, 2001), they are predicted to be intrinsically disordered in their N-terminal part flanking the primary degron (**Supplementary Figure 17**). The degron-flanking region therefore

likely serves as initiation site, or tertiary degron. In addition, we recently identified ubiquitination zones that lie in unstructured, flexible regions based on *in vitro* AUX/IAA ubiquitination data (Winkler *et al.*, under review).

Interestingly, the sequence composition of disordered regions has recently been shown to influence degradation (Fishbain *et al.*, 2015), which additionally supports the hypothesis that the highly divergent degron-flanking regions of AUX/IAAs (**Supplementary Figure 1**) contribute to their differential stability. Moreover, van der Lee *et al.* (2014) proposed that natural variation in the length and position of intrinsically disordered regions might contribute to differential protein half-lives.

With the objective to map regions outside the conserved primary degron that contribute to differential co-receptor assembly and stability, we focused on studying regions flanking the AUX/IAAs primary degron. Originally, experimental approaches to map the primary degron were based on truncating AUX/IAAs and subsequently assessing the stability of those truncations (Worley *et al.*, 2000; Ramos *et al.*, 2001). While this has been a valid and fruitful approach in the past and in our collaborative efforts (Guseman *et al.*, 2015; Moss *et al.*, 2015), it arguably has its limitations. Truncations are linear along the primary protein structure. However, the secondary and tertiary protein structure has to be considered, as it is crucial to protein function. Not only the three-dimensionality of rigidly folded, but also of highly dynamic structures must not be neglected. Therefore, in this work, a chimera approach was employed to map regions outside the primary degron that contribute to auxin co-receptor assembly and subsequent destabilization of AUX/IAAs. By using full-length chimeric AUX/IAAs it is more likely to preserve the folded or dynamic three-dimensional properties necessary for co-receptor complex formation, ubiquitination and subsequent degradation.

In order to narrow down features that contribute to a high or low affinity auxin co-receptor complex, two AUX/IAAs were selected for chimera design that had been shown to equip TIR1-containing auxin co-receptors with distinct affinities for complex assembly. In radioligand binding assays, the apparent K_D values for auxin co-receptor TIR1-IAA7 and TIR1-IAA12 complex formation were determined to be ~10 nM and ~300 nM, respectively (Calderón Villalobos *et al.*, 2012). Thus, IAA7 and IAA12 were promising candidates for this approach. Both IAA7 and IAA12 differ in their primary degron sequence. Replacing two crucial residues in the IAA12 primary degron for the conserved IAA7 GWPPVR residues could not restore high affinity for auxin (Calderón Villalobos *et al.*, 2012). This further corroborates that distinct features outside the primary degron equip IAA7 and IAA12 with unique properties in an auxin sensing complex. Comparison of IAA7 and IAA12 primary structure reveals regions

AUX/IAA

4-module chimera



5-module chimera



reduced compactness / disordered

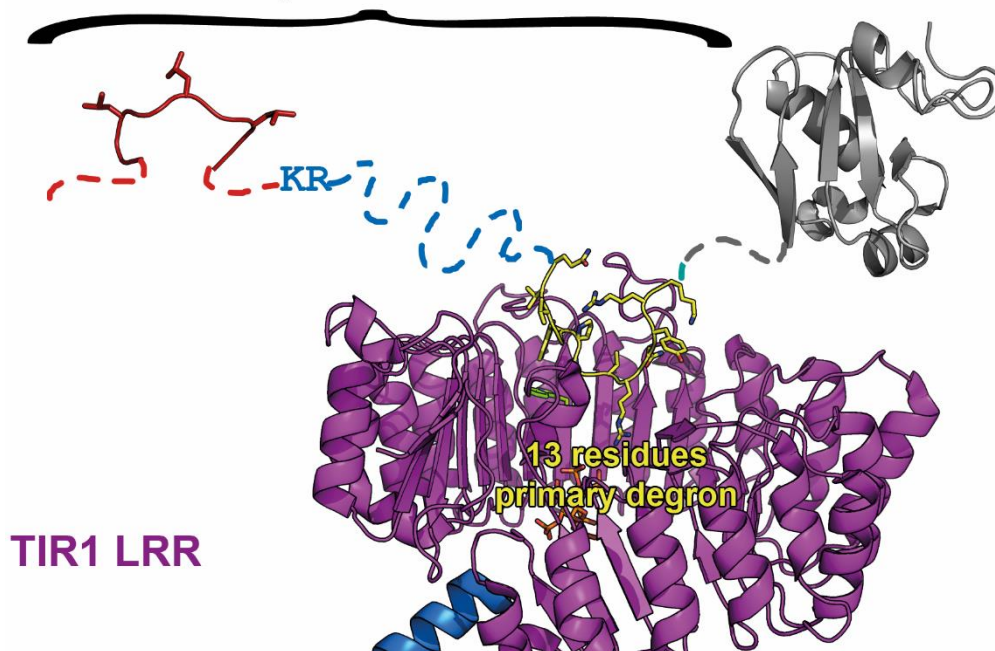


Figure 2-19: Scheme of chimera modules and regions of AUX/IAAs

Structural representation of TIR1 LRRs (purple cartoon representation) with auxin (green stick representation) bound at the bottom of the TIR1 binding pocket and the 13-residue IAA7 degron peptide (i.e. primary degron; yellow cartoon with side chains in stick representation) binding on top (PDB code: 2P1Q; Tan *et al.*, 2007). AUX/IAA regions N- and C-terminal of the primary degron which are predicted to be structurally disordered are represented as dashed line (**Supplementary Figure 17**). The C-terminal structurally compact PB1 domain (Phyre2 model of IAA1 PB1 (Kelley *et al.*, 2015)) is shown as a grey cartoon representation. EAR motif residues are shown in the same conformation as in IAA1 in complex with OstPR2 (PDB code: 5C7F; Ke *et al.*, 2015). Two AUX/IAA schemes above the structural representation with the same color-code depict the design of four or five modules for the chimera approach. The 5-module chimera comprise the modules domain I-containing N-terminus (DI N-ter; red), linker (blue) delimited by the conserved KR duplet and the primary degron, primary degron (yellow), degron-tail (DT, turquoise), and PB1 domain (grey). 4-module chimera comprise the same modules, except that DT and PB1 domain are consolidated as a single module. Note that across AUX/IAAs, the DI N-ter, linker, as well as DT module are highly variable in length and sequence composition (**Supplementary Figure 1**).

surrounding the conserved primary degron are highly variable in length and amino acid content (**Supplementary Figure 3**, **Supplementary Table 3**), thus likely responsible for the differences.

An IAA7 truncation comprising the N-terminal part of the protein including the primary degron provided a TIR1-containing co-receptor with the same high affinity for complex formation as a full-length IAA7 (Calderón Villalobos *et al.*, 2012). Therefore, we hypothesized that additional determinants for co-receptor assembly lie in the N-terminal degron-flanking region. To examine the influence of that region, we designed modules for the chimeras the

following way. The 13-residue primary degron was defined as one module (module 3 “degron”), since its role is well-characterized, and it was shown to not influence co-receptor assembly alone. Furthermore, the degron-flanking C-terminal part of the AUX/IAA protein was defined as one module (module 4). It comprises a highly variable region which we termed the “degron-tail” (DT), as well as the highly conserved, structurally compact PB1 domain. The highly conserved KR duplet that has been suggested to be required for basal destabilization of AUX/IAAs (Dreher *et al.*, 2006), served as a suitable delimitation to specify two modules in the remaining N-terminal part of the protein: the domain I-containing N-terminus (DI N-ter; module 1), and the variable region between KR duplet and primary degron, which was termed the “linker” (module 2, **Figure 2-19**).

2.2.1 The influence of degron-flanking regions on auxin-dependent TIR1/AFB-AUX/IAA interaction is highly interconnected

Based on the hypothesis that additional determinants for co-receptor assembly lie in the N-terminal degron-flanking region, truncated chimeras with swapped modules 1 to 3 were generated and compared with full-length IAA7 and IAA12 in a Y2H assay for auxin-dependent interaction with TIR1/AFBs (**Supplementary Figure 38**). Full-length IAA7 interacted more strongly with TIR1/AFBs than full-length IAA12 which usually showed no or very weak TIR1/AFB interaction in yeast (as was shown before by Calderón Villalobos *et al.*, 2012). Interestingly, chimeras clearly grouped into weakly and strongly interacting ones. Whenever module 1 was IAA12-derived, chimeras interacted more strongly with TIR1/AFB1/AFB2 than those with an IAA7-derived module 1. This effect of IAA7- or IAA12-derived module 1 on interaction strength contrasted with full-length IAA7 and IAA12 interaction behavior, and indicates that the C-terminal DT+PB1-containing region likely has an effect on determining differences in auxin-dependent TIR1/AFB interaction. Also, expression of the AD-fusion of full-length IAA12 but none of the truncated chimeras lacking the DT+PB1-containing C-terminal part caused impaired yeast growth in our Y2H assays, suggesting a negative effect of the DT+PB1-containing region of IAA12 for overexpression in yeast (**Supplementary Figure 40**).

These observations prompted us to include the DT+PB1-containing C-terminal part, now corresponding to the fourth and fifth module, to obtain full-length chimeras for interaction analysis. For the 4-module approach, a C-terminal module that includes both DT and PB1 was used in swapping. For the 5-module approach, the C-terminal module was split into two individual modules DT and PB1 (**Figure 2-19, Supplementary Table 12**). The aforementioned preliminary assays were performed with 3-module combinations generated by overlap PCR, and Gateway-cloned into yeast vectors. This caused typical Gateway-cloning scars to be included. Therefore, full-length chimeras for subsequent assessments were GoldenGate-

assembled (Marillonnet and Werner, 2015). This ensured consistent two-residue linkers for tag fusion, scar-less module assembly, and no additional sequence extensions in 4- and 5-module chimeric constructs.

First, all 16 possible 4-module chimeras – including full-length IAA7 (7-7-7-7) and IAA12 (12-12-12-12) – were generated and tested for auxin-dependent interaction with TIR1 in yeast (**Figure 2-20 A**). Again, AD-chimeras grouped into weakly and strongly interacting ones. In contrast to the assessment of preliminary truncated chimeras (**Supplementary Figure 38**), this time, the shared chimeric module was the C-terminal DT+PB1-containing region (**Figure 2-20 A**; module 4; grey). All seven chimeras with IAA7-derived DT+PB1 grouped as strong interactors, while the seven chimeras with IAA12-derived DT+PB1 were weakly interacting, and also showed signs of toxicity to yeast as did full-length IAA12 (**Figure 2-20 A**). To test whether differences in protein expression levels caused these interaction patterns, crude protein preparations from diploid yeast used in the Y2H assay were used in immunoblot analysis and probed for AD-chimera levels. Interestingly, immunoblots showed higher amounts of protein, whenever the chimeric construct contained an IAA7-derived DT+PB1 module (**Supplementary Figure 40**). This suggests that the amount of AD-chimera fusion protein might be reflected in the observed interaction strength.

Since this effect in expression was correlated to module 4, we wanted to narrow down the region in this module of IAA7 and IAA12 that caused the observed differences. Overall, the primary structure of the two AUX/IAAs is highly conserved in the PB1 domain, but high variability in length and amino acid content are present in the loop connecting helices $\alpha 1$ and $\alpha 1'$ of PB1 domain (Han *et al.*, 2014; Dinesh *et al.*, 2015), in the C-terminus and, most interestingly, in the DT – the region connecting the highly conserved primary degron and the PB1 domain. It is likely that the observed differences between IAA7 and IAA12 in auxin-mediated TIR1 interaction are mediated by specific residues in the DT. Therefore, the C-terminal module was separated into a DT-containing and PB1-containing module resulting in 5-module chimeras (**Figure 2-19, Supplementary Table 12**).

To detect a possible influence of swapping the linker, the primary degron, or the DT, eight relevant 5-module chimeras were first tested in the Y2H system for differential auxin-dependent interaction with TIR1 (**Figure 2-20 B**). The expression levels of 5-module chimeras were not as strongly correlated with the reporter output (**Figure 2-20 B, Supplementary Figure 41**) as in the 4-module chimera assessment in yeast (**Figure 2-20 A, Supplementary Figure 40**). Unlike the 4-module chimeras, the 5-module chimeras interacted with TIR1 in dependency of auxin in a more similar manner, but differed from 7-7-7-DT7-7 and 12-12-12-

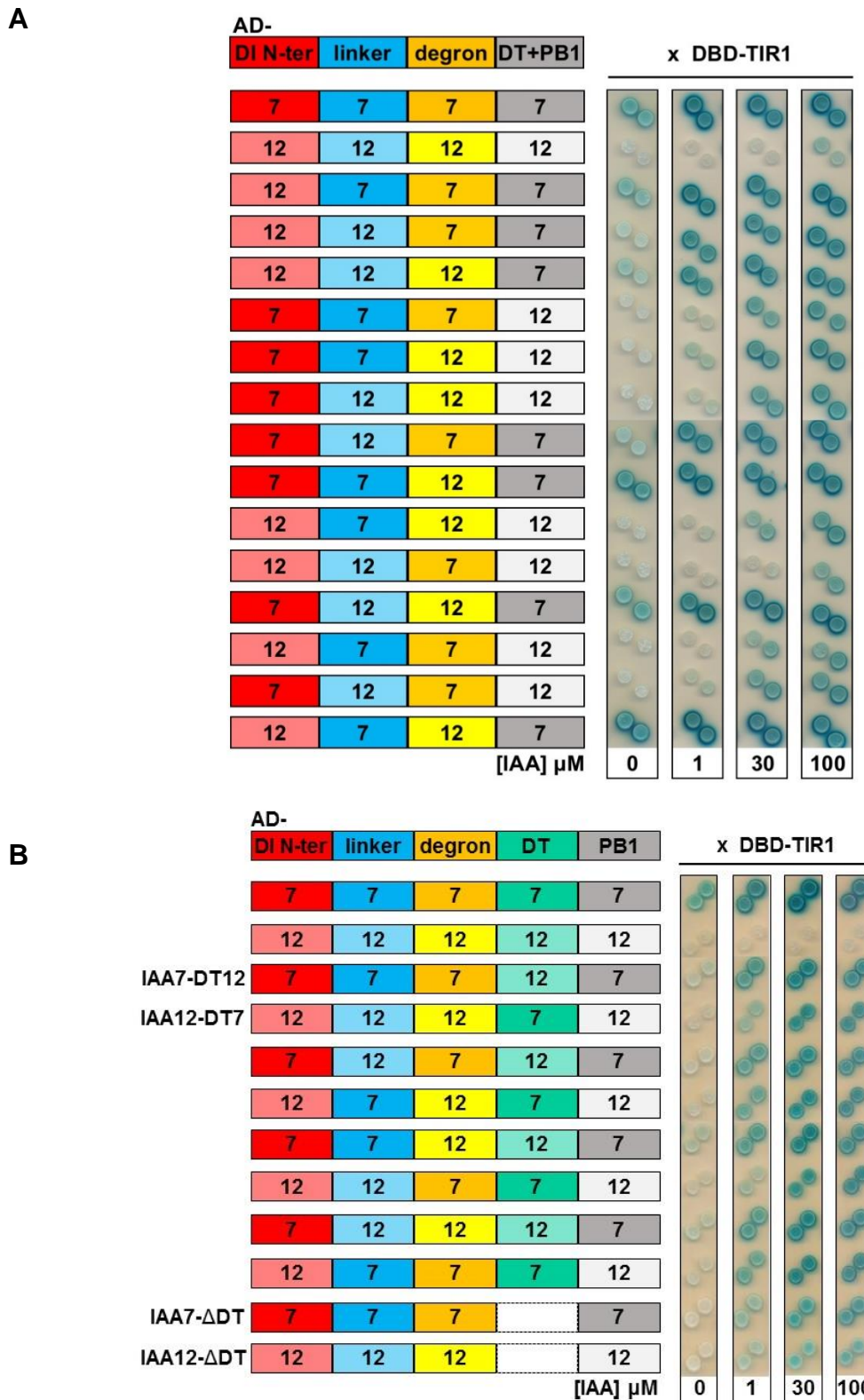


Figure 2-20: Auxin-dependent interaction of chimeric IAA7/IAA12 with TIR1 in yeast

Diploid yeast expressing full-length AD-chimeras and DBD-TIR1 were tested for β -Gal reporter activity on selective induction medium with 0, 1, 30, or 100 μ M IAA. Yeast cell dispersions of the same OD_{600} were spotted on selective induction medium plates and pictures taken after three days of growth at 30°C. **A.** AD-chimeras contain four modules as depicted in the scheme on the left: 1) DI N-ter (red), 2) linker (blue), 3) degron (yellow), 4) degron-tail (DT) and PB1 (grey). An independent experiment including interactions of AFB1 and AFB2 with chimeras is shown in **Supplementary Figure 39**. **Supplementary Figure 40** shows protein expression levels of 4-module chimeras in yeast. **B.** AD-chimeras contain five modules as depicted in the scheme on the left: 1) DI N-ter (red), 2) linker (blue),

3) degron (yellow), 4) DT (turquoise), 5) PB1 (grey). The two chimeras with a dashed white box in place of a DT module correspond to full-length IAA7 and IAA12 with a deleted DT module. **Supplementary Figure 41** shows protein expression levels of 5-module chimeras in yeast.

DT12-12 controls. 7-7-7-DT7-7 clearly showed interaction with TIR1 in the absence of auxin. Few of the chimeras showed very weak (7-7-7-DT12-7; 7-7-12-DT12-7; 7-12-12-DT12-7), and the remaining chimeras showed no basal interaction (**Figure 2-20 B**). Chimeras interacted more strongly with TIR1 at 1 μ M IAA, and even more at 30 μ M IAA, but interaction strength remained at the same level when IAA concentration was raised to 100 μ M (**Figure 2-20 B**). Slightly weaker or delayed response to an increasing auxin concentration was observed in chimeras 12-12-12-DT7-12 and 12-12-7-DT7-12 (**Figure 2-20 B**). Some weakly interacting chimeras shared an IAA12-derived DI N-ter and PB1. One could speculate that DI N-ter and PB1 might contribute to the weak or strong interaction of IAA12 and IAA7, respectively, with TIR1 in yeast. However, it is important to note that these common features do occur in other chimeras that do not show the same interaction behavior. Therefore, a definite influence of one region on co-receptor assembly cannot be concluded from these results. Rather, the results suggest a strong interplay of all regions in co-receptors assembly. This might be due to the highly flexible nature of degron-flanking regions. These regions might adopt an architecture with highly dynamic intramolecular, as well as intermolecular interactions upon association with TIR1.

To find out whether the DT is required for co-receptor assembly, an IAA7 and an IAA12 variant that each lack the DT (7-7-7- Δ DT-7 and 12-12-12- Δ DT-12) were included in the Y2H interaction assay. Both AUX/IAA variants were able to interact with TIR1 depending on auxin. The interaction was weaker compared with 7-7-7-DT7-7 and most of the chimeras, but interestingly, 12-12-12- Δ DT-12 interacted more strongly and in auxin-responsive manner compared with 12-12-12-DT12-12. This indicates that, on the one hand, the DT is likely dispensable for auxin-dependent interaction with TIR1. On the other hand, the observed very weak interaction of 12-12-12-DT12-12 with TIR1 and/or toxic expression of 12-12-12-DT12-12 in yeast might be caused by the IAA12 DT region or part of it.

2.2.2 The degron-tail (DT) is required for AUX/IAA destabilization *in vivo*

Since regions outside the primary degron have been implicated to play a role not only in co-receptor assembly but also in subsequent AUX/IAA destabilization (Worley *et al.*, 2000; Zenser *et al.*, 2001; Dreher *et al.*, 2006; Havens *et al.*, 2012), we used AUX/IAA degradation as yet another read-out to explore differences between AUX/IAA targets. We implemented a ratiometric auxin sensor approach (in collaboration with Sophia Samodelov and Matias Zurbriggen, University of Düsseldorf), where chimeric IAA7/IAA12 were expressed as firefly

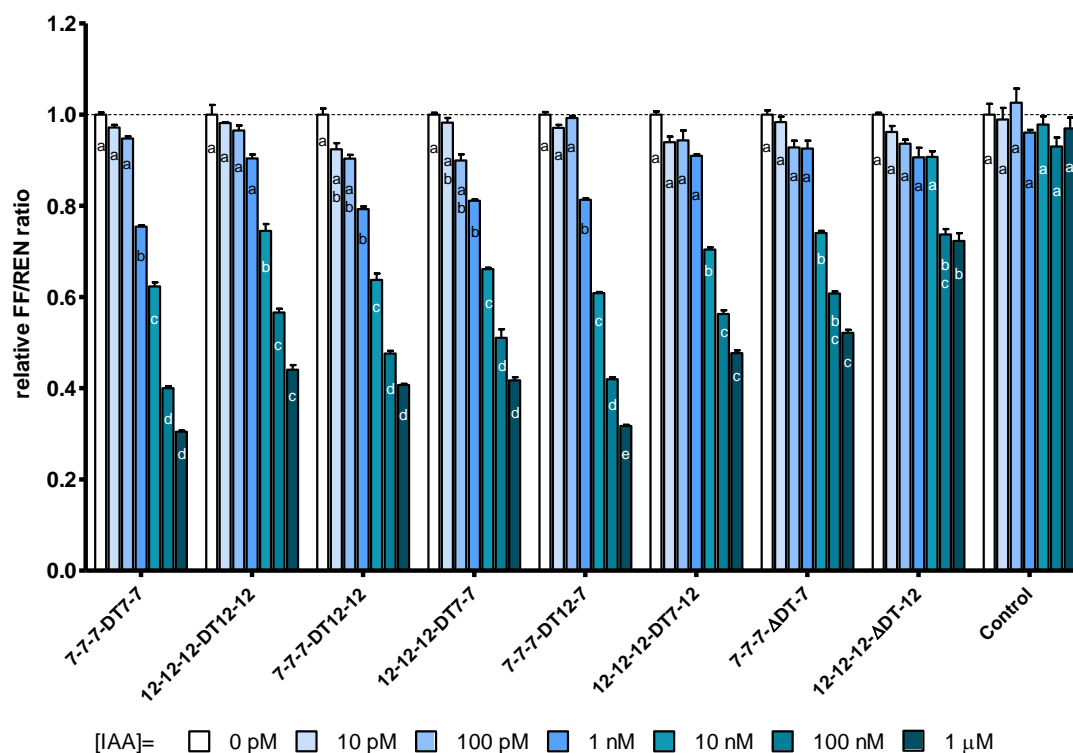


Figure 2-21: Auxin sensitivity of chimeric IAA7/IAA12 degradation in Arabidopsis mesophyll protoplasts

IAA7/IAA12 chimeras (see schemes in **Figure 2-19**, **Figure 2-20**, and **Supplementary Table 12**) were fused as sensor modules to firefly luciferase (FF) in frame with a self-splicing renilla luciferase (REN) fusion for normalization of expression and expressed in Arabidopsis mesophyll protoplasts (Wend *et al.*, 2013). Accordingly, a ratio below 1 indicates degradation of FF and sensor modules in relation to constant REN expression. This ratiometric quantification of FF/REN reporter activity was performed after 30 min incubation of protoplasts in indicated auxin concentrations ([IAA]), which gives a measure for auxin sensitivity of degradation of the respective chimera, and indirectly, allows conclusion about the degradation rates. Relative FF/REN ratios, normalized to 0 pM-added IAA for each construct are shown. A construct lacking an auxin-responsive sensor module served as a negative control (Wend *et al.*, 2013). Absolute FF and REN expression is shown in **Supplementary Figure 42**. Statistical contrast between concentration groups is shown for each construct indicated with lower case letters. One-way ANOVAs were performed from the raw data for each of the constructs individually with a Tukey-Kramer method in RLPLOT, with a p -value of < 0.05 .

luciferase (FF) fusions in frame with a self-splicing normalization construct of renilla luciferase (REN) in Arabidopsis protoplasts (Wend *et al.*, 2013). After addition of different concentrations of IAA, and subsequent normalization, the luciferase reporter signals provide a measure for auxin sensitivity of chimera degradation. Expectedly, addition of no auxin or picomolar IAA concentrations, did not cause a significant reduction in protein levels in any of the full-length or chimeric versions of IAA7 and IAA12 (**Figure 2-21**). While full-length IAA7 levels are significantly reduced upon incubation with 1 nM IAA, full-length IAA12 was only significantly reduced upon 10 nM IAA (**Figure 2-21**). Chimera 7-7-7-DT12-7 behaved similar to 7-7-7-DT7-7 in that a first significant reduction of protein was caused by incubation with 1 nM IAA. Incubation with 10 nM, 100 nM and 1 μM IAA each caused a significant reduction of protein for both chimeras 7-7-7-DT7-7 and 7-7-7-DT12-7. Also, chimera 12-12-12-DT7-12 behaved similar to 12-12-12-DT12-12. Their protein levels were significantly reduced upon

addition of 10 nM IAA and again upon addition of 100 nM IAA (**Figure 2-21**). This indicates that *in vivo* auxin sensitivity and degradation dynamics of IAA7 and IAA12 are not affected by DT swapping.

Interestingly, when the DT region was deleted from IAA7 or IAA12 (7-7-7- Δ DT-7 and 12-12-12- Δ DT-12), the proteins became stabilized. Significant protein level reduction of 7-7-7- Δ DT-7 and 12-12-12- Δ DT-12 could only be caused by IAA concentrations one order of magnitude higher compared to full-length controls 7-7-7-DT7-7 and 12-12-12-DT12-12, respectively (**Figure 2-21**). Especially 12-12-12- Δ DT-12 protein levels were not reduced as much as those of other chimeras tested, even at high IAA concentrations (**Figure 2-21**). This suggests that the DT region plays a role in auxin sensitivity and subsequent destabilization of IAA7 and IAA12 in general. Nevertheless, since swapping the DT did not impact auxin sensitivity of chimera degradation, the DT appears not to carry an IAA7- or IAA12-specific feature that is transferable among chimeric constructs.

Taken together, the assessment of AUX/IAA degron-flanking regions revealed that the AUX/IAA DT plays a role in AUX/IAA stability. Therefore, it might contribute to the AUX/IAA degron. Interestingly, the DT seems dispensable in the preceding auxin receptor complex formation. Therefore, its precise role in AUX/IAA turnover remains to be further characterized in future studies.

3 Discussion

3.1 Combinatorial events in auxin co-receptor assembly

The large combinatorial potential of TIR1/AFB1-5 and canonical AUX/IAAs has been proposed to provide plants with a plethora of specialized auxin-sensing co-receptors (Calderón Villalobos *et al.*, 2012; Rosquete *et al.*, 2012; Vanneste and Friml, 2012). This array of co-receptor pairs with distinct auxin sensing properties might likely allow the continued assessment of auxin levels in plants (Abel, 2007). To date, only a few auxin-dependent co-receptor combinations have been biochemically characterized (Calderón Villalobos *et al.*, 2012). Although two recent synthetic biology studies provided a comprehensive co-receptor reconstitution in yeast, their AUX/IAA stability read-out is somewhat indirect or even arbitrary. These analyses relied on the assembly of a hybrid SCF^{TIR1} from Arabidopsis and yeast, and on the activity of the yeast E1, E2s and 26S proteasome (Havens *et al.*, 2012; Shimizu-Mitao and Kakimoto, 2014). The current work provides a first direct assessment of auxin-dependent Arabidopsis TIR1/AFB1/AFB2:AUX/IAA interaction. Even though these assays were carried out in the heterologous yeast system, they provide a direct reporter read-out of ligand-dependent PPI. By establishing a comprehensive interaction matrix between TIR1/AFB1/AFB2 and AUX/IAAs, we could make predictions in the assembly of putative auxin co-receptors (**Figure 2-2**). We focused our analyses on members of the *TIR1/AFB1-3* clade, of which *lof* mutants have been thoroughly studied (Dharmasiri *et al.*, 2005b; Parry *et al.*, 2009). Initial studies of *afb4* and *afb5* mutants first attributed an unconventional role in auxin signaling to the *AFB4/AFB5* clade, which has diverged from the *TIR1/AFB1-3* clade (Parry *et al.*, 2009). Therefore, AFB4 and AFB5 were intentionally excluded from our analysis. Just recently, AFB4 and AFB5 were confirmed to act in a similar fashion to other members of the family (Prigge *et al.*, 2016). AFB3, as well as two AUX/IAAs, IAA15 and IAA29, could not be included due to difficulties expressing functional protein in yeast. Remarkably, both Havens *et al.* (2012) and Shimizu-Mitao and Kakimoto (2014) reported they were unable to express either AFB3 or AFB1 capable of degrading AUX/IAAs in yeast. This could indicate that AFB1 and AFB3 require plant-specific factors or modifications for stability and function. Although functional AFB1 was successfully expressed in yeast for auxin-dependent AUX/IAA interaction (Calderón Villalobos *et al.*, 2012 and this work), it cannot be excluded that AFB1, requires plant-specific factors at least for AUX/IAA ubiquitination and destabilization.

We observed that for TIR1 and AFB2, auxin-dependent interaction was strongest with the majority of AUX/IAAs. This is consistent with pull-down results by Parry *et al.* (2009) that indicated TIR1 and AFB2 as the strongest interactors of the family. In addition, there has been

genetic evidence that attributed the most prominent role in auxin signaling to *TIR1* and *AFB2* (Dharmasiri *et al.*, 2005b; Parry *et al.*, 2009). Furthermore, *AFB2* could not complement for the loss of *TIR1* even when expressed under the *TIR1* promoter (Parry *et al.*, 2009). Indeed, the interaction patterns of *TIR1* and *AFB2* with AUX/IAAs observed, although similar, show differences (**Figure 2-2**). Although *AFB2* exhibits very strong auxin-mediated interaction with few AUX/IAAs in yeast, the number of strong auxin-mediated *TIR1*-AUX/IAA interactions exceeds those with *AFB2* (**Figure 2-2**). This indicates that the auxin-dependent interaction patterns of *TIR1*/*AFB2* with few AUX/IAAs might be the underlying cause for their hierarchical roles in auxin signaling observed in the previous genetic studies and in pull-down experiments (Parry *et al.*, 2009). The fact that AUX/IAA degradation could only be reconstituted in the presence of *TIR1* and *AFB2*, but not with *AFB1* and *AFB3* in yeast (Havens *et al.*, 2012; Shimizu-Mitao and Kakimoto, 2014), might also hint at a prevalent role of *TIR1* and *AFB2*.

The idea that *AFB1* plays a less important role in auxin signaling (Parry *et al.*, 2009) is substantiated by the finding that *AFB1* interacted with fewer AUX/IAAs in yeast in comparison to *TIR1* and *AFB2* (**Figure 2-2**). Nevertheless, few auxin-mediated *AFB1*:AUX/IAA interactions were strong, indicating that distinct AUX/IAAs preferentially pair up with *AFB1* to form auxin co-receptors. Among those are *IAA5*, *IAA6*, *IAA8*, *IAA27* and *IAA17*, for which no *in vivo* associations with *AFB1* have hitherto been reported. The key to characterizing the specific biological functions of *AFB1* and these candidate AUX/IAAs might lie in exploring the co-receptors they potentially form, rather than studying the components apart. We recently showed that *IAA6* exhibited the same auxin sensitivity of degradation in wild-type and *AFB1*-deficient *Arabidopsis* protoplasts (Winkler *et al.*, under review). This indicates that the preferential *AFB1*-*IAA6* pairing observed in yeast might be compensated in *AFB1*-deficient plants by pairing of *IAA6* with other *TIR1*/*AFBs*.

Furthermore, there is a number of AUX/IAAs that interact with *TIR1*/*AFB1*/*AFB2* auxin-independently in yeast. Among these are *IAA9* and *IAA17*, which were also shown to be rapidly degraded in the absence of auxin relying on *TIR1* and *AFB2* in yeast (Shimizu-Mitao and Kakimoto, 2014). But whether such auxin-independent target recognition is relevant *in planta* remains to be explored.

The *TIR1*/*AFB*:AUX/IAA interaction matrix generated in this study provides a quantitative assessment, hinting at sensitivities and interaction preferences of different co-receptor combinations. It needs to be noted, though, that the Y2H interaction read-out could be compromised through degradation of AUX/IAAs by the yeast UPS, since *TIR1*/*AFBs* could assemble into yeast SCF complexes (Nishimura *et al.*, 2009; Havens *et al.*, 2012). Therefore,

specific TIR1/AFB-AUX/IAA co-receptors require further validation through orthogonal biochemical approaches providing quantitative measures – of auxin affinities, for instance – as done here for selected co-receptor pairs.

Altogether, the yeast interaction matrix for potential auxin co-receptor assembly presented here adds to the study of combinatorial PPIs in auxin signaling, e.g. the interactions among AUX/IAAs (Kim *et al.*, 1997; Ouellet *et al.*, 2001), and between AUX/IAAs and ARFs mentioned previously in **Section 1.2.1.3** (Vernoux *et al.*, 2011; Piya *et al.*, 2014). All these diverse interaction capacities and alternatives likely facilitate the specific regulation of the specialized growth and developmental responses by auxin (**Figure 3-2**).

3.2 Auxin co-receptors might differentially assemble based on variable loop regions in TIR1, AFB1, AFB2 and AFB3

To pin down molecular features in TIR1, AFB1, AFB2, and AFB3 that contribute to differential auxin co-receptor formation, structural modeling for AFB1-3 was performed in the present work. This approach revealed that AFB2 exhibits a shorter, more flexible loop-12 that could account for better accessibility of the AUX/IAA primary degron to the binding site (**Figure 2-1**). As mentioned previously, AFB2, like TIR1, is a strong interactor of AUX/IAAs in auxin-dependent *in vitro* pull-down experiments and our Y2H assays (Parry *et al.*, 2009; Calderón Villalobos *et al.*, 2012 and this thesis). TIR1 F351 located in loop-12 has been proposed to undergo conformational changes upon auxin and AUX/IAA binding and to act as a ‘fastener’ to interact with AUX/IAA and prevent it from dissociating (Hao and Yang, 2010). If this holds true, dissociation rates of AFB2-based co-receptor complexes should be much faster, since the residue to exert this proposed fastening mechanism is lacking in AFB2 loop-12. Interestingly, just as AFB2, AFB5 loop-12 is also lacking a residue homologous to F351 and shortened by one residue in comparison to TIR1 loop-12. SPR data showed much faster dissociation rates of AFB5 and auxins from immobilized IAA7 degron peptides in comparison to TIR1 (Calderón Villalobos *et al.*, 2012; Lee *et al.*, 2014). Whether, in AFB2, the contribution of easier auxin-dependent AUX/IAA association outweighs a faster dissociation or vice versa remains to be determined experimentally. Our comparison of equilibrium dissociation constants of TIR1-IAA1/IAA2 and AFB2-IAA1/IAA2 suggests that possibly faster association and dissociation rates in AFB2 co-receptor complexes balance out to result in a similar equilibrium dissociation constant as in TIR1 co-receptor complexes (**Figure 2-7 B** and **Figure 2-8**).

While the distinct AFB2 loop-12 was the most prominent finding in this modeling approach, the sequences of AFB1-3 all show variation in their loop-12 residues in comparison to TIR1

(**Figure 2-1 C**). AFB1 possesses a loop-12 of similar length as TIR1, and the aromatic residue F351 is replaced by a negatively charged amino acid (D347) in our structural alignment, which could also contribute to different AUX/IAA binding properties. AFB3 has a loop-12 that is one residue longer than that of TIR1/AFB1, and F351 is replaced by H347 – again a non-conservative exchange that might influence co-receptor assembly. Furthermore, AFB3 has a cluster of three acidic residues (E349, E350, D351) located in loop-12 in contrast to only one or no acidic residue in TIR1/AFB1 and AFB2, respectively. Although this AFB3 acidic cluster is pointing away from the AUX/IAA primary degron, it is possible that it promotes or prevents PPI with other proteins or other regions of the AUX/IAAs. In yeast-based AUX/IAA degradation assays, AFB1 and AFB3 did not promote AUX/IAA degradation as TIR1 and AFB2 did (Havens *et al.*, 2012; Shimizu-Mitao and Kakimoto, 2014). This further substantiates results from Parry *et al.* (2009), that AFB1 and AFB3 are weaker AUX/IAA target receptors. Taken together, loop-12 of TIR1/AFB1-3 is key and exhibits interesting variations in amino acid composition and structure that likely contribute to differential co-receptor formation and bring about their partially distinct functions. Future structural studies of co-receptor assembly as well as loop-12 swapping or mutational studies will corroborate these *in silico* findings.

3.3 Sister pair genes *IAA1* and *IAA2* show evidence for purifying selection, possibly hinting at conserved, crucial function

In most studies involving the *AUX/IAAs*, authors selected representatives from every clade to reflect a broad spectrum of differential function within the family (Dreher *et al.*, 2006; Calderón Villalobos *et al.*, 2012; Gilkerson *et al.*, 2015). A functional comparison between the nine Arabidopsis *AUX/IAA* sister pairs (**Figure 1-5 B**) has been missing so far. To explore functional diversification of the *AUX/IAA* protein family, two *AUX/IAA* sister pairs were initially selected in frame of this thesis. Biochemical characterization with regard to their function in the auxin co-receptor system was initiated for the *IAA1* and *IAA2*, as well as the *IAA6* and *IAA19* sister pair. *IAA6*- and *IAA19*-containing co-receptors were eventually independently characterized in a Master's thesis (Winkler, 2015; Winkler *et al.*, under review), while *IAA1*- and *IAA2*-containing co-receptors were the focus of this work.

IAA1 and *IAA2* gene products can constitute auxin co-receptors with TIR1 and AFB2 *in vitro*. Thus, when ternary complex assembly with ³H-IAA was assessed, TIR1-*IAA1* and TIR1-*IAA2* co-receptor combinations exhibited a similar high affinity of around 60 nM (**Figure 2-7**). In contrast, *IAA19* and *IAA6* have been shown to provide a TIR1-containing auxin co-receptor with significantly different affinities of $K_D = 15.6 \pm 2.0$ nM and 72.0 ± 10.5 nM, respectively (Winkler *et al.*, under review). Have then some *AUX/IAA* ohnologs diversified with regard to

co-receptor affinity while others did not? Might the diversification be based on specific and local features in their coding sequences?

IAA1 and IAA2 show a higher sequence identity (75%) than IAA6 and IAA19 (61.4%). This might hint at IAA1 and IAA2 being prone to more similar interaction behavior than IAA6 and IAA19. Furthermore, we employed a sliding window analysis, comparing 80 *A. thaliana* ecotypes and *A. lyrata*, to map selection signatures at specific regions across the coding sequence of the *AUX/IAA* sister pairs. We used the dN/dS ratio as an indicator for purifying ($dN/dS < 1$), neutral ($dN/dS = 1$), or positive ($dN/dS > 1$) selection pressure acting on the specific region of the coding sequences in question. This analysis revealed different patterns in both, IAA1/IAA2 and IAA6/IAA19, sister pairs. Here, we showed that dN/dS ratios for *IAA1* and *IAA2* are low (<1) throughout all sequence regions in sliding window analysis, indicating purifying selection acting on these genes (**Figure 2-3 B**). Consistent with *in vitro* binding assays, there seems to be no functional divergence arising in either *IAA1* or *IAA2*. In contrast, the *IAA6/IAA19* sister pair exhibits differences. Sliding window analysis revealed an overall low dN/dS for both *IAA19* and *IAA6* (<1). However, distinct peaks of dN/dS values in two regions (>5 and >50) of *IAA6*, indicate increased sequence divergence and suggest positive selection and hence evolving functional innovation (Winkler *et al.*, under review). Consequently, positive selection pressure seems to be acting on specific limited regions of selected *AUX/IAA* genes. Yet, overall, *AUX/IAAs* seem to have evolved mainly under the influence of purifying selection (Paponov *et al.*, 2009).

While there are no hints for functional diversification in coding sequence that results in different sensing properties in IAA1 and IAA2, this sister pair's retention might also be based on sub- and/or neofunctionalization on the expression level (Duarte *et al.*, 2006). *IAA1* and *IAA2* expression levels throughout cell-types, developmental stages and Arabidopsis ecotypes differ significantly. *IAA2* is generally expressed more highly than *IAA1* (**Figure 2-3 A** and **Supplementary Figure 4** to **Supplementary Figure 6**). Consistent with the results from Paponov *et al.* (2009) and Duarte *et al.* (2006), our analysis which is based on a broader set of publicly available expression data than the previous studies, indicates that *IAA1/IAA2* sister pair exhibits regulatory diversification. Their different expression domains and levels likely play a role in tissue- and cell-type specific auxin responses (Teale *et al.*, 2006; Paponov *et al.*, 2008). *IAA1* and *IAA2* promoter sequences are predicted to contain different putative transcription factor binding sites, which remain to be experimentally confirmed (**Supplementary Table 4** and **Supplementary Table 5**). In conclusion, both, changes in expression patterns (this work and Paponov *et al.*, 2009), and changes in the coding

sequences (Winkler *et al.*, under review), seem to have driven the radiation of *AUX/IAA* family. Whether one of these diversification modes is the main theme in *AUX/IAA* evolution will become clearer upon further functional studies of more *AUX/IAA* sister pairs.

3.4 TIR1-IAA1 and TIR1-IAA2 auxin co-receptors

To test our hypothesis that different co-receptor combinations provide plant cells with a range of auxin sensitivities, it was crucial to biochemically evaluate the sensing capabilities of selected auxin co-receptors. The determinant event for auxin sensing is the formation of a TIR1/AFB:auxin:AUX/IAA ternary complex. It cannot be excluded that other factors enhance or alleviate auxin sensing capability *in vivo*. Thus, affinity measurements with purified co-receptor proteins *in vitro* are highly informative. In the current work, auxin co-receptors TIR1-IAA1, TIR1-IAA2, AFB2-IAA1 and AFB2-IAA2 have been shown to form ternary complexes with ^3H -IAA *in vitro* with K_D values of 55 nM, 69 nM, 81 nM, 48 nM, respectively, which are not significantly different from one another (**Figure 2-7, Figure 2-8, Table 2-1, Supplementary Table 6**). These co-receptors constitute auxin sensors of high affinity *in vitro*, albeit not as high as e.g. TIR1-IAA7 ($K_D \approx 17$ nM)(Calderón Villalobos *et al.*, 2012) or TIR1-IAA19 ($K_D \approx 16$ nM)(Winkler *et al.*, under review). The auxin affinity of TIR1-IAA1 was roughly determined with 44 nM previously (Calderón Villalobos *et al.*, 2012). The current thorough assessment of dissociation constant substantiates this dissociation constant. Thus, TIR1-IAA1 and TIR1-IAA2 classify as medium-high affinity IAA co-receptors together with TIR1-IAA28, AFB5-IAA7 ($K_D \approx 75$ nM and 51 nM, respectively)(Calderón Villalobos *et al.*, 2012), and TIR1-IAA6 ($K_D \approx 72$ nM)(Winkler *et al.*, under review).

Likely, also AFB2-IAA1 and AFB2-IAA2 classify as such. Nevertheless, expression and purification of enough, highly pure AFB2 protein proved very challenging. It needs therefore to be considered that only two independent saturation binding experiments with samples in duplicates contributed to affinity determination, and AFB2-IAA1 affinity for auxin could only be determined with a high standard error. It is interesting, though, that exchange of TIR1 for AFB2 seems not to influence complex assembly (also see discussion in **Section 3.2**).

While the saturation binding assays for determination of K_D values did not reveal differences between IAA1- and IAA2-containing co-receptors, it did not escape our attention that homologous competition binding experiments yielded different mean K_i values (**Figure 2-10, Supplementary Figure 15**) for TIR1-IAA1 and TIR1-IAA2 with IAA. The reason for this is yet unclear. However, since our K_i calculations factor in a previously determined K_D value (Cheng and Prusoff, 1973), we chose to attribute more weight to the K_D values directly obtained from saturation binding experiments. Differences between IAA1 and IAA2 in interaction with

TIR1/AFB1/AFB2 were also observed in Y2H assays. Therefore, the validation via orthogonal *in vitro* binding approaches is desirable and was initiated in frame of this work. Attempts to characterize ternary complex formation via isothermal titration calorimetry (ITC) were not successful, and thwarted by limited amounts of recombinant TIR1 protein, and poor stability of fully active wild-type IAA1 and IAA2 proteins. The generation of an IAA1 mutant version with reduced homotypic oligomerization (IAA1^{BM3}; **Figure 2-4**), and our finding that homotypic oligomerization is unlikely to affect co-receptor complex formation, might facilitate ITC and other *in vitro* approaches for characterization of binding in the future.

In light of the co-receptor affinities, an interesting scenario opens when one considers the overall higher expression levels of *IAA2* in comparison to *IAA1* (**Figure 2-3 A** and **Supplementary Figure 4** to **Supplementary Figure 6**). Assuming that no post-transcriptional regulations or subcellular localization alleviate those levels, and *IAA1* and *IAA2* are truly co-expressed in a cell, this would result in higher cellular *IAA2* protein concentrations. Since the K_D value describes the concentrations of free proteins and protein complex at equilibrium, and since the K_D values for TIR1:auxin:IAA1 and TIR1:auxin:IAA2 are almost identical, one could imagine the following hypothetical scenario. A higher concentration of *IAA2* protein in the cell will force the binding equilibrium towards more TIR1:auxin:IAA2 complex, and deplete TIR1 and auxin from forming complexes with *IAA1* (or other AUX/IAAs present at lower concentrations). Thus, *IAA2* might be ubiquitinated more efficiently than *IAA1*, and would be subject to a much higher turnover. Then, in analogy with findings by Guseman *et al.* (2015), distinct turnover rates might dictate timing of specific developmental responses. Consequently, despite the same K_D for auxin, TIR1-*IAA1* and -*IAA2* co-receptors might behave differently in or compete for co-receptor assembly due to their different concentrations in a cell. This is just a small hypothetical snapshot of the *in vivo* scenario. Although short and simple, many more interactors are involved in the nuclear auxin signaling pathway (Lokerse and Weijers, 2009). Higher levels of *IAA2* might also form more homomers, or be sequestered by other players, i.e. might repress more ARF activators and recruit more TPL/TPR co-repressors. Besides many interactors from the AUX/IAA family itself (Kim *et al.*, 1997; Tatematsu *et al.*, 2004; Vernoux *et al.*, 2011), there are reported physical interactions for both *IAA1* and *IAA2* with ARF4-10 and ARF19 (Tatematsu *et al.*, 2004; Vernoux *et al.*, 2011; Piya *et al.*, 2014) and with TPL/TPR1-4 (Causier *et al.*, 2012a). Additionally, *IAA1* has been reported to interact with ARF17 (Vernoux *et al.*, 2011). *IAA1* and *IAA2* also interact with themselves and with one another (**Figure 2-4**, **Supplementary Figure 8**) (Kim *et al.*, 1997; Vernoux *et al.*, 2011; Kim *et al.*, 2015).

The question whether the homotypic interactions of IAA1 and IAA2 affect auxin-mediated co-receptor assembly with TIR1 was assessed in this work. The amino acid substitution P61S in the IAA1 degron, that has been shown to abolish interaction with TIR1 (Yang *et al.*, 2004), can be mimicked in IAA2 (P66S) (**Figure 2-4**, also **Figure 2-9**). Thus, degron mutations do not affect interaction of IAA1 and IAA2 with themselves and with one another in yeast (**Figure 2-4**). This was actually expected, as PB1 domain of AUX/IAAs is regarded as a portable PPI domain (Guilfoyle and Hagen, 2012) that folds and functions independently for AUX/IAA and ARF PB1 domain interaction (Han *et al.*, 2014; Dinesh *et al.*, 2015). In this work, increasing amounts of those degron mutants were used alongside a fixed concentration of wild-type AUX/IAA to lower the amount of available degron per AUX/IAA oligomer in an equilibrium binding experiment with radiolabeled IAA and TIR1. Levels of bound IAA, and therefore amount of co-receptor complex remained constant, indicating that degrons of wild-type IAA1 or IAA2 remained accessible to auxin-mediated TIR1 binding. This was independent of IAA1 or IAA2 concentration as free monomers or oligomers. In addition, a recently generated basic patch mutant IAA1^{BM3} that exhibits reduced homotypic interaction, was able to undergo auxin-mediated interaction with TIR1 in yeast and in *in vitro* binding assays (**Figure 2-4** and **Figure 2-5**). This suggests that a prevalent monomeric state of IAA1 is at least not detrimental for auxin co-receptor formation. Based on these results, we postulate that TIR1 can bind AUX/IAAs in an auxin-dependent manner, irrespectively of AUX/IAA oligomerization state. This is most likely due to the modular constitution of AUX/IAAs, in which the PB1 domain independently folds into a compact structure, whereas the degron-containing N-terminal region exhibits reduced compactness and high flexibility. This flexibility might allow the recognition of the degron by TIR1, regardless of the PB1-mediated complex formation. Removal of PB1 from IAA1, IAA17 or IAA28 mildly accelerated their auxin-induced degradation in yeast, indicating that oligomerization might negatively influence the degradation of AUX/IAAs, but the effect was highly dependent on the type of AUX/IAA (Moss *et al.*, 2015). Since ARFs undergo interactions with AUX/IAAs in the same PB1-based manner, our observation might not only apply to homotypic but also to heterotypic ARF:AUX/IAA oligomers. It needs to be considered that the experiments employed in our *in vitro* binding approach did not involve a complete SCF complex but only TIR1:ASK complex. Whether the much larger SCF^{TIR1} can access the degrons in the same manner or whether oligomerization state of AUX/IAAs poses a steric hindrance is still an open question. Furthermore, AUX/IAAs' modular constitution includes the conserved EAR motif-containing DI for interaction with TPL/TPR co-repressors (**Figure 3-2**). A recent study demonstrated that a plant EAR-motif-carrying interactor of TPL showed increased affinity when in oligomeric state (Ke *et al.*, 2015).

It has been postulated that AUX/IAAs could insert into *AuxRE*-bound ARF dimers or oligomers and thereby disrupt efficient DNA-binding of ARFs and recruit co-repressors to the DNA (Han *et al.*, 2014). Han *et al.* (2014) also suggested that this insertion model would provide the possibility for rapid reestablishment of functional ARF oligomers and thus gene activation as soon as AUX/IAAs are removed. Since our results indicate that PB1 domain-mediated interactions do not interfere with degron recognition by TIR1, it is conceivable that AUX/IAA recognition for ubiquitination can take place right at the multimeric ARF-AUX/IAA repressor complex on the DNA. Recent mapping of *in vitro* ubiquitination sites for IAA6 and IAA19 revealed that invariant lysine residues in the PB1 domain implicated in electrostatic interactions for homo- and heterooligomerization of AUX/IAAs and ARFs are targeted for ubiquitination *in vitro* (Winkler *et al.*, under review). Ubiquitination of this site could serve as a mechanism to disrupt AUX/IAA PB1 domain-mediated interactions (Winkler *et al.*, under review). Consequently, AUX/IAAs inserted into ARF dimers or oligomers on the DNA might be dislodged through ubiquitination upon an auxin stimulus.

In recent years, a number of equilibrium dissociation constants (affinities) for different binding reactions in auxin signaling have been determined (Calderón Villalobos *et al.*, 2012; Han *et al.*, 2014; Dinesh *et al.*, 2015; Ke *et al.*, 2015; Korasick *et al.*, 2015; Winkler *et al.*, under review). For instance, the affinity of AUX/IAA dimer formation has been determined around 6 μM (Han *et al.*, 2014; Dinesh *et al.*, 2015), which is considerably weaker than the affinity for auxin co-receptor formation. Most affinities for auxin-dependent co-receptor formation determined so far are in the 10^{-8} M range (this work; Calderón Villalobos *et al.*, 2012; Winkler *et al.*, under review), and therefore comparable with the affinity determined for IAA17:ARF5 dimerization in calorimetric experiments (Han *et al.*, 2014). Applying this reductionist approach of employing *in vitro* approaches with few components, has greatly advanced our understanding of PPIs in the nuclear auxin signaling pathway. Hence, strength or preference of the interactions could be determined, or determinants of specificity and strength of PPIs could be identified. One needs also to consider the holistic view of the system. Affinities describe complex formation at equilibrium, whereas in the cell constantly rapid changes occur. Furthermore, local concentrations of proteins can vary due to the effect of macromolecular crowding inside the cell, which might influence the preference of molecular interactions in a different way than expected from *in vitro* data (Ellis, 2001).

3.5 Differential effects downstream of co-receptor formation

The biochemical characterization of TIR1-IAA1 and TIR1-IAA2 auxin co-receptors in this work not only included ternary complex assembly, but also the study of IAA1 and IAA2 as targets

for ubiquitination. This work demonstrates that IAA1 and IAA2 are targets for *in vitro* polyubiquitination by SCF^{TIR1}, and thus complements sparse data on AUX/IAA ubiquitination (dos Santos Maraschin *et al.*, 2009; Gilkerson *et al.*, 2015; Winkler *et al.*, under review).

Furthermore, this work demonstrated that despite the similar auxin affinities of TIR1-IAA1 and TIR1-IAA2 co-receptors, differences between IAA1 and IAA2 as targets in SCF^{TIR1}-mediated ubiquitination are plausible. Surprisingly, IAA1 ubiquitination was hardly auxin-responsive at the very same IAA concentrations that induced a clear increase in IAA2 ubiquitination. How can this higher responsiveness be explained, when TIR1, which was used in IVU assays, assembles with auxin and both AUX/IAA targets with the same affinity?

First, the fact that in IVU assays, TIR1 is assembled into a complete SCF complex interacting with E2~Ub might differentially influence the interaction with IAA1 and IAA2. Both targets might exhibit slight differences in conformation when associating with the full E3 complex, SCF^{TIR1}. SCF complexes can modify, in a rather nonspecific manner, lysines located in a so-called ubiquitination zone (Mattioli and Sixma, 2014). Thus, IAA1 and IAA2 might differ in their ubiquitination zones when associated with SCF^{TIR1}. Also, different rates of ubiquitination on IAA1 and IAA2 by SCF^{TIR1} are conceivable. Secondly, the covalent attachment of Ub might influence the dissociation rate of the target from the E3 complex. Such differences might reflect in the outcome of IVU. As expected, introducing a single amino acid exchange in the core degron of IAA1 (IAA1^{P61S/axr5-1}) that corresponds to the *axr5-1* mutation abolished its ubiquitination. Interestingly, the same mutation in IAA2 (IAA2^{P66S}) led to a strong reduction of Ub-conjugation (**Figure 2-12**). Although IAA2^{P66S} did not undergo auxin-mediated interaction with TIR1 in yeast and binding assays (**Figure 2-5** and **Figure 2-9**), we cannot exclude that residual interaction despite the mutation might be the reason. IAA3 carrying the *shy2-2* mutation, for example, has been shown to residually interact with TIR1 in an auxin-dependent manner, even though a proline of the core degron was mutated (Tian *et al.*, 2003). The differential effect on IVU by the same mutation in IAA1 and IAA2 further supports the presence of intrinsic differences between the two closely related AUX/IAAs, which are not reflected in the affinity of ternary complex formation. One might reason that IAA2 shows stronger differences in Ub conjugation because it might carry more target lysines for ubiquitination. While IAA1 carries 16 lysines, none of which seems preferred or even required for ubiquitination (Gilkerson *et al.*, 2015), IAA2 carries 18 lysines (**Supplementary Figure 2**). Lysine residues are highly conserved between IAA1 and IAA2 in the PB1 domain. They show, however, some variance in the N-terminal part, which is where ubiquitination zones might differ between the sister pair and could possibly result in differential ubiquitination. As

Gilkerson *et al.* (2015) demonstrated, even when all lysines of IAA1 are mutated, the protein still becomes efficiently destabilized. Ubiquitination of non-canonical serines and threonines via oxy-ester linkages is likely the reason. It seems, that regardless of the state of its ubiquitination zones, the IAA1 ubiquitination and degradation is absolutely essential for plant proteostasis. It would be interesting to establish in the future, how important IAA2 lysines or non-canonical ubiquitination target residues are.

The lack of auxin-dependent IAA1 ubiquitination at the experimental conditions tested here is puzzling (**Figure 2-13, Figure 2-14**). Many findings indicate that auxin enhances IAA1 interaction with SCF^{TIR1} (Yang *et al.*, 2004), interaction with TIR1/AFB1/AFB2 in yeast (this work), and degradation of IAA1 (Zenser *et al.*, 2001; Havens *et al.*, 2012; Shimizu-Mitao and Kakimoto, 2014; Gilkerson *et al.*, 2015). A possible explanation might be the absence of additional factors in our *in vitro* approach, which probably influence auxin-mediated IAA1 ubiquitination. Also, auxin concentrations higher or lower than those tested here, might show a response in IAA1 ubiquitination. In addition, it is possible that IAA1 protein stability is compromised *in vitro*. While the IAA1 primary degron might be functional for auxin-dependent TIR1 recognition, the intrinsically disordered N-terminal part might not adopt the ensemble of structural conformations necessary for auxin-responsive ubiquitination.

It is possible that the differential ubiquitination of IAA1 and IAA2 is reflected in the Y2H assay. In yeast, IAA1 showed a stronger auxin-mediated interaction with TIR1/AFB1/AFB2 than IAA2 (**Figure 2-2, Figure 2-9**). As IAA2 seems to be more efficiently, and auxin-dependently ubiquitinated, it might be turned-over more efficiently by the yeast UPS after an auxin surge. Thus, a more stable IAA1 would yield a stronger Y2H reporter output due to its more prevalent PPI with TIR1/AFBs.

We are aware that our IVU assay system also requires further fine-tuning in the future. We observed unspecific ubiquitination signal likely due to ubiquitinated CUL1 species (**Figure 2-11**), as also Wu *et al.* (2003) and Duda *et al.* (2008) report. Possibly, reducing the amount of free Ub used in the reactions could diminish this unspecific signal. Furthermore, to achieve a complete picture of ubiquitination dynamics, testing a broader range of auxin concentrations in the IVU might be helpful. The use of GST-tagged versions of AUX/IAAs was necessary in all our *in vitro* assays so far for satisfying stability of AUX/IAAs, which are highly prone to aggregate. This could be circumvented in the future by using AUX/IAA mutant versions with reduced homomerization, such as the IAA1^{BM3} mutant generated in frame of this work. IAA1^{BM3} exhibited enhanced stability upon freezing and thawing, and much higher yields during affinity purification were obtained. Furthermore, IAA1^{BM3} could be handled at 10-fold

the concentration of wild-type IAA1. Therefore, it is a promising variant for further studies that require tag removal, higher amounts and concentrations. Our IVU approach also opens up the opportunity to identify potential ubiquitination sites or zones in IAA1 and IAA2 as has been recently accomplished for IAA6 and IAA19 (Winkler, 2015; Winkler *et al.*, under review). Additionally, many other aspects of AUX/IAA ubiquitination can be studied via IVU experiments in the future. For example, one can explore differential Ub sites and Ub linkages, E2 specificity, or influence of additional regulatory processes such as neddylation.

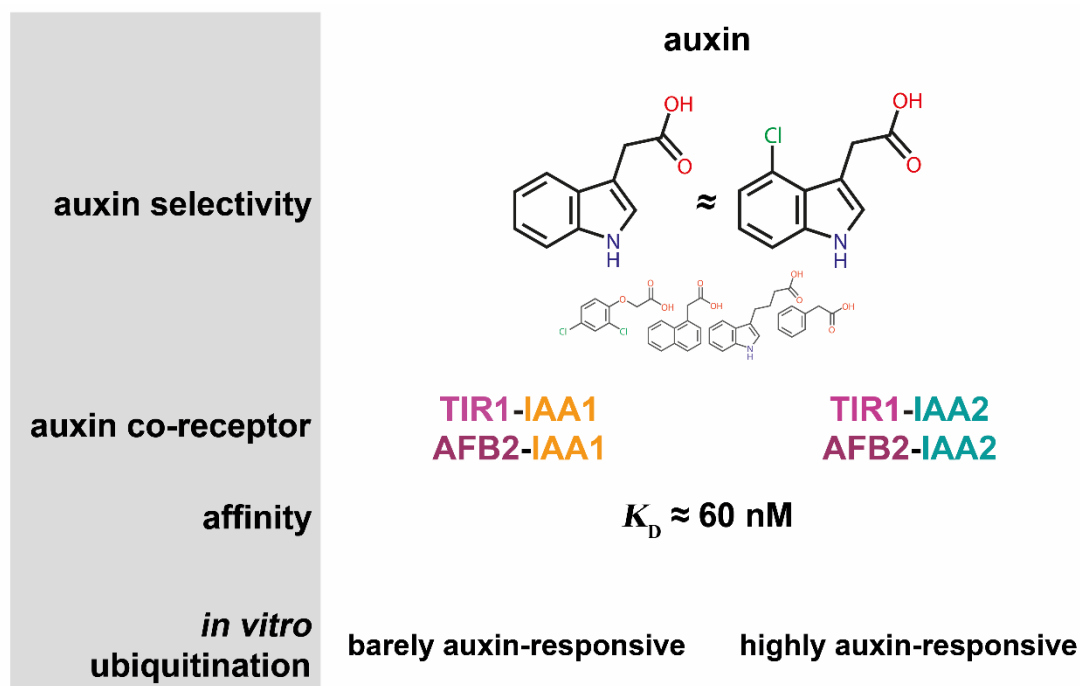


Figure 3-1: Summary of biochemical characterization of TIR1-IAA1 and TIR1-IAA2 auxin co-receptors

Ternary receptor complexes TIR1:auxin:IAA1 and TIR1:auxin:IAA2, and likely, also AFB2:auxin:IAA1 and AFB2:auxin:IAA2 assemble with similar high affinity of around 60 nM *in vitro*. TIR1-IAA1 and -IAA2 are high affinity co-receptors for IAA and 4-Cl-IAA, whereas 2,4-D, NAA, IBA, and PAA are bound with less affinity. Biochemical output of highly similar receptor complex formation, namely IAA1 and IAA2 ubiquitination exhibits differences. While IAA2 undergoes highly auxin-responsive ubiquitination, IAA1 does not.

3.6 *In vivo* studies of IAA1 and IAA2 in auxin receptor formation

The subsequent question this work aimed to answer was how does AUX/IAA stability mirror auxin receptor affinities and target ubiquitination. To comparatively study the stability of IAA1 and IAA2 *in vivo*, several approaches were implemented. We performed transient transfection of *Nicotiana benthamiana* leaves and transfection of Arabidopsis mesophyll protoplast to express tagged IAA1 and IAA2 versions. Treatments with protein synthesis inhibitors, proteasome inhibitors and auxin were implemented. Protein extraction, and immunoblot analysis of tagged IAA1 and IAA2 was employed, but yielded no consistent results (data not shown). Nevertheless, we successfully established a number of stable lines overexpressing YFP-IAA1 and YFP-IAA2 translational fusions in wild-type and different *tir1/afb*

mutant backgrounds. These lines will surely provide a broad tool set for future IAA1 and IAA2 ubiquitination studies. Also, these transgenic lines will allow analyses of IAA1 and IAA2 stability, as well as co-receptor assembly under limited TIR1/AFB availability *in vivo*.

Initial characterization of our set of transgenic lines yielded interesting hints to the role of *IAA1* and *IAA2* *in planta*. Intriguingly, overexpression of *YFP-IAA1* resulted in a broad distribution of transgene transcript levels in independent transformants seemingly unconnected with the genetic background. In contrast, *YFP-IAA2* transcript levels were low in all transgenic lines (**Figure 2-16**). Hence, it is possible that *YFP-IAA2* overexpression is suppressed through posttranscriptional mechanism, or that lines with higher transcript levels were not viable. Endogenous *IAA2* transcript levels are significantly higher than those of *IAA1* across tissues and developmental stages (**Figure 2-3 A**). Thus, overexpression of *YFP-IAA2* only marginally added to overall *IAA2* transcript in all transgenic lines tested (**Supplementary Figure 22**). This observation suggests that *IAA2* transcript is restricted to a tightly controlled maximum level. In contrast, no such regulation or restriction seems to apply to *IAA1* transcript levels. While the nature of the regulatory mechanism remains to be identified, it hints at a crucial role of *IAA2* transcript levels *in planta*.

Interestingly, no *YFP-IAA2* overexpressing line could be established in the *tir1-1 afb2-3* background (Table 2-2, **Supplementary Table 7**), which allows speculation that high levels of *YFP-IAA2* protein and the failure to recognize them through SCF^{TIR1} and SCF^{AFB2} for degradation could be highly detrimental for the plant. Consistently, *YFP-IAA2* protein levels in transgenic lines were very low in comparison to *YFP-IAA1* levels. While treatment with proteasome inhibitor and a *tir1-1* or *tir1-1 afb3-4* genetic background could partially stabilize *YFP-IAA2* levels, they remained at the detection limit despite the enrichment step via immunoprecipitation (**Figure 2-18, Supplementary Figure 24**). Moreover, no *gof* mutant for *IAA2* has been isolated to date which, together with the aforementioned hints for its tight regulation and the evidence for high endogenous expression levels, could be indicative of *IAA2* playing an even more crucial role in auxin signaling than *IAA1*.

These transgenic lines also displayed a range of *YFP-IAA1* and *YFP-IAA2* protein levels. Of course, the transcript levels and thereby protein levels are influenced by the position of transgene insertion (Gelvin, 2003). Therefore, direct comparison of AUX/IAA stabilization among *tir1/afb* backgrounds is not possible at this point. For the same reason, a robust phenotypic assessment of these transgenic lines is not yet feasible. However, from our initial analyses, we tentatively state that, as expected, *IAA1* and *IAA2* proteins can be stabilized through combining transcriptional overexpression and translational YFP fusion with

TIR1/AFBs deficiency (**Figure 2-18, Supplementary Figure 24**). Preliminary phenotypic screening provided hints for a negative correlation of transgene level and hypocotyl elongation in dark-grown seedlings of *YFP-IAA1* overexpressor lines (**Supplementary Table 9**). This is consistent with the phenotype of the *axr5-1* mutant that expresses a stabilized version of IAA1 protein. Hypocotyls of dark-grown *axr5-1* seedlings are longer than wild-type (Yang *et al.*, 2004). This is also in line with results from a study with dexamethasone-inducible overexpression of stabilized IAA1 protein, which showed that hypocotyl elongation of dark-grown transgenic seedlings was significantly inhibited in the presence of dexamethasone compared to uninduced seedlings (Park *et al.*, 2002). Together, this suggests that at least the *YFP-IAA1* overexpression lines generated in frame of this thesis show auxin-related, relevant phenotypes.

For future studies, lines carrying the same transgenic allele in the different *tir1/afb* mutant backgrounds have to be generated through crosses. By crossing a representative medium overexpressor into a different genetic background, all combinations of *tir1/afb* single or multiple mutant as well as wild-type background can be obtained (**Supplementary Table 11**). Phenotypic studies with lines generated through crosses will target auxin-related phenotypes guided by previous studies with stabilized IAA1 (Park *et al.*, 2002; Yang *et al.*, 2004), and allow to subsequently quantify grades of phenotype severeness between *tir1/afb* mutant backgrounds. Such analysis could provide important hints for co-receptor assembly and downstream responses with *IAA1* and *IAA2* *in vivo*.

While on the long term the very high overexpressor lines likely carrying multiple T-DNA insertions are more prone to undergo silencing of transgene expression (Gelvin, 2003), these lines might be more advantageous in order to study *in vivo* co-receptor assembly on the protein level. Since mapping of IAA1 ubiquitination sites *in vivo* has proven challenging, likely due to low *IAA1* expression (Gilkerson *et al.*, 2015), high overexpression levels might facilitate the recovery of sufficient modified protein species. This will facilitate future studies of e.g. *in vivo* ubiquitination including the mapping of IAA1 *in vivo* ubiquitination sites.

3.7 Redefining the degron

In recent years, evidence had accumulated that regions outside the highly conserved primary degron influence auxin co-receptor assembly (Calderón Villalobos *et al.*, 2012) as well as AUX/IAA stability (Worley *et al.*, 2000; Zenser *et al.*, 2001; Dreher *et al.*, 2006; Havens *et al.*, 2012). Furthermore, the definition of degrons in UPS target proteins has been lately refined. A degron is likely tripartite rather than solely a sequence motif for recognition by an E3 ligase (Guharoy *et al.*, 2016). As explained before, AUX/IAAs are intriguing candidates for a

refinement of the degron concept in plant UPS targets (review **Section 2.2** for a detailed tripartite degron definition). The primary degron encompasses the highly conserved 13 residues, first identified as necessary and sufficient for degradation by Ramos *et al.* (2001). The AUX/IAA N-terminal part, comprising primary degron-flanking regions, is predicted to be intrinsically disordered. This is a prerequisite for initiation of engagement by the proteasome – a tertiary degron (**Supplementary Figure 17**) (Prakash *et al.*, 2004; Fishbain *et al.*, 2011). Moreover, AUX/IAA disordered region varies in length and sequence composition among the members of the protein family. This led us to hypothesize that differences in auxin co-receptor assembly, and AUX/IAA stability might arise from those variations. Indeed, recent studies showed that sequence composition of disordered segments influences protein half-life (van der Lee *et al.*, 2014; Fishbain *et al.*, 2015).

IAA7 and IAA12 are two rather distantly related AUX/IAAs with dissimilar degron-flanking regions (**Figure 1-5 B, Supplementary Figure 3, Supplementary Table 3**). Also, IAA7 and IAA12 exhibit distinct auxin binding affinities in TIR1-containing co-receptors (Calderón Villalobos *et al.*, 2012). The relatively high sensitivity of IAA12 degradation to PAA in yeast (Shimizu-Mitao and Kakimoto, 2014), might indicate that co-receptors containing IAA12 might have specialized to sense auxins other than IAA. It is yet to be determined whether IAA12 has specialized in providing ligand specificity to an auxin co-receptor. To narrow down features that differentially contribute to co-receptor assembly, IAA7 and IAA12 were used in a chimera approach in frame of this work. From our experiments, a single region directing differential co-receptor assembly could not be identified with certainty. 4-module, but not 5-module chimeric constructs showed expression levels in yeast that correlated with the nature of the C-terminal module (**Figure 2-20, Supplementary Figure 40 and Supplementary Figure 41**). Similarly, attempts to express GST-tagged chimeras in *E. coli*, made evident that proteins containing the degron-tail (DT) and PB1 of IAA7 generally expressed with higher yields than those with DT and PB1 of IAA12 (data not shown). Together, these observations in the yeast and bacterial heterologous expression suggest that the C-terminal module might have had an effect on the physicochemical stability of the protein. IAA7-derived C-terminal part appears more advantageous than an IAA12-derived one. This finding was further corroborated by the observation that the DT is dispensable for auxin-mediated interaction with TIR1 in yeast. DT deletion, especially in case of IAA12, seemed to have an advantageous effect on yeast growth and expression (**Figure 2-20 B, Supplementary Figure 41**). However, no such effects were observed in protoplast expression (**Supplementary Figure 42**). Furthermore, yeast interaction data were to be validated through *in vitro* binding assays. Expression of chimeric constructs in *E. coli* and their purification, however, proved challenging. Either AUX/IAA chimeras

exhibited insufficient yield or stability during expression and purification, or were not active in binding experiments (data not shown). Even though seamless chimeras were designed, synthesis of unstable, or misfolded protein cannot be ruled out. One needs to point out that the chimera approach employed here is valid and highly suitable for the analysis in contrast to a truncation analysis. Conserved residues and motifs were carefully chosen as delimitations of modules, as opposed to progressively and linearly shortening residues that might partake in a three-dimensional conformation or intramolecular interaction (**Figure 3-2**). By providing all domains of the full-length protein, albeit derived from different family members, aberrant secondary or tertiary structural conformation is likely circumvented. However, it is also possible that IAA7 and IAA12 are too distantly related to reconstitute a functional chimeric AUX/IAA.

In contrast to the yeast data and recombinant expression in *E. coli*, the expression of functional chimeric IAA7 and IAA12 C-terminal LUC fusions in Arabidopsis protoplasts was viable. We implemented a stability assessment via ratiometric sensor approach established by Wend *et al.* (2013). Interestingly, we found that the high and low K_D values measured *in vitro* for TIR1-IAA7 and TIR1-IAA12 auxin co-receptors, respectively, are likely reflected in auxin sensitivity of IAA7-LUC and IAA12-LUC degradation in protoplasts. While a treatment with 1 nM exogenously applied IAA caused a significant reduction of IAA7-LUC protein levels, a 10-fold higher IAA concentration was required to cause a significant reduction in IAA12-LUC levels (**Figure 2-21**). In protoplasts, not only TIR1 but also AFBs likely assemble with IAA7 and IAA12 (Dharmasiri *et al.*, 2005b; Parry *et al.*, 2009; Calderón Villalobos *et al.*, 2012). Thus, this correlation of *in vitro* auxin affinity of TIR1-IAA7 and -IAA12 co-receptors with *in vivo* auxin sensitivity of IAA7 and IAA12 degradation hints at the following. On the one hand, TIR1 might be the main contributor to IAA7 and IAA12 auxin-dependent recognition and degradation. On the other hand, AFBs might have very similar binding affinities for IAA7 and IAA12.

Furthermore, ratiometric *in vivo* degradation assays revealed that DT removal reduced auxin sensitivity of IAA7 and IAA12 degradation (**Figure 2-21**). This suggests that the DT does play a role in degradation, even though it did not contribute to auxin-mediated interaction of AUX/IAA chimera with TIR1 in yeast (**Figure 2-20 B**). This could possibly be due to the DT carrying residues irrelevant to complex assembly, but particularly essential for AUX/IAA ubiquitination and their subsequent degradation. Several lysine residues can be found in the DT (**Supplementary Table 12** and **Supplementary Figure 3**), that could possibly provide an obligatory ubiquitination zone (secondary degron). Swapping of the DT module between IAA7 and IAA12, however, did not have significant effects on auxin sensitivity of their degradation

(Figure 2-21). This indicates that the DT, although essential for destabilization, can be interchanged between AUX/IAAs. Thus it does not carry the features responsible for the different auxin sensitivities of IAA7 and IAA12 turn-over.

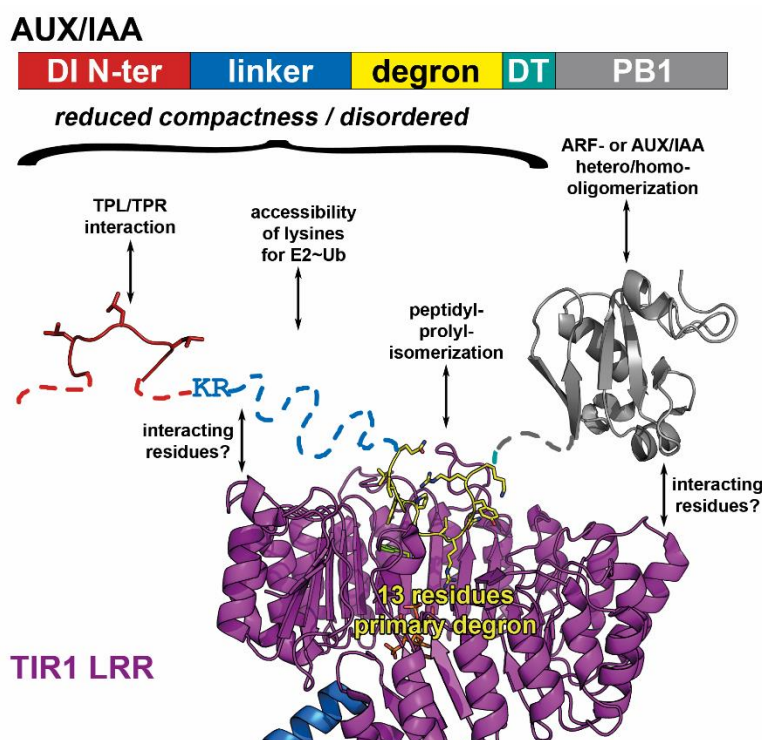


Figure 3-2: Scheme of AUX/IAAs regions and their potential roles in co-receptor formation

Structural representation of TIR1 LRRs (purple cartoon representation) with auxin (green stick representation) bound at the bottom of the TIR1 binding pocket and the 13-residue IAA7 degron peptide (i.e. primary degron; yellow cartoon with side chains in stick representation) binding on top (PDB code: 2P1Q; Tan *et al.*, 2007). AUX/IAA regions N- and C-terminal of the primary degron which are predicted to be structurally disordered are represented as dashed line. The C-terminal structurally compact PB1 domain (Phyre2 model of IAA1 PB1 (Kelley *et al.*, 2015)) is shown as a grey cartoon representation. EAR motif residues are shown in the same conformation as in IAA1 in complex with OsTPR2 (PDB code: 5C7F; Ke *et al.*, 2015). AUX/IAA scheme with same color code depicting regions assessed in this work's chimera approach. Domain I-containing N-terminus (DI N-ter; red), linker (blue) delimited by the conserved KR duplet and the primary degron, primary degron (yellow), degron-tail (DT, turquoise), and PB1 domain (grey). Black arrows show reported or putative interactions that could potentially influence co-receptor assembly, including TPL/TPR interaction (Ke *et al.*, 2015), AUX/IAA residues outside the primary degron interacting with TIR1, AUX/IAA lysine residues that need to be accessible for ubiquitination, peptidyl-prolyl isomerization in the AUX/IAA degron core (Jing *et al.*, 2015), and oligomerization with ARFs or AUX/IAAs via PB1 domain (Han *et al.*, 2014; Dinesh *et al.*, 2015).

In a parallel study, Moss *et al.* (2015) utilized a synthetic auxin-mediated AUX/IAA degradation system in yeast (Havens *et al.*, 2012), and a subset of AUX/IAAs served to define regions (rate motifs) that fine-tune auxin-induced degradation rates. By assessing serial truncations of IAA1, IAA17 and IAA28, the region necessary to recapitulate full-length degradation dynamics was narrowed down to lie between DI and PB1 domain. These rate motifs correspond to the modules *linker*, *degron*, and *degron-tail* defined in the present work (*NdC fragment* according to the Moss *et al.* nomenclature). Further truncations revealed different contributions of the linker and DT region to degradation dynamics in the studied AUX/IAAs. Removal of the linker,

resulting in a fragment including only degron and DT, strongly slowed IAA1, mildly slowed IAA3 and IAA17, and did not affect IAA28 degradation. On the other hand, removal of the DT, resulting in a linker plus degron fragment, strongly slowed IAA28, moderately slowed IAA3 and IAA17, and weakly slowed IAA1 degradation (Moss *et al.*, 2015). This is consistent with our results where DT removal from IAA7 and IAA12 reduced auxin sensitivity of their degradation *in vivo* (**Figure 2-21**).

For, IAA1 and IAA17 the major contributor in the linker to degradation dynamics of IAA1 and IAA17 was shown to be the conserved KR duplet, whereas IAA28 seems to be a natural variant lacking this motif (Moss *et al.*, 2015). Varying the length of the linker, i.e. the distance between KR and degron, did not affect degradation dynamics, although proximity of KR and degron seemed to correlate with the magnitude of the effect the linker had on degradation dynamics (Moss *et al.*, 2015). A role for KR in full-length IAA7 auxin-dependent binding by TIR1 was demonstrated in radioligand binding assays (Calderón Villalobos *et al.*, 2012). In AlphaScreen competition and Y2H experiments by Moss *et al.* (2015), however, KR in an IAA1 NdC fragment was not found to contribute to auxin-dependent binding by TIR1. Whether there are differences between AUX/IAA family members regarding the contribution of their KR motif to complex formation, or whether differences are intrinsic to full-length AUX/IAAs versus truncations lacking DI and PB1 domain as utilized in Calderón Villalobos *et al.* (2012) and Moss *et al.* (2015), respectively, remains to be elucidated.

Moss *et al.* further addressed the contribution of rate motif-containing, degron-flanking sequences to auxin-dependent binding to TIR1. Whereas for IAA1, rate-motifs in the DT contribute to auxin-dependent TIR1 binding, rate-motifs in the IAA28 DT do not (Moss *et al.*, 2015). These findings from assays with IAA1 and IAA28 truncations suggest that the interaction strength in these auxin co-receptor complexes does not translate directly into AUX/IAA degradation rates. This is consistent with our observation that DT deletion does not affect auxin-dependent interaction of IAA7 and IAA12 with TIR1 in yeast, but reduces auxin sensitivity of AUX/IAA degradation *in vivo*. This might hint at an uncoupling of interaction and target degradation, at least with regard to the DT and the studied AUX/IAAs. In contrast, mutations in the immediate N-terminal proximity of the IAA14 core degron that progressively slow degradation, also gradually reduce binding affinity with auxin and TIR1 (Guseman *et al.*, 2015), indicating that for this particular AUX/IAA and/or in this particular region interaction and target degradation are very well connected.

In addition, it needs to be noted that IAA1 and IAA28 truncations, that were sufficient to recapitulate the degradation dynamics of full-length proteins, exhibited a strong increase in

affinity in *in vitro* auxin-binding experiments (Moss *et al.*, 2015) compared to full-length IAA1 and IAA28 (this work and Calderón Villalobos *et al.*, 2012). This indicates that the truncations could recapitulate degradation dynamics of full-length proteins but not co-receptor complex formation, and therefore calls into question whether deletion of rate-motifs provides a true picture of the effects on complex formation.

In conclusion, the KR, linker and DT contain rate motifs that fine-tune AUX/IAA degradation dynamics, however, the magnitude of the effect of each rate motif appears to vary among AUX/IAAs.

3.8 Co-receptors perceiving auxins other than IAA

Several synthetic and natural compounds have been shown to possess auxinic activity (Woodward and Bartel, 2005). Furthermore, there is structural and *in vitro* biochemical evidence for binding of IAA, NAA and 2,4-D by a TIR1-IAA7 degron peptide co-receptor complex (Tan *et al.*, 2007; Calderón Villalobos *et al.*, 2012; Lee *et al.*, 2014). *In vitro* binding data established high nanomolar affinities for several co-receptor combinations with IAA, and for the TIR1-IAA7 co-receptor with the synthetic auxin picloram (Calderón Villalobos *et al.*, 2012). Moreover, SPR-based *in vitro* binding studies with TIR1, AFB5 and IAA7 degron peptides could establish k_{off} rates for IAA, and the synthetic auxins Fluoroxypyr and Triclopyr (Lee *et al.*, 2014). However, the binding capability of full-length auxin co-receptors still remained elusive, especially for the natural auxins, 4-Cl-IAA, IBA and PAA (Simon and Petrasek, 2011).

The present work presents *in vitro* affinities for the co-receptors TIR1-IAA1 and TIR1-IAA2 in complex with these natural auxins (**Figure 2-10, Supplementary Figure 15**). Interestingly, 4-Cl-IAA binds to these co-receptors with nanomolar affinity close to that of IAA, suggesting that 4-Cl-IAA might be perceived by TIR1-IAA1 and TIR1-IAA2 co-receptors at physiological concentrations in the cell. This is consistent with IAA and 4-Cl-IAA inducing AUX/IAA degradation at similar concentrations in yeast (Shimizu-Mitao and Kakimoto, 2014). Although, the occurrence of 4-Cl-IAA as an auxin seems restricted to the *Fabeaceae* family (Lam *et al.*, 2015), this finding indicates that TIR1/AFB-AUX/IAA co-receptors rather than other auxin binding components are responsible for 4-Cl-IAA sensing. *Fabeaceae* orthologs of TIR1 and IAA1/IAA2 are likely candidates for 4-Cl-IAA perception in this family. Furthermore, two lines of evidence suggest a role of 4-Cl-IAA or a yet unknown chlorinated auxin in *Arabidopsis*. First, the high affinity of AFB4/5 for picloram (Calderón Villalobos *et al.*, 2012; Prigge *et al.*, 2016), a synthetic auxin, could hint at a specialization of these FBPs for perception of a chlorinated endogenous auxin. Second, Shimizu-Mitao and Kakimoto (2014) report that in yeast,

degradation of IAA31, which carries a degenerate primary degron, was induced only by 4-Cl-IAA but not by IAA. To further address the role and sensing of endogenous chlorinated auxins, it would be interesting to test 4-Cl-IAA binding in AFB5-based co-receptors (as also suggested by Lee *et al.*, 2014), and screen for yet undetected chlorinated auxins that naturally occur in plants.

In this work, we also established K_i values for binding of synthetic auxins 2,4-D and NAA by TIR1-IAA1 and TIR1-IAA2 co-receptor pairs (**Figure 2-10, Supplementary Figure 15**). These K_i values lie in the low micromolar range, i.e. a one to two orders of magnitude weaker affinity compared with IAA and 4-Cl-IAA. This is likely due to fewer intermolecular interactions of 2,4-D and NAA with the TIR1 binding pocket compared with indole-ring based auxins IAA and 4-Cl-IAA, that form an additional hydrogen bond through their amine group (Tan *et al.*, 2007; Hao and Yang, 2010). The reason for the high activity of 2,4-D and NAA in plants might lie in their cellular stability and transport characteristics (Woodward and Bartel, 2005; De Rybel *et al.*, 2009).

Furthermore, we found that the natural auxins IBA and PAA bound to TIR1-IAA1 and TIR1-IAA2 co-receptors with affinities in the high micromolar range, i.e. three to four orders of magnitude weaker than IAA and 4-Cl-IAA (**Figure 2-10, Supplementary Figure 15**). This suggests that these natural auxins are unlikely candidates for perception by TIR1-IAA1 and TIR1-IAA2 co-receptors. Previously, it has been reported that IBA was ineffective to elicit degradation of any AUX/IAAs in yeast (Shimizu-Mitao and Kakimoto, 2014), further supporting the conception that IBA action in Arabidopsis relies on its conversion to IAA rather than direct perception (Zolman *et al.*, 2000; Strader and Bartel, 2011). PAA has been reported at high endogenous levels (e.g. up to ≈ 4000 pmol/g fresh weight in young shoots of barley) – often, but not always, surpassing IAA levels (Sugawara *et al.*, 2015). However, even these high nanomolar/low micromolar concentrations are not suitable for perception with a K_i value only in the high micromolar range as determined here for TIR1-IAA1 and TIR1-IAA2 co-receptors. Curiously, Sugawara *et al.* (2015) provide some evidence that PAA acts through the TIR1/AFB auxin signaling pathway. They showed that in a Y2H assay, PAA promotes interaction of TIR1/AFB2/AFB5 with IAA3, IAA5, IAA7, IAA8, IAA12, and IAA28 at very high concentrations of 100 μ M and 1 mM. In pull-down assays, PAA promoted interaction of TIR1 with IAA7 but not with IAA3 (Sugawara *et al.*, 2015). Note, that IAA3 is closely related to IAA1 and IAA2 studied in this thesis (**Figure 1-5 B**). Another study reports that although overall PAA was less effective than IAA in inducing AUX/IAA degradation in yeast, exceptionally, PAA sensitivities of TIR1-IAA12 and TIR1-IAA13 co-receptor complexes were higher than that of

other co-receptor pairs (Shimizu-Mitao and Kakimoto, 2014). This is not quite consistent with the Y2H interactions reported by Sugawara *et al.* (2015), but taken together, one may speculate that TIR1-IAA1 and TIR1-IAA2 might not primarily be a co-receptor combination responsible for PAA perception. Other distinct AUX/IAA clades, for instance IAA12/IAA13 could eventually participate in formation of PAA co-receptors. The lower affinity for PAA measured in competition binding assays might not be as pronounced for co-receptors containing AUX/IAAs other than IAA1/IAA2, and reflect an affinity that corresponds to the high endogenous PAA levels in many plant tissues (Sugawara *et al.*, 2015).

3.9 Challenging the co-receptor model – auxin as an orthosteric regulator of target-recognition by SCF^{TIR1}

The elucidation of the structural basis of auxin perception by Tan *et al.* (2007), provided evidence that auxin is not an allosteric regulator of SCF^{TIR1}, and auxin binding does not induce significant conformational changes. Rather, auxin enhances the AUX/IAA target-binding activity of TIR1 by acting as a ‘molecular glue’ instead of an allosteric switch (Tan *et al.*, 2007). Perception of the phytohormone jasmonate (JA) – precisely, of its bioactive form (3R,7S)-jasmonoyl-L-isoleucine (JA-Ile) – functions analogous to auxin perception. The FBP COI1 JA-Ile-dependently recognizes JAZ repressors for ubiquitination and subsequent degradation to activate a transcriptional response (Katsir *et al.*, 2008; Yan *et al.*, 2009). When JA-Ile perception was studied on the structural level, researchers found that a COI1:JAZ complex, rather than COI1 alone, functions as the genuine high-affinity JA-Ile receptor in a *co-receptor* form (Sheard *et al.*, 2010). The *co-receptor* model and terminology as a concept describing two interacting proteins providing full capability of hormone sensing, whose binding takes place at their PPI interface, was hypothesized and demonstrated for auxin perception soon after (Calderón Villalobos *et al.*, 2010; Calderón Villalobos *et al.*, 2012). However, in both auxin and jasmonate perception, the target alone (AUX/IAA or JAZ, respectively), does not exhibit a measurable affinity for the hormone (Dharmasiri *et al.*, 2005a; Yan *et al.*, 2009; Sheard *et al.*, 2010). A low hormone affinity of the FBP alone, could be demonstrated for COI1 in a JA-linked sepharose binding assay, where recombinant COI1 could be specifically retained (Yan *et al.*, 2009). For TIR1/AFBs, the early receptor studies reported binding of radiolabeled IAA to myc-tagged SCF^{TIR1} that was immunoprecipitated from transgenic plant extracts (Dharmasiri *et al.*, 2005a; Kepinski and Leyser, 2005). This suggests that auxin binds to the SCF^{TIR1} complex rather than to the AUX/IAA. However, TIR1 was only partially purified and not recombinantly expressed from heterologous system in this particular experiment. As Lee *et al.* (2014) argue, the complete auxin co-receptor complex has been found necessary in all binding assay formats so far. Binding to TIR1/AFBs alone has not yet been recorded, although this must

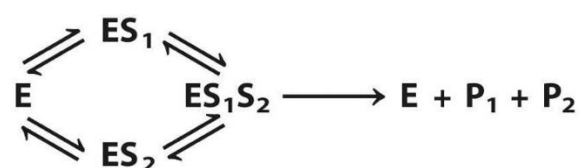
precede co-receptor assembly given that the binding pocket is completely occluded by degron association (Tan *et al.*, 2007; Lee *et al.*, 2014). Altogether, this suggests rather unequal roles in hormone binding for FBP and target, which together form the so-called *co-receptor*.

In the research field dealing with small-molecule modulation of PPIs, auxin is regarded as PPI stabilizer (Milroy *et al.*, 2014; Cesa *et al.*, 2015), in particular it could be classified as an orthosteric stabilizer of PPIs (Fischer *et al.*, 2015).

From an enzymology point of view, we are looking at a reaction involving two substrates, S_1 and S_2 (**Figure 3-3**), and an $SCF^{TIR1/AFB}$:auxin:AUX/IAA ternary complex (i.e. ES_1S_2 according to **Figure 3-3**). This reaction leads to the catalytic turnover of one substrate S_2 , namely the AUX/IAA, to the ubiquitinated product, AUX/IAA- Ub_n (P_2), by the enzyme (E) $SCF^{TIR1/AFB}$. Since auxin, corresponding to substrate S_1 , is not altered in the reaction, S_1 is in fact identical with P_1 (**Figure 3-3**). Next, one needs to ask whether the mechanism obeys a random or ordered mechanism. The study by Tan *et al.* (2007) indicates that an access of auxin to the binding pocket of TIR1 after degron binding is unlikely, thus a random binding mechanism for ternary complex formation seems improbable. Instead, a sequential (or ordered) binding mechanism appears applicable (**Figure 3-3**). A study employing an *in silico* molecular dynamics approach suggested that auxin acts as a conformational inducer leading F82 in the binding pocket of TIR1 to undergo a conformational change to accommodate subsequent binding of AUX/IAAs (Hao and Yang, 2010). This further substantiates a stepwise binding of auxin to TIR1 first, followed by AUX/IAA binding to the TIR1:auxin complex.

Enzyme reaction involving a ternary complex

Random order



Ordered



Figure 3-3: Model of a two-substrate enzyme reaction involving a ternary complex

A ternary complex can be formed either by a random (top row) or ordered (bottom row) mechanism. In this scheme, an enzyme E forms complexes with substrates S_1 and S_2 , resulting in products P_1 and P_2 , respectively. Since ternary complex formation in auxin sensing also includes an enzyme entity (the SCF^{TIR1}) and two binding partners, namely auxin (corresponding to S_1) and AUX/IAA (corresponding to S_2), it is standing to reason to classify it into one of the modes of mechanism. Figure modified from Nelson and Cox (2012).

This two-step binding reaction has been taken into account for determining dissociation constants for auxin co-receptor complexes via radioligand binding experiments, as expounded

in **Section 2.1.3.3**. As mentioned there, only the apparent dissociation constant K'_D has been assessable so far (**Figure 2-6** net reaction **(3)** corresponds to **Figure 3-4** dashed box).

Considering the aforementioned aspects, I would like to propose a refined concept of auxin perception in which TIR1 is regarded as the sole auxin receptor. TIR1 is used in an exemplary way here. Obviously, the described model can be applied to all TIR1/AFBs, and can even be transferred to COI1:JA-Ile:JAZ complex formation. The receptor TIR1 is part of the greater enzymatic entity SCF^{TIR1} and becomes modified through binding of the orthosteric regulator auxin (**Figure 3-4**, orange box). This renders SCF^{TIR1} to be in a modified or activated form, SCF^{TIR1*} , that can bind the AUX/IAA substrate with high affinity (**Figure 3-4**, green box). Subsequently, the AUX/IAA- Ub_n product is catalyzed through rounds of exchange of E2 for $E2\sim Ub$ after discharge of activated Ub to the AUX/IAA (**Figure 3-4**).

Furthermore, there are indications that SCF^{TIR1} might exhibit “basal”, auxin-independent, low affinity for some AUX/IAAs (Calderón Villalobos et al., 2012, and this thesis **Figure 2-2**, **Figure 3-4**, blue box). Also, the auxin-less SCF^{TIR1} :AUX/IAA complex was shown to lead to AUX/IAA ubiquitination *in vitro* (this thesis **Figure 2-13** mainly for IAA1; **Figure 3-4**, grey reaction arrows). However, basal auxin-independent degradation could not be observed in yeast (Havens et al., 2012), and when observed *in vivo*, it is most likely due to low endogenous auxin levels (Dreher et al., 2006; dos Santos Maraschin et al., 2009).

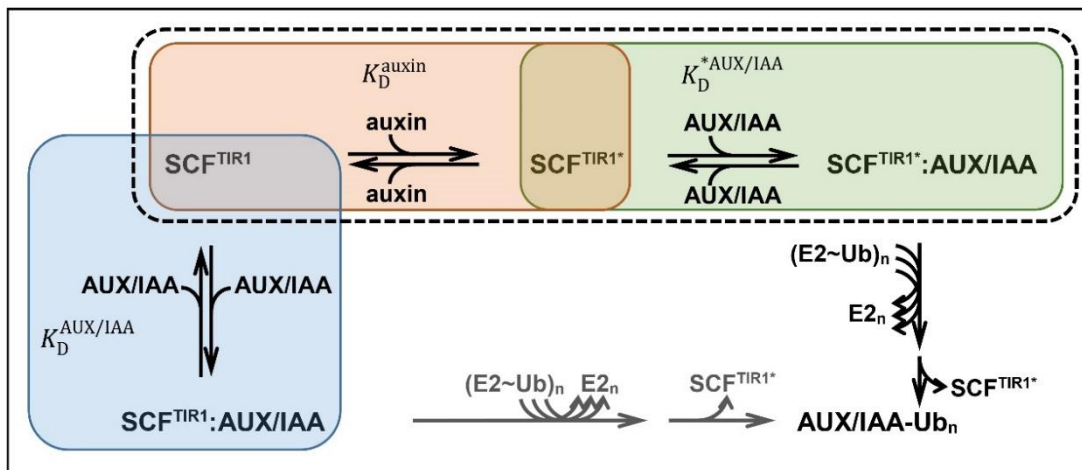


Figure 3-4: Hypothesis of partial binding reactions occurring in auxin co-receptor complex formation

The first binding reaction involves binding of auxin to SCF^{TIR1} to yield activated SCF^{TIR1*} (orange box) The dissociation constant of this binding reaction is here referred to as K_D^{auxin} . In a following binding reaction with dissociation constant $K_D^{*AUX/IAA}$, AUX/IAA binds to SCF^{TIR1*} and results in an $SCF^{TIR1*}:AUX/IAA$ (green box). This complex can then undergo polyubiquitination, here, signified by several reaction arrows indicating discharges of Ub from $E2\sim Ub$ to the AUX/IAA resulting in polyubiquitinated AUX/IAA (AUX/IAA- Ub_n). Alternatively, AUX/IAAs might bind to SCF^{TIR1} without a preceding auxin binding reaction to orthosterically activate TIR1 ($K_D^{AUX/IAA}$; blue box). Whether this results in AUX/IAA ubiquitination remains to be clarified (grey reaction arrows).

To confirm this model, the following assessments would be required. First, and most importantly, to confirm that TIR1 is a true receptor, the dissociation constant for binding of auxin to SCF^{TIR1} (K_D^{auxin} ; **Figure 3-4**, orange box) has to be determined. This has proven elusive in radioligand binding experiments, most likely due to auxin separating from TIR1 with high dissociation rates (for limitations of the radioligand binding approach also see Hellmuth and Calderón Villalobos (2016)). To establish alternative methods for determining this binding affinity, initial experiments have been performed in the course of this dissertation project using ITC and microscale thermophoresis. However, limitations in TIR1 protein expression yields and protein stability have impeded successful establishment of these methods. Second, it would be interesting to establish dissociation constants for binding of the different AUX/IAAs to the TIR1:auxin complex, or TIR1* ($K_D^{*\text{AUX/IAA}}$; **Figure 3-4**, green box). Expectably, the $K_D^{*\text{AUX/IAA}}$ values of different AUX/IAAs will exhibit the variation which until now has only been assessable in the apparent dissociation constants determined in this work and in Calderón Villalobos *et al.* (2012), as well as (Winkler *et al.*, under review). $K_D^{*\text{AUX/IAA}}$ can actually be calculated if the apparent dissociation constant (K'_D) of ternary complex formation (**Figure 3-4**, dashed box) and K_D^{auxin} (**Figure 3-4**, orange box) are known, since $K'_D = K_D^{\text{auxin}} * K_D^{*\text{AUX/IAA}}$. Experimentally, both K_D^{auxin} and $K_D^{*\text{AUX/IAA}}$ could be assessed in SPR experiments for example. For this, TIR1 protein will have to be immobilized on the chip, while auxin and AUX/IAA serve as analytes whose binding response is to be recorded. Although, IAA is a small analyte compound (175 Da), it should be detectable in SPR and could serve for determination of K_D^{auxin} . Next, adding AUX/IAA to immobilized TIR1 under buffer conditions saturating it with auxin, could serve to determine $K_D^{*\text{AUX/IAA}}$. This, however, has drawbacks, since at equilibrium, auxin will not be bound to all TIR1 molecules, turning them to TIR1*. Thus, AUX/IAAs might also exhibit basal binding to TIR1 (**Figure 3-4**, blue box). To overcome this heterogeneity of the immobilized receptor, one might have to draw upon cross-linking auxin into the TIR1 binding pocket. Only with a uniform fraction of orthosterically activated TIR1*, $K_D^{*\text{AUX/IAA}}$ can be experimentally determined with accuracy. Thirdly, basal TIR1:AUX/IAA interaction can be measured with immobilized TIR1 and AUX/IAA analyte. AUX/IAA oligomerization events could interfere with detection of the binding response of AUX/IAA to TIR1 in SPR assays. As discussed in **Section 3.4**, AUX/IAA mutant versions that are unable to form homomers, could serve well in *in vitro* binding experiments to address binding to TIR1 or TIR1*.

3.10 Concluding remarks

Taken together, this work contributed important insights to the understanding of the mechanism of auxin perception. We identified selected co-receptors that exhibit a similar auxin selectivity and high affinity for IAA, yet, they differ in their ubiquitination output. This indicates that the auxin co-receptor system offers plasticity on many levels. Open questions remain about the fine-tuning of receptor complex formation and AUX/IAA ubiquitination and most importantly, about its *in vivo* implications. The biochemical characterization of selected auxin receptors performed in this thesis can be exemplary for further studies on other auxin-co-receptor pairs. Also, the approaches and insights from this work can be instructive for investigations on analogous systems, since auxin is archetypal for perception and signaling of other plant hormones. As mentioned above, the plant hormone JA-Ile is perceived in a similar manner by a co-receptor complex and mediates repressor turnover by its corresponding E3 ligase. This gains tremendous relevance considering the large number of plant LRR-FBPs with the majority yet to be characterized. But also in the mammalian system, small molecule-mediated target recognition by E3 ligases has been reported (Ito *et al.*, 2010; Fischer *et al.*, 2014a). This highlights the importance of small molecule-mediated modulation of SCF complexes, which might be a wide-spread mechanism regulating target stability.

4 Summary

The phytohormone auxin – with its prevalent natural form indole-3-acetic acid (IAA) – is a key regulator of plant growth and development. It activates expression of auxin response genes by promoting the turnover of AUX/IAA transcriptional repressors. The TIR1/AFB target receptors of SCF-type E3 ubiquitin-ligases auxin-dependently bind the degron of AUX/IAs, thus targeting them for ubiquitination and subsequent proteasomal degradation. SCF^{TIR1/AFB} together with various AUX/IAs act as auxin co-receptors. Due to their modular and dynamic assembly, co-receptor combinations can potentially result in an array of auxin sensors impacting *in vivo* plasticity in growth and developmental responses. In this work, we have shown that auxin co-receptor complexes undergo multifaceted assembly. Differential auxin-dependent co-receptor assembly was assessed in a quantitative Y2H assay. This allowed the comparison of following aspects of co-receptor formation: (1) absolute strength of basal and auxin-dependent TIR1/AFB:AUX/IAA interaction, (2) relative auxin response of the interaction, and (3) patterns of preferred TIR1/AFB-AUX/IAA combinations, demonstrating that distinct features of AUX/IAs contribute to auxin-dependent co-receptor assembly. To identify sequence and structural determinants of auxin sensing in TIR1/AFBs and AUX/IAs, we employed a structural homology modeling approach for AFB1-3 on the one hand, and a AUX/IAA chimera approach on the other hand. Structural models revealed intriguing features of AFB2 loop-12 which might play a role in AUX/IAA target selectivity. Experiments with chimeric AUX/IAs revealed that the degron-tail – a short variable sequence C-terminal of the AUX/IAA degron – seemed to be required for AUX/IAA turnover *in vivo*. Furthermore, through this study, the body of biochemical information on auxin-sensors could be enlarged by specific affinities of four more receptor combinations. TIR1-IAA1, TIR1-IAA2, and, for the first time AFB2-containing receptors, AFB2-IAA1 and AFB2-IAA2, have been shown to constitute auxin receptors with similar high affinity ($K_D \approx 60$ nM). Biochemical analyses also revealed that not only IAA but also the natural auxin 4-Cl-IAA can be perceived by TIR1-IAA1 and TIR1-IAA2 co-receptors. Among the many PPIs that putatively accompany auxin co-receptor formation, here, AUX/IAA homomerization was studied and found to not influence co-receptor assembly. Although seemingly redundant with regard to auxin sensing, IAA1 and IAA2 exhibited differential auxin-responsive ubiquitination *in vitro*. This points to a possible functional diversification in IAA1 and IAA2 turnover. Finally, for future studies on *in vivo* auxin co-receptor assembly, AUX/IAA ubiquitination and half-life, stable lines overexpressing translational fusions of YFP to IAA1 and IAA2 in different *tir1/afb* mutant backgrounds have been generated and validated. Taken together, this thesis provided important insight on the mechanism of auxin sensing.

5 Zusammenfassung

Das Phytohormon Auxin – in seiner natürlich vorkommenden, häufigsten Form Indol-3-essigsäure (IAA) – ist maßgeblich an der Steuerung nahezu aller pflanzlicher Wachstums- und Entwicklungsprozesse beteiligt. Es löst den Abbau von AUX/IAA Transkriptions-Repressoren aus und aktiviert somit die Expression auxinabhängiger Gene. TIR1/AFB-Proteine, die in E3-Ubiquitinligasen vom SCF-Typ spezifisch Zielproteine erkennen, binden auxinvermittelt das AUX/IAA-Degron und leiten somit Ubiquitinierung und nachfolgenden proteasomalen Abbau der AUX/IAAs ein. SCF^{TIR1/AFBs} agieren zusammen mit AUX/IAAs als Auxin-Korezeptorkomplexe. Aufgrund ihrer modularen und dynamischen Zusammensetzung liegt es nahe, dass verschiedene Korezeptor-Kombinationen ein breites Spektrum an Auxin-Sensoren ermöglichen, die *in vivo* die Plastizität von Wachstum und Entwicklung beeinflussen. In der vorliegenden Arbeit wurde die facettenreiche Zusammensetzung und Funktion von Auxin-Korezeptoren untersucht. Zunächst wurden differentielle Auxin-Korezeptor-Interaktionen in einem quantitativen Hefe-Dihybrid-Experiment analysiert. Dadurch konnten folgende Aspekte der Korezeptoren-Formation verglichen werden: (1) absolute auxinunabhängige und -abhängige TIR1/AFB:AUX/IAA Interaktionsstärke, (2) relative Auxinabhängigkeit der Interaktionen sowie (3) Muster bevorzugter TIR1/AFB:AUX/IAA-Kombinationen. Dies zeigt, dass individuelle Eigenschaften der AUX/IAAs zur auxinabhängigen Assemblierung der Korezeptoren beitragen. Um in TIR1/AFBs und AUX/IAAs Eigenschaften auf Sequenz- und Strukturebene ausfindig zu machen, die die Auxin-Perzeption bestimmen, wurden verschiedene Ansätze verfolgt. Zunächst wurden Unterschiede zwischen TIR1 sowie AFB1, AFB2 und AFB3 mittels homologiebasierter Strukturmodellierung aufgeklärt. Es konnte gezeigt werden, dass ein kürzerer und flexiblerer Loop-12 in AFB2 möglicherweise ein geringeres sterisches Hindernis für die AUX/IAA-Bindung darstellt. Diese Beobachtung eröffnet neue Perspektiven zur Analyse der SCF^{TIR1/AFB} Zielprotein-Selektivität. Weiterhin wurden chimäre AUX/IAAs erzeugt und untersucht und ergaben, dass ein kurzer, variabler Sequenzabschnitt unmittelbar C-terminal des AUX/IAA-Degrone für deren Abbau *in vivo* erforderlich ist. Weiterhin konnten die biochemischen Daten zu Auxin-Rezeptoren um Affinitätswerte für vier weitere Korezeptor-Paare erweitert werden. TIR1-IAA1, TIR1-IAA2 sowie AFB2-IAA1 und AFB2-IAA2 konstituieren Rezeptoren, die Auxin mit hoher Affinität binden ($K_D \approx 60$ nM). Auch das natürlich in Pflanzen vorkommende Auxin 4-Chlor-IAA kann mit ähnlich hoher Affinität von TIR1-IAA1- und -IAA2-Rezeptorkomplexen gebunden werden. Darüber hinaus konnte gezeigt werden, dass AUX/IAA-Homomerisierung die Ausbildung eines Auxin-Rezeptorkomplexes nicht beeinflusst. Die noch wenig erforschte Ubiquitinierung von AUX/IAAs wurde anhand von IAA1 und IAA2, die sehr ähnliche Rezeptorkomplexe ausbilden,

untersucht. Interessanterweise weisen IAA1 und IAA2 Unterschiede in der Auxinresponsivität der Ubiquitinierung *in vitro* auf, was auf funktionelle Unterschiede insbesondere hinsichtlich der Stabilität dieser AUX/IAAs *in vivo* hindeutet. Schließlich wurden für weiterführende *in vivo*-Untersuchungen zur Auxin-Rezeptorkomplex-Assemblierung sowie zur AUX/IAA-Ubiquitinierung und -Stabilität ein Instrumentarium transgener Linien generiert und validiert. Diese überexprimieren translationelle YFP-AUX/IAA-Fusionen in TIR1/AFB-defizienten Mutanten. Zusammenfassend konnten somit im Rahmen dieser Dissertation wichtige Erkenntnisse über den Mechanismus der Auxin-Wahrnehmung in Pflanzen gewonnen werden.

6 Material and Methods

6.1 Material

6.1.1 Chemicals and supplies

Unless otherwise indicated, chemicals were obtained from the following suppliers: BD Difco, Carl Roth, Clontech Laboratories, Duchefa Biochemie, Merck, including Merck Millipore and Sigma-Aldrich, and Serva Electrophoresis. Cell culture and molecular biology supplies and kits were obtained from Bio&Sell, Life Technologies and Thermo Fisher Scientific. Primer synthesis as well as sequencing was performed by Eurofins Genomics.

6.1.2 Bacterial and yeast strains, insect cell culture, and plasmid vectors

The following bacterial strains were used molecular cloning purposes: *Escherichia coli* DH5 α (Thermo Fisher Scientific), *Escherichia coli* TOP10 (Thermo Fisher Scientific), and *Escherichia coli* XL1 blue (Agilent Technologies). *Escherichia coli* One Shot[®] ccdB Survival[™] 2 T1R (Thermo Fisher Scientific) was used to propagate empty Gateway[®] vectors. *Escherichia coli* BL21 (DE3) (Agilent Technologies) was used for protein expression. *Agrobacterium tumefaciens* GV3101 (Koncz and Schell, 1986) was used for plant transformation via floral dip and transient transformation in *Nicotiana benthamiana*.

Spodoptera frugiperda cell line Sf9 (Thermo Fisher Scientific) was used for baculovirus amplification and baculovirus-mediated protein expression.

The following yeast strains were used for PPI analyses via Y2H: *Saccharomyces cerevisiae* EGY48 (*MAT α*) (Clontech Laboratories) carrying reporter gene plasmid pSH18-34 (Thermo Fisher Scientific), and *Saccharomyces cerevisiae* YM4271 (*MAT α*) (Clontech Laboratories). Plasmid vectors listed in **Table 6-1** were used and/or generated in frame of this work, for instance for molecular cloning, recombinant expression, and Y2H. Plasmid vectors assembled through or adapted for Golden Gate modular cloning are listed separately in **Section 6.6.8**.

Table 6-1: Plasmid vectors used and/or generated, their purpose and features

Plasmid	Purpose and features	Reference
pDONR [™] 221	Gateway cloning <ul style="list-style-type: none"> <i>attP1</i>, <i>attP2</i>, <i>rrnB</i> T1 and T2, pUC ori, Kan^r, <i>ccdB</i> 	Thermo Fisher Scientific
pENTR/SD/D-TOPO	Gateway cloning <ul style="list-style-type: none"> <i>attL1</i>, <i>attL2</i>, <i>rrnB</i> T1 and T2, T7 gene 10 translation enhancer, RBS, TOPO[®] recognition sites, Kan^r, pUC ori 	Thermo Fisher Scientific
pGEX-4T-3 (Gateway compatible)	Protein expression in <i>E. coli</i>	GE Healthcare Life Sciences

	<ul style="list-style-type: none"> N-ter GST tag, thrombin site, tac Promoter, lac Operator, <i>lac</i>^q, RBS, Amp^r, pBR322 ori 	<ul style="list-style-type: none"> Gateway cassette insertion (see Section 6.6.8)
pLexA	Y2H protein expression <ul style="list-style-type: none"> <i>GAL1</i> promoter, N-ter DBD (LexA), <i>HIS3</i>, Amp^r 	Clontech (Gyuris <i>et al.</i> , 1993)
pB42AD (Gateway compatible)	Y2H protein expression <ul style="list-style-type: none"> <i>GAL1</i> promoter, N-ter AD (B42), N-ter HA epitope tag, <i>TRP1</i>, Amp^r Gateway version was provided by the host lab 	Clontech (Gyuris <i>et al.</i> , 1993)
pSH18-34	Y2H reporter plasmid <ul style="list-style-type: none"> <i>LacZ</i> (reporter) under control of 8LexA operators, 2μ ori, pUC ori, <i>URA3</i>, Amp^r 	Thermo Fisher Scientific
pB7WGY2	binary plant expression vector <ul style="list-style-type: none"> <i>attR1</i>, <i>attR2</i>, <i>ccdB</i>, CaMV 35S promoter and terminator, N-ter EYFP tag, LB, RB, Bar 	Karimi <i>et al.</i> (2002), Karimi <i>et al.</i> (2005)

6.2 Media

E. coli, yeast, insect cell, Agrobacterium, and Arabidopsis media used are listed with their composition and optional supplements in **Table 6-2**. All media were sterilized at 120° C and 2 bar for 15 min.

For bacterial selection, the corresponding antibiotics were added to LB or 2x YT medium. Protein expression in bacteria was induced by addition of isopropyl- β -D-1-thiogalactopyranoside (IPTG).

Yeast selection was based on dropout medium. To select for the corresponding auxotrophic markers dropout supplements were added to synthetic defined (SD) medium. SD medium was prepared with glucose for propagation of yeast carrying plasmids. For Y2H assays, SD selective induction medium was prepared with galactose for induction of protein expression, raffinose as additional carbon source, Dropout supplement for selection, and 5-bromo-4-chloro-3-indolyl- β -D-galactopyranoside (X-Gal) as a chromogenic reporter substrate.

Table 6-2: Media composition and supplements

medium type	composition	supplements	Reference
0.5x MS (<i>A. thaliana</i>)	2.203 g/L MS with vitamins (Duchefa), 10 g/L MES, 1% (w/v) sucrose pH 5.7 (with KOH)	8-10 g/L Plant Agar (Duchefa) 5 g/L Agargel (Sigma-Aldrich) 10 μ g/mL Basta® (200 g/L Glufosinat-ammonium; Bayer)	Murashige and Skoog (1962)
LB (Miller) (<i>E. coli</i> , <i>A. tumefaciens</i>)	10 g/L bacto tryptone, 10 g/L NaCl, 5 g/L yeast extract, pH 7.5 (with NaOH)	10 g/L Agar-agar 50 μ g/mL Kanamycin 50 μ g/mL Ampicillin 50 μ g/mL Hygromycin 100 μ g/mL Rifampicin 100 μ g/mL Spectinomycin	Bertani (1951)
2x YT (<i>E. coli</i>)	31 g/L 2x YT (Carl Roth)	50 μ g/mL Ampicillin 0.5-1 mM Isopropyl- β -D-1-thiogalactopyranoside (IPTG)	
SD (<i>S. cerevisiae</i>)	6.7 g/L Yeast Nitrogen Base without amino acids (BD),	20 g/L Agar-agar	Clontech Yeast Protocols (PT3024-1)

	Dropout Supplement (-Ura; -Ura,-His; -Ura,-His,-Trp depending on selection; Clontech), 2% (w/v) D(+)-glucose pH 5.8		
SD selective induction medium for Y2H (<i>S. cerevisiae</i>)	6.7 g/L Yeast Nitrogen Base without amino acids (BD), -Ura,-His,-Trp-Dropout Supplement (Clontech)	20 g/L Agar-agar 2% D(+)-galactose, 1% D(+)- raffinose, BU salts, 80 mg/L 5-bromo-4-chloro-3- indolyl-b-D-galactopyranoside (X- Gal) according to Clontech Yeast Protocols (PT3024-1)	Clontech Yeast Protocols (PT3024- 1)
YPD (<i>S. cerevisiae</i> YM4271)	20 g/L Peptone, 10 g/L yeast extract, 2% (w/v) D-glucose, pH 6.5	20 g/L Agar-agar	Clontech Yeast Protocols (PT3024- 1)
SF-900™ II SFM (<i>Sf9</i>)	ready-to-use serum-free medium	1-2x Penicillin-Streptomycin- Glutamine (Thermo Fisher Scientific)	Thermo Fisher Scientific
SF-4 BaculoExpress ICM (<i>Sf9</i>)	ready-to-use serum-free medium	1-2x Penicillin-Streptomycin- Glutamine (Thermo Fisher Scientific)	Bio&SELL

6.3 Plant material and cultivation

6.3.1 Plant lines

All experiments were performed using *Arabidopsis thaliana* ecotype Columbia-0 (Col-0). Mutant lines *tir1-1*, *afb2-3*, *afb3-4*, *tir1-1 afb2-3*, *tir1-1 afb3-4* (Ruegger *et al.*, 1998; Dharmasiri *et al.*, 2005b; Parry *et al.*, 2009) were either obtained via NASC or provided by the host lab.

6.3.2 Plant cultivation under sterile conditions

For sterile cultivation of plants, *Arabidopsis* seeds were surface sterilized for five min in 70% ethanol, followed by eight min incubation in 4.5% NaClO (v/v) with 0.01% Triton X-100 (v/v). Next, seeds were washed three times in sterile water and resuspended in sterile water or 0.1% agar for sowing on 0.5x MS plates. Seeds were stratified for at least two days at 4° C in the dark. Typically, plants were cultivated for propagation in growth chambers or cabinets under continuous light or long day conditions (16 hours day, 8 hours night) with ca. 130 $\mu\text{mol}/(\text{m}^2\text{s})$ light fluency at 20-22° C and 60 % relative humidity. Specific growth conditions are described for experiments individually where necessary. For selection procedures plants were grown on 0.5x MS plates supplied with 10 $\mu\text{g}/\text{mL}$ BASTA.

6.3.3 Plant cultivation on soil

Cultivation of *Arabidopsis* plants on soil was performed in growth chambers under long day conditions with ca. 100-130 $\mu\text{mol}/(\text{m}^2\text{s})$ light fluency at 20-22° C and 60 % relative humidity. Specific growth conditions are described for experiments individually where necessary. Plants for transformation, selection and propagation purposes were grown in the greenhouse under long day conditions at 18–20° C and 55–65 % relative humidity. The substrate used was “Einheitserde Typ GS 90” mixed with vermiculite (1–2 mm) in a 4:3 ratio.

6.3.4 Floral-dip transformation of *Arabidopsis*

Flowering *Arabidopsis* Col-0 plants were stably transformed with the *floral dip* method (Logemann *et al.*, 2006). *Agrobacterium* carrying the plasmid vector for expression of the gene of interest were streaked on two to three LB medium plates containing the corresponding antibiotics. After two days of incubation at 28° C, *Agrobacterium* cells were resuspended in liquid LB and diluted to an OD_{600} of 2.0. Next, 5 % (w/v) saccharose was added to the cell suspension in a 4:1 ratio. Silwet-L77 was added to a final concentration of 0.03 % (v/v). Plants were dipped upside down into the cell suspension and gently agitated for ten seconds, so that all flowers were thoroughly immersed. Afterwards, plants were kept moist and dark by wrapping the tray with foil and covering it for 24 hours. For setting of seeds, transformed plants were continued to be cultivated in the greenhouse under conditions given above (Section 6.3.3).

6.3.4.1 Selection procedures

T1 Seeds were harvested from transformed plants and densely sown on soil in large trays, stratified, and afterwards grown in the greenhouse. Circa 5-7 days after germination, the seedlings were sprayed with 80 mg/L Basta® solution every two to three days until Basta®-resistant seedlings were visible. The resistant seedlings (T1) were transferred to individual pots and cultivated further in the greenhouse for seed setting. Approximately ten independent T1 lines per construct and genetic background were isolated, and T1 lines were numbered (#1-#10). The *Agrobacterium*-mediated transformation procedure applied here, causes multiple insertion of transgene into the plant genome (Gelvin, 2003; Glowacka *et al.*, 2016). To reduce, at least to some extent, the likelihood of selecting transgenic lines with multiple insertions, the transformants were selected to show a 3:1 segregation in the T2 generation. To that end, T2 seeds were sown on 0.5x MS plates (ca. 100 seeds) containing 10 $\mu\text{g}/\text{mL}$ BASTA®. If T2 seedlings showed a 3:1 segregation, T2 seeds from the corresponding T1 line were selected for further propagation. In the case of YFP stable expression lines, ca. 5-

day old T2 seedlings were assayed for YFP expression through fluorescence microscopy, and the observed signal strength was recorded. Approximately ten T2 seedlings were then further propagated until setting of T3 seeds. T2 individuals (and thereby the resulting T3 seed batches) were numbered with a second numeral (e.g. #1.1-#1.10, #5.1-#5.10, ...). T3 seeds were again sown on Basta®-containing medium in plates to select for homozygous lines. These lines were used for determination of transcript levels of the transgene in seedlings via reverse transcription quantitative real-time PCR (RT-qPCR). Since T3 seed yield was overall low and seeds showed a low germination rate, T4 seeds were raised from the selected lines, and subsequent experiments were performed with T4 seedling material.

6.4 Bacterial and yeast general procedures

6.4.1 *Escherichia coli* and *Agrobacterium tumefaciens* cultivation

E. coli was cultivated overnight (16 hours) at 37° C either on LB plates or in LB liquid medium containing appropriate antibiotics. Liquid cultures were incubated with shaking at 140 to 180 rpm. Cultivation conditions for expression cultures are described below.

A. tumefaciens was cultivated on LB plates plus corresponding antibiotics at 28° C for two days. 5 mL-overnight cultures in liquid LB plus corresponding antibiotics were incubated shaking at 28° C and 140 to 180 rpm.

Stocks of *E. coli* clones were prepared from overnight cultures mixed with glycerol to a final concentration of 30% (v/v). Stocks of *A. tumefaciens* clones were prepared from overnight cultures mixed with glycerol to a final concentration of 30% (v/v), or with DMSO to a final concentration of 7% (v/v). Stocks were flash-frozen in liquid nitrogen and stored at -80° C.

6.4.2 *Escherichia coli* and *Agrobacterium tumefaciens* transformation

6.4.2.1 Transformation of chemically competent *E. coli*

Chemically competent *E. coli* DH5 α , XL1 blue, *ccdB* survival, TOP10, or BL21 (DE3) cells were transformed through heat shock method as follows. 50 μ L chemically competent cells were thawed on ice, carefully mixed with ca. 1 μ L plasmid DNA (ca. 100 ng/ μ L), and incubated for 20 min on ice, before applying a 30 seconds heat shock at 42° C in a water bath. Following this, cells were chilled on ice for two min before adding 0.5-1 mL liquid LB medium. Subsequently, transformed cells were incubated horizontally shaking at 37° C for one hour and then plated on LB plates containing antibiotics for selection of the transformed plasmid.

6.4.2.2 Transformation of electrocompetent *A. tumefaciens*

Electrocompetent *A. tumefaciens* GV3101 cells were transformed through electroporation. 50 μ L competent cells were carefully mixed with 1-2 μ L plasmid DNA (ca. 100 ng/ μ L) and pulsed in a 2 mm electroporation cuvette with a 2.5 kV pulse (BIO RAD MicroPulser Electroporator). 1 mL liquid LB medium was added and cells were incubated horizontally shaking at 28° C for two hours and then plated on LB plates containing Rifampicin and Gentamycin (see **Table 6-2**), as well as antibiotics for selection of the transformed plasmid.

6.4.3 *Saccharomyces cerevisiae* cultivation

S. cerevisiae was cultivated on SD dropout medium plates for propagations of plasmid carrying strains three days at 30° C. Only untransformed *S. cerevisiae* strain YM4271 and yeast mating were cultivated on non-selective YPD plates three days at 30° C. 3-5 mL overnight cultures in liquid SD dropout medium for preparation of stocks (see below) or expression tests (see **Section 6.7.8**) were incubated with vigorous shaking of at least 180 rpm. SD medium was supplied with either glucose, or with galactose/raffinose for propagation or for hybrid protein expression, respectively.

Stocks of haploid or diploid yeast clones were generated by growing overnight cultures in selective SD medium, recovering the cells by centrifugation and resuspending them in freezing medium (YPD, 25% glycerol (v/v)). Stocks were frozen and stored at -80° C.

6.4.4 *Saccharomyces cerevisiae* transformation with LexA Y2H plasmid vectors

Transformations of *S. cerevisiae* strains YM4271 or EGY48/pSH18-34 with plasmids carrying genes of interest for hybrid protein expression pB42AD or pLexA, respectively, were performed according to Clontech Yeast Protocols Handbook PT3024-1 (PR13103; 2001) Small-scale Lithium acetate (LiAc) Yeast Transformation Procedure. Liquid YPD or SD/-Ura was inoculated with few colonies of YM4271 or EGY48/pSH18-34, respectively, and cells were well dispersed. The cell suspension was transferred into 50 mL of YPD or SD/-Ura medium and incubated overnight at 30° C with shaking until stationary growth phase ($OD_{600} > 1.5$). Following this, part of the overnight culture was added to 300 mL YPD to reach an OD_{600} of 0.2–0.3 and incubated with shaking at 30°C for at least three hours until OD_{600} had doubled (0.4–0.6). Cells were harvested by centrifuging at 1000 x g for five min at RT, washed twice with sterile, deionized water (first wash 150 mL, second wash 50 mL), and finally resuspended in 1.5 mL TE/LiAc (10 mM Tris-HCl, 1 mM EDTA, 0.1 M lithium acetate, pH 7.5). Carrier DNA

was denatured before use by placing it in a boiling water bath for 20 min and immediately cooling it on ice for at least five min. For each transformation, 0.1 mg of plasmid DNA and 0.1 mg of carrier DNA, ssDNA from salmon testes (Sigma-Aldrich), were added to a 1.5-mL tube and mixed. Then, 0.1 mL of yeast competent cells were added to each tube and mixed by vortexing. Subsequently, 0.6 mL of sterile PEG/LiAc solution (10 mM Tris-HCl, 1 mM EDTA, 0.1 M lithium acetate, 40% (w/v) PEG4000, pH 7.5) was added to each tube and vortexed vigorously for ten seconds. The mixture was incubated at 30°C for 30 min horizontally shaking at 180 rpm. Following this, 70 µL of DMSO was added and mixed with cells by gentle inversion, before a heat shock was applied for 15 min in a 42°C water bath. Cells were briefly chilled on ice for 1-2 min and then recovered from the suspension by centrifuging for five seconds at 14 000 rpm at RT. The supernatant was removed and cells were washed twice in 0.5 mL of sterile TE buffer (10 mM Tris-HCl, 1 mM EDTA, pH 7.5). Cells were then resuspended in 0.5 mL TE buffer for plating on SD medium plates containing dropout supplement selecting for desired transformants, and incubated at 30° C for three to four days. Individual colonies were tested for presence of the plasmid by colony PCR, as described below. Expression levels for hybrid proteins were determined in diploid yeasts via immunoblot as described below.

6.5 Insect cell and Baculovirus general procedures

6.5.1 Cultivation of *Sf9* cells

Procedures involving *Sf9* insect cells and baculovirus were almost strictly performed according to “Guide to Baculovirus Expression Vector Systems (BEVS) and Insect Cell Culture Techniques” instruction manual (Invitrogen, now Thermo Fisher Scientific).

6.5.1.1 Suspension cultures

Sf9 cells (Thermo Fisher Scientific) were maintained as 30 mL suspension cultures in 250 mL polycarbonate cell culture flasks with vent cap (Corning®) in ready-to-use serum-free medium supplemented with Penicillin-Streptomycin-Glutamine (see **Table 6-2**) at 28° C gently agitating at 85 rpm. Cultures were passaged every two to three days. For that, cell density was first determined using a Neubauer counting chamber, before culture was split to 0.8×10^6 cells/mL into fresh medium.

6.5.1.2 Adhesive cultures

Sf9 cells (Thermo Fisher Scientific) were also cultivated 30 mL adhesive cultures in polystyrene cell culture dish with grid (15 cm diameter, Corning®) in ready-to-use serum-free medium supplemented with Penicillin-Streptomycin-Glutamine at 28° C. Cells were seeded at 40-50 %

confluency and grown to 70 % confluency for infection with Baculovirus. Confluency was determined using a stereomicroscope.

6.5.2 Freezing, storage and thawing of Sf9 cell stocks

For storing insect cell stocks, Sf9 cells at a low passage were recovered from a suspension culture by centrifuging for three min at 150 xg and RT, after cell density had been determined. Cells were then carefully resuspended in freezing medium [50 % (v/v) fresh Sf9 medium, 50% used Sf9 medium (supernatant from centrifugation), 7.5 % DMSO, 10 % BSA] to a density of 1×10^7 cells/mL. Aliquots of 1 mL were slowly cooled down 30 min at 4° C, 30 min at -20° C, one hour at -80° C, and finally stored in liquid nitrogen. Cells were thawed from stocks in a RT water bath, followed by addition of 1 mL Sf9 medium while stock culture was still partially frozen. When almost all visible frozen particles had disappeared in the stock vial, the content was immediately transferred to a flask with 30 mL fresh Sf9 medium for cultivation as above.

6.5.3 Baculovirus amplification and storage

Baculoviruses for expression were provided by the host lab (Tan *et al.*, 2007; Calderón Villalobos *et al.*, 2012 and unpublished)(also see **Section 6.7.4.2**). To amplify virus, adhesive Sf9 cultures were infected at ca. 70 % confluency. First, medium was removed from plates, 1-2 mL of virus was added (depending on virus titer) and incubated for one hour at RT on a rocker gently moving to evenly spread low virus volume across the whole plate surface. Following this, 30 mL fresh medium was added to the plates and incubated for three days at 28° C. Successful virus infection was evaluated using a stereomicroscope to observe confluency, cell shape and attachment. Amplified virus was harvested by detaching the culture from plate through pipetting, separating the cells from the medium by centrifugation, and filter-sterilizing (0.22 µm pore size syringe filter) and storing the virus-containing supernatant at 4° C in the dark. The infected cell material was usually subjected to an expression test or discarded.

6.6 Molecular biology methods

6.6.1 Polymerase chain reaction (PCR)

6.6.1.1 Standard and colony PCRs

Unless otherwise indicated, standard PCRs, including colony PCRs, were performed using DreamTaq™ Green PCR Master Mix (2x; Thermo Fisher Scientific).

A typical 10 µL PCR reaction consisted of:

- 5 μL DreamTaq™ Green Mastermix (2x)
- 0.75 μL forward primer (final concentration: 1.5 μM)
- 0.75 μL reverse primer (final concentration: 1.5 μM)
- 1 μL template DNA or cell material from a single bacterial or yeast colony
- ad 10 μL deionized water

The thermal profile used is shown in **Table 6-3**. The annealing temperature was typically set to 4–5 K lower than the melting temperature (T_m) of primers used. All primers used in this work are listed in **Supplementary Table 13** to **Supplementary Table 18**. The synthesis time for the expected amplicon was calculated based on a polymerase synthesis velocity of ca. 1 kb/min. For colony PCR from yeast, cells were pre-treated by boiling in 20 mM NaOH for 45 min at 95° C and using 1 μL of the extract as a template.

Table 6-3: Thermal profile for DreamTaq™ PCR

number of cycles	temperature	duration	phase
1	95° C	2 min	initial denaturation/activation
35	95° C	20 s	denaturation
	$T_m - 5$ K	30 s	annealing
	72° C	1 min/kb	extension
1	72° C	15 min	final extension

Following this, the reactions were analyzed via agarose gel electrophoresis (**Section 6.6.4**).

6.6.1.2 High-fidelity PCR for molecular cloning

Amplification of *AUX/IAA* coding sequences from Col-0 wild-type cDNA was performed with gene-specific primers designed to suffice requirements for Gateway entry clone generation with pENTR/SD/D-TOPO or pDONR221 vectors (see **Supplementary Table 13** and **Supplementary Table 14**). To ensure error-free fragment amplification, Phusion™ High-Fidelity PCR Master Mix with HF Buffer (Thermo Fisher Scientific) was used here according to manufacturer’s instructions. Typically, first a 10 μL test reaction was performed to optimize the conditions until one amplicon of predicted size was detectable in agarose gel electrophoresis. Subsequently, a 50 μL reaction was performed for loading on a preparative agarose gel for gel extraction of the amplified DNA fragment.

A typical 50 μL PCR reaction consisted of:

- 25 μL Phusion Master Mix (2x)
- 1.25 μL of 20 μM forward primer (final concentration: 0.5 μM)
- 1.25 μL of 20 μM reverse primer (final concentration: 0.5 μM)
- 1 μL template Arabidopsis Col-0 wild-type cDNA (ca. 50-200 ng)
- ad 50 μL deionized water

The thermal profile used is shown in **Table 6-4**. The annealing temperature was typically set to 4–5 K lower than the melting temperature (T_m) of primers used. Primers used are listed in

Supplementary Table 13 and **Supplementary Table 14**. The synthesis time for the expected amplicon was calculated based on a polymerase synthesis velocity of ca. 15-30 s/min.

Table 6-4: Thermal profile Phusion™ High-Fidelity PCR

number of cycles	temperature	duration	phase
1	98° C	30 sec	initial denaturation/activation
35	98° C	10 s	denaturation
	$T_m - 5$ K or max. 72° C	30 s	annealing
	72° C	15-30 s/kb	extension
1	72° C	10 min	final extension

6.6.2 Overlap extension PCRs

Before GoldenGate cloning was used to generate chimeras, truncated test chimeras were generated via overlap extension PCR for initial experiments (**Supplementary Figure 38**)(Wurch *et al.*, 1998). These chimeras consisted only of N-ter DI, linker and degon, and were only used in preliminary Y2H experiments shown in **Supplementary Figure 38**. High-fidelity Phusion PCR was performed and fragments were gel-purified as described in **Sections 6.6.1.2** and **6.6.5**. Fragments of *IAA12* and *IAA7* CDS were amplified with primers listed in **Table 6-5** from full-length expression constructs generated before. These primers carry a sequence specific for one gene, and a neighboring sequence overlap that is specific for the other gene. In a subsequent PCR, fragments were allowed annealing through their overlapping sequences, and extended through Dream Taq polymerase in a reaction mixture and with a thermal profile as described in **Section 6.6.1.1**, excluding primers. These annealing products were then used in a PCR reaction with *attB* primers (**Supplementary Table 14**) to amplify a full chimeric AUX/IAA for BP recombination into pDONR221 as described below (see **Section 6.6.7.2**). The final PCR product was gel-purified before BP reaction was performed. All PCR reaction mixtures were at a volume of 50 μ L.

Table 6-5: Primers used in overlap PCR for generation of chimeras

Primer	template gene	5'->3' sequence
7Li-12DII_F	At3g23050.1,At1g04550.2	TGCTAAAGCACAAAGTGGTAG
12Li-7DII_F	At1g04550.2,At3g23050.1	TCGTTCAAGTCAAGTGGTGG
12Li-7DII_R	At3g23050.1,At1g04550.2	CCACCACTTGACTTGAACGA
12DI-7Li_R	At1g04550.2,At3g23050.1	AGCCTCTCTTAGACCCAACG
7DI-12Li_R	At3g23050.1,At1g04550.2	CAGAGCGTTTGCTTCCCACC
7Li-12DII_R	At1g04550.2,At3g23050.1	CTACCACTTGTGCTTTAGCA
7DI-12Li_F	At3g23050.1,At1g04550.2	GGTGGGAAGCAAACGCTCTG
12DI-7Li_F	At1g04550.2,At3g23050.1	CGTTGGGTCTAAGAGAGGCT

6.6.3 Site-directed mutagenesis of plasmids

Site-directed mutageneses, for example for generation of *AUX/IAA* gain-of-function (gof) variants, or BM3 variant of *IAA1*, were performed with QuikChange II Site-Directed Mutagenesis Kit (Agilent) according to manufacturer's instructions. Primers used for mutagenesis are listed in **Supplementary Table 15**. Reaction products were transformed into competent *E. coli* cells provided with the kit, or into chemically competent *E. coli* DH5 α , TOP10, or XL1 blue as described above.

6.6.4 Agarose gel electrophoresis

PCR products were analyzed depending on fragment size on 1-2 % Agarose gels through electrophoretic separation. Gels were prepared by dissolving agarose in 1x TAE buffer (40 mM Tris-HCl pH 7.6, 20 mM acetic acid, 1 mM EDTA) and brief boiling, followed by addition of Serva DNA Stain G (Serva; 3 μ L/100 mL) for DNA staining before casting. Samples were loaded onto the gel, and where necessary, 10 μ L sample were mixed with 2 μ L 6x Orange G loading buffer (0.25 % (w/v) Orange-G, 30 % glycerol) beforehand. 1x TAE was used as running buffer. Electrophoretic separation was typically performed at 100-120 V. Analysis and documentation of electrophoresis gels was done with a UV transilluminator.

6.6.5 DNA extraction from agarose gel after electrophoretic separation

Extraction of DNA fragments amplified from PCR was performed with QIAquick[®] Gel Extraction Kit (QIAGEN) from TAE/Agarose gel according to manufacturer's instructions. Purified fragments were then used for TOPO[®] Cloning reaction with pENTR/SD/D-TOPO, or BP reaction with pDONR221 (Thermo Fisher Scientific).

6.6.6 DNA isolation

6.6.6.1 Plasmid DNA isolation from *E. coli*

6.6.6.1.1 Plasmid Mini-Preps

Isolation of plasmid DNA was performed with QIAprep[®] Spin Miniprep Kit (QIAGEN) according to manufacturer's instruction using a table top centrifuge. Plasmid DNA concentrations were spectrophotometrically determined with the Infinite[®] 200 NanoQuant (TECAN) device.

6.6.6.1.2 Phenol/chloroform extraction of plasmid DNA

Cloning procedures for *AUX/IAAs* into pENTR/SD/D-TOPO were marked by a low yield of positive clones after transformation into *E. coli*. Therefore, a larger number of colonies than usual was screened for positives with the following crude extraction method using a table top

centrifuge. 0.5 mL of a 5 mL-overnight culture was transferred to a 1.5 mL-tube and centrifuged for 5 min at maximum speed at RT. After discarding the supernatant, the pellet was resuspended in 50 μ L TE buffer (10 mM Tris-HCl, 1 mM EDTA, pH 8.0). 50 μ L of phenol/chloroform/isoamylalcohol (25:24:1) was added and mixed vigorously by vortexing for one minute. After centrifuging at maximum speed for 5 min, 10 μ L of the upper aqueous phase containing plasmid DNA was transferred to a 200 μ L-PCR tube and mixed with 2 μ L Orange G loading dye (0.25 % (w/v) Orange-G, 30 % glycerol) and subsequently loaded onto a 1% TAE/agarose gel. Electrophoretic separation was performed at lower voltage (80-100 V) to ensure separation of plasmids with and without inserts. Single positive clones identified via this method were then used to isolate plasmid DNA of high purity with method described in above.

6.6.7 Gateway cloning

The Gateway system (Thermo Fisher Scientific) was employed for molecular cloning to obtain translational fusions of *AUX/IAAs* for expression in yeast (Y2H), in plants (overexpression of YFP fusions) and in *E. coli* (overexpression of GST fusions). Entry clones were initially generated via the Topoisomerase-assisted pENTR/SD/D-TOPO vector system (pENTR™ Directional TOPO® Cloning Kit, Thermo Fisher Scientific), and later mainly with the recombinase-assisted cloning through attachment (*att*) sites and the pDONR system (Gateway® Technology, Thermo Fisher Scientific).

6.6.7.1 Directional cloning in pENTR/SD/D-TOPO

To obtain Arabidopsis *AUX/IAAs* coding sequences for Gateway cloning, *AUX/IAAs* were amplified from Col-0 wild-type cDNA with gene specific primers as described above. For entry clone generation with the pENTR/SD/D-TOPO system, primers listed in **Supplementary Table 13** were used. The forward primer carried the required CACC extension at the 5' end, and reverse primers were designed to include the stop codon. Amplification products were purified via gel extraction. The TOPO® cloning reaction was performed according to manufacturer's instructions and reaction products were either transformed into One Shot® Competent *E. coli* cells provided with the TOPO® Cloning Kit according to manufacturer's instructions, or transformed into chemically competent *E. coli* DH5 α , or XL1 blue cells as described above. Positive transformants were confirmed via colony PCR with vector-specific M13_for (**Supplementary Table 16**) and gene-specific pENTR-RV primer (**Supplementary Table 13**), or via Phenol/chloroform extraction of plasmid DNA (see **Section 6.6.6.1.2**). Confirmed positive clones were then sequenced with the M13 uni (-21) primer provided by the sequencing service (Eurofins Genomics).

6.6.7.2 Gateway recombination in pDONR221

To obtain Arabidopsis AUX/IAAs coding sequences for Gateway cloning, AUX/IAAs were amplified from Col-0 wild-type cDNA with gene specific primers as described above. For entry clone generation with the Gateway® system, primers with *attB1* and *attB2* sites listed in **Supplementary Table 14** were used. These primers were designed to include the stop codon. Amplification products were purified via gel extraction. BP recombination reactions were performed with Gateway BP Clonase II enzyme mix (Thermo Fisher Scientific). 150 ng purified PCR product and 150 ng plasmid DNA were mixed with TE buffer (10 mM Tris-HCl pH 8.0, 1 mM EDTA) to a total volume of 8.5 µL. Next, 1.5 µL BP-Clonase™ II Enzyme Mix was added and incubated at 25° C for at least one hour. The reaction was terminated by addition of 1 µL proteinase K and incubation at 37° C for 10 min. Typically, 1 µL of reaction mixture was used in subsequent transformation. Reaction products were transformed into chemically competent *E. coli* DH5α, or XL1 blue cells. Positive transformants were confirmed via colony PCR with vector-specific M13_for (**Supplementary Table 16**) and gene-specific primer (**Supplementary Table 13** and **Supplementary Table 14**), and then sequenced with the M13 uni (-21) primer provided by the sequencing service (Eurofins Genomics).

6.6.7.3 Gateway-conversion of pGEX-4T-3

Conversion of pGEX-4T-3 (GE Healthcare) into a version compatible with the Gateway system was performed with the Gateway® Vector Conversion System (Thermo Fisher Scientific) according to manufacturer's instructions. The vector was restricted with *EcoRI*. The Fill-in reaction with DNA Polymerase I, Large (Klenow) Fragment (Thermo Fisher Scientific) and Calf Intestinal Alkaline Phosphatase (CIAP; Thermo Fisher Scientific) reaction to remove 5' phosphate, as well as ligase reaction with T4 ligase (Thermo Fisher Scientific) required for the procedure were performed according to manufacturer's instructions. A Gateway cassette frame RfC.1 was ligated into the restriction site resulting in the vector map shown in **Supplementary Figure 48**.

6.6.7.4 Recombination into destination vectors

To create expression clones via the Gateway system, entry clones and destination vectors were combined in an LR reaction with Gateway® LR Clonase™ II Enzyme Mix (Thermo Fisher Scientific). 150 ng plasmid DNA of entry clone was mixed with 150 ng empty destination vector and TE buffer to a total volume of 8.5 µL. 1.5 µL LR Clonase™ II Enzyme Mix were then added, and the mixture incubated at 25° C for at least one hour. The reaction was terminated by addition of 1 µL proteinase K and incubation at 37° C for 10 min. Typically, 1 µL of reaction

mixture was used in subsequent transformation. Reaction products were transformed into chemically competent *E. coli* DH5 α , or XL1 blue cells. Positive transformants were confirmed via colony PCR with a combination of vector-specific (**Supplementary Table 16**) and gene-specific (**Supplementary Table 13** and **Supplementary Table 14**) primer, and then sequenced with a suitable primer.

6.6.8 Golden Gate modular cloning (MoClo) assembly of chimeras

Golden Gate Modular Cloning (MoClo) assembly (Engler and Marillonnet, 2013, 2014) was employed for 4-module and 5-module chimera assembly (**Supplementary Figure 43**) from *IAA7* and *IAA12*. A standard Golden Gate cloning procedure with one-step one-pot reaction including restriction enzyme and T4 DNA ligase (Werner *et al.*, 2012) was applied. MoClo vectors were kindly provided by Sylvestre Marillonnet (Department of Cell and Metabolic Biology, Leibniz Institute of Plant Biochemistry)(Weber *et al.*, 2011; Engler *et al.*, 2014). Modules of *IAA7* and *IAA12* (modules 1, 2, 3, 4, 4-1 and 4-2 corresponding to N-ter DI, Linker, degenon, DT+PB1, DT and PB1, respectively) were Phusion PCR-amplified with primers listed in **Supplementary Table 17**, gel-purified, and subsequently *BsaI*-cloned into pAGM1311 Level - 1 vector with kanamycin resistance (**Supplementary Figure 44**). Conserved amino acids in *IAA7* and *IAA12* sequence were chosen as module borders for scarless assembly (see **Supplementary Table 12** and **Supplementary Figure 44**). Directional assembly of modules to a full length chimeric *AUX/IAA* was then performed by *BpiI*-cloning into pAGM4031 Level 0 vector with spectinomycin resistance. The resulting, assembled chimeras in Level 0 were subsequently named pLUZ2 plasmids (see **Supplementary Figure 43** for an overview of all chimeras generated). As a last step, Level 0 chimeras were *BsaI*-cloned into Level 1 vectors for different purposes, including Y2H, *E. coli* and plant expression. Cloning was facilitated by blue/white selection. For this purpose, *E. coli* DH10B cells were plated on selective LB medium including 20 μ M X-Gal. Plasmids were verified by sequencing in each Level. MoClo strategy is visualized in **Supplementary Figure 44** to **Supplementary Figure 47**. Assembly or adaptation of Level 1 vectors is described below.

6.6.8.1 Generation of Golden Gate-compatible Level 1 vectors

Expression vectors pLUZ5 and pLUZ6 (vectors for AD LexA Y2H expression, and N-terminal GST fusion for *E. coli* expression, respectively) for Level 1 cloning were generated by removing *BsaI* sites from the vector backbone of pB42AD and pGEX-4T-3 (see **Table 6-1**), respectively, with site-directed mutagenesis using primers G717c FW and G717c RV (**Supplementary Table 17**). Additionally, a *LacZa* cassette for blue/white selection was amplified from pAGM3582 with GEXpr1_GG forward primer or b42pr1_GG forward primer for subsequent cloning into pGEX-

4T-3 or pB42AD, respectively and b42pr1_GG reverse primer (**Supplementary Table 17**). Through this amplification, *LacZα* cassette was framed by *BsaI* sites. *LacZα* was then cloned into pGEX-4T-3 and pB42AD *EcoRI* and *XhoI* multiple cloning site (**Supplementary Figure 46**). Maps of the resulting vectors are shown in **Supplementary Figure 49** and **Supplementary Figure 50**.

A binary vector for VENUS expression in plants (Level 1) was assembled from MoClo tool set kindly provided by Sylvestre Marillonnet (affiliation as stated above)(Engler *et al.*, 2014). First, a VENUS coding sequence was generated through site directed mutagenesis on YFP from pB7WGY2. Primers in **Supplementary Table 15** were used to introduce F47L, F65L, M154T, V164A, S176G. The VENUS coding sequence was then amplified with Venus GG FW und VENUS_NS GG RV primers (**Supplementary Table 17**) to include *BsaI* sites and *Bpil* sites for Level 1 cloning, and *BsaI*-cloned into pAGM1276, resulting in pLUZ1. MoClo elements in the following order were *BsaI*-cloned into the pICH75044 binary vector backbone: two times Cauliflower Mosaic virus 35S promoter from pICH45089, Tomato Mosaic Virus Ω 5'UTR from pAGT707, VENUS coding sequence from pLUZ1, chimera coding sequence from pLUZ2, U1 3'NTR from pICH53411 and Octopine synthase terminator from pICH53444. This yielded pLUZ3 plasmids where pLUZ2 chimera plasmids were used in the assembly. For an unspecific control plasmid, the phosphinothricin acetyltransferase gene (*Bar*) from pICH42222 was inserted instead of the chimeras from pLUZ2, resulting in the pLUZ4 control plasmid (**Supplementary Figure 47**).

6.6.9 Analysis of transcript levels from Arabidopsis seedlings

To determine transcript levels in transgenic or wildtype and mutant Arabidopsis seedlings, reverse transcription quantitative real-time PCR (RT-qPCR) was employed.

6.6.9.1 Harvesting of plant material and RNA isolation

For determination of overexpression transcript levels, T3 seedlings were cultivated on 0.5x MS plates and grown at 22°C under long day conditions (16/8) with ca. 100 $\mu\text{mol}/(\text{m}^2\text{s})$ light fluency and 60% relative humidity in a growth chamber for 5 days (118 hours). Ca. 100 mg plant material was harvested per sample, frozen in liquid nitrogen, and stored at -80° C until further processing. Triplicate samples were collected and processed individually. Isolation of total RNA was performed with RNeasy Plant Mini Kit (QIAGEN) according to manufacturer's instructions including DNase I treatment with RNase-Free DNase Set (QIAGEN). Frozen plant material was ground using a Tissue Lyser II (QIAGEN) bead mill and

glass beads (4 mm diameter). RNA concentrations were spectrophotometrically determined with the Infinite 200 NanoQuant (TECAN) device.

6.6.9.2 RNA agarose gel electrophoresis

For quality control of isolated RNA, an agarose gel electrophoresis was performed. Samples were mixed with 0.5 volumes of denaturing sample buffer (8 M Urea, 0.25 % w/v bromophenol blue, 0.25 % w/v xylene cyanol), incubated for ten min at 65° C, and chilled on ice for five min. Following this, RNA samples were electrophoretically separated on a TAE/Agarose gel as described above. Before performing RNA agarose gel electrophoresis, the gel chamber and parts were thoroughly cleaned by soaking in 1% SDS solution and rinsing with sterile water.

6.6.9.3 Quality control to detect DNA contamination in RNA preparations

In order to test for contamination with genomic DNA, RNA preparations were diluted corresponding to the cDNA dilutions finally used in RT-qPCR and used just as cDNA as template in a RT-qPCR reaction (see **Section 4.5.9.5**). When resulting cycle threshold (Ct) values were >30 or no Ct value resulted, contamination with genomic DNA could be neglected, and samples were used for cDNA synthesis and subsequent transcript level quantification.

6.6.9.4 cDNA synthesis

RNA preparations obtained and checked with above-mentioned methods were subjected to reverse transcription reactions to obtain cDNA representing the transcript levels of the corresponding samples. To that end, 1.5 µg RNA were used as a template. The cDNA synthesis was performed with RevertAid™ First Strand cDNA Synthesis Kit (Thermo Fisher Scientific) according to manufacturer's instructions. The optional denaturing step was omitted. Oligo(dT) primer was used. The resulting samples containing cDNA were subsequently diluted to test primer. For RT-qPCR, 1:10 dilutions were used.

6.6.9.5 Quantitative Real-Time-PCR (RT-qPCR)

RT-qPCRs were performed with Fast SYBR Green Mastermix (Thermo Fisher Scientific) according to manufacturer's instructions. Typically, a 10 µL reaction was set up as follows:

- 5 µL Fast SYBR Green Mastermix 5x
- 4 µL RT-qPCR forward and reverse primer mix (final concentration 0.25 µM each)
- 1 µL cDNA (1:10 dilution)
[alternatively: 1 µL RNA (dilution corresponding to cDNA dilution) for quality control]

Primers used for RT-qPCR were designed with the Primer3Plus tool (<http://www.bioinformatics.nl/cgi-bin/primer3plus/primer3plus.cgi/>)(Untergasser *et al.*, 2007), and are listed in **Supplementary Table 18**. The thermal profile is shown in **Table 6-6**. Fluorescence was measured at the end of the annealing phase and a dissociation curve was recorded during the last cycle. The PCR was performed on a MX3005P QPCR system (Agilent Technologies).

Table 6-6: Thermal profile for RT-qPCR

number of cycles	temperature	duration	fluorescence measurement
1	95° C	10 min	
45	95° C	30 s	
	60° C	1 min	* (end)
	72° C	30 s	
1	95° C	1 min	
	60° C	30 s	*(continuous)
	72° C	30 s	*

DNA generated in PCR cycles is quantifiable through fluorescence spectrometry. The Ct value serves as characteristic parameter at the end of a RT-qPCR run, and describes the number of amplification cycles that were necessary to have the fluorescence of amplified DNA exceed a threshold of background fluorescence. Consequently, the Ct value corresponds to the transcript amount. For relative quantification of transcripts, the constitutively expressed gene *PP2A* (AT1G13320) was always detected in parallel in every RT-qPCR sample and used as a reference gene (Czechowski *et al.*, 2005). Ct of the gene of interest was subtracted from Ct of *PP2A* to obtain the Δ Ct value. Assuming a doubling of DNA with every PCR cycle, transcript amounts were calculated $2^{\Delta Ct}$, since they increase exponentially with the number of cycles. As a result, transcript amounts relative to the reference gene *PP2A* were plotted for (**Supplementary Figure 23** and **Supplementary Figure 37**).

6.6.9.5.1 Data analysis

For transcript analysis, where comparison of different genes was essential (as in **Figure 2-16**, **Figure 2-17**, **Supplementary Figure 22**), data analysis was performed considering amplification efficiency as follows. Raw fluorescence data was exported from MXPro software and analyzed via Real-time PCR Miner (Zhao and Fernald, 2005) with default settings for Stratagene MX3000 platform. The outputs “AverageEfficiency_OfGenes” and “CT” from Miner were used to calculate the transcript amount X with the equation $X = \frac{1}{(1 + \text{AverageEfficiency_OfGenes})^{CT}}$. Relative transcript amounts were obtained by dividing X_{gene} by $X_{\text{reference } PP2A}$ and means of biological replicates were plotted with Prism 5 (GraphPad Software, Inc.). Analysis of frequency distribution was done in Prism 5 (GraphPad Software, Inc.).

6.7 Biochemical methods

6.7.1 Protein quantitation

Protein quantitation was performed either by roughly estimating the protein concentration of a preparation of interest by assessing it on an SDS-PAGE next to known amounts of bovine serum albumin (BSA), or with the following protein assays. Routinely, Bradford Protein Assay (BIO-RAD) was used by mixing 200 μ L of Bradford solution with 10 μ L of sample in a 96-well flat-bottom transparent plate and measuring absorbance at 595 nm after at least five min of incubation at RT for each sample. A standard curve was obtained by using known concentrations of BSA. Occasionally, Pierce BCA Protein Assay Kit (Thermo Fisher scientific) according to manufacturer's instructions was also implemented. For these purposes, Pierce™ Bovine Serum Albumin Standard Ampules, 2 mg/mL or Pierce™ Bovine Serum Albumin Standard Pre-Diluted Set (Thermo Fisher Scientific) was used.

6.7.2 SDS-PAGE

Electrophoretic separation of proteins was performed using Sodium dodecyl sulfate polyacrylamide gel electrophoresis (SDS-PAGE, Laemmli, 1970). Protein samples or extracts were mixed with 4x SDS-PAGE loading buffer (200 mM Tris-HCl, pH 6.8, 8% (w/v) SDS, 0.4% Bromophenol blue, 50% (v/v) glycerol, 20% (v/v) β -Mercaptoethanol) before loading onto gels consisting of a stacking and a resolving gel. See **Table 6-7** for composition. Typically, mini gels were prepared. For analysis of IVUs for example, maxi gels with a 5-15% polyacrylamide gradient were prepared using a gradient former (BioRAD) and a P1 peristaltic pump (Pharmacia). See **Table 6-8** for composition.

SDS-PAGE was performed in running buffer (25 mM Tris-HCl pH8.3, 192 mM glycine, 0.1% (w/v) SDS). For mini gels SDS-PAGE was run at RT at 100 V until samples had migrated through the stacking gel, and subsequently at 200-250 V during migration through the resolving gel. Maxi gradient SDS-PAGE were run at 90-110 V at 4° C until dye front had reached the lower rim of the gel.

Table 6-7: SDS-PAGE mini gel composition

Composition of stacking and resolving gel for different polyacrylamide concentrations of 8%, 10%, and 12% in the resolving gel.

SDS-PAGE mini gel	stacking gel		resolving gel	
polyacrylamide concentration	4 %	8%	10%	12%
components				

deionized water	3 mL	4.73 mL	4.13 mL	3.43 mL
40% acrylamide/bisacrylamide (37.5:1)	0.7 mL	2.7 mL	3.3 mL	4.0 mL
1.5 M Tris-HCl, 0.4% (w/v) SDS, pH 8.8	-	2.5 mL	2.5 mL	2.5 mL
0.5 M Tris-HCl, 0.4% (w/v) SDS, pH 6.8	1.25 mL	-	-	-
10% ammonium persulphate	25 μ L	60 μ L	60 μ L	60 μ L
<i>N, N, N', N'</i> -tetramethylethylenediamine	20 μ L	13 μ L	13 μ L	13 μ L
total volume	5 mL	10 mL	10 mL	10 mL

Table 6-8: SDS-PAGE maxi gradient gel composition

5% and 15% resolving gel mixes were combined to cast a gradient gel with a gradient maker and peristaltic pump.

SDS-PAGE maxi gradient gel	stacking gel		gradient resolving gel
polyacrylamide concentration	4 %	5%	15%
components			
deionized water	6.44 mL	8.39 mL	2.96 mL
40% acrylamide/bisacrylamide (37.5:1)	1.00 mL	1.69 mL	5.06 mL
1.5 M Tris-HCl, 0.4% (w/v) SDS, pH 8.8	-	3.38 mL	3.38 mL
0.5 M Tris-HCl, 0.4% (w/v) SDS, pH 6.8	2.50 mL	-	-
glycerol	-	-	2.14 mL
10% ammonium persulphate	33.33 μ L	27.00 μ L	27.00 μ L
<i>N, N, N', N'</i> -tetramethylethylenediamine	25.00 μ L	18.00 μ L	18.00 μ L
total volume	10 mL	13.5 mL	13.5 mL

6.7.2.1 Coomassie staining

SDS-PAGE gels were routinely stained with Coomassie to detect protein amounts \geq 100ng. To this end, gels were incubated in Coomassie staining solution (40% Ethanol (v/v), 10% acetic acid (v/v), 0.1% (w/v) Coomassie Brilliant Blue R250) at RT. Following the staining, the gel was rinsed with deionized water and destained in destaining solution (40% Ethanol (v/v), 10% acetic acid (v/v)) for 0.5-1 hour. Afterwards gels were stored in deionized water until documentation through scanning.

6.7.2.2 Silver staining

To detect lower amounts of protein (\leq 100 ng), SDS-PAGE gels were silver-stained according to the following protocol. First, gels were incubated for minimum one hour in fixing solution (50% ethanol, 10% acetic acid), followed by sensitizing for 45 min in sensitizer solution (0.02% (w/v) sodium thiosulphate in water). Gels were then rinsed in 20% ethanol two times for ten min each rinse, followed by four washes with deionized water for ten min each time. Following this, gels were incubated in 12 mM AgNO₃ solution for one hour, and dipped into a container with deionized water for approximately ten seconds. To develop, gels were placed into developer solution (3% (w/v) sodium carbonate, 250 μ L 37% (v/v) formaldehyde, 0.0012% sodium thiosulphate) until bands appeared at the desired intensity. Developing was

stopped by incubation in 4% Tris, 2% (v/v) acetic acid for minimum 30 min. Afterwards, gels were rinsed and stored in deionized water until documentation through scanning.

6.7.3 Immunoblotting (Western Blot)

Proteins separated via SDS-PAGE were transferred to nitrocellulose membrane (Amersham Protran, 0.45 μ m) through semi-dry blotting with Towbin transfer buffer with SDS [25 mM Tris, 192 mM Glycine, 20% (v/v) Methanol, 1.3 mM SDS, pH 8.3 (without adjustment)] at 20 V for 60 to 120 min depending on electrophoretic mobility of proteins and pore size of SDS-PAGE gel. After transfer, membranes were incubated for two hours in blocking solution (3-5% milk powder (w/v) in PBS-T or TBS-T) gently agitating at RT. Buffer systems were used depending on detection methods: PBS(-T) and TBS(-T) were applied for Horseradish peroxidase (HRP) or alkaline phosphatase (AP) detection, respectively. First antibody was applied as dilution indicated in **Table 6-9** in blocking solution. Membranes were incubated with gentle agitation in first antibody usually overnight at 4°C or for at least two hours at RT. Membranes were washed three times for five min with PBS or TBS and once for ten min in PBS-T or TBS-T. Secondary antibody was usually applied as dilution indicated in **Table 6-10** in PBS-T or TBS-T with gentle agitation for at least two hours at RT or overnight at 4° C. Washing was repeated as above. Horseradish peroxidase (HRP) detection was performed with SuperSignal West Pico Chemoluminescent Substrate (Thermo Fisher Scientific) according to manufacturer's instruction and chemoluminescent signal detected with X-ray films. Alkaline phosphatase (AP) detection was performed by incubating membrane in substrate solution (100 mM Tris-HCl, pH 9.5, 5 mM MgCl₂, 100 mM NaCl, 0.165 mg/mL Nitro blue tetrazolium, 0.33 mg/mL 5-Bromo-4-chloro-3-indolyl phosphate) until colorimetric detection of alkaline phosphatase activity and subsequently stopped by rinsing with water.

Table 6-9: Primary antibodies used in immunoblotting procedures

primary antibody	in	clonality	dilution	manufacturer	identifier
α -Glutathione-S-Transferase (GST)	rabbit	poly	1:2000	Sigma-Aldrich	G7781
α -Tubulin (YL1/2)	rat	mono	1:1000	abcam	ab6160
α -6xHis tag	rabbit	poly	1:1000	abcam	ab9108
α -LexA DNA BD	rabbit	poly	1:1000	abcam	ab14553
α -HA (F-7)	mouse	mono	1:1000	Santa Cruz Biotechnology	sc-7392
α -Ub (P4D1)	mouse	mono	1:1000	Santa Cruz Biotechnology	sc-8017
α -GFP (FL)	rabbit	poly	1:1000	Santa Cruz Biotechnology	sc-8334
α -Actin (plant) (10-3B)	mouse	mono	1:2000	Sigma-Aldrich	A0480

Table 6-10: Secondary antibodies used in immunoblotting procedures

Secondary Antibody	in	dilution	manufacturer	identifier
α -rabbit AP	goat	1:10'000	Sigma-Aldrich	A3687
α -mouse AP	goat	1:10'000	Sigma-Aldrich	A2179
α -rat AP	goat	1:5000-1:10000	Chemicon International	AP136A
α -mouse HRP	goat	1:10'000	thermo scientific	31430
α -rabbit HRP	goat	1:10'000	Santa Cruz Biotechnology	sc-2004
α -rat HRP	goat	1:10'000	abcam	ab97057
α -goat AP	rabbit	1:10.000-30.000	Sigma-Aldrich	A4187

6.7.4 Recombinant protein expression

6.7.4.1 GST-AUX/IAA expression in *E. coli*

GST-IAA1 and -IAA2 wild-type and mutant proteins were expressed from the pGEX-4T-3 (Gateway version) plasmid as N-terminal GST fusions in *E. coli* BL21 (DE3) cells. After selection of an expression clone, a 20-50 mL pre-culture in LB medium including 100 μ g/mL Ampicillin was inoculated and grown overnight at 37° C with 180 rpm shaking to stationary phase. Following this, an 1 L expression culture of 2x YT medium including 100 μ g/mL Ampicillin in a baffled flask was inoculated with 8-15 mL of pre-culture, and grown at 37° C with 160 rpm shaking for approximately three hours to an OD₆₀₀ of just below 1. To prepare for induction, the culture was chilled on ice-water for 15-20 min, and then, IPTG was added to a final concentration of 0.5 mM as an inducer. The expression was continued to incubate with 160 rpm shaking at 30° C for 8 to 16 hours. The cells were harvested by centrifugation and frozen at -20° C until further processing.

6.7.4.2 TIR1-ASK1 and AFB2-ASK1 expression with Baculovirus expression system (BEVS)

Baculoviruses for expression of GST-tagged TIR1 (TIR1 in pFB-GTE) and His₆-tagged ASK1 (ASK1 in pFB-HTB), as well as GST-AFB2 and His₆-ASK1 from a dual expression plasmid (pFB-Dual) were kindly provided by the host lab and generated in the Zheng lab (University of Washington)(Tan *et al.*, 2007; Calderón Villalobos *et al.*, 2012 and unpublished).

Expression cultures of *Sf9* cells were first raised to a volume of up to 100 mL in 250 mL polycarbonate cell culture flasks with vent cap (Corning®) or up to 1 L in 2.8 L Fernbach glass flasks in ready-to-use serum-free medium supplemented with Penicillin-Streptomycin-Glutamine (Table 6-2). To reach the final expression volume, cells at a density of approximately 3.0 * 10⁶ cells/mL were diluted to approximately 0.8 * 10⁶ cells/mL by adding

fresh medium. When the desired volume was reached, cells were grown for 1-2 days to a density of 1.5 to 2×10^6 cells/mL and centrifuged gently at $170 \times g$ for five to seven min at RT. The supernatant was removed and 3-15 mL virus added directly to the pellet and incubated gently agitating at 85 rpm at 28°C for one hour. The amount used to infect was approximated according to small-scale expression tests with the respective virus batch prior to the larger-scale expression. After this incubation, the cells were added to the 1.5- or 2-fold amount of medium consisting of equal parts of old medium (supernatant) and fresh medium in fresh flasks. The expression continued for 72 hours with cultures gently agitating at 85 rpm at 28°C . Cells were then harvested as described below.

6.7.5 Protein extraction from *E. coli* and *Sf9* cells

For protein extraction, cells were subjected to lysis. First, cell pellets were resuspended in 2-5 mL/g lysis buffer (20 mM Tris-HCl, pH 8.0, 200 mM NaCl, 5 mM DTT, 1 mM PMSF) mixed with cOmplete™, Mini, EDTA-free Protease Inhibitor Cocktail (Roche; 1 tablet per 50 mL). Cells were disrupted by sonification (Bandelin Sonopuls HD 3200, MS73 or MS72 sonotrode) 4-5 times for one min at 90% power with one second-pulses and 1 second-intervals on ice in a 4°C cold laboratory. Alternatively, cells were disrupted via French Press (Constant Systems TS 0.75) at 1.3 kbar and 4°C . In this case, PMSF and DTT were excluded from the lysis buffer and added to the lysate after French Press procedure. The lysates were cleared via centrifugation at $48000 \times g$ for 30 min at 4°C . For insect cell lysates, the clarification was repeated.

6.7.6 Protein purification

6.7.6.1 GST affinity purification

AUX/IAAs, as well as TIR1 and AFB2 were expressed as N-terminally GST-tagged recombinant proteins in *E. coli* or *Sf9* insect cells, respectively. For GST-AUX/IAAs and GST-AFB2, a one-step affinity purification was performed. GST-TIR1 was affinity-purified followed by tag-cleavage and anion exchange chromatography.

6.7.6.1.1 Gravity flow affinity purification

Gluthathione Sepharose® 4B (GE Healthcare) or Protino® Glutathione Agarose 4B (Macherey Nagel) were used as a matrix for affinity purification of GST-tagged AUX/IAA and TIR1/AFB2 proteins. Matrix was prepared according to manufacturer's instructions. Typically, cleared lysates from 1 L expression cultures were applied two times to 1 mL matrix (binding capacity: 8 mg GST/mL matrix) in a 25 mL flow column (BIO-RAD) by gravity flow. Three washes with 25 mL binding buffer (20 mM Tris-HCl, pH 8.0, 200 mM NaCl, 5 mM DTT) and 0.5 mL elution buffer (50 mM Tris-HCl, pH 8.0, 200 mM NaCl, 10 mM reduced Glutathione(GSH)) were

performed. Elution was accomplished by adding 500 μ L elution buffer to the closed column, incubating for ten min and subsequently collecting the eluate. This was repeated two to three times to obtain a total of three to four elutions, which were pooled after analysis on a SDS-PAGE. The whole procedure was performed at 4° C.

6.7.6.1.2 FPLC assisted affinity purification

Alternatively, GST-tagged AUX/IAAs and TIR1/AFB2 proteins were affinity-purified using GSTrap® 4B 1 mL (GE Healthcare) or Protino® GST/4B 1mL (Macherey Nagel) columns with ÄKTA pure chromatography system (GE Healthcare). Sample application was performed at a flow-rate of 0.5 mL/min, followed by washing with 10 column volumes (CV) binding buffer (20 mM Tris-HCl, pH 8.0, 200 mM NaCl, 5 mM DTT) at 1 mL/min flow rate, which usually caused absorbance at 280 nm to drop to baseline indicating complete removal of unbound protein. Elution was run at 0.5 mL/min with 100 % elution buffer (20 mM Tris-HCl, pH 8.0, 200 mM NaCl, 5 mM DTT) applied with pausing the system every 2 mL for ten min for longer incubation of column material in elution buffer yielding higher concentrated elution fractions. 0.5-1 mL fractions were collected of a total elution volume of 15 mL. Elution fractions were analyzed on SDS-PAGE and afterwards pooled accordingly.

6.7.6.2 Protein tag cleavage

GST-TIR1 was subjected to tag cleavage with tobacco etch virus (TEV) protease (Sigma-Aldrich; 10 units/ μ g) in batch or on column according to manufacturer's instructions. Typically, after buffer exchange to TEV cleavage buffer (25 mM Tris-HCl pH 8.0, 200 mM NaCl, 14 mM β -mercaptoethanol) 1 unit of TEV was used to cleave 2 μ g GST-TIR1 at 4° C overnight or at 30° C for one to two hours.

6.7.6.3 FPLC-assisted anion exchange chromatography

To remove TEV and cleaved GST from TIR1:His₆-ASK1 complex, anion exchange chromatography using a Mono Q 5/50 GL (GE Healthcare) 1 mL column. The following buffers were used:

- Equilibration buffer (20 mM Tris-HCl pH 8.0)
- Wash buffer (20 mM Tris-HCl pH 8.0, 1 M NaCl)
- Elution buffer (20 mM Tris-HCl pH 8.0, 200 mM NaCl)

After equilibration according to manufacturer's instructions with equilibration buffer, sample was applied with 0.5mL/min flow rate to the column and subsequently a gradient of elution buffer from 0% to 100% was applied over 20 CVs. The column was washed and equilibrated according to manufacturer's instructions. Flow rate for all phases was 2 ml/min.

6.7.7 General protein handling procedures

6.7.7.1 Protein concentration

After purification, proteins were concentrated when necessary using Amicon® Ultra Centrifugal Filters (EMD Millipore) with a 10K or 30K molecular weight cut-off according to manufacturer's instructions. Concentrators were also used for buffer exchange alternative to dialysis. Protein concentration was always performed at 4° C.

6.7.7.2 Dialysis

After GST-affinity purification, GST-AUX/IAs were dialyzed against binding buffer excluding glycerol (50 mM Tris-HCl, pH 8.0, 200 mM NaCl, 0.1% (v/v) Tween-20, excluding 10% (v/v) glycerol) with Spectra/Por® Dialysis Membrane with 3.5K or 6-8K molecular weight cut-off (Spectrum Laboratories). 10% (v/v) glycerol was added afterwards. Typically, dialysis was performed until GSH concentration was below approximately 0.01 mM.

6.7.7.3 Storage

Typically, purified proteins were kept in storage buffer (50 mM Tris-HCl, 200 mM NaCl, 5 mM DTT, 10 % (v/v) glycerol), aliquoted, flash-frozen in liquid nitrogen and stored at -80°. Wild-type AUX/IAA proteins were stored for maximum 5 days at 4° C.

6.7.8 Yeast protein extraction and expression analysis

To verify expression of hybrid proteins in yeast, diploid yeasts were grown in 3 mL selective induction medium (Gal/Raf/-Ura/-His/-Trp) overnight at 30° C with shaking at ≥ 180 rpm. Next, the OD₆₀₀ of the cultures was determined, and all cultures diluted to the lowest OD₆₀₀ with Gal/Raf/-Ura/-His/-Trp. The cultures were grown for an additional 0.5-1 hour at 30° C with shaking at ≥ 180 rpm, before recovering the yeast cells by centrifugation at RT for five min with 3200 x g. Yeast cells were then washed twice with 0.5 mL ice-cold, sterile water, transferred to 1.5-mL tubes and kept on ice for further processing. After washing, the cell pellet was resuspend 0.5 mL sample buffer (60 mM Tris-HCl pH 6.8, 10% (v/v) glycerol, 2% (w/v) SDS, 5% (v/v) β -Mercaptoethanol, 0.025% (w/v) Bromophenolblue) to which 1 mM PMSF, 1 mM Benzamidine and cComplete™, Mini, EDTA-free Protease Inhibitor Cocktail (Roche; 1 tablet per 50 mL) were added just prior to use. Following this, ca. 250 μ L acid-washed glass beads (0.5 μ m diameter; Sigma-Aldrich) were added, and samples vortexed at maximum speed five times for 45 seconds to break yeast cells and chilled on ice in between. Next, samples were centrifuged at 4°C with maximum speed for five min and the lysate (supernatant without interphase) transferred to a fresh tube. Samples were denatured for five min at 95° C before 20 μ L sample were loaded onto SDS-PAGE for electrophoretic separation followed by

immunoblotting as described below. Fusion proteins expressed from pB42AD and pLexA were detected with primary antibody α -HA (mouse) and α -LexA (rabbit), respectively (see **Table 6-9**). Loading controls were probed with α -tubulin (rat) (see **Table 6-10**).

6.7.9 Plant protein extraction

For analysis of overexpression of YFP fusion proteins in transgenic lines, seedlings were grown on 0.5x MS plates at long day conditions (16 hours day/ 8 hours night), 22° C and 90 μ mol/(m²s) for six days. 90-110 seedlings were transferred to 5 mL liquid 0.5x MS with 50 μ M MG-132 (stock dissolved in DMSO) or mock (corresponding volume of DMSO) in 6-well plates, vacuum-infiltrated for ten min, and incubated for 20 hours in a light room at 22° C gently agitating at 80 rpm. Seedlings were removed from the liquid medium and drained well on tissue paper, the fresh weight determined (approximately 300 mg) and flash frozen in liquid nitrogen to be stored at -80° C.

Frozen plant material was ground with mortar and pestil or using a Tissue Lyser II (QIAGEN) bead mill and glass beads (4 mm diameter) under liquid nitrogen. The ground plant material was resuspended in 50 μ L cold plant extraction buffer (50 mM Tris-HCl, pH 7.8, 100 mM NaCl, 10% (v/v) glycerol, 0.5 mM EDTA, 0.5% (v/v) NP-40) mixed with 1 mM PMSF and cComplete™, Mini, EDTA-free Protease Inhibitor Cocktail (Roche; 1 tablet per 50 mL). After transferring to 1.5 mL-tubes, the extract was cleared by centrifugation in a cooled table-top centrifuge at maximum speed for ten min. The supernatant was transferred to a fresh tube and clarification repeated. Cleared extracts were then used for immunoprecipitation procedures.

6.7.9.1 GFP-Trap immunoprecipitation

For immunoprecipitation, samples were diluted with dilution buffer (50 mM Tris-HCl pH7.8, 100 mM NaCl, 0.5 mM EDTA) to reduce NP-40 concentration. 15 μ L lysate were taken for input control to analyze in α -Actin immunoblot. GFP-Trap_A (Chromotek) slurry was washed in dilution buffer according to manufacturer's instructions. 20 μ L GFP-Trap_A slurry was added to lysate and incubated with slow end-over-end rotation at 4° C for one hour. Samples were centrifuged at 3500 x g for five min at 4° C to pellet the beads and the supernatant removed. GFP-trap beads were then washed twice with 500 μ L dilution buffer and centrifuged as above. After removal of supernatant, 100 μ L 2x Laemmli buffer (120 mM Tris-HCl pH 6.8, 4% (w/v) SDS, 20% (v/v) glycerol, 0.02% (w/v) bromophenol blue, 10% β -mercaptoethanol) were added to the loaded beads and boiled at 95° C for ten min to release the fusion protein. The beads were pelleted at 5000 x g for five min at 4° C. 20 μ L of sample were loaded onto SDS-PAGE for further analysis.

6.7.10 *In vitro* ubiquitination assays

In vitro ubiquitination (IVU) assays were performed as previously described (Winkler, 2015; Winkler *et al.*, under review). Proteins were expressed and purified as previously described, and kept in storage buffer (50 mM Tris-HCl, 200 mM NaCl, 5 mM DTT, 10 % (v/v) glycerol). Expression and purification of Uba1, Ubc8 and CUL1-RBX1 are described elsewhere (Winkler, 2015; Winkler *et al.*, under review). Untagged *Arabidopsis thaliana* Ubiquitin (Ub) was purchased from BostonBiochem (#U-100At).

In brief, two mixtures (A and B) were prepared in parallel (see **Table 6-11**) in reaction buffer (30 mM Tris-HCl pH 7.5, 100 mM NaCl, 1 mM DTT, 5 mM MgCl₂, 1 μM ZnCl₂, 2 mM ATP). For activation and E2-conjugation of Ub, E1 and E2 enzymes, as well as Arabidopsis Ub were combined in mix A. For preassembly of the SCF^{TIR1}:auxin:AUX/IAA complex, E3 components HsCUL1:MmRBX1 and AtASK1:AtTIR1, as well as target GST-IAA1 or -IAA2 and auxin were combined in mix B.

Table 6-11: Components in mixes A and B for *in vitro* ubiquitination reactions, their molecular weights and final concentrations

protein mix A	molecular weight in kDa	final concentration in μM
AtUb	8.6	130
His ₆ -AtUba1	123.3	1
His ₆ -AtUbc8	19.2	10
protein mix B	final concentration in μM	
MmCUL1-HsRBX1	101.1	0.5
AtTIR1-ASK1	85	0.5
GST-AtIAA1/-IAA2	47.7/46.8	10
auxin (IAA)	0.175	as indicated for individual experiments

Both mixtures were incubated for five min at 25 °C with 500 rpm orbital shaking. By combining mix A containing ubiquitin charged E2 (E2~Ub) and mix B containing SCF^{TIR1}:auxin:AUX/IAA complexes, the ubiquitination reactions were initiated (time point 0) and continued to be incubated at 25 °C with 500 rpm orbital shaking. 5 μL samples were taken from the reaction at indicated time points and immediately mixed with 3 μL SDS-PAGE loading buffer. 10 μL loading control samples were taken at the end of a IVU series. Samples were then separated on gradient SDS-PAGE and immunoblotted with α-Ubiquitin and α-GST antibodies to detect proteins covalently modified with Ub moieties, and to detect unmodified as well as covalently modified GST-AUX/IAA protein species, respectively.

6.8 Protein-Protein Interaction analyses

6.8.1 Yeast Two Hybrid Assay

Yeast Two Hybrid assay was performed using the LexA System following Clontech Yeast Protocols Handbook (PT3024-1). Plasmids encoding the AD-fusions were transformed into *Saccharomyces cerevisiae* strain YM4271 (*MAT α*), whereas plasmids encoding DBD-fusions were transformed into strain EGY48/pSH18-34 (*MAT α*). Non-Gateway DBD-TIR1/AFB clones were kindly provided by the host lab (Calderón Villalobos *et al.*, 2012). Diploid yeasts were generated via mating. To this end, haploid yeast were streaked in crosses on YPD plates, incubated at 30° C for ca. 24 hours, and subsequently cells from the area, where streaked strains intersected, were picked. These cells were then streaked on selective SD/-Ura/-His/-Trp medium for selection of diploid yeast and incubated at 30° C for 2 to 3 days. For evaluating protein-protein interaction, two forms of β -Galactosidase (β -Gal) reporter assays were carried out (see below).

6.8.1.1 Plate Y2H assay

For a plate Y2H assay, diploid yeasts were dispersed in ca. 200 μ L sterile water, diluted to a uniform OD₆₀₀ and then spotted on selective (-Ura/-His/-Trp) induction [2% (w/v) galactose, 1% (w/v) raffinose] media supplemented with 80 mg/L X-Gal and auxins for assessing β -Gal (*LacZ*) reporter gene expression. 3-5 μ L droplets were spotted. After incubation at 30° C for 2 to 5 days, and/or appearance of blue-colored yeast colonies, plates were scanned for documentation of results.

6.8.1.2 Quantitative ONPG-based Y2H assay

For a quantitative Y2H assay, diploid yeasts were dispersed in selective induction medium, diluted to a uniform OD₆₀₀, and used to inoculate triplicate 500 μ L- liquid culture samples in selective (-Ura/-His/-Trp) induction [2% (w/v) galactose, 1% (w/v) raffinose] media supplemented with 25 μ M IAA or mock in 96-deep well-plates. These cultures were grown at 30° C with vigorous shaking (180-200 rpm) over two nights (ca. 30 hours) to an OD₆₀₀ between 1 and 2. For later normalization, OD₆₀₀ of cultures was measured in a spectrophotometric plate reader infinite M1000 (TECAN). Cultures were centrifuged for five min at 1000 x g at 4° C and supernatant discarded. Cells were washed twice with 500 μ L Z-buffer (0.1 M sodium phosphate buffer pH 7.1, 10 mM KCl, 1 mM MgSO₄), and finally resuspended in 500 μ L Z-buffer. To lyse yeast cells, five freeze-thaw cycles were applied with 20 min freezing in liquid nitrogen and 30 min thawing in a 37° C water bath. Extracts were frozen in liquid nitrogen and stored at -80° C for less than a week. Extracts were then used to assess *LacZ* reporter gene expression, by adding 12 μ L yeast extract to 88 μ L ONPG-substrate solution (0.685 mg/mL

ONPG in Z buffer) and incubating for 4 hours at 30° C in the dark. Absorbance of ONPG turnover by LacZ was measured at 420 nm wavelength with spectrophotometric plate reader infinite M1000 (TECAN).

6.8.1.2.1 Data processing

Absorbance measurements of triplicate samples were processed in MS Excel the following way. First, null measurements were averaged and subtracted from sample measurements. Next OD₄₂₀ recorded in ONPG assay was normalized against OD₆₀₀ of cultures before processing. Means of triplicate samples were calculated. Further data analysis and visualization was done in R (available at <http://cran.r-project.org>; R Development Core Team, 2012) Heatmap.2 function of the gplots package was used with hclust hierarchical clustering with the default complete linkage method and Euclidean distance measure.

6.8.2 Radioligand Binding Assays

6.8.2.1 Considerations taken for equilibrium binding assays involving

TIR1:auxin:AUX/IAA complex formation

For the equilibrium binding assays we are following the assumptions of the law of mass action:

1. We assume that all of TIR1:ASK1 receptors have only one IAA binding site that is equally accessible to all of ³H-IAA ligand. The presence of only one IAA binding site has been shown in structural studies (Tan *et al.*, 2007). Although, there might be fractions of ASK1-less TIR1 potentially behaving differently from TIR1:ASK1, it is highly likely for those to be inactive or of negligible quantity. Also, TIR1:ASK1:AUX/IAA complexes might form ligand-independently to an extent, which we think are also of negligible quantity.
2. We assume that there are no states of partial binding, i.e. that TIR1:ASK1 exists either free or bound to ³H-IAA.
3. From the structural studies of (Tan *et al.*, 2007), we can be sure the assumption that neither ligand nor receptor are altered by binding,
4. and the assumption that binding is reversible is met. Also, the fact that homologous competition binding approaches could be successfully implemented demonstrates that TIR1:ASK1:auxin binding is reversible.

Furthermore, we designed the TIR1:AUX/IAA stoichiometric ratio to saturate the reaction with AUX/IAA protein. Thereby an effect of AUX/IAA availability (but not of the intrinsic nature as component of the co-receptor complex) for the second partial binding reaction (**Figure 3-4**) can be excluded, in order to compare apparent dissociation constants from complex

formation with either IAA1 or IAA2. Assuming that in GST-AUX/IAA preparations only a fraction of total protein is active, ratio of GST-AUX/IAA to TIR1/AFB is kept high (10^2 - 10^3 -fold).

6.8.2.2 Radioligand filter binding assays

Radioligand binding assays were performed as described in (Calderón Villalobos *et al.*, 2012; Hellmuth and Calderón Villalobos, 2016) using 8-20 nM purified TIR1:ASK1 protein complexes or 6-10 nM GST-AFB2:ASK1, as well as 0.7-8 μ M GST-tagged AUX/IAAs or their mutant versions and radiolabeled IAA [5- 3 H] (3 H-IAA) with a specific activity of 25 Ci/mmol (American Radiolabeled Chemicals, Inc.). All reactions were carried out in a volume of 100 μ L. Samples were prepared in duplicates or triplicates. To reach equilibrium binding, samples were incubated with orbital shaking for 30-90 min on ice, and subsequently immobilized on glass fiber filters with a vacuum manifold. Filter discs were incubated overnight in scintillation liquid (EcoScint, National Diagnostics or FilterSafe, Zinsser Analytik) until scintillation counting was performed with Beckman LSC 5000 (one minute 3 H; counting efficiency 60%).

6.8.2.2.1 Saturation binding and one-point binding assays

For saturation binding and one-point binding assays, non-specific binding was determined using 1-5 mM cold IAA (ca. 10^4 -fold excess with respect to maximum [3 H-IAA]). Specific binding was then calculated by subtracting non-specific from total binding. Raw data plots of total and non-specific binding are shown in **Supplementary Figure 11**. Cpm values obtained from scintillation counting were subsequently converted to binding sites (in fmol) per TIR1/AFB2 protein amount (in mg), and – in the case of saturation binding experiments – plotted against radioligand concentration. Saturation binding curves were fitted and K_D values obtained, using non-linear regression for a one-site, hyperbolic binding curve (Prism 5, GraphPad Software, Inc.).

6.8.2.2.2 Competition binding assays

For competition binding assays, ASK1:TIR1 as well as GST-AUX/IAA proteins were incubated with a fix concentration of 70 nM 3 H-IAA. After scintillation counting, cpm values were normalized as follows: total binding (in absence of unlabeled competitor) was set to 100% and non-specific binding (at maximum concentration of unlabeled competitor) was set to 0%. Data were plotted against the logmolar concentration of competitor and fitted with built-in analysis (one-site fit LogIC50) of Prism5, GraphPad Software, Inc. to obtain IC_{50} values. K_i values were calculated using the Cheng-Prusoff equation (Cheng and Prusoff, 1973) with K_D

values of 55 nM and 69 nM for TIR1-IAA1 and TIR1-IAA2, respectively, obtained from saturation binding experiments with ^3H -IAA.

6.8.2.2.3 Kinetic binding assay

Kinetic binding assay was performed to approximate the time frame for equilibrium establishment. Samples containing 8 nM TIR1:ASK1, 2 μM GST-AUX/IAA and 75 nM ^3H -IAA were set up for total binding (without cold IAA) and non-specific binding (including 1 mM cold IAA) in duplicates, and harvested to filter discs after different times of incubation with shaking on ice. Cpm values were plotted against incubation time and curves were fitted according to “One phase exponential association” model (Prism 5, GraphPad, Inc.).

6.9 Protoplast-based stability assays

6.9.1 Plasmid construction

Sensor constructs for expression in plant protoplasts were generated as previously described by (Wend *et al.*, 2013). In brief, the cDNA of AUX/IAA proteins to be used as sensor modules (SM) (constructs pLUZ2-1 through pLUZ2-16 and pLUZ19, pLUZ20, pLUZ11, pLUZ12; see **Supplementary Figure 43**) was PCR-amplified and Gibson-cloned into the existing pMIR expression vector, replacing the sensor module (L2min17-Luc), to encode for renilla-2A-SM-firefly under the control of a CaMV 35S promoter.

6.9.2 Plant material

A. thaliana (Col-0) seeds were plated in a line on autoclaved filter paper stripes (200-300 seeds/strip) placed on 12 cm square plates (Greiner Bio-One, Germany) containing SCA culture medium. After 24 h incubation at 4 °C, the plates were placed in a growth chamber, with a 16 h light regime at 23 °C. 2 to 3-week old plantlets were used for protoplast isolation.

6.9.3 Protoplast isolation, transformation and auxin treatment

Tissue pre-plasmolysis, digestion, protoplast isolation and transformation were performed according to Ochoa-Fernandez *et al.* (2016). For each construct tested, five separate transformations with 500 000 protoplasts in a final volume of 1.6 mL were performed in a 6-well plate (Corning Incorporated, Germany), sealed with parafilm, and incubated in the dark for 24 h. Before induction with auxin, the replicate transformations were pooled and 1 mL of protoplast solution was transferred into a well of a 2 mL deep-well storage plate (ABgene, Germany) for every concentration of auxin to be tested. Serial dilutions of auxin solutions in PCA-M medium (PCA salts, 600 mOsm mannitol, pH 5.8) were prepared at a 11-fold concentration and 100 μL were added to the 1 mL of protoplasts to obtain the appropriate

auxin end-concentration. Samples were incubated in the dark for 30 min before measurement of luciferase activity.

6.9.4 Inducers

Indole-3-acetic acid (IAA) (Sigma Aldrich, St. Louis, MO) was prepared as 50 mM stock in 95 % ethanol.

6.9.5 Luminescence analysis

In order to determine luciferase activity, 80 μ L of protoplast suspensions were used for luminescence determinations in 96-well flat-bottom white plates (Corning Incorporated, Germany). Firefly and Renilla luminescence was directly monitored using either a Synergy 4 multimode microplate reader (BioTek Instruments Inc., Winooski, VT), or an Infinite M200 Pro (Tecan Group Ltd., Männedorf, Switzerland) after addition of 20 μ L of either firefly luciferase substrate (20 mM Tricine, 2.67 mM $MgSO_4$, 0.1 mM EDTA, 33.3 mM DTT, 0.52 mM ATP, 0.27 mM Acetyl-CoA, 5 mM NaOH, 50 mM $MgCO_3$, 0.47 mM luciferin) or renilla luciferase substrate (472 μ M coelenterazine stock solution in methanol; diluted directly before use, 1:15 in PBS).

6.9.6 Statistical analysis

One-way ANOVA was performed using RlPlot version 1.5.

6.10 Physiological assays

6.10.1 Root elongation assay

For root elongation assays (REA), seedlings were sown on 0.5x MS plates with 15 g/L Agargel, stratified for two days at 4° C in the dark and cultivated at long-day conditions (16 hours day/ 8 hours night), 22° C, 90 μ mol/(m²s) for four days. Seedlings were then transferred to plates containing indicated concentrations of auxin and further cultivated. Plates were scanned 2, 3, and 4 days after transfer (dpt).

6.10.2 Temperature-induced hypocotyl elongation

For assays to assess temperature-induced hypocotyl elongation (TIHE), seedlings were grown on 0.5x MS plates with 15 g/L Agargel including sucrose, sealed with parafilm, and cultivated at long-day conditions (16 hours day/ 8 hours night), 20° C, 95 μ mol/(m²s) for one day. Then one set was kept at these growing conditions, while a duplicate set was shifted from 20° C to 28° C and photos for analysis of hypocotyl length were taken seven days after shifting.

6.10.3 Measurements and data analyses

Root and hypocotyl measurements were performed using ImageJ (Schneider *et al.*, 2012) with NeuronJ plugin (Meijering *et al.*, 2004) or with the Root Detection software

(<http://www.labutils.de/rd.html>). Rosette leaves area was quantified with Easy Leaf Area (Easlon and Bloom, 2014). Statistical analysis was performed in Prism 5 (GraphPad Software, Inc.).

6.11 *In silico* analyses

6.11.1 Homology modeling of auxin receptor complexes

Homology modeling has been performed using YASARA (Krieger *et al.*, 2009). Ligands, as well as co-crystallized IAA7 degrons were taken over from templates. Template structures not containing the degron were discarded. Remaining templates are: 2P1N, 2P1O, 2P1Q (Tan *et al.*, 2007). These templates have been taken from pdb_redo (Joosten *et al.*, 2014) and provided as input for homology modeling applying default parameters. Models were refined during a short molecular dynamics simulation using the force field YASARA2 (Krieger *et al.*, 2002). Resulting 3D models have been validated with Procheck (Laskowski *et al.*, 1993), ProSA2 (Sippl, 1993) and Qmean (Benkert *et al.*, 2008).

6.11.2 Gene expression data analysis

AtGenExpress (Schmid *et al.*, 2005; <http://jsp.weigelworld.org/AtGenExpress/resources/>), and Arabidopsis eFP (Winter *et al.*, 2007; <http://www.bar.utoronto.ca/>) were used to retrieve and compare *A. thaliana* expression profiles for IAA1 and IAA2 in different natural accessions (Lempe *et al.*, 2005), and developmental stages, as well as different tissues including: root cells types (Birnbaum *et al.*, 2003; Nawy *et al.*, 2005), microgametogenesis (Honys and Twell, 2004), embryo development (Casson *et al.*, 2005), flowers (Lempe *et al.*, 2005), xylem & cork (Zhao *et al.*, 2005), guard & mesophyll cells (Yang *et al.*, 2008), stem epidermis (Suh *et al.*, 2005), stigma & ovaries (Swanson *et al.*, 2005), pollen germination (Qin *et al.*, 2009), shot apical (Yadav *et al.*, 2009), trichomes (Marks *et al.*, 2009; Gilding and Marks, 2010). Statistical analysis was performed in Prism 5 (GraphPad Software, Inc.).

6.11.3 Sequence divergence between *A. thaliana* and *A. lyrata*

Nucleotide divergence rates (dN/dS) between 21,574 *A. thaliana* and *A. lyrata* orthologs were calculated using several functions implemented in the orthologR R package (<https://github.com/HajkD/orthologR>) as reported previously (Drost *et al.*, 2015). IAA1 and IAA2 *A. thaliana* sequences and the BLASTp (BLAST version 2.2.21) reciprocal best hit in *A. lyrata* were used to generate sequence alignments using the L-INS-i option in MAFFT (Katoh *et al.*, 2005). The resulting protein alignment and the corresponding nucleotide sequences were used to compute codon alignments with Pal2Nal (Suyama *et al.*, 2006). The codon alignments were used to compute the nucleotide divergence by a sliding window analysis

(window size: 15, step: 3) with DnaSPv5.1 (Librado and Rozas, 2009). The computation of dN/dS for specific amino acids was based on the model of (Chen *et al.*, 2004) using the R/Bioconductor package CorMut (Li *et al.*, 2014).

7 References

- Abas, L., Benjamins, R., Malenica, N., Paciorek, T., Wisniewska, J., Moulinier-Anzola, J.C., Sieberer, T., Friml, J., *et al.* (2006). Intracellular trafficking and proteolysis of the Arabidopsis auxin-efflux facilitator PIN2 are involved in root gravitropism. *Nat Cell Biol* **8**, 249-256.
- Abel, S., Oeller, P.W., and Theologis, A. (1994). Early auxin-induced genes encode short-lived nuclear proteins. *Proc Natl Acad Sci U S A* **91**, 326-330.
- Abel, S., Nguyen, M.D., and Theologis, A. (1995). The PS-IAA4/5-like family of early auxin-inducible mRNAs in Arabidopsis thaliana. *J Mol Biol* **251**, 533-549.
- Abel, S., and Theologis, A. (1995). A polymorphic bipartite motif signals nuclear targeting of early auxin-inducible proteins related to PS-IAA4 from pea (*Pisum sativum*). *Plant J* **8**, 87-96.
- Abel, S., and Theologis, A. (1996). Early genes and auxin action. *Plant Physiol* **111**, 9-17.
- Abel, S. (2007). Auxin is surfacing. *ACS Chem Biol* **2**, 380-384.
- Arase, F., Nishitani, H., Egusa, M., Nishimoto, N., Sakurai, S., Sakamoto, N., and Kaminaka, H. (2012). IAA8 involved in lateral root formation interacts with the TIR1 auxin receptor and ARF transcription factors in Arabidopsis. *PLoS One* **7**.
- Bachmair, A., Novatchkova, M., Potuschak, T., and Eisenhaber, F. (2001). Ubiquitylation in plants: a post-genomic look at a post-translational modification. *Trends Plant Sci* **6**, 463-470.
- Bai, C., Sen, P., Hofmann, K., Ma, L., Goebel, M., Harper, J.W., and Elledge, S.J. (1996). SKP1 connects cell cycle regulators to the ubiquitin proteolysis machinery through a novel motif, the F-box. *Cell* **86**, 263-274.
- Ballas, N., Wong, L.M., and Theologis, A. (1993). Identification of the auxin-responsive element, AuxRE, in the primary indoleacetic acid-inducible gene, PS-IAA4/5, of pea (*Pisum sativum*). *J Mol Biol* **233**, 580-596.
- Benjamins, R., and Scheres, B. (2008). Auxin: the looping star in plant development. *Annu Rev Plant Biol* **59**, 443-465.
- Benkert, P., Tosatto, S.C., and Schomburg, D. (2008). QMEAN: A comprehensive scoring function for model quality assessment. *Proteins* **71**, 261-277.
- Benkova, E., Michniewicz, M., Sauer, M., Teichmann, T., Seifertova, D., Jurgens, G., and Friml, J. (2003). Local, efflux-dependent auxin gradients as a common module for plant organ formation. *Cell* **115**, 591-602.
- Bertani, G. (1951). Studies on lysogeny. I. The mode of phage liberation by lysogenic *Escherichia coli*. *J Bacteriol* **62**, 293-300.
- Birnbaum, K., Shasha, D.E., Wang, J.Y., Jung, J.W., Lambert, G.M., Galbraith, D.W., and Benfey, P.N. (2003). A gene expression map of the Arabidopsis root. *Science* **302**, 1956-1960.
- Boer, D.R., Freire-Rios, A., van den Berg, W.A., Saaki, T., Manfield, I.W., Kepinski, S., Lopez-Vidriero, I., Franco-Zorrilla, J.M., *et al.* (2014). Structural basis for DNA binding specificity by the auxin-dependent ARF transcription factors. *Cell* **156**, 577-589.
- Calderón Villalobos, L.I., Tan, X., Zheng, N., and Estelle, M. (2010). Auxin perception--structural insights. *Cold Spring Harb Perspect Biol* **2**.
- Calderón Villalobos, L.I., Lee, S., De Oliveira, C., Ivetac, A., Brandt, W., Armitage, L., Sheard, L.B., Tan, X., *et al.* (2012). A combinatorial TIR1/AFB-Aux/IAA co-receptor system for differential sensing of auxin. *Nat Chem Biol* **8**, 477-485.

- Casson, S., Spencer, M., Walker, K., and Lindsey, K.** (2005). Laser capture microdissection for the analysis of gene expression during embryogenesis of Arabidopsis. *Plant J* **42**, 111-123.
- Causier, B., Ashworth, M., Guo, W., and Davies, B.** (2012a). The TOPLESS interactome: a framework for gene repression in Arabidopsis. *Plant Physiol* **158**, 423-438.
- Causier, B., Lloyd, J., Stevens, L., and Davies, B.** (2012b). TOPLESS co-repressor interactions and their evolutionary conservation in plants. *Plant Signal Behav* **7**, 325-328.
- Cesa, L.C., Mapp, A.K., and Gestwicki, J.E.** (2015). Direct and Propagated Effects of Small Molecules on Protein-Protein Interaction Networks. *Front Bioeng Biotechnol* **3**, 119.
- Chandler, J.W.** (2016). Auxin response factors. *Plant Cell Environ* **39**, 1014-1028.
- Chapman, E.J., and Estelle, M.** (2009). Mechanism of auxin-regulated gene expression in plants. *Annu Rev Genet* **43**, 265-285.
- Chen, L., Perlina, A., and Lee, C.J.** (2004). Positive selection detection in 40,000 human immunodeficiency virus (HIV) type 1 sequences automatically identifies drug resistance and positive fitness mutations in HIV protease and reverse transcriptase. *J Virol* **78**, 3722-3732.
- Chen, L., and Hellmann, H.** (2013). Plant E3 ligases: flexible enzymes in a sessile world. *Mol Plant* **6**, 1388-1404.
- Chen, Z.J., and Sun, L.J.** (2009). Nonproteolytic functions of ubiquitin in cell signaling. *Mol Cell* **33**, 275-286.
- Cheng, Y., and Prusoff, W.H.** (1973). Relationship between the inhibition constant (K₁) and the concentration of inhibitor which causes 50 per cent inhibition (I₅₀) of an enzymatic reaction. *Biochem Pharmacol* **22**, 3099-3108.
- Chhun, T., Taketa, S., Tsurumi, S., and Ichii, M.** (2004). Different Behaviour of Indole-3-Acetic Acid and Indole-3-Butyric Acid in Stimulating Lateral Root Development in Rice (*Oryza sativa* L.). *Plant Growth Regulation* **43**, 135-143.
- Colon-Carmona, A., Chen, D.L., Yeh, K.C., and Abel, S.** (2000). Aux/IAA proteins are phosphorylated by phytochrome in vitro. *Plant Physiol* **124**, 1728-1738.
- Conant, G.C., and Wolfe, K.H.** (2008). Turning a hobby into a job: how duplicated genes find new functions. *Nat Rev Genet* **9**, 938-950.
- Crooks, G.E., Hon, G., Chandonia, J.M., and Brenner, S.E.** (2004). WebLogo: a sequence logo generator. *Genome Res* **14**, 1188-1190.
- Czechowski, T., Stitt, M., Altmann, T., Udvardi, M.K., and Scheible, W.R.** (2005). Genome-wide identification and testing of superior reference genes for transcript normalization in Arabidopsis. *Plant Physiol* **139**, 5-17.
- Darwin, C., and Darwin, F.** (1881). *The power of movement in plants.* (New York: Appleton).
- Davuluri, R.V., Sun, H., Palaniswamy, S.K., Matthews, N., Molina, C., Kurtz, M., and Grotewold, E.** (2003). AGRIS: Arabidopsis gene regulatory information server, an information resource of Arabidopsis cis-regulatory elements and transcription factors. *BMC Bioinformatics* **4**, 25.
- De Rybel, B., Audenaert, D., Beeckman, T., and Kepinski, S.** (2009). The past, present, and future of chemical biology in auxin research. *ACS Chem Biol* **4**, 987-998.
- Dezfulian, M.H., Jalili, E., Roberto, D.K., Moss, B.L., Khoo, K., Nemhauser, J.L., and Crosby, W.L.** (2016). Oligomerization of SCFTIR1 Is Essential for Aux/IAA Degradation and Auxin Signaling in Arabidopsis. *PLoS Genet* **12**.
- Dharmasiri, N., Dharmasiri, S., Jones, A.M., and Estelle, M.** (2003). Auxin action in a cell-free system. *Curr Biol* **13**, 1418-1422.
- Dharmasiri, N., Dharmasiri, S., and Estelle, M.** (2005a). The F-box protein TIR1 is an auxin receptor. *Nature* **435**, 441-445.

- Dharmasiri, N., Dharmasiri, S., Weijers, D., Lechner, E., Yamada, M., Hobbie, L., Ehrismann, J.S., Jurgens, G., *et al.* (2005b). Plant development is regulated by a family of auxin receptor F box proteins. *Dev Cell* **9**, 109-119.
- Dinesh, D.C., Kovermann, M., Gopalswamy, M., Hellmuth, A., Calderón Villalobos, L.I., Lilie, H., Balbach, J., and Abel, S. (2015). Solution structure of the PslAA4 oligomerization domain reveals interaction modes for transcription factors in early auxin response. *Proc Natl Acad Sci U S A* **112**, 6230-6235.
- Dinesh, D.C., Villalobos, L.I., and Abel, S. (2016). Structural Biology of Nuclear Auxin Action. *Trends Plant Sci* **21**, 302-316.
- Ding, X., Richter, T., Chen, M., Fujii, H., Seo, Y.S., Xie, M., Zheng, X., Kanrar, S., *et al.* (2009). A rice kinase-protein interaction map. *Plant Physiol* **149**, 1478-1492.
- dos Santos Maraschin, F., Memelink, J., and Offringa, R. (2009). Auxin-induced, SCF(TIR1)-mediated poly-ubiquitination marks AUX/IAA proteins for degradation. *Plant J* **59**, 100-109.
- Dreher, K.A., Brown, J., Saw, R.E., and Callis, J. (2006). The Arabidopsis Aux/IAA protein family has diversified in degradation and auxin responsiveness. *Plant Cell* **18**, 699-714.
- Drost, H.G., Gabel, A., Grosse, I., and Quint, M. (2015). Evidence for active maintenance of phylotranscriptomic hourglass patterns in animal and plant embryogenesis. *Mol Biol Evol* **32**, 1221-1231.
- Duarte, J.M., Cui, L., Wall, P.K., Zhang, Q., Zhang, X., Leebens-Mack, J., Ma, H., Altman, N., *et al.* (2006). Expression pattern shifts following duplication indicative of subfunctionalization and neofunctionalization in regulatory genes of Arabidopsis. *Mol Biol Evol* **23**, 469-478.
- Dubrovsky, J.G., Napsucialy-Mendivil, S., Duclercq, J., Cheng, Y., Shishkova, S., Ivanchenko, M.G., Friml, J., Murphy, A.S., *et al.* (2011). Auxin minimum defines a developmental window for lateral root initiation. *New Phytol* **191**, 970-983.
- Duda, D.M., Borg, L.A., Scott, D.C., Hunt, H.W., Hammel, M., and Schulman, B.A. (2008). Structural insights into NEDD8 activation of cullin-RING ligases: conformational control of conjugation. *Cell* **134**, 995-1006.
- Easlon, H.M., and Bloom, A.J. (2014). Easy Leaf Area: Automated digital image analysis for rapid and accurate measurement of leaf area. *Appl Plant Sci* **2**.
- Ellis, R.J. (2001). Macromolecular crowding: obvious but underappreciated. *Trends Biochem Sci* **26**, 597-604.
- Engler, C., and Marillonnet, S. (2013). Combinatorial DNA assembly using Golden Gate cloning. *Methods Mol Biol* **1073**, 141-156.
- Engler, C., and Marillonnet, S. (2014). Golden Gate cloning. *Methods Mol Biol* **1116**, 119-131.
- Engler, C., Youles, M., Gruetzner, R., Ehnert, T.M., Werner, S., Jones, J.D., Patron, N.J., and Marillonnet, S. (2014). A golden gate modular cloning toolbox for plants. *ACS Synth Biol* **3**, 839-843.
- Epstein, E., and Ludwig-Müller, J. (1993). Indole-3-butyric acid in plants: occurrence, synthesis, metabolism and transport. *Physiologia Plantarum* **88**, 382-389.
- Falkenberg, B., Witt, I., Zanol, M.I., Steinhauser, D., Mueller-Roeber, B., Hesse, H., and Hoefgen, R. (2008). Transcription factors relevant to auxin signalling coordinate broad-spectrum metabolic shifts including sulphur metabolism. *Journal of Experimental Botany* **59**, 2831-2846.
- Finet, C., Berne-Dedieu, A., Scutt, C.P., and Marletaz, F. (2013). Evolution of the ARF gene family in land plants: old domains, new tricks. *Mol Biol Evol* **30**, 45-56.
- Fischer, E.S., Bohm, K., Lydeard, J.R., Yang, H., Stadler, M.B., Cavadini, S., Nagel, J., Serluca, F., *et al.* (2014a). Structure of the DDB1-CRBN E3 ubiquitin ligase in complex with thalidomide. *Nature* **512**, 49-53.

- Fischer, G., Rossmann, M., and Hyvonen, M.** (2015). Alternative modulation of protein-protein interactions by small molecules. *Curr Opin Biotechnol* **35**, 78-85.
- Fischer, I., Dainat, J., Ranwez, V., Glemin, S., Dufayard, J.F., and Chantret, N.** (2014b). Impact of recurrent gene duplication on adaptation of plant genomes. *BMC Plant Biol* **14**, 151.
- Fishbain, S., Prakash, S., Herrig, A., Elsasser, S., and Matouschek, A.** (2011). Rad23 escapes degradation because it lacks a proteasome initiation region. *Nat Commun* **2**, 192.
- Fishbain, S., Inobe, T., Israeli, E., Chavali, S., Yu, H., Kago, G., Babu, M.M., and Matouschek, A.** (2015). Sequence composition of disordered regions fine-tunes protein half-life. *Nat Struct Mol Biol* **22**, 214-221.
- Friml, J., Benkova, E., Blilou, I., Wisniewska, J., Hamann, T., Ljung, K., Woody, S., Sandberg, G., et al.** (2002a). AtPIN4 mediates sink-driven auxin gradients and root patterning in Arabidopsis. *Cell* **108**, 661-673.
- Friml, J., Wisniewska, J., Benkova, E., Mendgen, K., and Palme, K.** (2002b). Lateral relocation of auxin efflux regulator PIN3 mediates tropism in Arabidopsis. *Nature* **415**, 806-809.
- Friml, J.** (2003). Auxin transport - shaping the plant. *Curr Opin Plant Biol* **6**, 7-12.
- Friml, J., Vieten, A., Sauer, M., Weijers, D., Schwarz, H., Hamann, T., Offringa, R., and Jurgens, G.** (2003). Efflux-dependent auxin gradients establish the apical-basal axis of Arabidopsis. *Nature* **426**, 147-153.
- Fukaki, H., Tameda, S., Masuda, H., and Tasaka, M.** (2002). Lateral root formation is blocked by a gain-of-function mutation in the SOLITARY-ROOT/IAA14 gene of Arabidopsis. *Plant J* **29**, 153-168.
- Fukazawa, J., Ito, T., Kamiya, Y., Yamaguchi, S., and Takahashi, Y.** (2015). Binding of GID1 to DELLAs promotes dissociation of GAF1 from DELLA in GA dependent manner. *Plant Signal Behav* **10**.
- Gagne, J.M., Downes, B.P., Shiu, S.H., Durski, A.M., and Vierstra, R.D.** (2002). The F-box subunit of the SCF E3 complex is encoded by a diverse superfamily of genes in Arabidopsis. *Proc Natl Acad Sci U S A* **99**, 11519-11524.
- Gelvin, S.B.** (2003). Agrobacterium-mediated plant transformation: the biology behind the "gene-jockeying" tool. *Microbiol Mol Biol Rev* **67**, 16-37.
- Gilding, E.K., and Marks, M.D.** (2010). Analysis of purified glabra3-shapeshifter trichomes reveals a role for NOECK in regulating early trichome morphogenic events. *Plant J* **64**, 304-317.
- Gilkerson, J., Kelley, D.R., Tam, R., Estelle, M., and Callis, J.** (2015). Lysine Residues Are Not Required for Proteasome-Mediated Proteolysis of the Auxin/Indole Acidic Acid Protein IAA1. *Plant Physiol* **168**, 708-720.
- Girod, P.A., Carpenter, T.B., van Nocker, S., Sullivan, M.L., and Vierstra, R.D.** (1993). Homologs of the essential ubiquitin conjugating enzymes UBC1, 4, and 5 in yeast are encoded by a multigene family in Arabidopsis thaliana. *Plant J* **3**, 545-552.
- Glowacka, K., Kromdijk, J., Leonelli, L., Niyogi, K.K., Clemente, T.E., and Long, S.P.** (2016). An evaluation of new and established methods to determine T-DNA copy number and homozygosity in transgenic plants. *Plant Cell Environ* **39**, 908-917.
- Gray, W.M., del Pozo, J.C., Walker, L., Hobbie, L., Risseuw, E., Banks, T., Crosby, W.L., Yang, M., et al.** (1999). Identification of an SCF ubiquitin-ligase complex required for auxin response in Arabidopsis thaliana. *Genes Dev* **13**, 1678-1691.
- Gray, W.M., Kepinski, S., Rouse, D., Leyser, O., and Estelle, M.** (2001). Auxin regulates SCF(TIR1)-dependent degradation of AUX/IAA proteins. *Nature* **414**, 271-276.
- Grossmann, K.** (2010). Auxin herbicides: current status of mechanism and mode of action. *Pest Manag Sci* **66**, 113-120.
- Guharoy, M., Bhowmick, P., Sallam, M., and Tompa, P.** (2016). Tripartite degrons confer diversity and specificity on regulated protein degradation in the ubiquitin-proteasome system. *Nat Commun* **7**, 10239.

- Guilfoyle, T.J., and Hagen, G.** (2007). Auxin response factors. *Curr Opin Plant Biol* **10**, 453-460.
- Guilfoyle, T.J., and Hagen, G.** (2012). Getting a grasp on domain III/IV responsible for Auxin Response Factor-IAA protein interactions. *Plant Sci* **190**, 82-88.
- Guseman, J.M., Hellmuth, A., Lanctot, A., Feldman, T.P., Moss, B.L., Klavins, E., Calderón Villalobos, L.I., and Nemhauser, J.L.** (2015). Auxin-induced degradation dynamics set the pace for lateral root development. *Development* **142**, 905-909.
- Gyuris, J., Golemis, E., Chertkov, H., and Brent, R.** (1993). Cdi1, a human G1 and S phase protein phosphatase that associates with Cdk2. *Cell* **75**, 791-803.
- Hagen, G., and Guilfoyle, T.** (2002). Auxin-responsive gene expression: genes, promoters and regulatory factors. *Plant Mol Biol* **49**, 373-385.
- Hamann, T., Mayer, U., and Jurgens, G.** (1999). The auxin-insensitive bodenlos mutation affects primary root formation and apical-basal patterning in the Arabidopsis embryo. *Development* **126**, 1387-1395.
- Hamann, T., Benkova, E., Baurle, I., Kientz, M., and Jurgens, G.** (2002). The Arabidopsis BODENLOS gene encodes an auxin response protein inhibiting MONOPTEROS-mediated embryo patterning. *Genes Dev* **16**, 1610-1615.
- Han, M., Park, Y., Kim, I., Kim, E.H., Yu, T.K., Rhee, S., and Suh, J.Y.** (2014). Structural basis for the auxin-induced transcriptional regulation by Aux/IAA17. *Proc Natl Acad Sci U S A* **111**, 18613-18618.
- Hao, G.F., and Yang, G.F.** (2010). The role of Phe82 and Phe351 in auxin-induced substrate perception by TIR1 ubiquitin ligase: a novel insight from molecular dynamics simulations. *PLoS One* **5**.
- Hatfield, P.M., Gosink, M.M., Carpenter, T.B., and Vierstra, R.D.** (1997). The ubiquitin-activating enzyme (E1) gene family in Arabidopsis thaliana. *Plant J* **11**, 213-226.
- Havens, K.A., Guseman, J.M., Jang, S.S., Pierre-Jerome, E., Bolten, N., Klavins, E., and Nemhauser, J.L.** (2012). A synthetic approach reveals extensive tunability of auxin signaling. *Plant Physiol* **160**, 135-142.
- Hellmuth, A., and Calderón Villalobos, L.I.** (2016). Radioligand Binding Assays for Determining Dissociation Constants of Phytohormone Receptors. *Methods Mol Biol* **1450**, 23-34.
- Hershko, A., and Ciechanover, A.** (1998). The ubiquitin system. *Annu Rev Biochem* **67**, 425-479.
- Herud, O., Weijers, D., Lau, S., and Jurgens, G.** (2016). Auxin responsiveness of the MONOPTEROS-BODENLOS module in primary root initiation critically depends on the nuclear import kinetics of the Aux/IAA inhibitor BODENLOS. *Plant J* **85**, 269-277.
- Holland, A.J., Fachinetti, D., Han, J.S., and Cleveland, D.W.** (2012). Inducible, reversible system for the rapid and complete degradation of proteins in mammalian cells. *Proc Natl Acad Sci U S A* **109**, 3350-3357.
- Honys, D., and Twell, D.** (2004). Transcriptome analysis of haploid male gametophyte development in Arabidopsis. *Genome Biol* **5**, R85.
- Hua, Z., and Vierstra, R.D.** (2011). The cullin-RING ubiquitin-protein ligases. *Annu Rev Plant Biol* **62**, 299-334.
- Iglesias, M.J., Terrile, M.C., Windels, D., Lombardo, M.C., Bartoli, C.G., Vazquez, F., Estelle, M., and Casalongue, C.A.** (2014). MiR393 regulation of auxin signaling and redox-related components during acclimation to salinity in Arabidopsis. *PLoS One* **9**.
- Ito, T., Ando, H., Suzuki, T., Ogura, T., Hotta, K., Imamura, Y., Yamaguchi, Y., and Handa, H.** (2010). Identification of a primary target of thalidomide teratogenicity. *Science* **327**, 1345-1350.
- IUPAC-IUB, C.o.B.N.C.** (1968). A One-Letter Notation for Amino Acid Sequences*. *European Journal of Biochemistry* **5**, 151-153.

- Jing, H., Yang, X., Zhang, J., Liu, X., Zheng, H., Dong, G., Nian, J., Feng, J., *et al.* (2015). Peptidyl-prolyl isomerization targets rice Aux/IAs for proteasomal degradation during auxin signalling. *Nat Commun* **6**, 7395.
- Joosten, R.P., Long, F., Murshudov, G.N., and Perrakis, A. (2014). The PDB_REDO server for macromolecular structure model optimization. *IUCrJ* **1**, 213-220.
- Kagale, S., Links, M.G., and Rozwadowski, K. (2010). Genome-wide analysis of ethylene-responsive element binding factor-associated amphiphilic repression motif-containing transcriptional regulators in Arabidopsis. *Plant Physiol* **152**, 1109-1134.
- Kagale, S., and Rozwadowski, K. (2011). EAR motif-mediated transcriptional repression in plants: an underlying mechanism for epigenetic regulation of gene expression. *Epigenetics* **6**, 141-146.
- Kanke, M., Nishimura, K., Kanemaki, M., Kakimoto, T., Takahashi, T.S., Nakagawa, T., and Masukata, H. (2011). Auxin-inducible protein depletion system in fission yeast. *BMC Cell Biol* **12**, 8.
- Karcz, W., and Burdach, Z. (2002). A comparison of the effects of IAA and 4-Cl-IAA on growth, proton secretion and membrane potential in maize coleoptile segments. *J Exp Bot* **53**, 1089-1098.
- Karimi, M., Inze, D., and Depicker, A. (2002). GATEWAY vectors for Agrobacterium-mediated plant transformation. *Trends Plant Sci* **7**, 193-195.
- Karimi, M., De Meyer, B., and Hilson, P. (2005). Modular cloning in plant cells. *Trends Plant Sci* **10**, 103-105.
- Katayama, M. (2000). Synthesis and biological activities of 4-chloroindole-3-acetic acid and its esters. *Biosci Biotechnol Biochem* **64**, 808-815.
- Katoh, K., Kuma, K., Toh, H., and Miyata, T. (2005). MAFFT version 5: improvement in accuracy of multiple sequence alignment. *Nucleic Acids Res* **33**, 511-518.
- Katsir, L., Schillmiller, A.L., Staswick, P.E., He, S.Y., and Howe, G.A. (2008). COI1 is a critical component of a receptor for jasmonate and the bacterial virulence factor coronatine. *Proc Natl Acad Sci U S A* **105**, 7100-7105.
- Kazan, K., and Manners, J.M. (2009). Linking development to defense: auxin in plant-pathogen interactions. *Trends Plant Sci* **14**, 373-382.
- Ke, J., Ma, H., Gu, X., Thelen, A., Brunzelle, J.S., Li, J., Xu, H.E., and Melcher, K. (2015). Structural basis for recognition of diverse transcriptional repressors by the TOPLESS family of corepressors. *Sci Adv* **1**.
- Kelley, L.A., Mezulis, S., Yates, C.M., Wass, M.N., and Sternberg, M.J. (2015). The Phyre2 web portal for protein modeling, prediction and analysis. *Nat Protoc* **10**, 845-858.
- Keminer, O., and Peters, R. (1999). Permeability of single nuclear pores. *Biophys J* **77**, 217-228.
- Kepinski, S., and Leyser, O. (2005). The Arabidopsis F-box protein TIR1 is an auxin receptor. *Nature* **435**, 446-451.
- Kim, B.C., Soh, M.C., Kang, B.J., Furuya, M., and Nam, H.G. (1996). Two dominant photomorphogenic mutations of Arabidopsis thaliana identified as suppressor mutations of hy2. *Plant J* **9**, 441-456.
- Kim, J., Harter, K., and Theologis, A. (1997). Protein-protein interactions among the Aux/IAA proteins. *Proc Natl Acad Sci U S A* **94**, 11786-11791.
- Kim, M.J., Kim, M., Lee, M.R., Park, S.K., and Kim, J. (2015). LATERAL ORGAN BOUNDARIES DOMAIN (LBD)10 interacts with SIDECAR POLLEN/LBD27 to control pollen development in Arabidopsis. *Plant J* **81**, 794-809.
- Kögl, F., and Haagen-Smit, A.J.H. (1931). Über die Chemie des Wuchsstoffs.
- Komander, D., and Rape, M. (2012). The ubiquitin code. *Annu Rev Biochem* **81**, 203-229.

- Koncz, C., and Schell, J.** (1986). The promoter of TL-DNA gene 5 controls the tissue-specific expression of chimaeric genes carried by a novel type of *Agrobacterium* binary vector. *Molecular and General Genetics MGG* **204**, 383-396.
- Korasick, D.A., Enders, T.A., and Strader, L.C.** (2013). Auxin biosynthesis and storage forms. *J Exp Bot* **64**, 2541-2555.
- Korasick, D.A., Westfall, C.S., Lee, S.G., Nanao, M.H., Dumas, R., Hagen, G., Guilfoyle, T.J., Jez, J.M., et al.** (2014). Molecular basis for AUXIN RESPONSE FACTOR protein interaction and the control of auxin response repression. *Proc Natl Acad Sci U S A* **111**, 5427-5432.
- Korasick, D.A., Chatterjee, S., Tonelli, M., Dashti, H., Lee, S.G., Westfall, C.S., Fulton, D.B., Andreotti, A.H., et al.** (2015). Defining a two-pronged structural model for PB1 (Phox/Bem1p) domain interaction in plant auxin responses. *J Biol Chem* **290**, 12868-12878.
- Kraft, E., Stone, S.L., Ma, L., Su, N., Gao, Y., Lau, O.S., Deng, X.W., and Callis, J.** (2005). Genome analysis and functional characterization of the E2 and RING-type E3 ligase ubiquitination enzymes of *Arabidopsis*. *Plant Physiol* **139**, 1597-1611.
- Krieger, E., Koraimann, G., and Vriend, G.** (2002). Increasing the precision of comparative models with YASARA NOVA--a self-parameterizing force field. *Proteins* **47**, 393-402.
- Krieger, E., Joo, K., Lee, J., Lee, J., Raman, S., Thompson, J., Tyka, M., Baker, D., et al.** (2009). Improving physical realism, stereochemistry, and side-chain accuracy in homology modeling: Four approaches that performed well in CASP8. *Proteins* **77 Suppl 9**, 114-122.
- Krogan, N.T., Ckurshumova, W., Marcos, D., Caragea, A.E., and Berleth, T.** (2012a). Deletion of MP/ARF5 domains III and IV reveals a requirement for Aux/IAA regulation in *Arabidopsis* leaf vascular patterning. *New Phytol* **194**, 391-401.
- Krogan, N.T., Hogan, K., and Long, J.A.** (2012b). APETALA2 negatively regulates multiple floral organ identity genes in *Arabidopsis* by recruiting the co-repressor TOPLESS and the histone deacetylase HDA19. *Development* **139**, 4180-4190.
- Kulathu, Y., and Komander, D.** (2012). Atypical ubiquitylation - the unexplored world of polyubiquitin beyond Lys48 and Lys63 linkages. *Nat Rev Mol Cell Biol* **13**, 508-523.
- Kuroda, H., Yanagawa, Y., Takahashi, N., Horii, Y., and Matsui, M.** (2012). A comprehensive analysis of interaction and localization of *Arabidopsis* SKP1-like (ASK) and F-box (FBX) proteins. *PLoS One* **7**.
- Laemmli, U.K.** (1970). Cleavage of structural proteins during the assembly of the head of bacteriophage T4. *Nature* **227**, 680-685.
- Lam, H.K., McAdam, S.A., McAdam, E.L., and Ross, J.J.** (2015). Evidence That Chlorinated Auxin Is Restricted to the Fabaceae But Not to the Fabeae. *Plant Physiol* **168**, 798-803.
- Laskowski, R.A., MacArthur, M.W., Moss, D.S., and Thornton, J.M.** (1993). PROCHECK: a program to check the stereochemical quality of protein structures. *Journal of Applied Crystallography* **26**, 283-291.
- Lau, S., De Smet, I., Kolb, M., Meinhardt, H., and Jurgens, G.** (2011). Auxin triggers a genetic switch. *Nat Cell Biol* **13**, 611-615.
- Lee, S., Sundaram, S., Armitage, L., Evans, J.P., Hawkes, T., Kepinski, S., Ferro, N., and Napier, R.M.** (2014). Defining binding efficiency and specificity of auxins for SCF(TIR1/AFB)-Aux/IAA co-receptor complex formation. *ACS Chem Biol* **9**, 673-682.
- Lempe, J., Balasubramanian, S., Sureshkumar, S., Singh, A., Schmid, M., and Weigel, D.** (2005). Diversity of flowering responses in wild *Arabidopsis thaliana* strains. *PLoS Genet* **1**, 109-118.
- Leyser, H.M., Pickett, F.B., Dharmasiri, S., and Estelle, M.** (1996). Mutations in the AXR3 gene of *Arabidopsis* result in altered auxin response including ectopic expression from the SAUR-AC1 promoter. *Plant J* **10**, 403-413.
- Li, H., Cheng, Y., Murphy, A., Hagen, G., and Guilfoyle, T.J.** (2009). Constitutive repression and activation of auxin signaling in *Arabidopsis*. *Plant Physiol* **149**, 1277-1288.

- Li, H., Tiwari, S.B., Hagen, G., and Guilfoyle, T.J. (2011). Identical amino acid substitutions in the repression domain of auxin/indole-3-acetic acid proteins have contrasting effects on auxin signaling. *Plant Physiol* **155**, 1252-1263.
- Li, Z., Huang, Y., Ouyang, Y., Jiao, Y., Xing, H., Liao, L., Jiang, S., Shao, Y., *et al.* (2014). CorMut: an R/Bioconductor package for computing correlated mutations based on selection pressure. *Bioinformatics* **30**, 2073-2075.
- Librado, P., and Rozas, J. (2009). DnaSP v5: a software for comprehensive analysis of DNA polymorphism data. *Bioinformatics* **25**, 1451-1452.
- Ljung, K., Bhalerao, R.P., and Sandberg, G. (2001). Sites and homeostatic control of auxin biosynthesis in Arabidopsis during vegetative growth. *Plant J* **28**, 465-474.
- Ljung, K., Hull, A.K., Kowalczyk, M., Marchant, A., Celenza, J., Cohen, J.D., and Sandberg, G. (2002). Biosynthesis, conjugation, catabolism and homeostasis of indole-3-acetic acid in Arabidopsis thaliana. *Plant Mol Biol* **49**, 249-272.
- Logemann, E., Birkenbihl, R.P., Ulker, B., and Somssich, I.E. (2006). An improved method for preparing Agrobacterium cells that simplifies the Arabidopsis transformation protocol. *Plant Methods* **2**, 16.
- Lokerse, A.S., and Weijers, D. (2009). Auxin enters the matrix--assembly of response machineries for specific outputs. *Curr Opin Plant Biol* **12**, 520-526.
- Long, J.A., Ohno, C., Smith, Z.R., and Meyerowitz, E.M. (2006). TOPLESS regulates apical embryonic fate in Arabidopsis. *Science* **312**, 1520-1523.
- Ludwig-Müller, J. (2000). Indole-3-butyric acid in plant growth and development. *Plant Growth Regulation* **32**, 219-230.
- Ludwig-Müller, J., and Cohen, J.D. (2002). Identification and quantification of three active auxins in different tissues of *Tropaeolum majus*. *Physiol Plant* **115**, 320-329.
- Ludwig-Müller, J., Vertocnik, A., and Town, C.D. (2005). Analysis of indole-3-butyric acid-induced adventitious root formation on Arabidopsis stem segments. *J Exp Bot* **56**, 2095-2105.
- Ludwig-Müller, J. (2011). Auxin conjugates: their role for plant development and in the evolution of land plants. *J Exp Bot* **62**, 1757-1773.
- Marillonnet, S., and Werner, S. (2015). Assembly of Multigene Constructs Using Golden Gate Cloning. *Methods Mol Biol* **1321**, 269-284.
- Marks, M.D., Wenger, J.P., Gilding, E., Jilk, R., and Dixon, R.A. (2009). Transcriptome analysis of Arabidopsis wild-type and gl3-sst sim trichomes identifies four additional genes required for trichome development. *Mol Plant* **2**, 803-822.
- Márquez, G., Alarcón, M.V., and Salguero, J. (2016). Differential responses of primary and lateral roots to indole-3-acetic acid, indole-3-butyric acid, and 1-naphthaleneacetic acid in maize seedlings. *Biologia Plantarum* **60**, 367-375.
- Marrocco, K., Lecureuil, A., Nicolas, P., and Guerche, P. (2003). The Arabidopsis SKP1-like genes present a spectrum of expression profiles. *Plant Molecular Biology* **52**, 715-727.
- Mattiroli, F., and Sixma, T.K. (2014). Lysine-targeting specificity in ubiquitin and ubiquitin-like modification pathways. *Nat Struct Mol Biol* **21**, 308-316.
- McSteen, P., and Leyser, O. (2005). Shoot branching. *Annu Rev Plant Biol* **56**, 353-374.
- Meijering, E., Jacob, M., Sarria, J.C., Steiner, P., Hirling, H., and Unser, M. (2004). Design and validation of a tool for neurite tracing and analysis in fluorescence microscopy images. *Cytometry A* **58**, 167-176.
- Michniewicz, M., Brewer, P.B., and Friml, J.I. (2007). Polar auxin transport and asymmetric auxin distribution. *Arabidopsis Book* **5**.
- Milroy, L.G., Grossmann, T.N., Hennig, S., Brunsveld, L., and Ottmann, C. (2014). Modulators of protein-protein interactions. *Chem Rev* **114**, 4695-4748.

- Mironova, V.V., Omelyanchuk, N.A., Wiebe, D.S., and Levitsky, V.G.** (2014). Computational analysis of auxin responsive elements in the *Arabidopsis thaliana* L. genome. *BMC Genomics* **15 Suppl 12**, S4.
- Mockaitis, K., and Estelle, M.** (2008). Auxin receptors and plant development: a new signaling paradigm. *Annu Rev Cell Dev Biol* **24**, 55-80.
- Möller, B., and Weijers, D.** (2009). Auxin control of embryo patterning. *Cold Spring Harb Perspect Biol* **1**.
- Moss, B.L., Mao, H., Guseman, J.M., Hinds, T.R., Hellmuth, A., Kovenock, M., Noorassa, A., Lanctot, A., et al.** (2015). Rate Motifs Tune Auxin/Indole-3-Acetic Acid Degradation Dynamics. *Plant Physiol* **169**, 803-813.
- Motulsky, H., and Neubig, R.** (2001). Analyzing radioligand binding data. *Curr Protoc Protein Sci* **Appendix 3**.
- Murashige, T., and Skoog, F.** (1962). A Revised Medium for Rapid Growth and Bio Assays with Tobacco Tissue Cultures. *Physiologia Plantarum* **15**, 473-497.
- Nagpal, P., Walker, L.M., Young, J.C., Sonawala, A., Timpfe, C., Estelle, M., and Reed, J.W.** (2000). AXR2 encodes a member of the Aux/IAA protein family. *Plant Physiol* **123**, 563-574.
- Nanao, M.H., Vinos-Poyo, T., Brunoud, G., Thevenon, E., Mazzoleni, M., Mast, D., Laine, S., Wang, S., et al.** (2014). Structural basis for oligomerization of auxin transcriptional regulators. *Nat Commun* **5**, 3617.
- Navarro, L., Dunoyer, P., Jay, F., Arnold, B., Dharmasiri, N., Estelle, M., Voinnet, O., and Jones, J.D.** (2006). A plant miRNA contributes to antibacterial resistance by repressing auxin signaling. *Science* **312**, 436-439.
- Nawy, T., Lee, J.Y., Colinas, J., Wang, J.Y., Thongrod, S.C., Malamy, J.E., Birnbaum, K., and Benfey, P.N.** (2005). Transcriptional profile of the *Arabidopsis* root quiescent center. *Plant Cell* **17**, 1908-1925.
- Nelson, D.L., and Cox, M.M.** (2012). *Lehninger Principles of Biochemistry*. (Freeman, W. H. & Company).
- Ngo, P., Ozga, J.A., and Reinecke, D.M.** (2002). Specificity of auxin regulation of gibberellin 20-oxidase gene expression in pea pericarp. *Plant Mol Biol* **49**, 439-448.
- Nishimura, K., Fukagawa, T., Takisawa, H., Kakimoto, T., and Kanemaki, M.** (2009). An auxin-based degron system for the rapid depletion of proteins in nonplant cells. *Nat Methods* **6**, 917-922.
- Nordstrom, A.C., Jacobs, F.A., and Eliasson, L.** (1991). Effect of Exogenous Indole-3-Acetic Acid and Indole-3-Butyric Acid on Internal Levels of the Respective Auxins and Their Conjugation with Aspartic Acid during Adventitious Root Formation in Pea Cuttings. *Plant Physiol* **96**, 856-861.
- Normanly, J.** (2010). Approaching cellular and molecular resolution of auxin biosynthesis and metabolism. *Cold Spring Harb Perspect Biol* **2**.
- Ochoa-Fernandez, R., Samodelov, S.L., Brandl, S.M., Wehinger, E., Muller, K., Weber, W., and Zurbriggen, M.D.** (2016). Optogenetics in Plants: Red/Far-Red Light Control of Gene Expression. *Methods Mol Biol* **1408**, 125-139.
- Oeller, P.W., Keller, J.A., Parks, J.E., Silbert, J.E., and Theologis, A.** (1993). Structural characterization of the early indoleacetic acid-inducible genes, PS-IAA4/5 and PS-IAA6, of pea (*Pisum sativum* L.). *J Mol Biol* **233**, 789-798.
- Oh, E., Zhu, J.Y., Ryu, H., Hwang, I., and Wang, Z.Y.** (2014). TOPLESS mediates brassinosteroid-induced transcriptional repression through interaction with BZR1. *Nat Commun* **5**, 4140.
- Ouellet, F., Overvoorde, P.J., and Theologis, A.** (2001). IAA17/AXR3: biochemical insight into an auxin mutant phenotype. *Plant Cell* **13**, 829-841.
- Overvoorde, P.J., Okushima, Y., Alonso, J.M., Chan, A., Chang, C., Ecker, J.R., Hughes, B., Liu, A., et al.** (2005). Functional genomic analysis of the AUXIN/INDOLE-3-ACETIC ACID gene family members in *Arabidopsis thaliana*. *Plant Cell* **17**, 3282-3300.

- Ozga, J.A., Reinecke, D.M., Ayele, B.T., Ngo, P., Nadeau, C., and Wickramarathna, A.D.** (2009). Developmental and hormonal regulation of gibberellin biosynthesis and catabolism in pea fruit. *Plant Physiol* **150**, 448-462.
- Padmanabhan, M.S., Shiferaw, H., and Culver, J.N.** (2006). The Tobacco mosaic virus replicase protein disrupts the localization and function of interacting Aux/IAA proteins. *Mol Plant Microbe Interact* **19**, 864-873.
- Paponov, I.A., Paponov, M., Teale, W., Menges, M., Chakrabortee, S., Murray, J.A., and Palme, K.** (2008). Comprehensive transcriptome analysis of auxin responses in Arabidopsis. *Mol Plant* **1**, 321-337.
- Paponov, I.A., Teale, W., Lang, D., Paponov, M., Reski, R., Rensing, S.A., and Palme, K.** (2009). The evolution of nuclear auxin signalling. *BMC Evol Biol* **9**, 126.
- Park, J.Y., Kim, H.J., and Kim, J.** (2002). Mutation in domain II of IAA1 confers diverse auxin-related phenotypes and represses auxin-activated expression of Aux/IAA genes in steroid regulator-inducible system. *Plant J* **32**, 669-683.
- Parry, G., Calderón Villalobos, L.I., Prigge, M., Peret, B., Dharmasiri, S., Itoh, H., Lechner, E., Gray, W.M., et al.** (2009). Complex regulation of the TIR1/AFB family of auxin receptors. *Proc Natl Acad Sci U S A* **106**, 22540-22545.
- Patton, E.E., Willems, A.R., Sa, D., Kuras, L., Thomas, D., Craig, K.L., and Tyers, M.** (1998). Cdc53 is a scaffold protein for multiple Cdc34/Skp1/F-box protein complexes that regulate cell division and methionine biosynthesis in yeast. *Genes Dev* **12**, 692-705.
- Pauwels, L., Barbero, G.F., Geerinck, J., Tilleman, S., Grunewald, W., Perez, A.C., Chico, J.M., Bossche, R.V., et al.** (2010). NINJA connects the co-repressor TOPLESS to jasmonate signalling. *Nature* **464**, 788-791.
- Perrot-Rechenmann, C.** (2010). Cellular responses to auxin: division versus expansion. *Cold Spring Harb Perspect Biol* **2**.
- Pierre-Jerome, E., Moss, B.L., Lanctot, A., Hageman, A., and Nemhauser, J.L.** (2016). Functional analysis of molecular interactions in synthetic auxin response circuits. *Proc Natl Acad Sci U S A* **113**, 11354-11359.
- Piya, S., Shrestha, S.K., Binder, B., Stewart, C.N., Jr., and Hewezi, T.** (2014). Protein-protein interaction and gene co-expression maps of ARFs and Aux/IAAs in Arabidopsis. *Front Plant Sci* **5**, 744.
- Ploense, S.E., Wu, M.F., Nagpal, P., and Reed, J.W.** (2009). A gain-of-function mutation in IAA18 alters Arabidopsis embryonic apical patterning. *Development* **136**, 1509-1517.
- Poupart, J., and Waddell, C.S.** (2000). The rib1 mutant is resistant to indole-3-butyric acid, an endogenous auxin in Arabidopsis. *Plant Physiol* **124**, 1739-1751.
- Prakash, S., Tian, L., Ratliff, K.S., Lehotzky, R.E., and Matouschek, A.** (2004). An unstructured initiation site is required for efficient proteasome-mediated degradation. *Nat Struct Mol Biol* **11**, 830-837.
- Prigge, M.J., Lavy, M., Ashton, N.W., and Estelle, M.** (2010). *Physcomitrella patens* auxin-resistant mutants affect conserved elements of an auxin-signaling pathway. *Curr Biol* **20**, 1907-1912.
- Prigge, M.J., Greenham, K., Zhang, Y., Santner, A., Castillejo, C., Mutka, A.M., O'Malley, R.C., Ecker, J.R., et al.** (2016). The Arabidopsis Auxin Receptor F-Box Proteins AFB4 and AFB5 Are Required for Response to the Synthetic Auxin Picloram. *G3 (Bethesda)* **6**, 1383-1390.
- Prince, V.E., and Pickett, F.B.** (2002). Splitting pairs: the diverging fates of duplicated genes. *Nat Rev Genet* **3**, 827-837.
- Prusty, R., Grisafi, P., and Fink, G.R.** (2004). The plant hormone indoleacetic acid induces invasive growth in *Saccharomyces cerevisiae*. *Proc Natl Acad Sci U S A* **101**, 4153-4157.

- Pufky, J., Qiu, Y., Rao, M.V., Hurban, P., and Jones, A.M.** (2003). The auxin-induced transcriptome for etiolated Arabidopsis seedlings using a structure/function approach. *Funct Integr Genomics* **3**, 135-143.
- Qin, Y., Leydon, A.R., Manziello, A., Pandey, R., Mount, D., Denic, S., Vasic, B., Johnson, M.A., et al.** (2009). Penetration of the stigma and style elicits a novel transcriptome in pollen tubes, pointing to genes critical for growth in a pistil. *PLoS Genet* **5**.
- R Development Core Team.** (2012). R: A Language and Environment for Statistical Computing. <http://cran.r-project.org>.
- Ramos, J.A., Zenser, N., Leyser, O., and Callis, J.** (2001). Rapid degradation of auxin/indoleacetic acid proteins requires conserved amino acids of domain II and is proteasome dependent. *Plant Cell* **13**, 2349-2360.
- Rashotte, A.M., Poupart, J., Waddell, C.S., and Muday, G.K.** (2003). Transport of the two natural auxins, indole-3-butyric acid and indole-3-acetic acid, in Arabidopsis. *Plant Physiol* **133**, 761-772.
- Ravid, T., and Hochstrasser, M.** (2008). Diversity of degradation signals in the ubiquitin-proteasome system. *Nat Rev Mol Cell Biol* **9**, 679-690.
- Reinecke, D.M., Ozga, J.A., and Magnus, V.** (1995). Effect of halogen substitution of indole-3-acetic acid on biological activity in pea fruit. *Phytochemistry* **40**, 1361-1366.
- Reinecke, D.M.** (1999). 4-Chloroindole-3-acetic acid and plant growth. *Plant Growth Regulation* **27**, 3-13.
- Remington, D.L., Vision, T.J., Guilfoyle, T.J., and Reed, J.W.** (2004). Contrasting modes of diversification in the Aux/IAA and ARF gene families. *Plant Physiol* **135**, 1738-1752.
- Rinaldi, M.A., Liu, J., Enders, T.A., Bartel, B., and Strader, L.C.** (2012). A gain-of-function mutation in IAA16 confers reduced responses to auxin and abscisic acid and impedes plant growth and fertility. *Plant Mol Biol* **79**, 359-373.
- Rogg, L.E., Lasswell, J., and Bartel, B.** (2001). A gain-of-function mutation in IAA28 suppresses lateral root development. *Plant Cell* **13**, 465-480.
- Rosquete, M.R., Barbez, E., and Kleine-Vehn, J.** (2012). Cellular auxin homeostasis: gatekeeping is housekeeping. *Mol Plant* **5**, 772-786.
- Rouse, D., Mackay, P., Stirnberg, P., Estelle, M., and Leyser, O.** (1998). Changes in auxin response from mutations in an AUX/IAA gene. *Science* **279**, 1371-1373.
- Ruegger, M., Dewey, E., Gray, W.M., Hobbie, L., Turner, J., and Estelle, M.** (1998). The TIR1 protein of Arabidopsis functions in auxin response and is related to human SKP2 and yeast gr1p. *Genes Dev* **12**, 198-207.
- Sabatini, S., Beis, D., Wolkenfelt, H., Murfett, J., Guilfoyle, T., Malamy, J., Benfey, P., Leyser, O., et al.** (1999). An auxin-dependent distal organizer of pattern and polarity in the Arabidopsis root. *Cell* **99**, 463-472.
- Sato, A., and Yamamoto, K.T.** (2008a). What's the physiological role of domain II-less Aux/IAA proteins? *Plant Signal Behav* **3**, 496-497.
- Sato, A., and Yamamoto, K.T.** (2008b). Overexpression of the non-canonical Aux/IAA genes causes auxin-related aberrant phenotypes in Arabidopsis. *Physiol Plant* **133**, 397-405.
- Scarpella, E., Barkoulas, M., and Tsiantis, M.** (2010). Control of leaf and vein development by auxin. *Cold Spring Harb Perspect Biol* **2**.
- Schlicht, M., Ludwig-Müller, J., Burbach, C., Volkmann, D., and Baluska, F.** (2013). Indole-3-butyric acid induces lateral root formation via peroxisome-derived indole-3-acetic acid and nitric oxide. *New Phytologist* **200**, 473-482.
- Schmid, M., Davison, T.S., Henz, S.R., Pape, U.J., Demar, M., Vingron, M., Scholkopf, B., Weigel, D., et al.** (2005). A gene expression map of Arabidopsis thaliana development. *Nat Genet* **37**, 501-506.

- Schneider, C.A., Rasband, W.S., and Eliceiri, K.W.** (2012). NIH Image to ImageJ: 25 years of image analysis. *Nat Methods* **9**, 671-675.
- Schneider, E.A., Kazakoff, C.W., and Wightman, F.** (1985). Gas chromatography-mass spectrometry evidence for several endogenous auxins in pea seedling organs. *Planta* **165**, 232-241.
- Sheard, L.B., Tan, X., Mao, H., Withers, J., Ben-Nissan, G., Hinds, T.R., Kobayashi, Y., Hsu, F.F., et al.** (2010). Jasmonate perception by inositol-phosphate-potentiated COI1-JAZ co-receptor. *Nature* **468**, 400-405.
- Shimizu-Mitao, Y., and Kakimoto, T.** (2014). Auxin sensitivities of all Arabidopsis Aux/IAAs for degradation in the presence of every TIR1/AFB. *Plant Cell Physiol* **55**, 1450-1459.
- Simon, S., and Petrasek, J.** (2011). Why plants need more than one type of auxin. *Plant Sci* **180**, 454-460.
- Sippl, M.J.** (1993). Recognition of errors in three-dimensional structures of proteins. *Proteins* **17**, 355-362.
- Skowyra, D., Craig, K.L., Tyers, M., Elledge, S.J., and Harper, J.W.** (1997). F-box proteins are receptors that recruit phosphorylated substrates to the SCF ubiquitin-ligase complex. *Cell* **91**, 209-219.
- Smalle, J., and Vierstra, R.D.** (2004). The ubiquitin 26S proteasome proteolytic pathway. *Annu Rev Plant Biol* **55**, 555-590.
- Stothard, P.** (2000). The sequence manipulation suite: JavaScript programs for analyzing and formatting protein and DNA sequences. *Biotechniques* **28**, 1102, 1104.
- Strader, L.C., Culler, A.H., Cohen, J.D., and Bartel, B.** (2010). Conversion of endogenous indole-3-butyric acid to indole-3-acetic acid drives cell expansion in Arabidopsis seedlings. *Plant Physiol* **153**, 1577-1586.
- Strader, L.C., and Bartel, B.** (2011). Transport and metabolism of the endogenous auxin precursor indole-3-butyric acid. *Mol Plant* **4**, 477-486.
- Stuttman, J., Lechner, E., Guerois, R., Parker, J.E., Nussaume, L., Genschik, P., and Noel, L.D.** (2009). COP9 signalosome- and 26S proteasome-dependent regulation of SCFTIR1 accumulation in Arabidopsis. *J Biol Chem* **284**, 7920-7930.
- Sugawara, S., Mashiguchi, K., Tanaka, K., Hishiyama, S., Sakai, T., Hanada, K., Kinoshita-Tsujimura, K., Yu, H., et al.** (2015). Distinct Characteristics of Indole-3-Acetic Acid and Phenylacetic Acid, Two Common Auxins in Plants. *Plant Cell Physiol* **56**, 1641-1654.
- Suh, M.C., Samuels, A.L., Jetter, R., Kunst, L., Pollard, M., Ohlrogge, J., and Beisson, F.** (2005). Cuticular lipid composition, surface structure, and gene expression in Arabidopsis stem epidermis. *Plant Physiol* **139**, 1649-1665.
- Sumimoto, H., Kamakura, S., and Ito, T.** (2007). Structure and function of the PB1 domain, a protein interaction module conserved in animals, fungi, amoebas, and plants. *Sci STKE* **2007**.
- Suyama, M., Torrents, D., and Bork, P.** (2006). PAL2NAL: robust conversion of protein sequence alignments into the corresponding codon alignments. *Nucleic Acids Res* **34**, 609-612.
- Swanson, R., Clark, T., and Preuss, D.** (2005). Expression profiling of Arabidopsis stigma tissue identifies stigma-specific genes. *Sexual Plant Reproduction* **18**, 163-171.
- Szemenyei, H., Hannon, M., and Long, J.A.** (2008). TOPLESS mediates auxin-dependent transcriptional repression during Arabidopsis embryogenesis. *Science* **319**, 1384-1386.
- Tan, X., Calderón Villalobos, L.I., Sharon, M., Zheng, C., Robinson, C.V., Estelle, M., and Zheng, N.** (2007). Mechanism of auxin perception by the TIR1 ubiquitin ligase. *Nature* **446**, 640-645.
- Tatematsu, K., Kumagai, S., Muto, H., Sato, A., Watahiki, M.K., Harper, R.M., Liscum, E., and Yamamoto, K.T.** (2004). MASSUGU2 encodes Aux/IAA19, an auxin-regulated protein that functions together with the transcriptional activator NPH4/ARF7 to regulate differential growth responses of hypocotyl and formation of lateral roots in Arabidopsis thaliana. *Plant Cell* **16**, 379-393.

- Teale, W.D., Paponov, I.A., and Palme, K.** (2006). Auxin in action: signalling, transport and the control of plant growth and development. *Nat Rev Mol Cell Biol* **7**, 847-859.
- Teixeira, M.C., Duque, P., and Sa-Correia, I.** (2007). Environmental genomics: mechanistic insights into toxicity of and resistance to the herbicide 2,4-D. *Trends Biotechnol* **25**, 363-370.
- Terrile, M.C., Paris, R., Calderón Villalobos, L.I., Iglesias, M.J., Lamattina, L., Estelle, M., and Casalongue, C.A.** (2012). Nitric oxide influences auxin signaling through S-nitrosylation of the Arabidopsis TRANSPORT INHIBITOR RESPONSE 1 auxin receptor. *Plant J* **70**, 492-500.
- Theologis, A., Huynh, T.V., and Davis, R.W.** (1985). Rapid induction of specific mRNAs by auxin in pea epicotyl tissue. *J Mol Biol* **183**, 53-68.
- Thines, B., Katsir, L., Melotto, M., Niu, Y., Mandaokar, A., Liu, G., Nomura, K., He, S.Y., et al.** (2007). JAZ repressor proteins are targets of the SCF(COI1) complex during jasmonate signalling. *Nature* **448**, 661-665.
- Thrower, J.S., Hoffman, L., Rechsteiner, M., and Pickart, C.M.** (2000). Recognition of the polyubiquitin proteolytic signal. *EMBO J* **19**, 94-102.
- Tian, Q., and Reed, J.W.** (1999). Control of auxin-regulated root development by the Arabidopsis thaliana SHY2/IAA3 gene. *Development* **126**, 711-721.
- Tian, Q., Uhlir, N.J., and Reed, J.W.** (2002). Arabidopsis SHY2/IAA3 inhibits auxin-regulated gene expression. *Plant Cell* **14**, 301-319.
- Tian, Q., Nagpal, P., and Reed, J.W.** (2003). Regulation of Arabidopsis SHY2/IAA3 protein turnover. *Plant J* **36**, 643-651.
- Timpte, C., Wilson, A.K., and Estelle, M.** (1994). The *axr2-1* mutation of Arabidopsis thaliana is a gain-of-function mutation that disrupts an early step in auxin response. *Genetics* **138**, 1239-1249.
- Timpte, C.S., Wilson, A.K., and Estelle, M.** (1992). Effects of the *axr2* mutation of Arabidopsis on cell shape in hypocotyl and inflorescence. *Planta* **188**, 271-278.
- Tiwari, S.B., Wang, X.J., Hagen, G., and Guilfoyle, T.J.** (2001). AUX/IAA proteins are active repressors, and their stability and activity are modulated by auxin. *Plant Cell* **13**, 2809-2822.
- Tiwari, S.B., Hagen, G., and Guilfoyle, T.** (2003). The roles of auxin response factor domains in auxin-responsive transcription. *Plant Cell* **15**, 533-543.
- Tiwari, S.B., Hagen, G., and Guilfoyle, T.J.** (2004). Aux/IAA proteins contain a potent transcriptional repression domain. *Plant Cell* **16**, 533-543.
- Uehara, T., Okushima, Y., Mimura, T., Tasaka, M., and Fukaki, H.** (2008). Domain II mutations in CRANE/IAA18 suppress lateral root formation and affect shoot development in Arabidopsis thaliana. *Plant Cell Physiol* **49**, 1025-1038.
- Ulmasov, T., Liu, Z.B., Hagen, G., and Guilfoyle, T.J.** (1995). Composite structure of auxin response elements. *Plant Cell* **7**, 1611-1623.
- Ulmasov, T., Hagen, G., and Guilfoyle, T.J.** (1997a). ARF1, a transcription factor that binds to auxin response elements. *Science* **276**, 1865-1868.
- Ulmasov, T., Murfett, J., Hagen, G., and Guilfoyle, T.J.** (1997b). Aux/IAA proteins repress expression of reporter genes containing natural and highly active synthetic auxin response elements. *Plant Cell* **9**, 1963-1971.
- Ulmasov, T., Hagen, G., and Guilfoyle, T.J.** (1999a). Activation and repression of transcription by auxin-response factors. *Proc Natl Acad Sci U S A* **96**, 5844-5849.
- Ulmasov, T., Hagen, G., and Guilfoyle, T.J.** (1999b). Dimerization and DNA binding of auxin response factors. *Plant J* **19**, 309-319.
- Untergasser, A., Nijveen, H., Rao, X., Bisseling, T., Geurts, R., and Leunissen, J.A.** (2007). Primer3Plus, an enhanced web interface to Primer3. *Nucleic Acids Res* **35**, W71-74.
- Uzunova, V.V., Quareshy, M., Del Genio, C.I., and Napier, R.M.** (2016). Tomographic docking suggests the mechanism of auxin receptor TIR1 selectivity. *Open Biol* **6**.

- van der Lee, R., Lang, B., Kruse, K., Gsponer, J., Sanchez de Groot, N., Huynen, M.A., Matouschek, A., Fuxreiter, M., *et al.* (2014). Intrinsically disordered segments affect protein half-life in the cell and during evolution. *Cell Rep* **8**, 1832-1844.
- Vanneste, S., and Friml, J. (2012). Plant signaling: Deconstructing auxin sensing. *Nat Chem Biol* **8**, 415-416.
- Varshavsky, A. (1991). Naming a targeting signal. *Cell* **64**, 13-15.
- Vernoux, T., Brunoud, G., Farcot, E., Morin, V., Van den Daele, H., Legrand, J., Oliva, M., Das, P., *et al.* (2011). The auxin signalling network translates dynamic input into robust patterning at the shoot apex. *Mol Syst Biol* **7**, 508.
- Vidal, E.A., Araus, V., Lu, C., Parry, G., Green, P.J., Coruzzi, G.M., and Gutierrez, R.A. (2010). Nitrate-responsive miR393/AFB3 regulatory module controls root system architecture in *Arabidopsis thaliana*. *Proc Natl Acad Sci U S A* **107**, 4477-4482.
- Vierstra, R.D. (2009). The ubiquitin-26S proteasome system at the nexus of plant biology. *Nat Rev Mol Cell Biol* **10**, 385-397.
- Voet, D., and Voet, J.G. (2004). *Biochemistry* (New York: John Wiley and Sons), pp. 1353-1354.
- Walsh, T.A., Neal, R., Merlo, A.O., Honma, M., Hicks, G.R., Wolff, K., Matsumura, W., and Davies, J.P. (2006). Mutations in an auxin receptor homolog AFB5 and in SGT1b confer resistance to synthetic picolinate auxins and not to 2,4-dichlorophenoxyacetic acid or indole-3-acetic acid in *Arabidopsis*. *Plant Physiol* **142**, 542-552.
- Wang, L., Kim, J., and Somers, D.E. (2013a). Transcriptional corepressor TOPLESS complexes with pseudoresponse regulator proteins and histone deacetylases to regulate circadian transcription. *Proc Natl Acad Sci U S A* **110**, 761-766.
- Wang, R., Zhang, Y., Kieffer, M., Yu, H., Kepinski, S., and Estelle, M. (2016). HSP90 regulates temperature-dependent seedling growth in *Arabidopsis* by stabilizing the auxin co-receptor F-box protein TIR1. *Nat Commun* **7**, 10269.
- Wang, S., Hagen, G., and Guilfoyle, T.J. (2013b). ARF-Aux/IAA interactions through domain III/IV are not strictly required for auxin-responsive gene expression. *Plant Signal Behav* **8**.
- Ward, J.J., Sodhi, J.S., McGuffin, L.J., Buxton, B.F., and Jones, D.T. (2004). Prediction and functional analysis of native disorder in proteins from the three kingdoms of life. *J Mol Biol* **337**, 635-645.
- Watanabe, E., Mano, S., Nomoto, M., Tada, Y., Hara-Nishimura, I., Nishimura, M., and Yamada, K. (2016). HSP90 Stabilizes Auxin-Responsive Phenotypes by Masking a Mutation in the Auxin Receptor TIR1. *Plant Cell Physiol* **57**, 2245-2254.
- Weber, E., Gruetzner, R., Werner, S., Engler, C., and Marillonnet, S. (2011). Assembly of designer TAL effectors by Golden Gate cloning. *PLoS One* **6**.
- Weijers, D., Schlereth, A., Ehrismann, J.S., Schwank, G., Kientz, M., and Jurgens, G. (2006). Auxin triggers transient local signaling for cell specification in *Arabidopsis* embryogenesis. *Dev Cell* **10**, 265-270.
- Weijers, D., and Wagner, D. (2016). Transcriptional Responses to the Auxin Hormone. *Annu Rev Plant Biol* **67**, 539-574.
- Weissman, A.M. (2001). Themes and variations on ubiquitylation. *Nat Rev Mol Cell Biol* **2**, 169-178.
- Wend, S., Dal Bosco, C., Kampf, M.M., Ren, F., Palme, K., Weber, W., Dovzhenko, A., and Zurbriggen, M.D. (2013). A quantitative ratiometric sensor for time-resolved analysis of auxin dynamics. *Sci Rep* **3**, 2052.
- Werner, S., Engler, C., Weber, E., Gruetzner, R., and Marillonnet, S. (2012). Fast track assembly of multigene constructs using Golden Gate cloning and the MoClo system. *Bioeng Bugs* **3**, 38-43.
- Wightman, F., and Lighty, D.L. (1982). Identification of phenylacetic acid as a natural auxin in the shoots of higher plants. *Physiologia Plantarum* **55**, 17-24.

- Wilson, A.K., Pickett, F.B., Turner, J.C., and Estelle, M.** (1990). A dominant mutation in *Arabidopsis* confers resistance to auxin, ethylene and abscisic acid. *Molecular and General Genetics MGG* **222**, 377-383.
- Winkler, M.** (2015). Master Thesis: Dissecting the dynamic turnover of transcriptional regulators in response to auxin (Martin-Luther University Halle-Wittenberg).
- Winkler, M., Hellmuth, A., Janitza, P., Niemeyer, M., Christ, G., Samodelov, S.L., Wilde, V., Majovsky, P., et al.** (under review). Variation in auxin sensing guides AUX/IAA destruction.
- Winter, D., Vinegar, B., Nahal, H., Ammar, R., Wilson, G.V., and Provart, N.J.** (2007). An "Electronic Fluorescent Pictograph" browser for exploring and analyzing large-scale biological data sets. *PLoS One* **2**.
- Woodward, A.W., and Bartel, B.** (2005). Auxin: regulation, action, and interaction. *Ann Bot* **95**, 707-735.
- Worley, C.K., Zenser, N., Ramos, J., Rouse, D., Leyser, O., Theologis, A., and Callis, J.** (2000). Degradation of Aux/IAA proteins is essential for normal auxin signalling. *Plant J* **21**, 553-562.
- Wu, G., Xu, G., Schulman, B.A., Jeffrey, P.D., Harper, J.W., and Pavletich, N.P.** (2003). Structure of a beta-TrCP1-Skp1-beta-catenin complex: destruction motif binding and lysine specificity of the SCF(beta-TrCP1) ubiquitin ligase. *Mol Cell* **11**, 1445-1456.
- Wurch, T., Lestienne, F., and Pauwels, P.J.** (1998). A modified overlap extension PCR method to create chimeric genes in the absence of restriction enzymes. *Biotechnology Techniques* **12**, 653-657.
- Xu, G., Ma, H., Nei, M., and Kong, H.** (2009). Evolution of F-box genes in plants: different modes of sequence divergence and their relationships with functional diversification. *Proc Natl Acad Sci U S A* **106**, 835-840.
- Yadav, R.K., Girke, T., Pasala, S., Xie, M., and Reddy, G.V.** (2009). Gene expression map of the *Arabidopsis* shoot apical meristem stem cell niche. *Proc Natl Acad Sci U S A* **106**, 4941-4946.
- Yan, D.W., Wang, J., Yuan, T.T., Hong, L.W., Gao, X., and Lu, Y.T.** (2013). Perturbation of auxin homeostasis by overexpression of wild-type IAA15 results in impaired stem cell differentiation and gravitropism in roots. *PLoS One* **8**.
- Yan, J., Zhang, C., Gu, M., Bai, Z., Zhang, W., Qi, T., Cheng, Z., Peng, W., et al.** (2009). The *Arabidopsis* CORONATINE INSENSITIVE1 protein is a jasmonate receptor. *Plant Cell* **21**, 2220-2236.
- Yang, X., Lee, S., So, J.H., Dharmasiri, S., Dharmasiri, N., Ge, L., Jensen, C., Hangarter, R., et al.** (2004). The IAA1 protein is encoded by AXR5 and is a substrate of SCF(TIR1). *Plant J* **40**, 772-782.
- Yang, Y., Costa, A., Leonhardt, N., Siegel, R.S., and Schroeder, J.I.** (2008). Isolation of a strong *Arabidopsis* guard cell promoter and its potential as a research tool. *Plant Methods* **4**, 6.
- Yilmaz, A., Mejia-Guerra, M.K., Kurz, K., Liang, X., Welch, L., and Grotewold, E.** (2011). AGRIS: the *Arabidopsis* Gene Regulatory Information Server, an update. *Nucleic Acids Res* **39**, D1118-1122.
- Yu, H., Moss, B.L., Jang, S.S., Prigge, M., Klavins, E., Nemhauser, J.L., and Estelle, M.** (2013). Mutations in the TIR1 auxin receptor that increase affinity for auxin/indole-3-acetic acid proteins result in auxin hypersensitivity. *Plant Physiol* **162**, 295-303.
- Yu, H., Zhang, Y., Moss, B.L., Bargmann, B.O., Wang, R., Prigge, M., Nemhauser, J.L., and Estelle, M.** (2015). Untethering the TIR1 auxin receptor from the SCF complex increases its stability and inhibits auxin response. *Nat Plants* **1**.
- Zenser, N., Ellsmore, A., Leasure, C., and Callis, J.** (2001). Auxin modulates the degradation rate of Aux/IAA proteins. *Proc Natl Acad Sci U S A* **98**, 11795-11800.
- Zenser, N., Dreher, K.A., Edwards, S.R., and Callis, J.** (2003). Acceleration of Aux/IAA proteolysis is specific for auxin and independent of AXR1. *Plant J* **35**, 285-294.

- Zhang, L., Ward, J.D., Cheng, Z., and Dernburg, A.F.** (2015). The auxin-inducible degradation (AID) system enables versatile conditional protein depletion in *C. elegans*. *Development* **142**, 4374-4384.
- Zhao, C., Craig, J.C., Petzold, H.E., Dickerman, A.W., and Beers, E.P.** (2005). The xylem and phloem transcriptomes from secondary tissues of the *Arabidopsis* root-hypocotyl. *Plant Physiol* **138**, 803-818.
- Zhao, S., and Fernald, R.D.** (2005). Comprehensive algorithm for quantitative real-time polymerase chain reaction. *J Comput Biol* **12**, 1047-1064.
- Zhao, Y.** (2014). Auxin biosynthesis. *Arabidopsis Book* **12**.
- Zheng, N., Wang, P., Jeffrey, P.D., and Pavletich, N.P.** (2000). Structure of a c-Cbl-Ubch7 complex: RING domain function in ubiquitin-protein ligases. *Cell* **102**, 533-539.
- Zheng, N., Schulman, B.A., Song, L., Miller, J.J., Jeffrey, P.D., Wang, P., Chu, C., Koepp, D.M., et al.** (2002). Structure of the Cul1-Rbx1-Skp1-F boxSkp2 SCF ubiquitin ligase complex. *Nature* **416**, 703-709.
- Zolman, B.K., Yoder, A., and Bartel, B.** (2000). Genetic analysis of indole-3-butyric acid responses in *Arabidopsis thaliana* reveals four mutant classes. *Genetics* **156**, 1323-1337.

8 Appendix

8.1 List of Publications

- Winkler, M., **Hellmuth, A.**, Janitza, P., Niemeyer, M., Christ, G., Samodelov, S.L., Wilde, V., Majovsky, P., Trujillo, M., Quint, M., Hoehenwarter, W., Zurbriggen, M.D., Calderón Villalobos, L.I. (*under revision*). Variation in auxin sensing guide AUX/IAA destruction.

Contribution:

Initiation of IAA6/IAA19 ohnolog characterization including initial molecular cloning of IAA6 and IAA19 CDS for yeast and *E.coli* expression, preliminary tests of *E.coli* expression, purification and auxin binding

- **Hellmuth, A.** and Calderón Villalobos, L.I. (2016). Radioligand binding assays for determining dissociation constants of phytohormone receptors. *Methods Mol Biol* 1450:23-34
- Moss, B.L., Mao, H., Guseman, J.M., Hinds, T.R., **Hellmuth, A.**, Kovenock, M., Noorassa, A., Lanctot, A., Villalobos, L.I., Zheng, N., Nemhauser, J.L. (2015). Rate motifs tune Aux/IAA degradation dynamics. *Plant Physiol.* 169.1, 803-813.

Contribution:

Assessment of binding affinity between TIR1 and IAA28 and IAA1 fragments (Supplementary Figure 5 B)

- Dinesh, D.C., Kovermann, M., Gopalswamy, M., **Hellmuth, A.**, Calderón Villalobos, L.I., Lilie, H., Balbach, J., Abel, S. (2015). Solution structure of the PsIAA4 oligomerization domain reveals interaction modes for transcription factors in early auxin response. *PNAS* 112.19, 6230-6235.

Contribution:

Generation of PsIAA4 mutant versions and preliminary Y2H assays for assessment of AUX/IAA homomerization in yeast

- Guseman, J.M., **Hellmuth, A.**, Lanctot, A., Feldman, J.P., Moss, B.L., Klavins, E., Calderón Villalobos, L.I., Nemhauser, J.L. (2015). Auxin-induced degradation dynamics set the pace for lateral root development. *Development* 142, 905-909.

Contribution:

Determination of *in vitro* auxin binding affinities of TIR1 and engineered IAA14 rate motif variants (Figure 1 D)

8.2 List of Figures

Figure 1-1: Structures of auxins	2
Figure 1-2: Ubiquitin proteasome system (UPS) and small-molecule mediated target recognition by SCF E3 Ub-ligases	6
Figure 1-3: Classical model of auxin signaling	9
Figure 1-4: Point mutations in AUX/IAA degrons cause grave phenotypes by interfering with their recognition by SCF ^{TIR1} -type E3 ligases	13
Figure 1-5: The gene families involved in auxin signaling have expanded and diversified during plant evolution	21
Figure 2-1: Homology models of AFB1-3 superimposed on TIR1 crystal structure	26
Figure 2-2: Quantitative assessment of TIR1/AFB1/AFB2:AUX/IAA interactions in yeast	32
Figure 2-3: Expression and nucleotide diversity of <i>IAA1</i> and <i>IAA2</i> ohnologs.....	35
Figure 2-4: PB1 basic patch mutant <i>IAA1</i> ^{BM3} shows reduced homotypic interaction	37
Figure 2-5: AUX/IAA oligomerization does not affect co-receptor complex formation.....	39
Figure 2-6: Hypothesized TIR1:auxin:AUX/IAA ternary complex formation	41
Figure 2-7: TIR1:auxin:IAA1 and TIR1:auxin:IAA2 complexes can be reconstituted <i>in vivo</i> and bind IAA with similar high affinity.....	42
Figure 2-8: AFB2:auxin:IAA1 and AFB2:auxin:IAA2 complexes can be reconstituted <i>in vitro</i> and bind IAA with a similar high affinity	43
Figure 2-9: Various auxins differentially promote TIR1/AFB:IAA1/IAA2 interaction in yeast	46
Figure 2-10: Various auxins can be bound by TIR1-IAA1 and TIR1-IAA2 co-receptors.....	48
Figure 2-11: Specificity of ubiquitination of IAA1 and IAA2 by Uba1, Ubc8, SCF ^{TIR1} and auxin <i>in vitro</i> ..	51
Figure 2-12: Ubiquitination of IAA1 and IAA2 <i>in vitro</i> relies on an intact core degron.....	53
Figure 2-13: Auxin dose response of <i>in vitro</i> ubiquitination reaction with targets IAA1 and IAA2	54
Figure 2-14: Time course of <i>in vitro</i> ubiquitination of targets IAA1 and IAA2 in the absence and presence of auxin.....	56
Figure 2-15: Schematic view of <i>in vivo</i> strategy to generate plant lines for co-receptor characterization	59
Figure 2-16: Transcript levels of transgenic <i>YFP-IAA1</i> and <i>-IAA2</i> overexpressor lines	61
Figure 2-17: Grouping and frequency distribution of expression levels in overexpressor lines	63
Figure 2-18: Overexpressed YFP-IAA1 or YFP-IAA2 proteins can be recovered from <i>35S::YFP-IAA1</i> or <i>35S::YFP-IAA2</i> transgenic lines and are stabilized upon MG-132 treatment	65
Figure 2-19: Scheme of chimera modules and regions of AUX/IAAs	69
Figure 2-20: Auxin-dependent interaction of chimeric IAA7/IAA12 with TIR1 in yeast.....	72
Figure 2-21: Auxin sensitivity of chimeric IAA7/IAA12 degradation in Arabidopsis mesophyll protoplasts	74
Figure 3-1: Summary of biochemical characterization of TIR1-IAA1 and TIR1-IAA2 auxin co-receptors	87
Figure 3-2: Scheme of AUX/IAAs regions and their potential roles in co-receptor formation.....	92
Figure 3-3: Model of a two-substrate enzyme reaction involving a ternary complex	97
Figure 3-4: Hypothesis of partial binding reactions occurring in auxin co-receptor complex formation	98

8.3 List of Tables

Table 2-1: Results from non-linear fit of radioligand binding data obtained for AFB2:auxin:IAA1 and AFB2:auxin:IAA2 complexes.....	44
Table 2-2: Selection of transgenic T3 lines.....	60
Table 6-1: Plasmid vectors used and/or generated, their purpose and features	104
Table 6-2: Media composition and supplements.....	105
Table 6-3: Thermal profile for DreamTaq™ PCR.....	112
Table 6-4: Thermal profile Phusion™ High-Fidelity PCR.....	113
Table 6-5: Primers used in overlap PCR for generation of chimeras.....	113
Table 6-6: Thermal profile for RT-qPCR.....	120
Table 6-7: SDS-PAGE mini gel composition	121
Table 6-8: SDS-PAGE maxi gradient gel composition	122
Table 6-9: Primary antibodies used in immunoblotting procedures	123
Table 6-10: Secondary antibodies used in immunoblotting procedures	124
Table 6-11: Components in mixes A and B for <i>in vitro</i> ubiquitination reactions, their molecular weights and final concentrations	129

8.4 List of Supplementary Figures

Supplementary Figure 1: Alignment of all Arabidopsis AUX/IAAs.	160
Supplementary Figure 2: MAFFT alignment of IAA1 and IAA2.....	160
Supplementary Figure 3: MAFFT alignment of IAA7 and IAA12.....	160
Supplementary Figure 4: Detailed expression level datasets of <i>IAA1</i> and <i>IAA2</i> as shown in Figure 2-3 A boxplot	162
Supplementary Figure 5: Detailed expression level datasets of <i>IAA1</i> and <i>IAA2</i> as shown in Figure 2-3 A boxplot	163
Supplementary Figure 6: Detailed expression level datasets of <i>IAA1</i> and <i>IAA2</i> as shown in Figure 2-3 A boxplot	163
Supplementary Figure 7: Immunoblot analysis of AD-AUX/IAA protein expression from yeast strains used in quantitative Y2H assay (Figure 2-2).....	168
Supplementary Figure 8: Auxin-independency and growth control of homo- and heteromerization matrix of AUX/IAAs in yeast	169
Supplementary Figure 9: GST-IAA1 and GST-IAA2 expression and purification in <i>E.coli</i>	170
Supplementary Figure 10: Binding kinetic of TIR1: ³ H-IAA:GST-AUX/IAA complex formation	171
Supplementary Figure 11: Raw data of total (colored circles) and non-specific (black squares) ³ H-IAA binding for TIR1/AFB2-IAA1/IAA2 co-receptors.....	174
Supplementary Figure 12: Specific binding data and curve fits for independent experiments underlying <i>KD</i> values shown in Figure 2-7	175
Supplementary Figure 13: AFB2:auxin:IAA1 and AFB2:auxin:IAA2 saturation binding data shown in Figure 2-8 and Table 2-1.....	176
Supplementary Figure 14: Immunoblot analysis of AD-AUX/IAA protein expression from yeast strains used in Y2H assay (Figure 2-9).....	178

Supplementary Figure 15: Summary of competition binding data with different auxins for co-receptors TIR1-IAA1 and TIR1-IAA2.....	178
Supplementary Figure 16: Competition binding data for (A) TIR1-IAA1 and (B) TIR1-IAA2 co-receptors and different auxins	179
Supplementary Figure 17: Disorder prediction for IAA1 and IAA2	180
Supplementary Figure 18: Specificity of ubiquitination of IAA1 and IAA2 by Uba1, Ubc8, SCF ^{TIR1} and auxin <i>in vitro</i>	181
Supplementary Figure 19: Loading control for IVU shown in Figure 2-12	182
Supplementary Figure 20: Auxin dose response of <i>in vitro</i> ubiquitination reaction with targets IAA1 and IAA2	182
Supplementary Figure 21: Loading control of IVU time course experiment (Figure 2-14)	183
Supplementary Figure 22: Comparison of transcript levels of transgenic and endogenous <i>IAA1</i> and <i>IAA2</i> in overexpressor lines	185
Supplementary Figure 23: Endogenous transcript levels of <i>TIR1</i> , <i>AFB1</i> , <i>AFB2</i> , <i>AFB3</i> as well as <i>IAA1</i> , <i>IAA</i> , <i>IAA19</i> and <i>GH3.1</i> genes in wild-type Col-0, <i>tir1/afb</i> and <i>axr5-1</i> mutant background	187
Supplementary Figure 24: Overexpressed YFP-IAA1 or YFP-IAA2 protein can be recovered from <i>35S::YFP-IAA1</i> or <i>35S::YFP-IAA2</i> transgenic lines and is stabilized upon MG-132 treatment	188
Supplementary Figure 25: Phenotypes of transgenic seedlings of <i>35S::YFP</i> , <i>35S::YFP-IAA1</i> and <i>35S::YFP-IAA2</i> overexpressor lines.....	191
Supplementary Figure 26: Phenotypes of 4-week old plants of <i>35S::YFP</i> , <i>35S::YFP-IAA1</i> and <i>35S::YFP-IAA2</i> overexpressor lines.....	192
Supplementary Figure 27: Root elongation assay with <i>35S::YFP</i> , <i>35S::YFP-IAA1</i> and <i>35S::YFP-IAA2</i> overexpressor lines	193
Supplementary Figure 28: Root elongation assay with <i>35S::YFP</i> , <i>35S::YFP-IAA1</i> and <i>35S::YFP-IAA2</i> overexpressor lines	194
Supplementary Figure 29: Elongation of roots at low light in 8-day old seedlings of <i>35S::YFP</i> , <i>35S::YFP-IAA1</i> and <i>35S::YFP-IAA2</i> overexpressor lines	195
Supplementary Figure 30: Elongation of hypocotyls at low light in 8-day old seedlings of <i>35S::YFP</i> , <i>35S::YFP-IAA1</i> and <i>35S::YFP-IAA2</i> overexpressor lines	196
Supplementary Figure 31: Elongation of hypocotyls in dark-grown 7-day old seedlings of <i>35S::YFP</i> , <i>35S::YFP-IAA1</i> and <i>35S::YFP-IAA2</i> overexpressor lines	197
Supplementary Figure 32: Elongation of hypocotyls in dark-grown 5-day old seedlings of <i>35S::YFP</i> , <i>35S::YFP-IAA1</i> and <i>35S::YFP-IAA2</i> overexpressor lines	197
Supplementary Figure 33: Elongation of hypocotyls in dark-grown 5-day old seedlings of <i>35S::YFP</i> , <i>35S::YFP-IAA1</i> and <i>35S::YFP-IAA2</i> overexpressor lines	198
Supplementary Figure 34: Number of axillary shoots in 5-week old plants of <i>35S::YFP</i> , <i>35S::YFP-IAA1</i> and <i>35S::YFP-IAA2</i> overexpressor lines.....	199
Supplementary Figure 35: Plant height of 5-week old plants of <i>35S::YFP</i> , <i>35S::YFP-IAA1</i> and <i>35S::YFP-IAA2</i> overexpressor lines.....	200
Supplementary Figure 36: Number of rosette leaves in 17-day old (A) and 20-day old (B) plants <i>35S::YFP</i> , <i>35S::YFP-IAA1</i> and <i>35S::YFP-IAA2</i> overexpressor lines	201
Supplementary Figure 37: Transcript levels of <i>IAA3</i> , <i>IAA4</i> , <i>IAA5</i> , and <i>IAA6</i> in seedlings of <i>35S::YFP</i> , <i>35S::YFP-IAA1</i> and <i>35S::YFP-IAA2</i> overexpressor lines	202
Supplementary Figure 38: Preliminary assessment of TIR1/AFB:AUX/IAA-chimera interaction in yeast	205

Supplementary Figure 39: Auxin-dependent interaction of chimeric IAA7/12 with TIR1/AFB1/AFB2 in yeast	205
Supplementary Figure 40: Immunoblot analysis of AD-4-module-chimera protein expression from yeast strains used in Y2H assay (Figure 2-20 A)	206
Supplementary Figure 41: Immunoblot analysis of AD-5-module-chimera protein expression from yeast strains used in Y2H assay (Figure 2-20 B)	207
Supplementary Figure 42: Absolute Firefly Luciferase (FF) and Renilla Luciferase (REN) expression	207
Supplementary Figure 43: Overview and nomenclature of 4-module (A) and 5-module (B) chimeric constructs	208
Supplementary Figure 44: Golden Gate Modular Cloning (MoClo) assembly strategy for 4-module and 5-module chimeras of <i>IAA7</i> and <i>IAA12</i>	209
Supplementary Figure 45: Details of 5-module MoClo assembly	210
Supplementary Figure 46: pLUZ5 and pLUZ6 vector adaptation for Golden Gate cloning compatibility from pB42AD and pGEX-4T-3, respectively	211
Supplementary Figure 47: MoClo assembly scheme for Level 1 binary vector for plant overexpression of N-terminally VENUS-tagged chimeras	211
Supplementary Figure 48: pGEX-4T-3 Gateway-adapted vector map	220
Supplementary Figure 49: pLUZ6 vector map	221
Supplementary Figure 50: pLUZ5 vector map	222

8.5 List of Supplementary Tables

Supplementary Table 1: Structurally aligned residues from AFB1, AFB2, and AFB3 models and TIR1 crystal structure (Figure 2-1)	157
Supplementary Table 2: Identity and similarity of IAA1 and IAA2 protein sequences	161
Supplementary Table 3: Identity and similarity of IAA7 and IAA12 protein sequences	161
Supplementary Table 4: List of predicted transcription factor (TF) or TF family binding sites (BS) in upstream region of <i>IAA1</i> (At4g14560)	164
Supplementary Table 5: List of predicted transcription factor (TF) or TF family binding sites (BS) in upstream region of <i>IAA2</i> (At3g23030)	166
Supplementary Table 6: Statistical analysis of radioligand binding data	177
Supplementary Table 7: Selection of transgenic T3 lines	184
Supplementary Table 8: Grouping of transgenic lines into high, medium and low overexpressors according to the frequency distribution analysis in Figure 2-17	186
Supplementary Table 9: Pearson correlation analysis for <i>YFP-IAA1</i> transgene expression level and selected phenotypic effects	189
Supplementary Table 10: Pearson correlation analysis for <i>YFP-IAA2</i> transgene expression level and selected phenotypic effects	190
Supplementary Table 11: Exemplary crossing scheme for generating lines that carry the same <i>35S::YFP-IAA1</i> or <i>35S::YFP-IAA2</i> locus in different <i>tir1/afb</i> single or double mutant backgrounds	203
Supplementary Table 12: Overview of chimera modules nomenclature and sequences	204
Supplementary Table 13: Primers for amplification of AUX/IAA CDS blunt end fragments for Directional TOPO cloning (Thermo Fisher Scientific)	212
Supplementary Table 14: Primers for amplification of AUX/IAA CDS <i>attB</i> site-containing fragments for Gateway cloning (Thermo Fisher Scientific)	213

Supplementary Table 15: Primers for site-directed mutagenesis (Agilent Technologies)	214
Supplementary Table 16: General primers	216
Supplementary Table 17: Primers applied in Golden Gate cloning procedures to amplify fragments and to verify cloning and transformation success in PCR	216
Supplementary Table 18: Primers used in RT-qPCR	218

8.6 Supplementary Figures and Tables

Supplementary Table 1: Structurally aligned residues from AFB1, AFB2, and AFB3 models and TIR1 crystal structure (Figure 2-1)

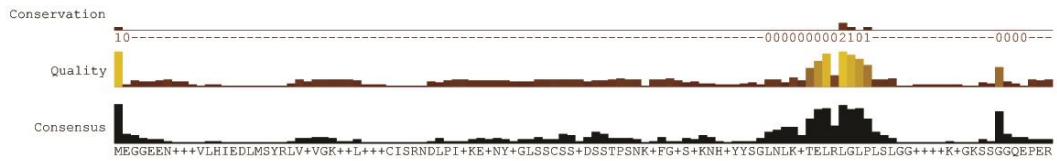
Black: Identical amino acids. Green: conserved changes in amino acid. Blue: non-conserved changes in amino acid. Function of TIR1 residues taken from Tan *et al.* (2007) and as indicated in the additional description.

TIR1	AFB1	AFB2	AFB3	additional description
auxin-binding/pocket formation				
R403	R399	R398	R400	anchoring carboxyl group of auxin
H78	H74	H73	H73	
R436	R432	R431	R433	
S438	S434	S432	S435	anchoring carboxyl group of auxin
S462	S458	S457	S459	
E487	E483	E482	E484	
M460	M456	M455	M457	
F79	F75	F74	F74	
L439	V435	L434	V436	backbone C=O with N-H of indole ring
AUX/IAA binding				
F82	Y78	F77	F77	F82 proposed to undergo conformational change (Hao et al. 2010)
F380	F376	F375	F377	
F351	D347	___	H347	loop-12, (F351 proposed as 'fastener' by Hao et al. 2010)
P347	P343	P343	P343	loop-12
P350	P346	L346	V346	loop-12
C405	C401	C400	C402	canopy
S440	S436	S435	S437	canopy
A464	A460	A459	A461	canopy
D170	D166	D165	D165	D170E enhanced degron interaction (Yu et al. 2015)
M473	L469	M468	M470	M473L enhanced degron interaction (Yu et al. 2015)
IP6 coordinating				
K74	K70	K69	K69	
K113	K109	K108	K108	
R114	R110	R109	R110	
R484	K480	K479	R481	
K485	K481	K480	K482	
R509	R505	R504	R506	

```

10      20      30      40      50      60      70      80      90      100     110
IAA10_ATIG04100.1  MNGLQEV-----CSSSGSVMI-----GLPAEEDEN--AAHSSDEDSCP-----DESVSETELDLALGLSI-----GRRK--
IAA11_AT4G28640.2  MRGG-----SASGSAS-----ALSNDENLV-----VSCEDSSSPIG-----NELELGLTLLS-----GRRGYR--
IAA12_ATIG04550.2  MRGVSE-----LEVGS-----NLPAESELELGLLGLSL-----GGGAWKE-----
IAA13_AT2G33310.2  MITE-----LEMGK-----GESELELGLLGLLGGTAAKIGKSGGGAWKE-----
IAA3_ATIG04240.1  M-----DE-----FVNLRKETEELRGLD-----GTDN-----
IAA4_AT5G43700.1  MEK-----VDVYDE-----LVNLRKATELRGLD-----GT-----
IAA2_AT3G23030.1  MA-----YEKVN-----ELNLRKDELRGLD-----GRTE-----
IAA1_AT4G14560.1  M-----EVTN-----GLNLRKDELRGLD-----GAQE-----
IAA17_ATIG04250.1  MM-----GSV-----ELNLRKETEELRGLD-----GGDT-----
IAA7_AT3G23050.1  MITG-----LMNLRKATELRGLD-----GGAE-----
IAA14_AT4G14550.1  M-----MNLKATELRGLD-----GGTE-----
IAA16_AT3G04730.1  M-----INFEATELRGLD-----GGNH-----
IAA27_AT4G29080.1  MS-----VSVAA-----EHDYIGLSEPTMEATMSDKTKTRDNNN--GLNFKATELRGLD-----SESSEPER
IAA8_AT2G22670.4  MSSGNDKIKQVLHIEDLMSYRLVSVKDELVTS--PCLKERNYVGLSDCSSVDSSTIPN--VVGKS--NLNFKATELRGLD-----ESQSPER
IAA9_AT5G65670.1  MSPPEELQSN--VSVASSSPTSNCISRNTLGLLKEHNYLGLSDCSSVGSSTLSP--LAEDDKA--TISLKAETEELRGLD-----GQSOPAR
IAA5_ATIG15580.1  MA-----NESN-----NLGLEITELRGLD-----GDTV-----
IAA6_ATIG52830.1  MA-----KE-----GLALEITELRGLD-----GDNY-----
IAA19_AT3G15540.1  ME-----KE-----GLGLEITELRGLD-----GRDVAEK-----
IAA15_ATIG80390.1  MSPPEEY-----VRVWPD-----SGDLGGTEELTALD-----GTPT-----
IAA18_ATIG51950.1  MEGYSRN-----GEISPKLL-----DLMIQPERRN-----WPHDEKNS--VFKTEEKKLELKLGLD-----SEED-----
IAA26_AT3G16500.1  MEGCPRN-----REIGPKLL-----DL-IPQGRK-----WYQEDKNN--TDQEKLELRGLD-----GGDE-----
IAA28_AT5G25890.1  ME-----EKKRLELRGLD-----EKKRLELRGLD-----
IAA20_AT2G46990.1  MGRGRS-----SSSSIESSSKSN--PFGASS--TRNLSFDLRLGLSFGT-----SSGTQYFNG
IAA30_AT3G62100.1  MGRGRS-----SSSSIESSCKSN--PFGVSS--NTRNLSFDLRLGLSFGS-----SSG-QYNG
IAA31_AT3G17600.1  MEVS-----TKPSPSSVNLSSL--TKPSPSSVNLSSL-----
IAA29_AT4G32280.1  M-----EIDLGLSLSP--HKSSKL--GFNF--
IAA34_ATIG15050.1  MYCSDPPHP--LH-----LVASDRQQ-----KDKHLLSWKKPTMDSQ--PLG--VFPNSPKYHPYYSQTTEFGGVIDLGLSLRT
IAA32_AT2G01200.2  M-----DPNTPAD--FFKGSKFHYIYSQTKKGGVIDLGLSLRT
IAA33_AT5G57420.1  MMSFEPSQ-----

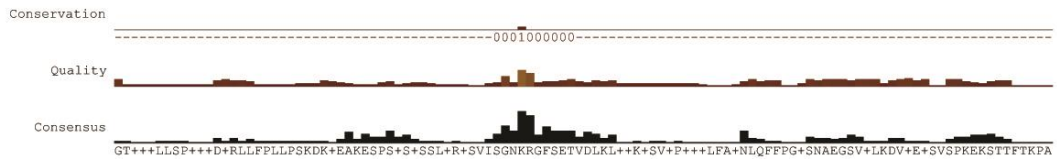
```



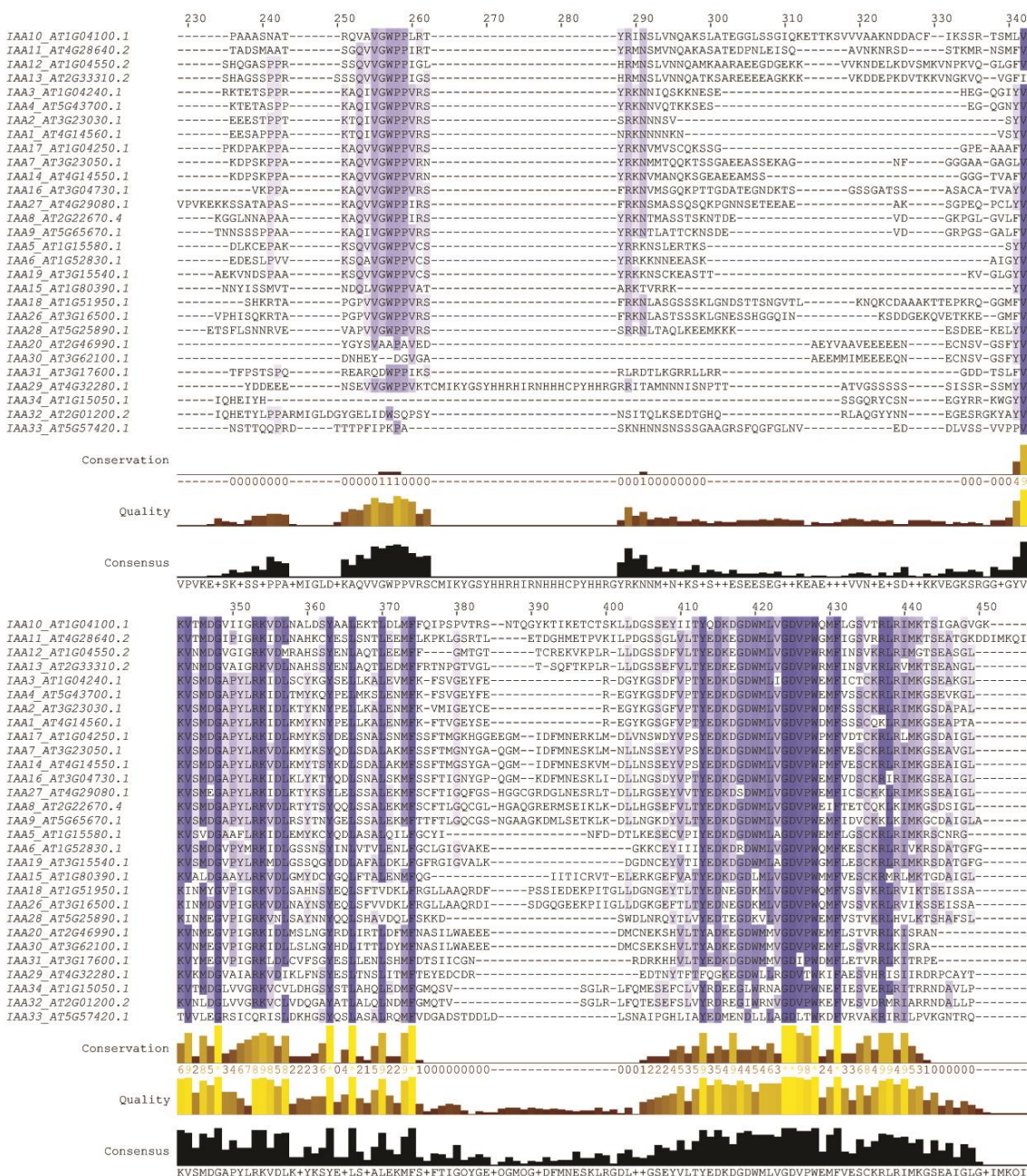
```

120     130     140     150     160     170     180     190     200     210     220
IAA10_ATIG04100.1  -----VRSLSLSSSSSLTRE--SGTKRSADSS-----
IAA11_AT4G28640.2  -----DCRVY-----ADSSSSSSSSSLSRASVIAGIKR-----
IAA12_ATIG04550.2  -----RGRIL-----TAKDFPS-----VGSKRAESS-----
IAA13_AT2G33310.2  -----RGRLL-----TAKDFPS-----VGSKRAADSA-----
IAA3_ATIG04240.1  -----VCEAKERVSCCN-----NNKRVLSTDEKEI-----ESSS-----
IAA4_AT5G43700.1  -----EETVSCG-----KSNRVLPATEKEI-----ESTG-----
IAA2_AT3G23030.1  -----KIKEEQVSCVK-----SNKRLFEETRD-----EKKRLELRGLD-----
IAA1_AT4G14560.1  -----EQLELSCVR-----SNKRRNNNDST-----
IAA17_ATIG04250.1  -----VAPV-----TGKRGFSETVDLKL-----NLNNE--PANKEGSTTH-DVVTF--DSKESAC-----
IAA7_AT3G23050.1  -----AVESPAKSA-----VSGKRGFSETVDLKL-----NLQ--SNKESVDL-KNVSA--VPKRTLL-----
IAA14_AT4G14550.1  -----TVESPAKSG-----VNGKRGFSETVDLKL-----NLQ--SNKQGVLDL--NTNG--APKERTL-----
IAA16_AT3G04730.1  -----GGMAGK-----VNGKRGFSETVDLKL-----NLS--STAMDSVS--KVDLE--MKRKY-----
IAA27_AT4G29080.1  V-----DSRF-----LALNKSSCPV-----SGAKRVFSDAINDSN--KWFVSPGTTATGDVSGSGPRTSVVKGDKSTTFPKPA
IAA8_AT2G22670.4  ETDPLGLSPRTPEKLLFPLLPKDKNGSATTGHNKVV--SGNKRGFADTWFDFSGVKSVPVGGG--INMML--SPKVKDVSXS--IQERSHA-----
IAA9_AT5G65670.1  DTELNLNLSPAKLDEKPFPLLPKDKDE-ICSSSQKNA--SGNKRGFSDTMDQFAEAKSSVYTEK--NWMFP--EAAATQSVTKKDVQON--IPKQGSST-----
IAA5_ATIG15580.1  -----VSGESI-----SGKKRASPEV-----E-----
IAA6_ATIG52830.1  -----SEISVCGSS-----KPKKRVLSDM-----MT--SSALDT--EN-EN--SVVSV-----
IAA19_AT3G15540.1  M-----MKKRAFTEM-----NMT--SSGSNS--DQCES--GVVSSGD-----
IAA15_ATIG80390.1  -----NASEGPKK-----FNGKRVLETVDLKL-----G-----
IAA18_ATIG51950.1  -----DDESMI-----RHMKKEPKDKSILSL--AGKYF-----SPSSTKTT-----
IAA26_AT3G16500.1  -----EDHSAIKKKNTE--IRNIRKETEDKSFHCF--NGNHF-----SPSNKTT-----
IAA28_AT5G25890.1  G-----CHOFTSNNN--INGSKQKSSTK-----
IAA20_AT2G46990.1  G-----
IAA30_AT3G62100.1  G-----
IAA31_AT3G17600.1  -----
IAA29_AT4G32280.1  -----DLNKHCAIEGAASCL--GTELRFEATFGLGNVEENCYMPKQRLPALNGQ--PNEEEDP--LESESSIV-----
IAA34_ATIG15050.1  -----
IAA32_AT2G01200.2  -----
IAA33_AT5G57420.1  -----DSLQRFHQD-----

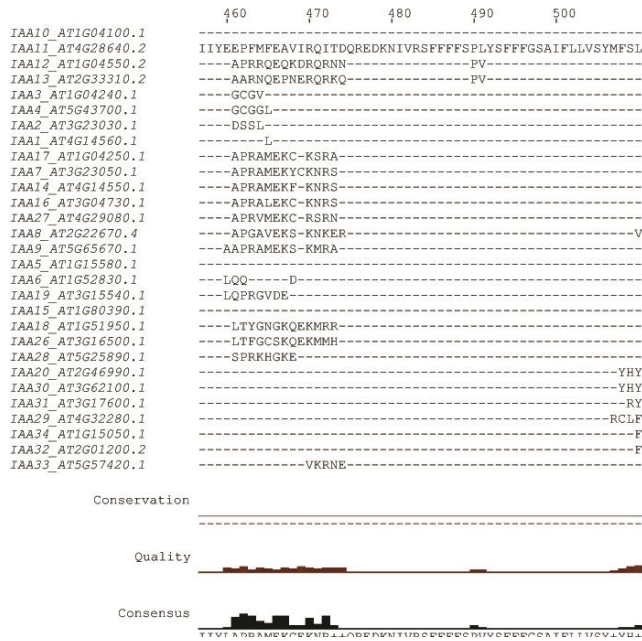
```



Supplementary Figure 1 continued next page



Supplementary Figure 1 continued next page



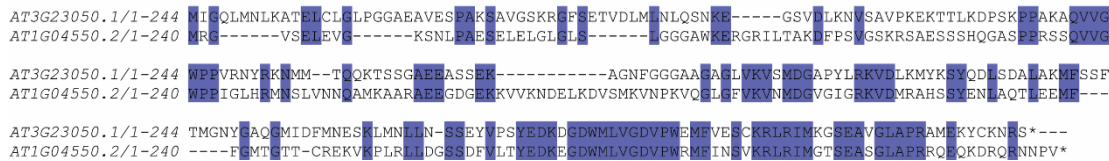
Supplementary Figure 1: Alignment of all Arabidopsis AUX/IAAs.

Alignment was taken and modified from (Winkler *et al.*, under review). Blue coloring indicates conservation level. Lighter and stronger blue denotes weaker or stronger conservation, respectively.



Supplementary Figure 2: MAFFT alignment of IAA1 and IAA2.

IAA1 (AT4G14560.1) and IAA2 (AT3G23030.1) protein sequences were aligned with MAFFT (Katoh *et al.*, 2005) at <http://www.ebi.ac.uk/Tools/msa/mafft/>, and identical amino acids colored in blue.



Supplementary Figure 3: MAFFT alignment of IAA7 and IAA12

IAA7 (AT3G23050.1) and IAA12 (AT1G04550.2) protein sequences were aligned with MAFFT (Katoh *et al.*, 2005) at <http://www.ebi.ac.uk/Tools/msa/mafft/>, and identical amino acids colored in blue.

Supplementary Table 2: Identity and similarity of IAA1 and IAA2 protein sequences

Using Sequence Manipulation Suite Ident and Sim (Stothard, 2000) at http://www.bioinformatics.org/sms2/ident_sim.html, identity and similarity of IAA1 and IAA2 were calculated. Input: MAFFT alignment of protein sequences of IAA1 (AT4G14560.1) and IAA2 (AT3G23030.1)(see **Supplementary Figure 2**). Similar residues were defined as followed: GAVLI, FYW, CM, ST, KRH, DENQ, P.

Results for IAA1 vs IAA2

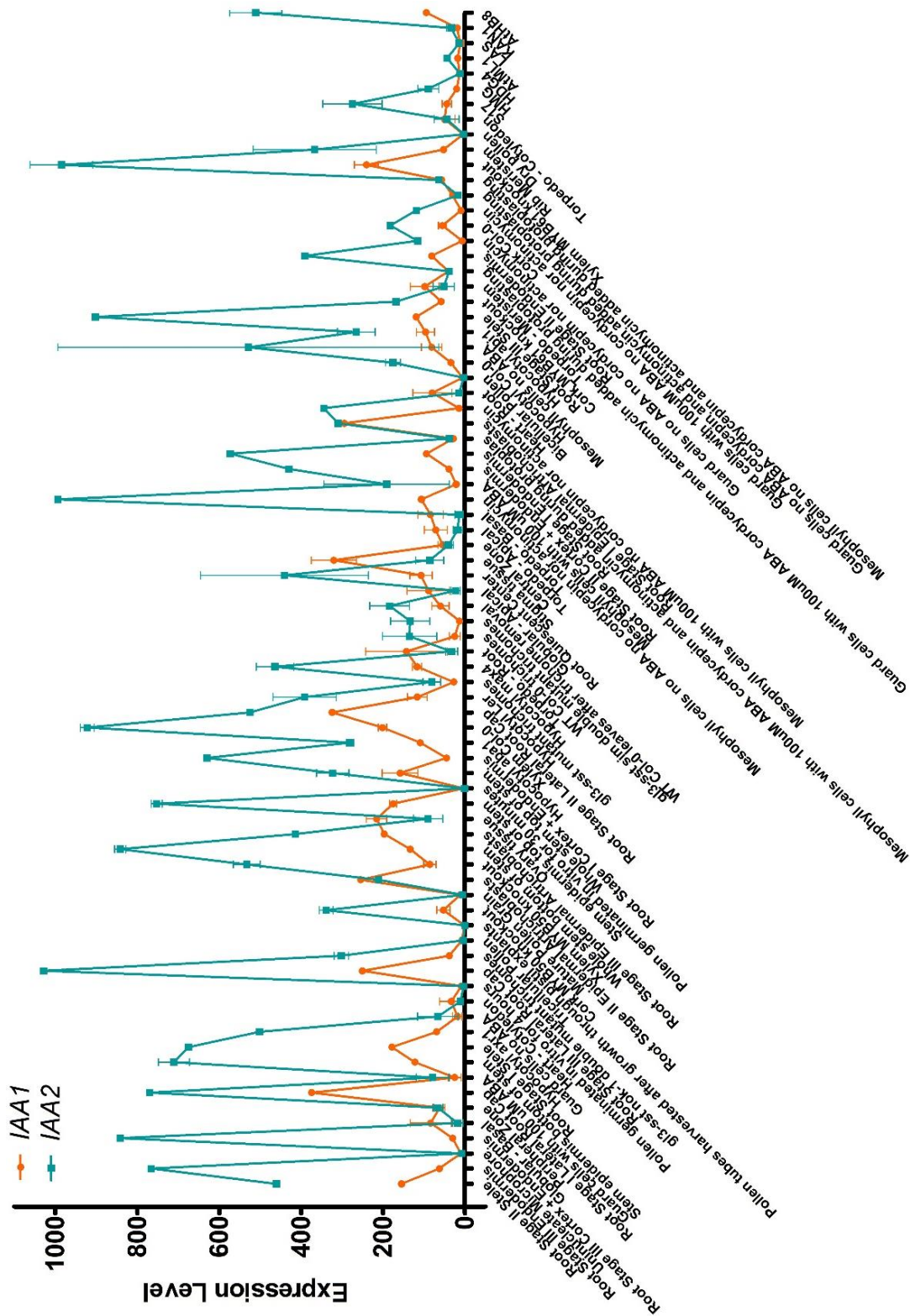
Alignment length:	176
Identical residues:	132
Similar residues:	11
Percent identity:	75.00
Percent similarity:	81.25

Supplementary Table 3: Identity and similarity of IAA7 and IAA12 protein sequences

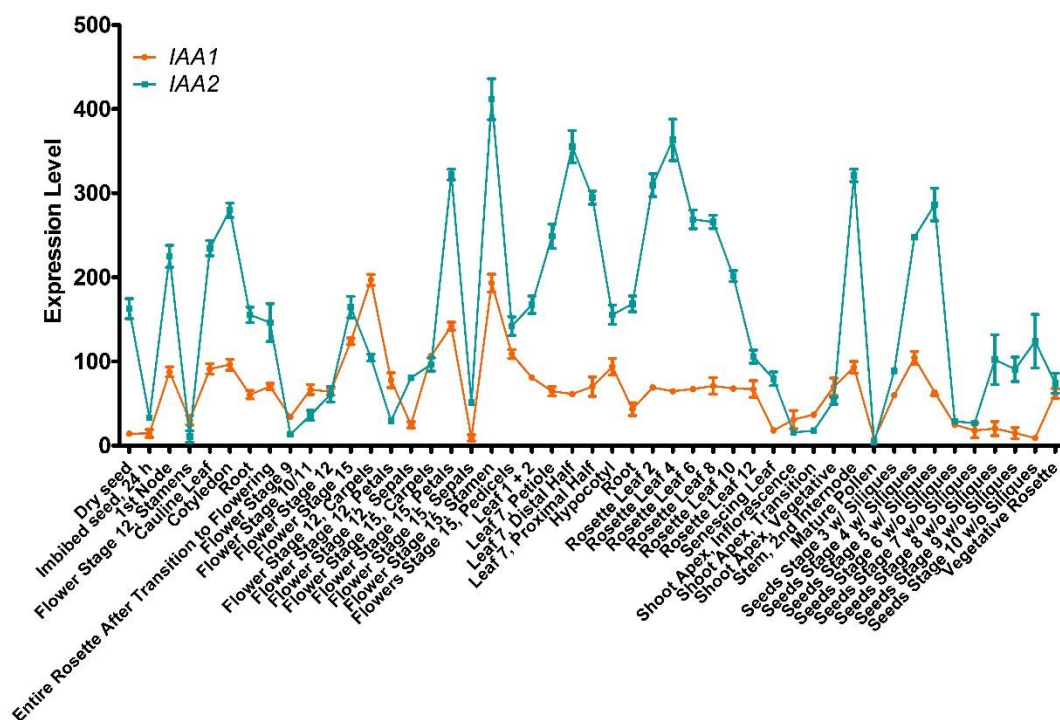
Using Sequence Manipulation Suite Ident and Sim (Stothard, 2000) at http://www.bioinformatics.org/sms2/ident_sim.html, identity and similarity of IAA7 and IAA12 were calculated. Input: MAFFT alignment of protein sequences of IAA1 (AT4G14560.1) and IAA2 (AT3G23030.1)(see **Supplementary Figure 3**). Similar residues were defined as followed: GAVLI, FYW, CM, ST, KRH, DENQ, P

Results for IAA7 vs IAA12

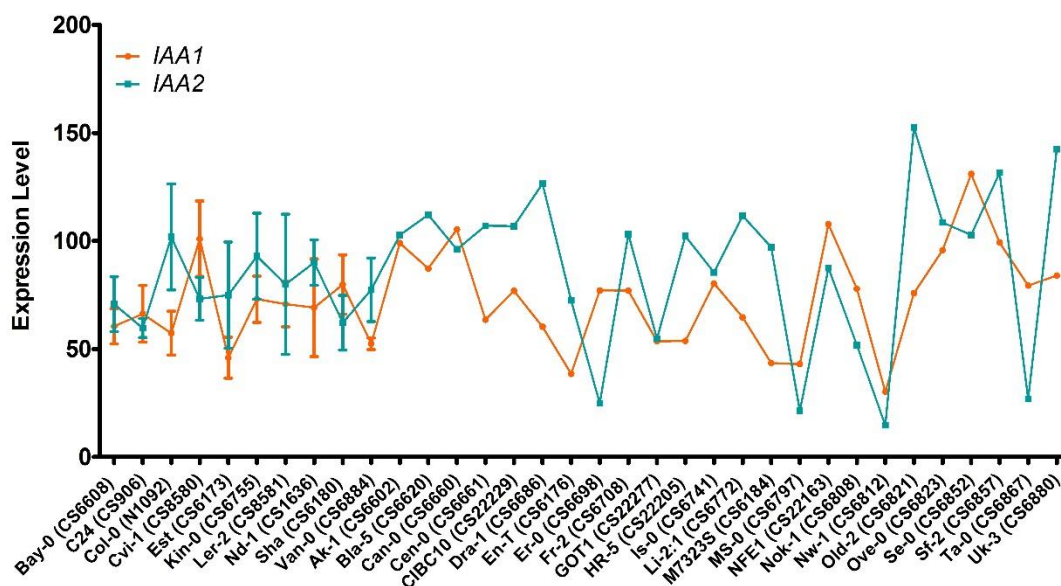
Alignment length:	265
Identical residues:	92
Similar residues:	31
Percent identity:	34.72
Percent similarity:	46.42



Supplementary Figure 4: Detailed expression level datasets of IAA1 and IAA2 as shown in Figure 2-3 A boxplot AtGenExpress datasets for Cell-type-specific expression. See Section 6.11.2 for detailed references.



Supplementary Figure 5: Detailed expression level datasets of IAA1 and IAA2 as shown in Figure 2-3 A boxplot AtGenExpress datasets for development-specific expression. See Section 6.11.2 for detailed references.



Supplementary Figure 6: Detailed expression level datasets of IAA1 and IAA2 as shown in Figure 2-3 A boxplot AtGenExpress datasets for expression in different *A. thaliana* ecotypes (natural variation dataset). See Section 6.11.2 for detailed references.

Supplementary Table 4: List of predicted transcription factor (TF) or TF family binding sites (BS) in upstream region of *IAA1* (At4g14560)

3 kb of the sequence upstream of the start site (ATG) were predicted as promotor, and analyzed with Arabidopsis Gene Regulatory Information Server for predicted *cis* regulatory motifs (<http://arabidopsis.med.ohio-state.edu/AtcisDB/>; Davuluri *et al.*, 2003; Yilmaz *et al.*, 2011). Predicted binding sites that occur in both *IAA1* and *IAA2* have been marked with identical colors in **Supplementary Table 4** and **Supplementary Table 5**.

IAA1

BS Name	BS Sequence	BS Family/TF
AtMYB2 BS in RD22	ctaacca	MYB
AtMYC2 BS in RD22	cacatg	BHLH
AtMYC2 BS in RD22	cacatg	BHLH
AtMYC2 BS in RD22	cacatg	BHLH
AtMYC2 BS in RD22	cacatg	BHLH
AtMYC2 BS in RD22	cacatg	BHLH
AtMYC2 BS in RD22	cacatg	BHLH
Bellringer/replumless/pennywise BS1 IN AG	aaattaa	Homeobox
ATB2/AtbZIP53/AtbZIP44/GBF5 BS in ProDH	actcat	bZIP
ATB2/AtbZIP53/AtbZIP44/GBF5 BS in ProDH	actcat	bZIP
W-box promoter motif	ttgacc	WRKY
W-box promoter motif	ttgacc	WRKY
W-box promoter motif	ttgact	WRKY
CArG promoter motif	ccaaaaagg	MADS
CArG promoter motif	cctttttgg	MADS
ARF1 binding site motif	tgtctc	ARF
ARF1 binding site motif	tgtctc	ARF
ATHB2 binding site motif	taataatta	HB
DPBF1&2 binding site motif	acacgtg	bZIP
DPBF1&2 binding site motif	acacgag	bZIP
DPBF1&2 binding site motif	acacatg	bZIP
DPBF1&2 binding site motif	acactag	bZIP
DPBF1&2 binding site motif	acactcg	bZIP
MYB binding site promoter	cacctacc	MYB
MYB4 binding site motif	aacaaac	MYB
MYB4 binding site motif	acctacc	MYB
MYB4 binding site motif	accaaac	MYB
MYB4 binding site motif	aactacc	MYB
RAV1-A binding site motif	caaca	ABI3VP1
RAV1-A binding site motif	caaca	ABI3VP1
RAV1-A binding site motif	caaca	ABI3VP1
RAV1-A binding site motif	caaca	ABI3VP1
RAV1-A binding site motif	caaca	ABI3VP1
RAV1-A binding site motif	caaca	ABI3VP1
RAV1-A binding site motif	caaca	ABI3VP1
RAV1-A binding site motif	caaca	ABI3VP1
RAV1-A binding site motif	caaca	ABI3VP1
LFY consensus binding site motif	ccaatg	LFY
ARF binding site motif	tgtctc	...
ARF binding site motif	tgtctc	...
BoxII promoter motif	ggttaa	...
EveningElement promoter motif	aaaatatct	...
EveningElement promoter motif	aaaatatct	...

GATA promoter motif [LRE]	agataa	...
GATA promoter motif [LRE]	agataa	...
GATA promoter motif [LRE]	tgatag	...
GATA promoter motif [LRE]	tgataa	...
GATA promoter motif [LRE]	agatag	...
GATA promoter motif [LRE]	tgataa	...
GATA promoter motif [LRE]	tgataa	...
GATA promoter motif [LRE]	agataa	...
G-box promoter motif [LRE]	cacgtg	...
G-box promoter motif [LRE]	cacgtg	...
Ibox promoter motif	gataag	...
Ibox promoter motif	gataag	...
L1-box promoter motif	taaatgca	...
T-box promoter motif	actttg	...
T-box promoter motif	actttg	...
T-box promoter motif	actttg	...
SORLIP1	agccac	...
SORLIP2	gggcc	...
SORLIP5	gagtgag	...

<http://arabidopsis.med.ohio-state.edu/AtcisDB/atcisview.html?id=At4g14560>

Supplementary Table 5: List of predicted transcription factor (TF) or TF family binding sites (BS) in upstream region of *IAA2* (At3g23030)

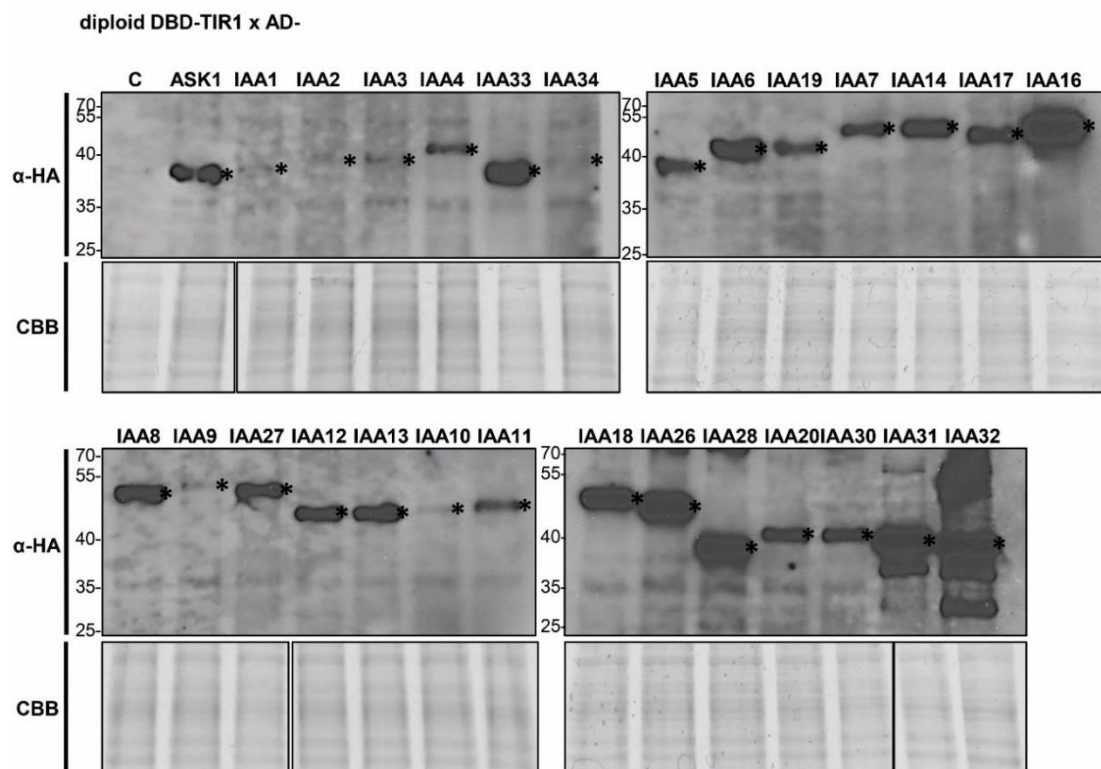
3 kb of the sequence upstream of the start site (ATG) were predicted as promotor, and analyzed with Arabidopsis Gene Regulatory Information Server for predicted *cis* regulatory motifs (<http://arabidopsis.med.ohio-state.edu/AtcisDB/>; Davuluri *et al.*, 2003; Yilmaz *et al.*, 2011). Predicted binding sites that occur in both *IAA1* and *IAA2* have been marked with identical colors in **Supplementary Table 4** and **Supplementary Table 5**.

IAA2

BS Name	BS Sequence	BS Family/TF
AtMYB2 BS in RD22	ctaacca	MYB
AtMYC2 BS in RD22	cacatg	BHLH
AtMYC2 BS in RD22	cacatg	BHLH
AtMYC2 BS in RD22	cacatg	BHLH
Bellringer/replumless/pennywise BS1 IN AG	aaattaa	Homeobox
Bellringer/replumless/pennywise BS1 IN AG	aaattaa	Homeobox
Bellringer/replumless/pennywise BS2 IN AG	aaattagt	Homeobox
Bellringer/replumless/pennywise BS3 IN AG	actaattt	Homeobox
ATB2/AtbZIP53/AtbZIP44/GBF5 BS in ProDH	actcat	bZIP
ATB2/AtbZIP53/AtbZIP44/GBF5 BS in ProDH	actcat	bZIP
ATB2/AtbZIP53/AtbZIP44/GBF5 BS in ProDH	actcat	bZIP
W-box promoter motif	ttgacc	WRKY
W-box promoter motif	ttgacc	WRKY
CARg promoter motif	cctttaagg	MADS
CARg promoter motif	ccaaaattgg	MADS
CARg promoter motif	ccaattttgg	MADS
CARg promoter motif	ccttaaagg	MADS
ARF1 binding site motif	tgtctc	ARF
ATHB2 binding site motif	taataatta	HB
DPBF1&2 binding site motif	acacacg	bZIP
DPBF1&2 binding site motif	acacaag	bZIP
DPBF1&2 binding site motif	acacaag	bZIP
MYB4 binding site motif	aacaaac	MYB
MYB4 binding site motif	aacaaac	MYB
RAV1-A binding site motif	caaca	ABI3VP1
RAV1-A binding site motif	caaca	ABI3VP1
RAV1-A binding site motif	caaca	ABI3VP1
RAV1-A binding site motif	caaca	ABI3VP1
RAV1-A binding site motif	caaca	ABI3VP1
RAV1-A binding site motif	caaca	ABI3VP1
RAV1-A binding site motif	caaca	ABI3VP1
LFY consensus binding site motif	ccattg	LFY
ABRE-like binding site motif	cacgtgga	...
ARF binding site motif	tgtctc	...
BoxII promoter motif	ggttaa	...
BoxII promoter motif	ggttaa	...
BoxII promoter motif	ggttaa	...
BoxII promoter motif	ggttaa	...
BoxII promoter motif	ggttaa	...
BoxII promoter motif	ggttaa	...
BoxII promoter motif	ggttaa	...
BoxII promoter motif	ggttaa	...
GATA promoter motif [LRE]	agataa	...
GATA promoter motif [LRE]	tgatag	...

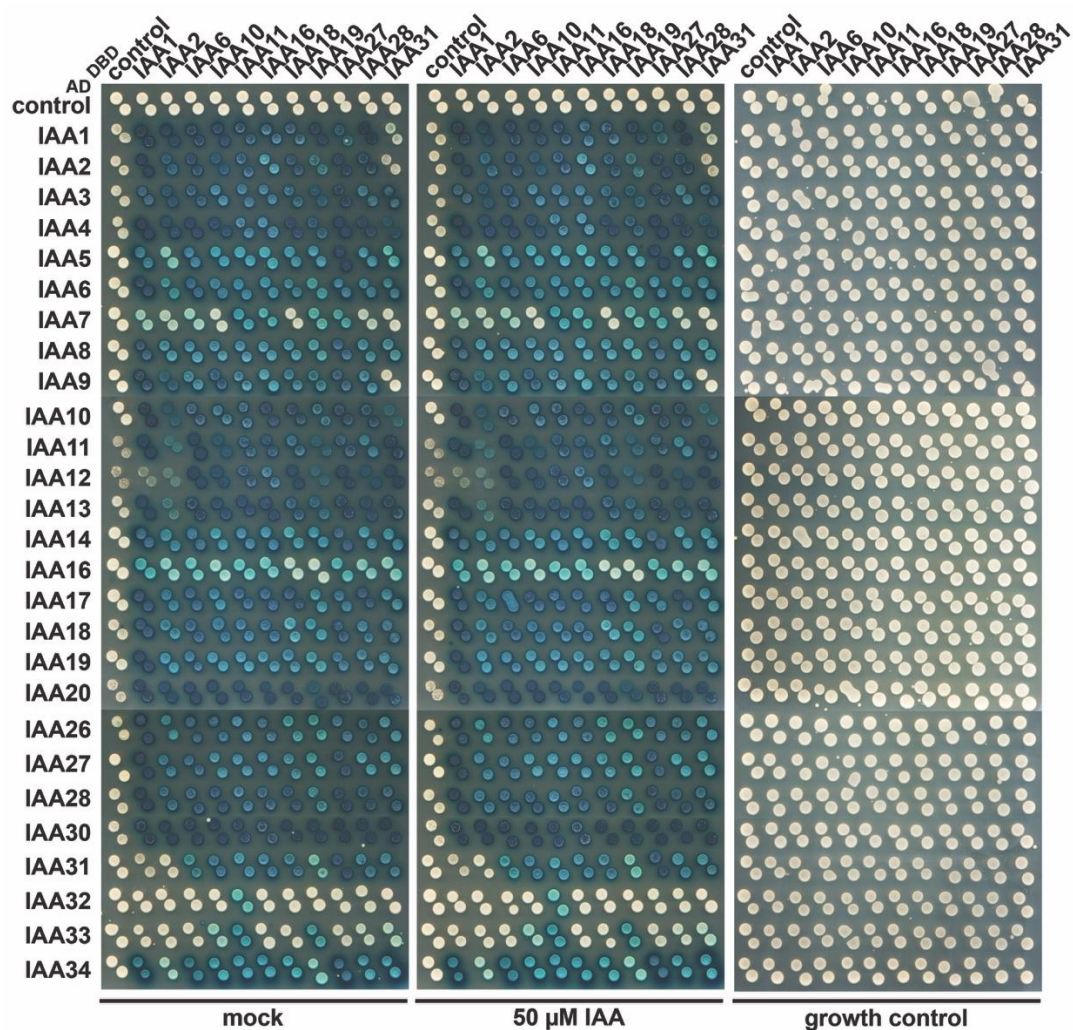
GATA promoter motif [LRE]	tgataa	...
GATA promoter motif [LRE]	tgataa	...
GATA promoter motif [LRE]	agataa	...
GATA promoter motif [LRE]	tgatag	...
GATA promoter motif [LRE]	agataa	...
GATA promoter motif [LRE]	agataa	...
GATA promoter motif [LRE]	agataa	...
G-box promoter motif [LRE]	cacgtg	...
G-box promoter motif [LRE]	cacgtg	...
GCC-box promoter motif	gccgcc	...
Ibox promoter motif	gataag	...
Ibox promoter motif	gataag	...
Ibox promoter motif	gataag	...
L1-box promoter motif	taaatgca	...
RY-repeat promoter motif	catgcatg	...
RY-repeat promoter motif	catgcatg	...
T-box promoter motif	actttg	...
T-box promoter motif	actttg	...

<http://arabidopsis.med.ohio-state.edu/AtcisDB/atcisview.html?id=At3g23030>



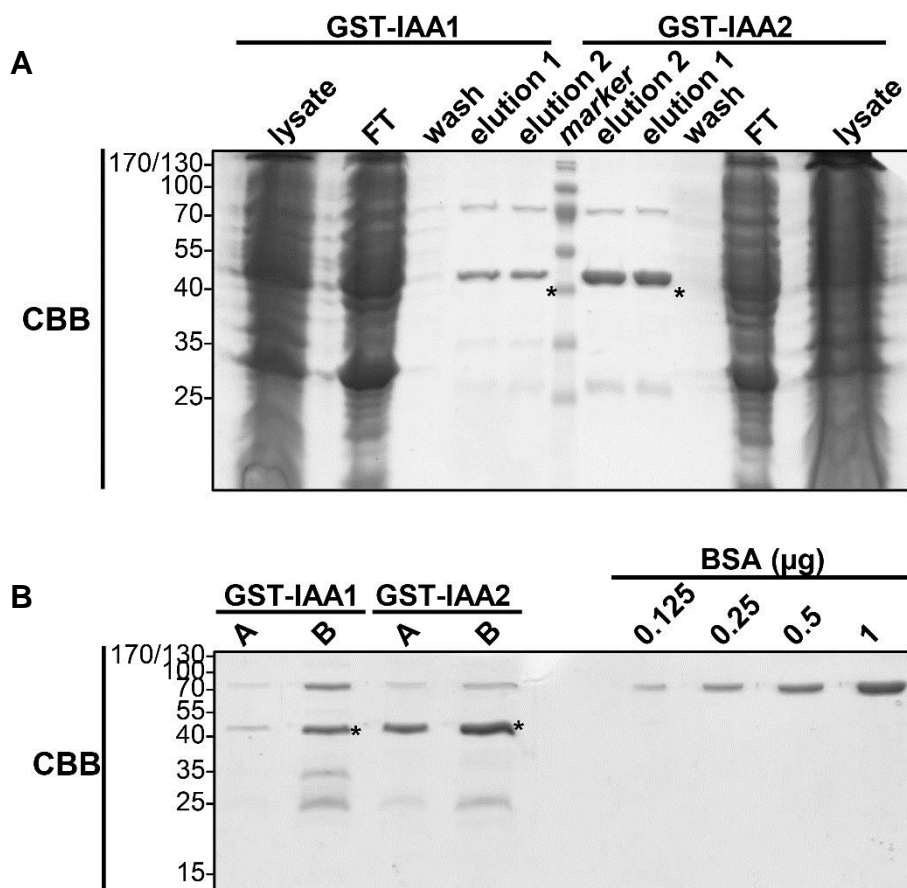
Supplementary Figure 7: Immunoblot analysis of AD-AUX/IAA protein expression from yeast strains used in quantitative Y2H assay (Figure 2-2)

Crude protein extracts were prepared from diploid yeasts expressing DBD-TIR1 and AD-AUX/IAA constructs. Yeast liquid cultures were grown in selective induction medium. Starting material was adjusted to similar amounts of yeast cells according to the culture OD_{600} . AD-fusion proteins carry an HA-tag between the AD and POI, and were therefore detected by immunoblotting with α -HA antibody (upper panels). Coomassie Brilliant Blue (CBB) staining of total protein is depicted as loading controls (lower panel). C: Control expressing DBD-TIR1 and AD empty vector. Asterisks denote AD-fusion protein. Protein levels of the DBD-TIR1/AFB expression constructs have been previously assessed (Calderon Villalobos et al., 2012).



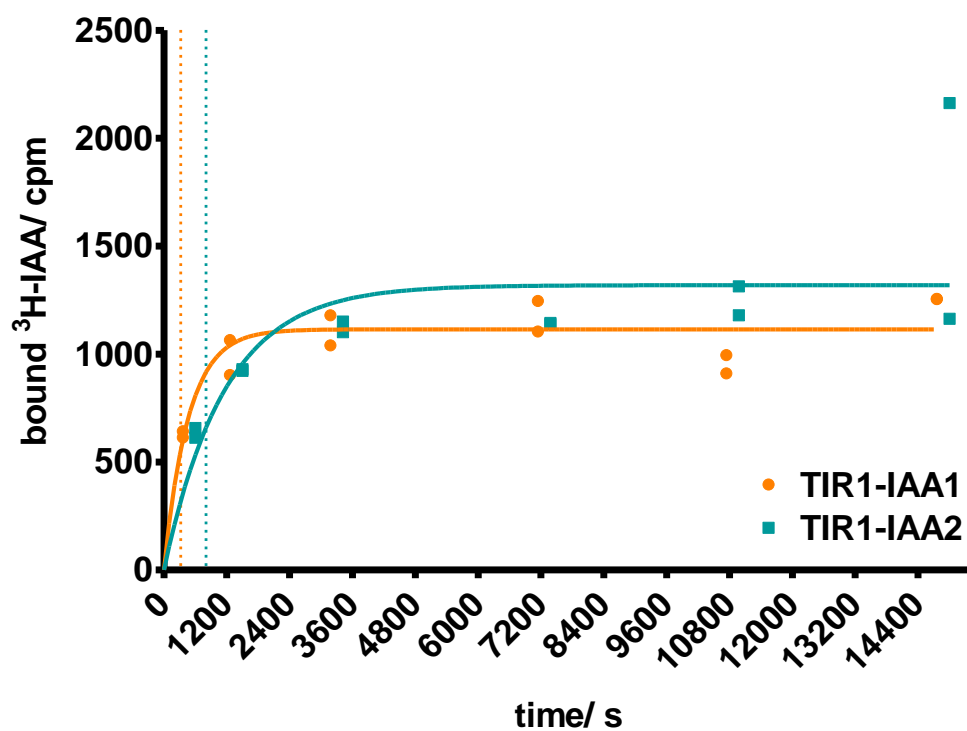
Supplementary Figure 8: Auxin-independency and growth control of homo- and heteromerization matrix of AUX/IAAs in yeast

To check for functional expression of AUX/IAAs in yeast, diploid yeast expressing AD-AUX/IAAs and DBD-AUX/IAAs were tested for β -Gal reporter activity indicative of PPI. Yeasts were grown on selective induction medium with or without 50 μ M IAA, or on SD medium without inducer as growth control. Yeast cell dispersions of the same OD₆₀₀ were spotted on medium plates and pictures taken after 3 days of growth at 30°C.

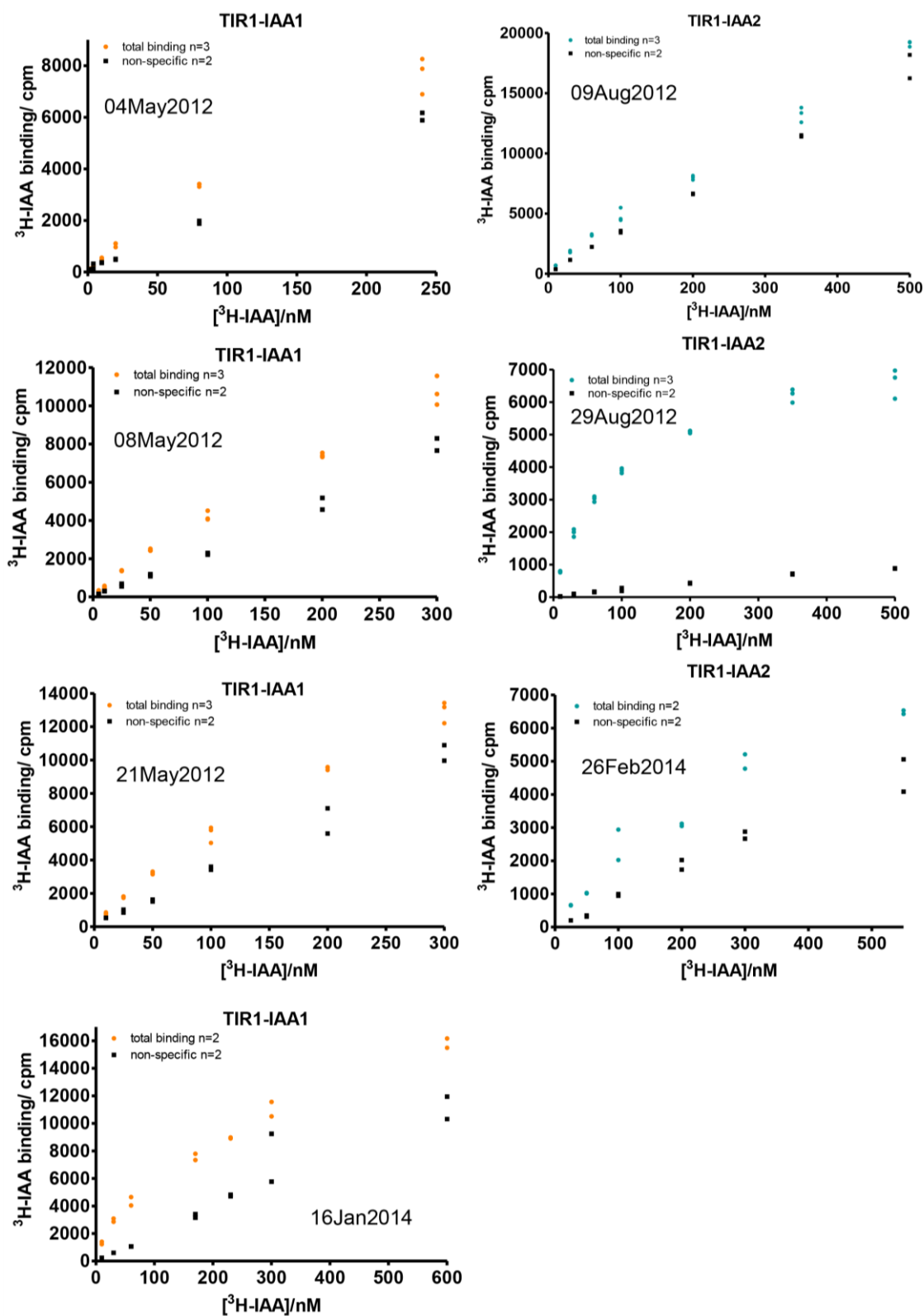


Supplementary Figure 9: GST-IAA1 and GST-IAA2 expression and purification in *E.coli*

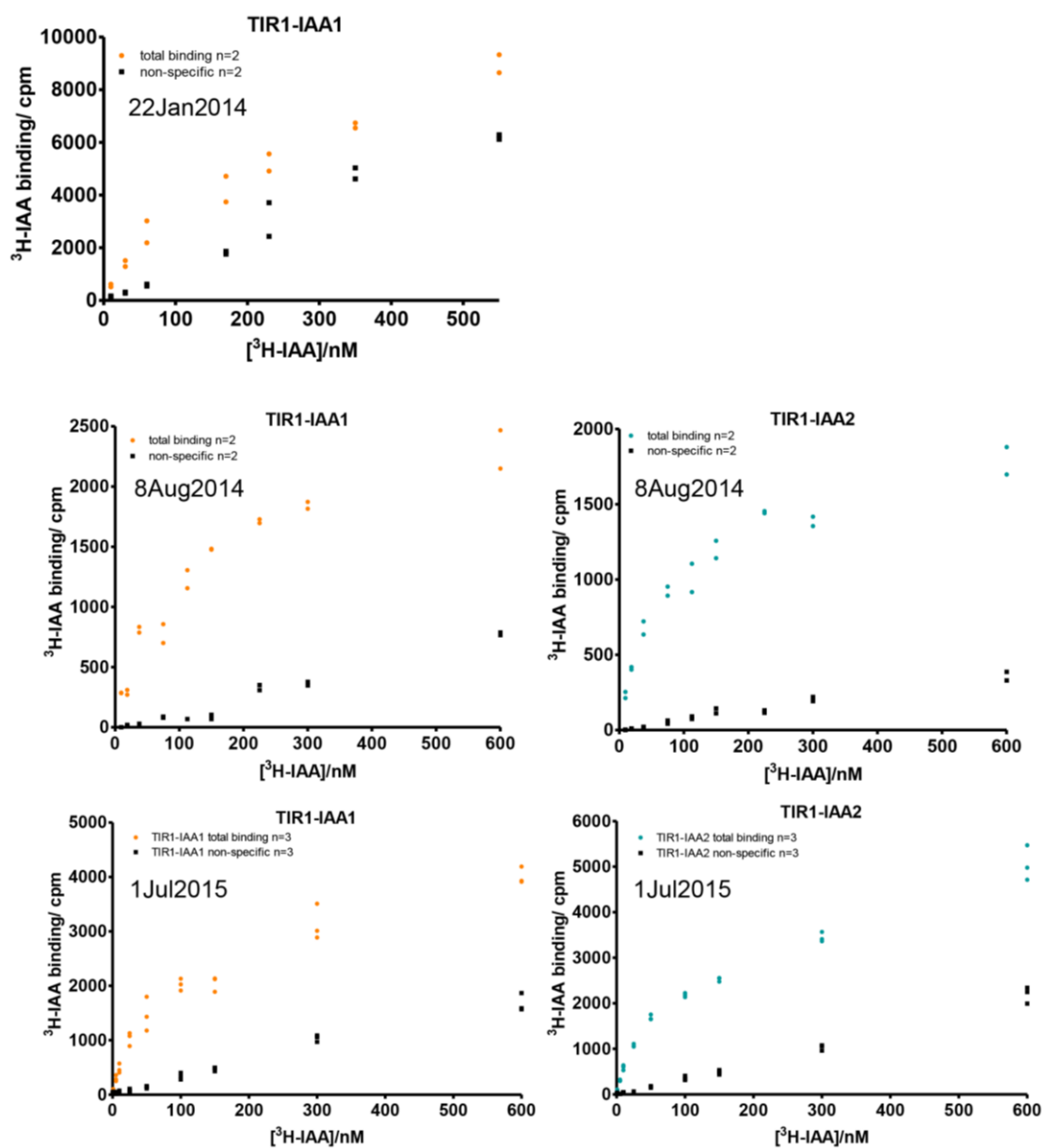
A. Typical 1-step affinity purification results are depicted. 4 μ L of crude lysate after lysis and clearance (lysate), 4 μ L of flow-through (FT) after application to GSTrap 4B 1mL column, 10 μ L of a mL wash fraction and 4 μ L of each 500 μ L-elution with 10 mM GSH were applied to 12% SDS-PAGE. Sufficiently pure GST-IAA1 or GST-IAA2 (marked with asterisk) was obtained in elution fractions. Elution fractions were pooled and dialyzed to remove GSH and concentrated. **B.** GST-IAA1 and GST-IAA2 are shown before (A) and after (B) buffer exchange and concentration (2 μ L per lane). Asterisk marks GST-IAA1/IAA2 protein of interest. Different amounts of BSA were loaded to estimate protein concentrations. CBB: Commassie Brilliant Blue stained SDS-PAGE.

**Supplementary Figure 10: Binding kinetic of TIR1:³H-IAA:GST-AUX/IAA complex formation**

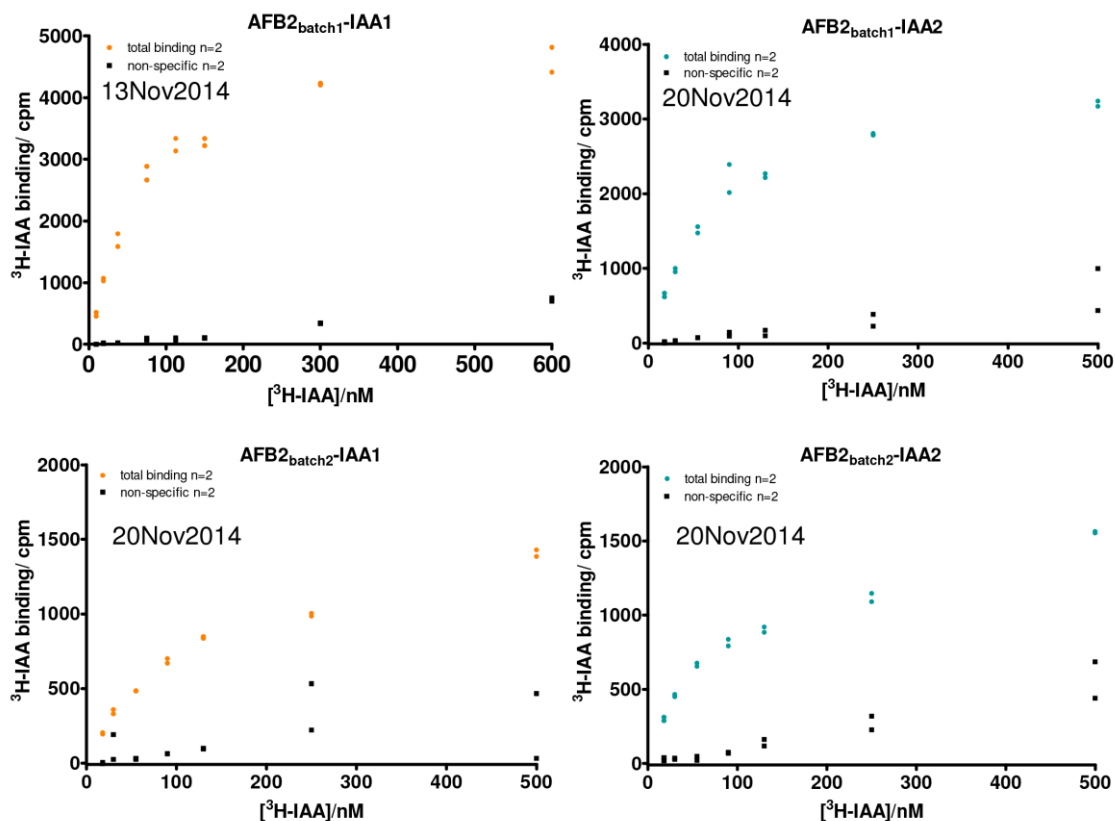
To estimate the incubation time needed until equilibrium is reached, a kinetic binding experiment was performed. Fixed concentrations of recombinant, highly pure TIR1:ASK1 (8 nM) and GST-AUX/IAA (2 μ M) were incubated with 75 nM ³H-IAA for indicated times. Samples containing co-receptor and radioligand for total binding, as well as identical samples with excess of unlabeled IAA (1 mM) for non-specific binding were measured. Specific binding was calculated by subtracting non-specific from total binding (n=2).



Supplementary Figure 9 (continued next page)

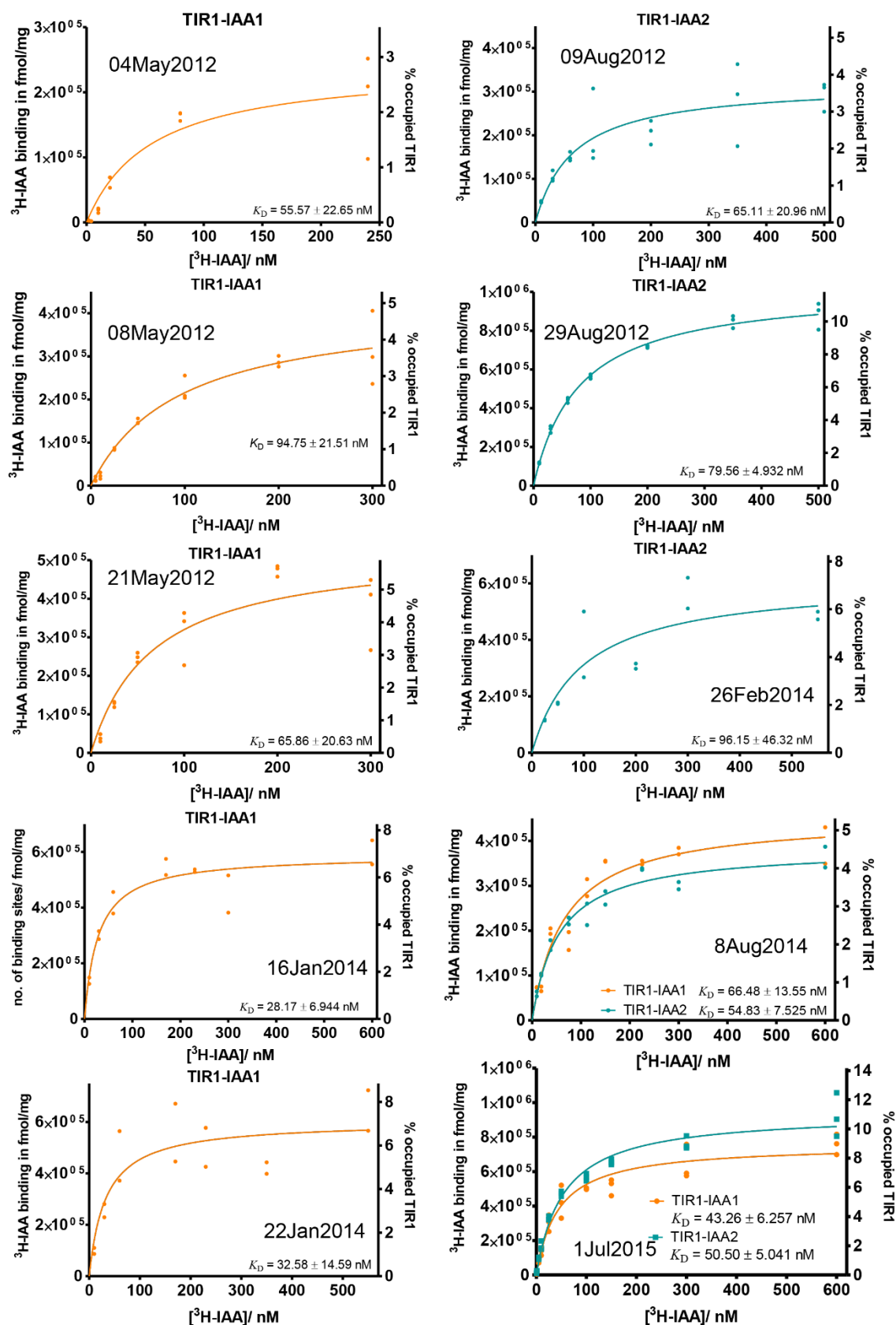


Supplementary Figure 9 (continued next page)



Supplementary Figure 11: Raw data of total (colored circles) and non-specific (black squares) ³H-IAA binding for TIR1/AFB2-IAA1/IAA2 co-receptors

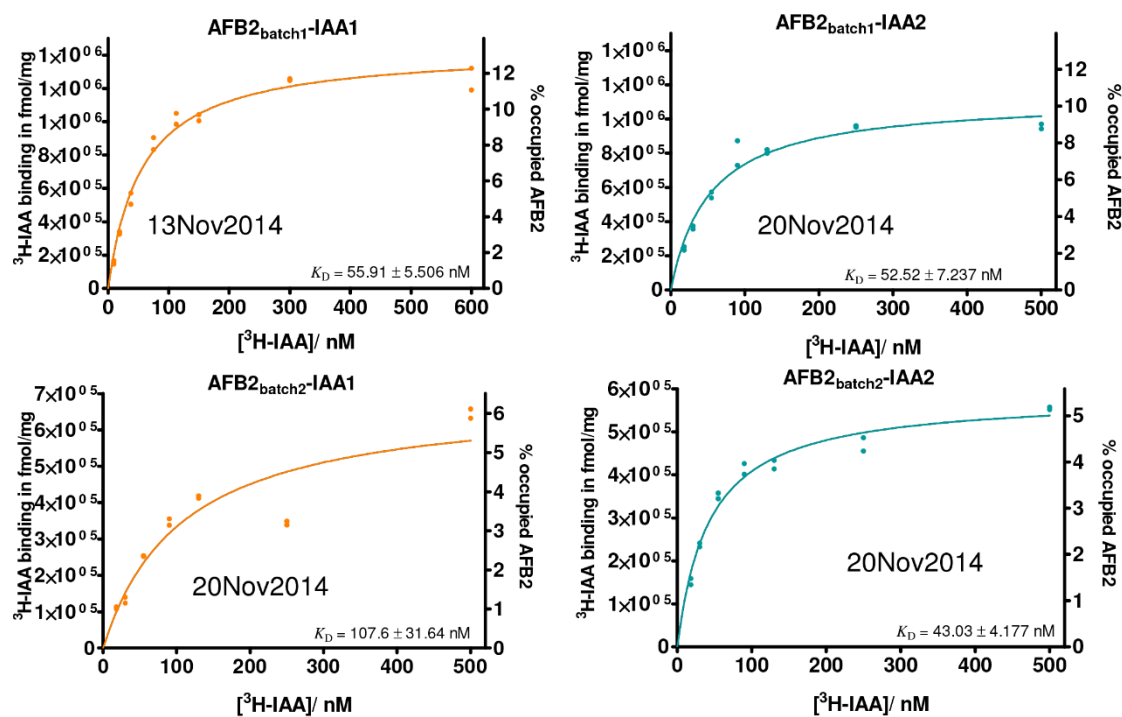
Cpm measurements were background-corrected by subtracting the mean count of at least two scintillation samples containing buffer-washed filter discs, which were run and measured alongside each individual experiment. n denotes number of replicates.



Supplementary Figure 12: Specific binding data and curve fits for independent experiments underlying K_D values shown in Figure 2-7

Specific binding was calculated for each experiment by subtracting non-specific from total binding, subsequently converted in binding sites in fmol per TIR1 amount in mg, and plotted against radioligand concentration. Data

points were fitted and K_D values obtained, using non-linear regression for a one-site, hyperbolic binding curve. Number of replicates as shown in **Supplementary Figure 11**.



Supplementary Figure 13: AFB2:auxin:IAA1 and AFB2:auxin:IAA2 saturation binding data shown in Figure 2-8 and Table 2-1

Here, AFB2 occupancy is additionally shown on the right hand y-axis.

Supplementary Table 6: Statistical analysis of radioligand binding data

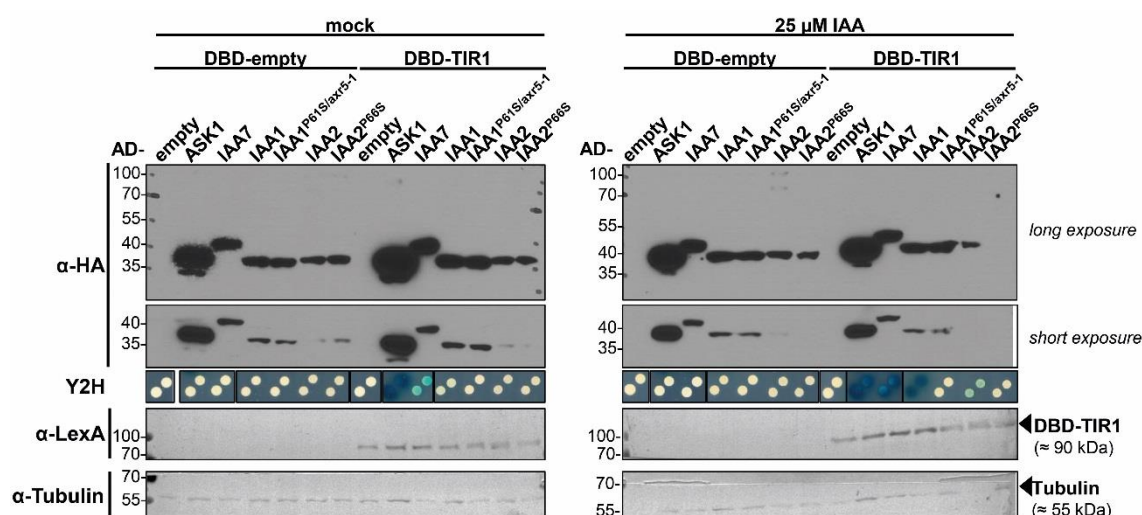
A. Statistical analysis for dissociation constants as shown in **Figure 2-7**. Mann-Whitney test (non-parametric test, two-tailed) was used to compare medians of K_D values of TIR1-IAA1 and TIR1-IAA2 co-receptors. **B.** Statistical analysis for dissociation constants determined from saturation binding experiments as shown in **Figure 2-7** and **Figure 2-8**. Non-parametric Kruskal-Wallis test followed by Dunn's multiple comparison comparing K_D of co-receptors TIR1/AFB2-IAA1/IAA2. K_D values do not differ significantly among these tested co-receptors. However, the small number of experiments for AFB2-containing receptors has to be taken into account.

A

K_D		Statistics	
TIR1-IAA1	TIR1-IAA2	Mann Whitney test	
55,57	65,11	<i>p</i> -value	0,4318
94,75	79,56	Exact or approximate <i>p</i> -value?	Exact
65,86	96,15	<i>p</i> -value summary	ns
28,17	54,83	Are medians signif. different? (<i>p</i> < 0.05)	No
32,58	50,5	One- or two-tailed <i>p</i> -value?	Two-tailed
66,48		Sum of ranks in column A,B	40 , 38
43,26		Mann-Whitney U	12

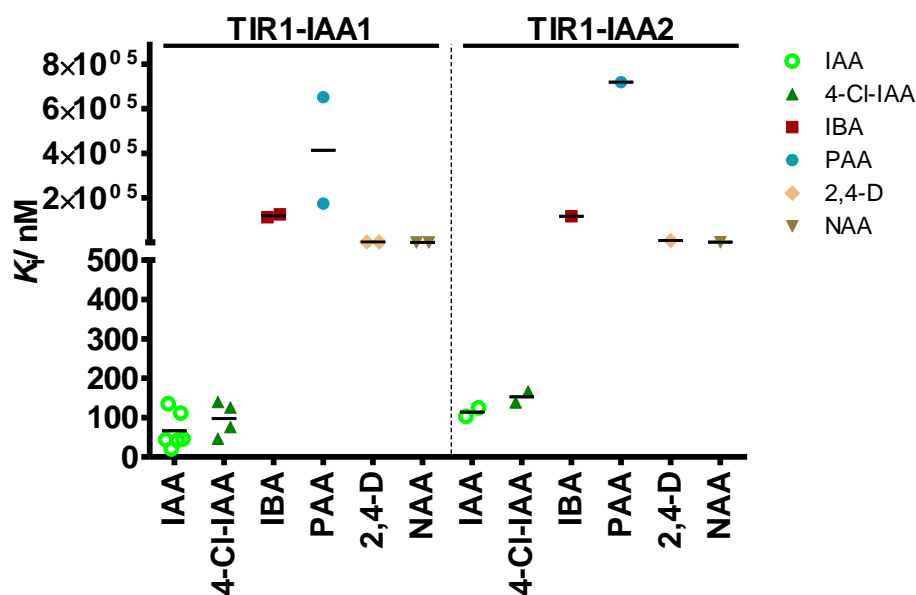
B

K_D				Kruskal-Wallis test			
TIR1-IAA1	TIR1-IAA2	AFB2-IAA1	AFB2-IAA2	P value			
55.57	65.11	55.91	52.52	0.2988			
94.75	79.56	107.6	43.03	Exact or approximate P value?	Gaussian Approximation		
65.86	96.15			P value summary	ns		
28.17	54.83			Do the medians vary signif. (P < 0.05)	No		
32.58	50.5			Number of groups	4		
66.48				Kruskal-Wallis statistic	3.674		
43.26				Dunn's Multiple Comparison Test			
				Difference in rank sum	Significant? P < 0,05?	Summary	
				TIR1-IAA1 vs TIR1-IAA2	-2.571	No	ns
				TIR1-IAA1 vs AFB2-IAA1	-5.071	No	ns
				TIR1-IAA1 vs AFB2-IAA2	2.929	No	ns
				TIR1-IAA2 vs AFB2-IAA1	-2.5	No	ns
				TIR1-IAA2 vs AFB2-IAA2	5.5	No	ns
				AFB2-IAA1 vs AFB2-IAA2	8	No	ns



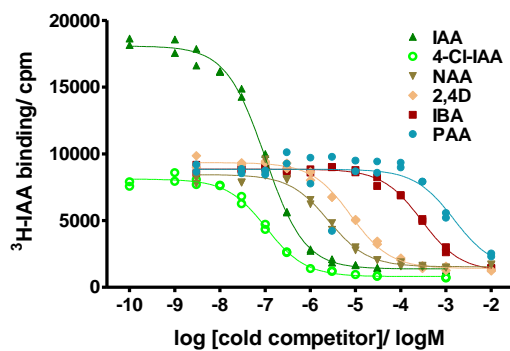
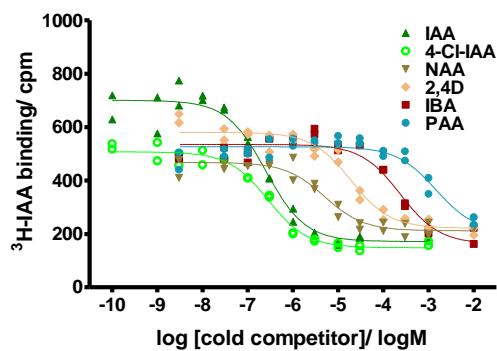
Supplementary Figure 14: Immunoblot analysis of AD-AUX/IAA protein expression from yeast strains used in Y2H assay (Figure 2-9)

Crude protein extracts were prepared from diploid yeasts expressing DBD-empty or DBD-TIR1 and AD-IAA1/IAA2 variants. Yeast liquid cultures were grown in selective induction medium in absence (mock) or presence of 25 μM IAA. Cell material for protein extraction was adjusted to similar amounts according to the culture OD_{600} . AD-fusion proteins carry an HA-tag between the AD and POI, and were therefore detected by immunoblotting with α -HA antibody (upper panel; long and short exposure of film). Below, Y2H reporter output as shown in **Figure 2-9** for the respective DBD-AD combination and auxin treatment. DBD-TIR1 was detected via α -LexA antibody. Extracts were probed with α -tubulin for loading control (lowest panel). Empty: empty vector control. AD-ASK1 and AD-IAA7 are usually highly expressed and shown as positive controls. ASK1 should be unaffected by TIR1- and auxin-mediated degradation.

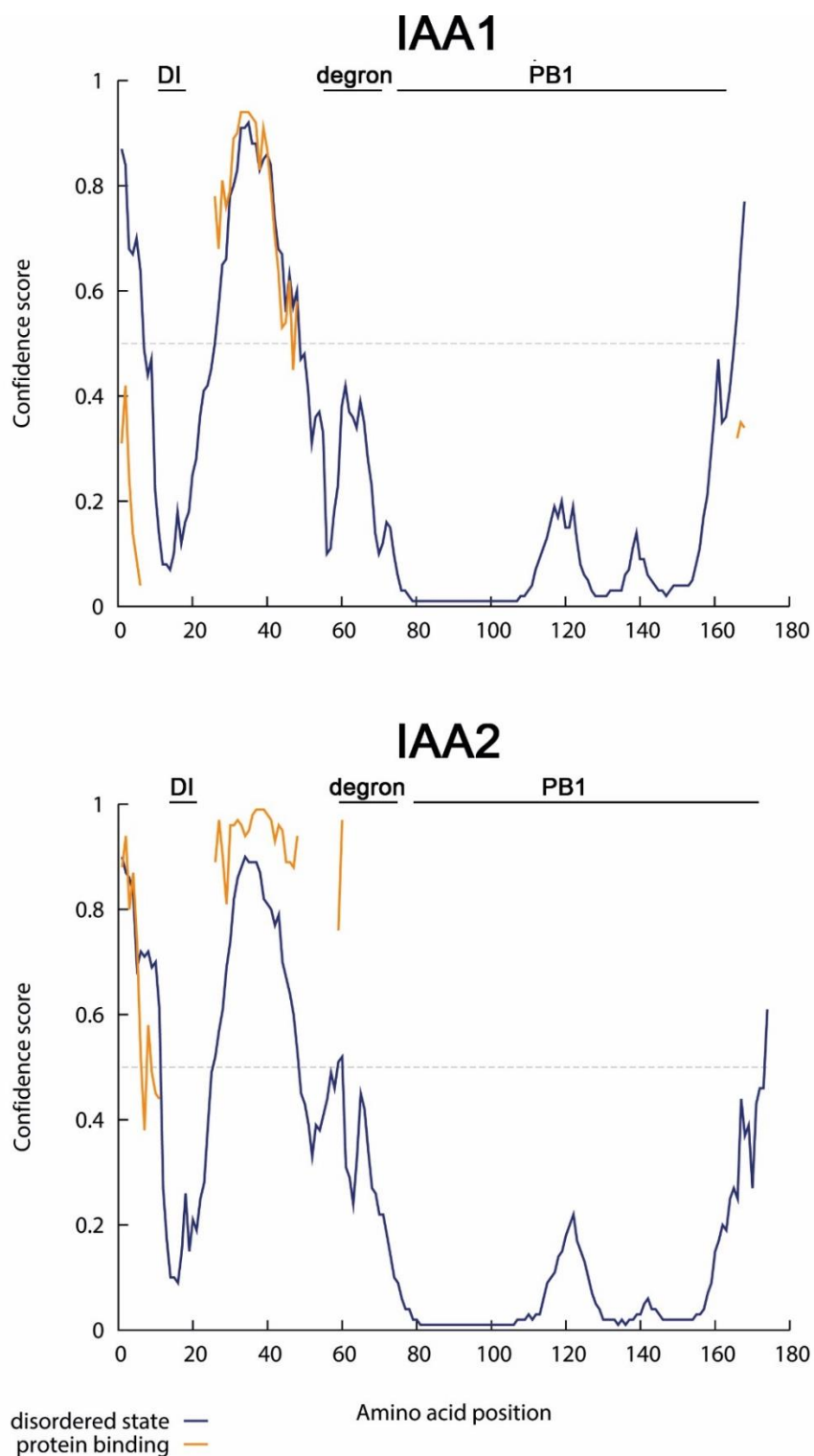


Supplementary Figure 15: Summary of competition binding data with different auxins for co-receptors TIR1-IAA1 and TIR1-IAA2

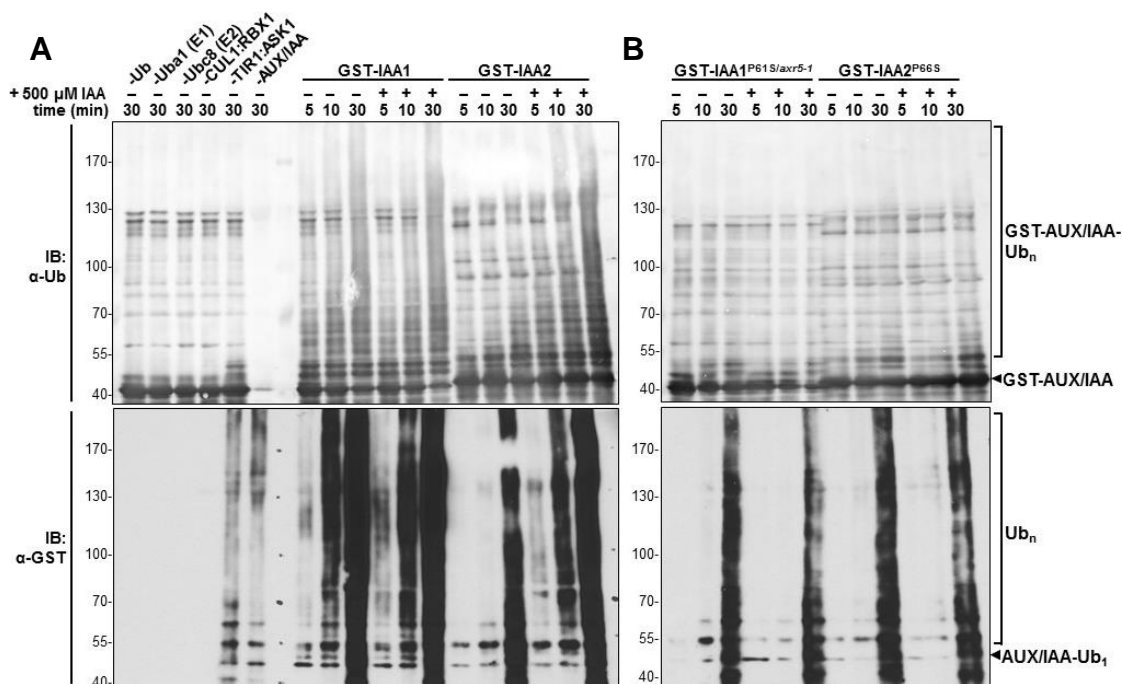
Scatter dot plot shows K_i values from independent competition binding experiments. Line denotes the mean K_i . K_i values have always been calculated via Cheng-Prusoff equation on the basis of the K_D values established in saturation binding experiments (**Figure 2-7 B**).

A TIR1-IAA1**B TIR1-IAA2****Supplementary Figure 16: Competition binding data for (A) TIR1-IAA1 and (B) TIR1-IAA2 co-receptors and different auxins**

Representation of absolute values of experiments shown in **Figure 2-10**. Radiolabel binding in cpm is plotted against the logmolar concentration of cold competitor. TIR1, GST-IAA1 or -IAA2 and 10 nM $^3\text{H-IAA}$ were combined into one master mix, which was used to set up samples with different competitors at different concentrations. There is a high total binding of $^3\text{H-IAA}$ in the presence of low concentrations of cold IAA especially in the TIR1-IAA1 co-receptor, but this effect was not observed consistently and therefore does not allow speculation about a positive effect of IAA on its own binding.

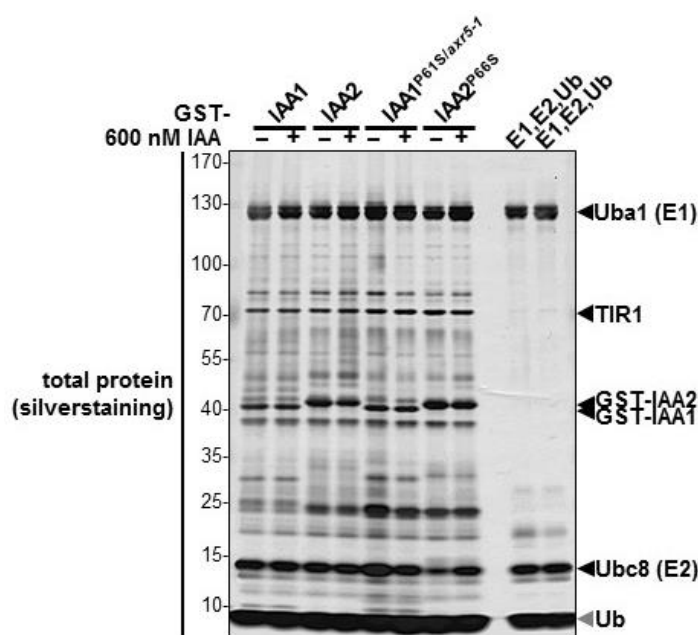
**Supplementary Figure 17: Disorder prediction for IAA1 and IAA2**

IAA1 and IAA2 protein sequences were analyzed via DISOPRED2 prediction server <http://bioinf.cs.ucl.ac.uk/index.php?id=806> (Ward *et al.*, 2004) with default options. Blue line shows disorder confidence levels against the sequence positions. The grey dashed horizontal line marks the threshold above which amino acids are regarded as disordered. For disordered residues, the orange line shows the confidence of disordered residues being involved in protein-protein interactions. Horizontal bars denote the approximate position of conserved domains domain I (DI), primary degron/domain II (degron), PB1 domain (PB1).



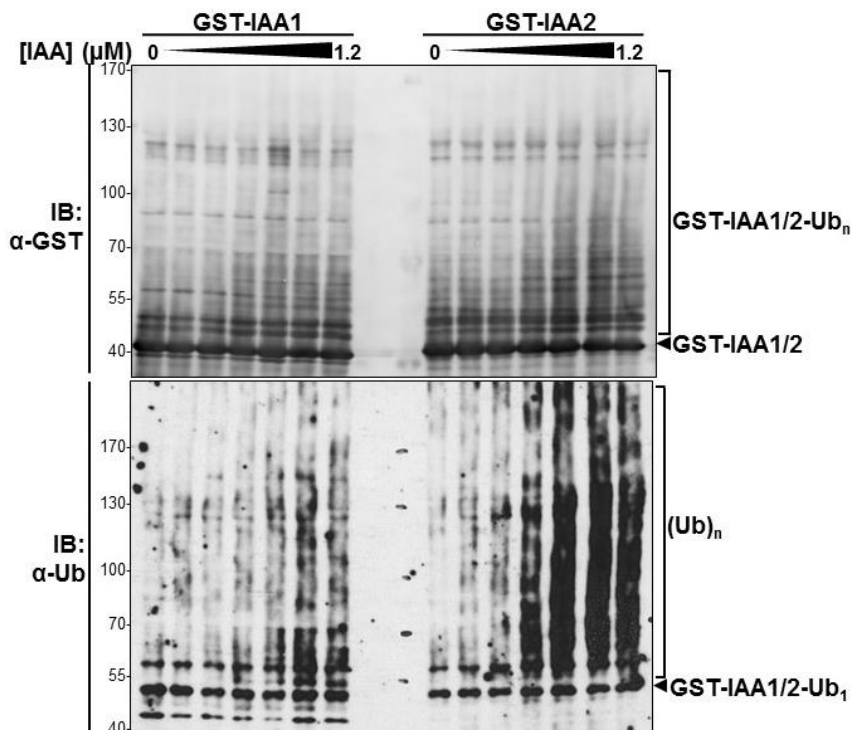
Supplementary Figure 18: Specificity of ubiquitination of IAA1 and IAA2 by Uba1, Ubc8, SCF^{TIR1} and auxin *in vitro*

Samples in A and B were loaded on 5-15% gradient SDS-PAGE and probed with α -GST antibody for detection of the GST-tagged AUX/IAA targets (upper immunoblot), or probed with α -Ub antibody for detection of Ub and thus ubiquitinated protein species (bottom immunoblot). Note that the α -GST immunoblot was accidentally shifted and therefore does not display even and distinct lanes (right upper panel). Unmodified targets GST-IAA1 and -IAA2 or monoubiquitinated species AUX/IAA-Ub₁ are denoted with a black triangle (\blacktriangle). **A.** Ubiquitination reactions were performed with GST-IAA1 as a target leaving out one component at a time as indicated (six lanes on the left hand side). Note that unspecific ubiquitination of proteins other than targets (bottom panel; "minus AUX/IAA" lane), as well as TIR1- and auxin-independent target ubiquitination ("minus TIR1:ASK1" lane, "minus auxin" lanes), can be detected. Reactions with GST-IAA1 and GST-IAA2 as targets in the presence or absence of 500 μ M IAA were used as positive controls and assessed over several time points (5, 10, 30 min; twelve lanes on the right hand side). **B.** Also, reactions with mutant variants GST-IAA1^{P61S/axr5-1} and GST-IAA2^{P66S} as targets were performed in the presence or absence of 500 μ M IAA over several time points (5, 10, 30 min). Even when using mutant versions of target protein, which are thought to not be bound by SCF^{TIR1}, ubiquitin signal is detected (right lower panel). However, higher molecular weight ubiquitinated target-specific species are only present in the positive control.



Supplementary Figure 19: Loading control for IVU shown in Figure 2-12

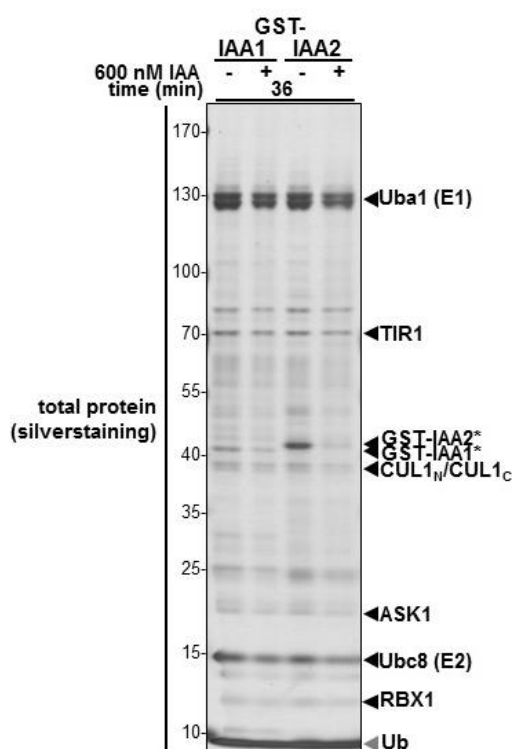
Ubiquitination reactions were performed with wild-type IAA1 and IAA2 and their corresponding degron mutants IAA1^{P61S/axr5-1} and IAA2^{P66S} as targets. Loading control samples were taken at the end of the reaction (20 min). Reactions were run in the absence or presence of 600 nM IAA. Samples were loaded on 5-15% gradient SDS-PAGE silver-stained for detection of total protein. Proteins are denoted with a black triangle. See **Table 6-11** for IVU components and their respective molecular weights.



Supplementary Figure 20: Auxin dose response of *in vitro* ubiquitination reaction with targets IAA1 and IAA2

Independent experiment to compare with **Figure 2-13**. Ubiquitination reactions were performed with wild-type IAA1 and IAA2 as targets and seven different auxin concentrations ([IAA]= 0; 0.006; 0.018; 0.1; 0.3; 0.6; 1.2 μ M). Samples were taken after the reaction had proceeded for 20 min. Samples were loaded on 5-15% gradient SDS-PAGE and probed with α -GST antibody (upper panel) for detection of the GST-tagged AUX/IAA targets, or with α -

Ubiquitin (α -Ub; bottom panel) antibody for detection of ubiquitinated protein species (denoted with bracket “(Ub)_n”) which might include ubiquitinated proteins other than AUX/IAA (see **Figure 2-11**). Unmodified targets GST-IAA1 and -IAA2 have a molecular weight of 46.8 kDa and 47.7 kDa, respectively, and are denoted with a black triangle (“GST-IAA1/IAA2”). GST-protein species >40 kDa are therefore indicative of ubiquitinated AUX/IAAs and denoted with bracket (“GST-IAA1/IAA2-Ub_n”).



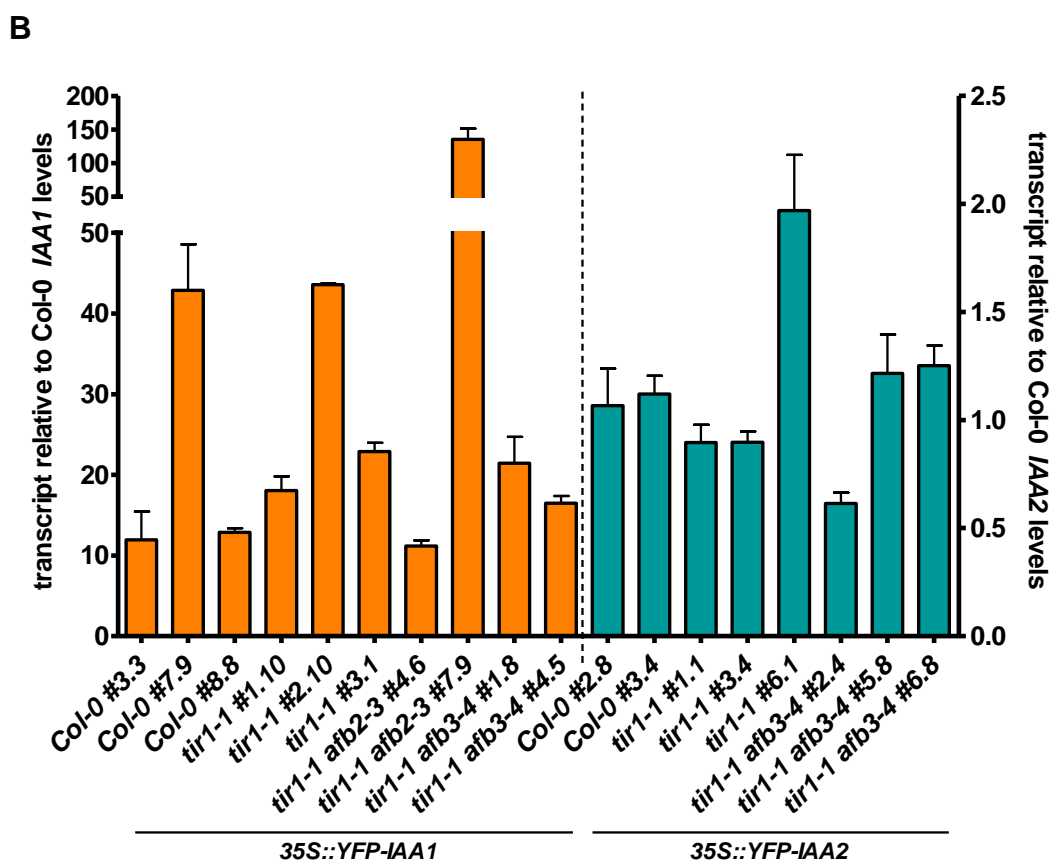
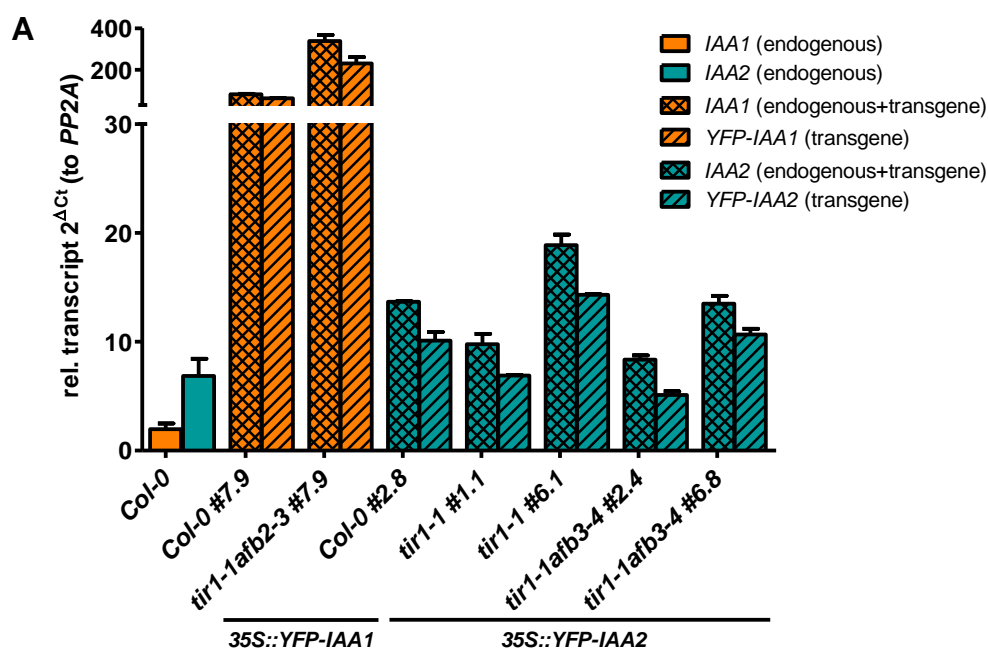
Supplementary Figure 21: Loading control of IVU time course experiment (Figure 2-14)

Loading control samples were taken at the end of the reaction time course (36 min). Reactions were run in the absence or presence of 600 nM IAA. Samples were loaded on 5-15% gradient SDS-PAGE silver-stained for detection of total protein. Proteins are denoted with a black triangle. See **Table 6-11** for IVU components and their respective molecular weights. The reduction of the amount of unmodified GST-IAA1/IAA2 protein through Ub-conjugation is evident in SDS-PAGE especially when comparing the reactions with and without auxin.

Supplementary Table 7: Selection of transgenic T3 lines

We generated Arabidopsis plants overexpressing YFP alone (\emptyset ; empty vector control), or N-terminal YFP fusions of *IAA1*, *IAA2*, *IAA7*, or *IAA12* under control of a 35S promoter. 35S::YFP-*IAA7* and -*IAA12* transformants were generated for reference purposes, since *IAA7* and *IAA12* are well characterized. Constructs for expression of transgenes with BASTA resistance marker were transformed into wild-type (Col-0) or mutant backgrounds (*tir1-1*, *afb1-3*, *afb2-3*, *afb3-4*, *tir1-1 afb2-3*, *tir1-1 afb3-4*). Seeds from transformed plants were first selected for about ten BASTA resistant T1 individuals, and individual transformants were numbered (#1, #2, #3...). Next, T2 seeds were tested for approximate 3:1 segregation on selection medium to ensure single insertions, and candidate lines were checked for YFP expression in seedlings via fluorescence microscopy (data not shown). T3 seeds derived from individual candidate T2 lines were numbered with a second numeral (e.g. #4.1, 4.2, 4.3...) and tested for homozygosity on selection medium. Ultimately, several homozygous T3 lines were established for part of the material. T3 lines in grey were excluded from the following analyses presented in this thesis (partly due to bad germination or ambiguous segregation).

	35S::YFP- \emptyset	<i>IAA1</i>	<i>IAA2</i>	<i>IAA7</i>	<i>IAA12</i>
T3 selection					
<i>Col-0</i>	- #4.9, #4.5, #4.6, #4.10 - #5.6, #5.7	- #3.5, #3.3 - #7.9 - #8.8, #8.2, #8.6	- #1.1, #1.2, #1.5 - #2.8 - #3.4, #3.9	—	—
<i>tir1-1</i>	- #3.1 - #6.10	- #1.10, #1.1, #1.8, #1.9 - #2.10 - #3.1, #3.10	- #1.1, #1.5 - #3.4, #3.2 - #6.1	—	—
<i>afb2-3</i>	- #1.3	—	- #1.2	—	—
<i>tir1-1 afb2-3</i>	- #4.7, #4.1 - #6.10	- #4.6 - #7.9 - #10.9	- #4.6, #4.2, #4.8, #4.9 - #5.9, #5.2 - #8.2, #8.4, #8.9	—	—
<i>tir1-1 afb3-4</i>	- #2.9, #2.3, #2.4, #2.5, #2.7 - #4.2 - #6.2	- #1.8, #1.2, #1.3, #1.5, #1.9 - #4.5, #4.3 - #10.9	- #2.4, #2.3, #2.6 - #5.8 - #6.8	—	—
T2 selection (positive for 3:1 segregation and YFP expression)					
<i>Col-0</i>	#4, #5	#3, #6, #7, #8, #10	#1, #2, #3, #10	#1, #8	#2, #4, #9
<i>tir1-1</i>	#1, #2, #3, #6	#1, #2, #3, #6, #8	#1, #3, #6, #7, #10	#1, #2, #5, #8	#9, #10
<i>afb1-3</i>	#3, #5	#5, #7, #9	#1, #2, #6, #8, #9	#3, #10	#6, #7, #8
<i>afb2-3</i>	#1	#1, #2, #7, #8	#1, #2	#1, #3, #5	#4, #5, #6, #8
<i>afb3-4</i>	#2, #3, #4	#7, #8	#1, #2, #3, #5	#5, #9	#2, #3, #5, #8
<i>tir1-1 afb2-3</i>	#1, #2, #4, #5, #6	#4, #7, #10	#4, #5, #6, #8	#2, #3, #5	#3, #4, #5, #6
<i>tir1-1 afb3-4</i>	#2, #3, #4, #6	#1, #4, #10	#2, #5, #6	#1, #8	#7, #8, #11
T1 selection					
<i>Col-0</i>	#1-12	#1-10	#1-10	#1-10	#1-10
<i>tir1-1</i>	#1-12	#1-10	#1-10	#1-10	#1-10
<i>afb1-3</i>	#1-6	#1-10	#1-10	#1-10	#1-10
<i>afb2-3</i>	#1-3	#1-10	#1-8	#1-10	#1-8
<i>afb3-4</i>	#1-8	#1-10	#1-8	#1-10	#1-10
<i>tir1-1 afb2-3</i>	#1-12	#1-10	#1-8	#1-5	#1-7
<i>tir1-1 afb3-4</i>	#1-8	#1-10	#1-11	#1-10	#1-11



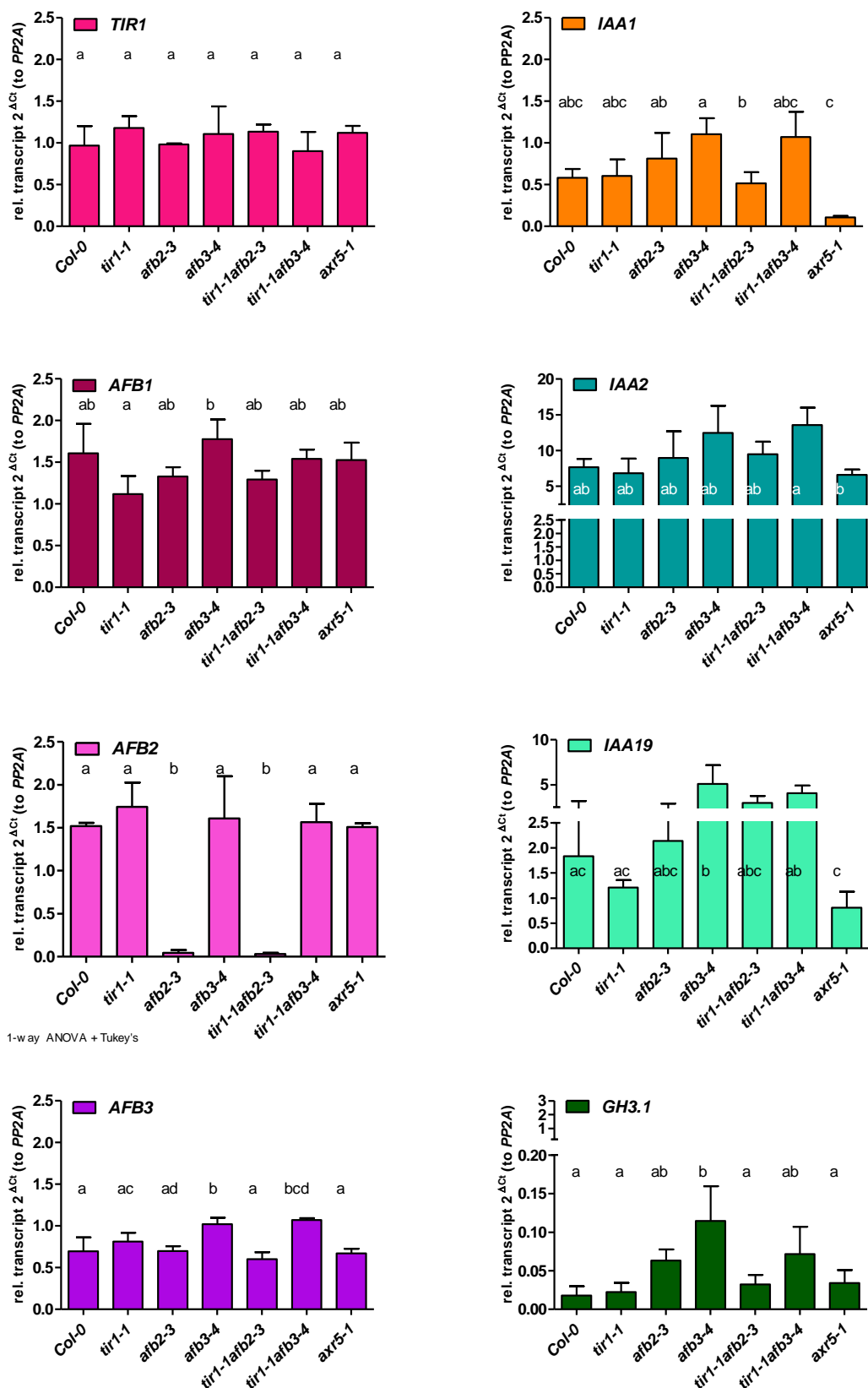
Supplementary Figure 22: Comparison of transcript levels of transgenic and endogenous IAA1 and IAA2 in overexpressor lines

Homozygous T3 lines overexpressing *YFP-IAA1* (orange) and *YFP-IAA2* (teal) in various genetic backgrounds. RNA from 5-day old seedlings was extracted, reverse transcribed and analyzed for the transgene expression level through RT-qPCR. **A.** Using *IAA1* or *IAA2* gene-specific primer pairs, the total transcript level including transgenic and endogenous *IAA1* or *IAA2* transcript, respectively, was determined for a selection of overexpressor lines. By combining primer for *YFP* and *IAA1* or *IAA2*, the levels of transgene transcript alone was determined. For comparison, the endogenous *IAA1* and *IAA2* transcript levels in Col-0 wild-type are shown, and have been used for relative representation of transcript levels in B. For all selected lines, three biological replicates, except for lines 35S::YFP-IAA2(*tir1-1*)#6.1 and 35S::YFP-IAA2(*tir1-1afb3-4*)#2.4 two biological replicates were analyzed. **B.** Rough

estimation of *IAA1* and *IAA2* transcript levels relative to endogenous *IAA1* or *IAA2* levels in Col-0 wild-type. Relative transcript levels of *YFP-IAA1* and *YFP-IAA2* (relative to *PP2A*) displayed in **Figure 2-16** were divided by the median expression of endogenous *IAA1* and *IAA2* in Col-0 wild-type (relative to *PP2A*), respectively (see A). This is represented as transcript relative to Col-0 *IAA1* (left axis) or *IAA2* (right axis) levels. Error bars denote standard error. All values were corrected for amplification efficiency (see **Section 6.6.9.5.1**).

Supplementary Table 8: Grouping of transgenic lines into high, medium and low overexpressors according to the frequency distribution analysis in Figure 2-17

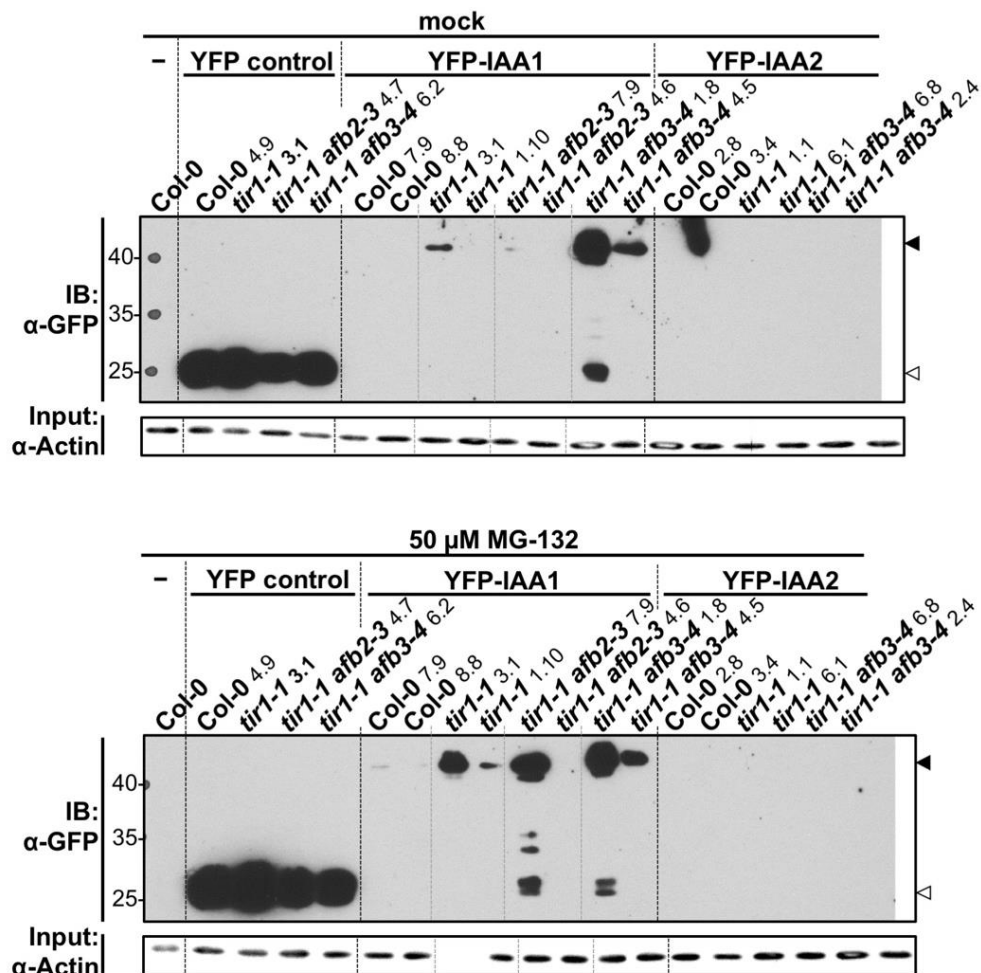
	35S::YFP-IAA1	35S::YFP-IAA2
Upper quartile High overexpressor	<i>tir1-1</i> #2.10 <i>tir1-1 afb2-3</i> #7.9	<i>tir1-1 afb3-4</i> #6.8 <i>tir1-1</i> #6.1
Interquartile range Medium overexpressor	<i>Col-0</i> #7.9 <i>Col-0</i> #8.8 <i>tir1-1</i> #1.10 <i>tir1-1</i> #3.1 <i>tir1-1 afb3-4</i> #1.8 <i>tir1-1 afb3-4</i> #4.5	<i>Col-0</i> #2.8 <i>Col-0</i> #3.4 <i>tir1-1</i> #3.4 <i>tir1-1 afb3-4</i> #5.8 <i>tir1-1 afb3-4</i> #6.8
Lower quartile Low overexpressor	<i>Col-0</i> #3.3 <i>tir1-1 afb2-3</i> #4.6	<i>tir1-1</i> #1.1 <i>tir1-1 afb3-4</i> #2.4



Supplementary Figure 23: Endogenous transcript levels of *TIR1*, *AFB1*, *AFB2*, *AFB3* as well as *IAA1*, *IAA2*, *IAA19* and *GH3.1* genes in wild-type Col-0, *tir1/afb* and *axr5-1* mutant background

Seedlings were grown on 0.5x MS plates for 7 days at 22°C under long day conditions (16 hours day/8 hours night) with 100-130 $\mu\text{mol}/(\text{m}^2\text{s})$ light fluency, and transcript levels of indicated genes determined via RT-qPCR. Transcript

levels are shown as relative to the reference gene *PP2A*. Transcript levels of *TIR1*, *AFB1*, *AFB2* and *AFB3* are consistent with characterization of mutant lines *tir1-1*, *afb2-3*, *afb3-4*, *tir1-1afb2-3*, and *tir1-1afb3-4* presented in Dharmasiri *et al.* (2005b) and Parry *et al.* (2009). Means of three biological samples are shown. Error bars denote standard deviation. 1-way ANOVA with Tukey's multiple comparisons were performed for statistical testing. Different letters denote significant ($p \leq 0.05$) differences.



Supplementary Figure 24: Overexpressed YFP-IAA1 or YFP-IAA2 protein can be recovered from *35S::YFP-IAA1* or *35S::YFP-IAA2* transgenic lines and is stabilized upon MG-132 treatment

7-day old seedlings of T4 transgenic lines were treated with 50 μ M MG-132 (right) or mock (left) for 16 hours, protein extracts were prepared and YFP-IAA1 and YFP-IAA2 fusion protein was enriched by immunoprecipitation through α -GFP-beads (GFPtrap). Equal amounts of sample were loaded and probed with α -GFP antibody to detect YFP fusion proteins. Filled triangles denote YFP-IAA1 (53.7 kDa), open triangles denote YFP (26.6 kDa). For loading control, input protein extract was probed with α -Actin antibody (input).

Supplementary Table 9: Pearson correlation analysis for *YFP-IAA1* transgene expression level and selected phenotypic effects

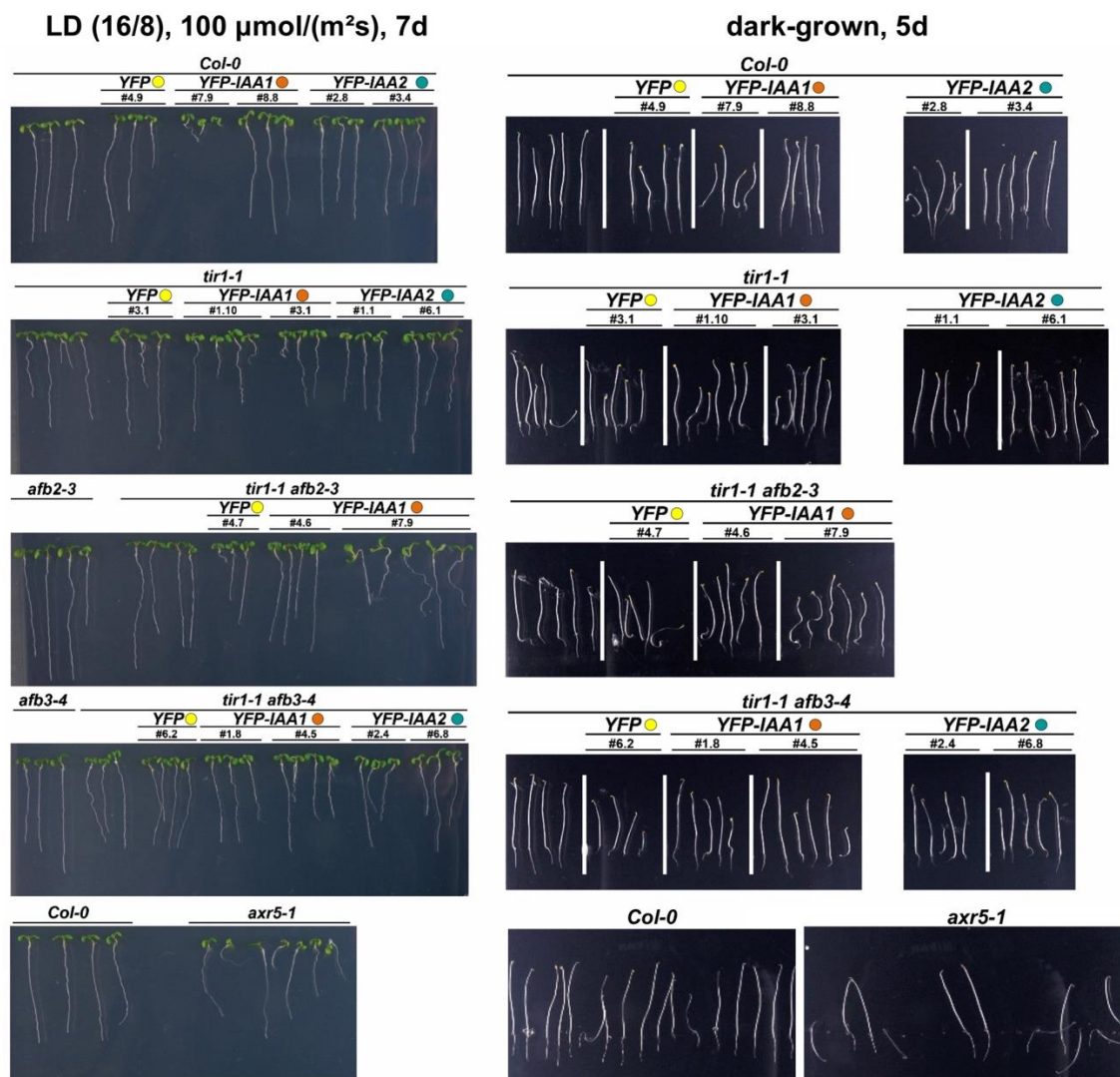
To test for correlation between transgene overexpression and phenotype, the correlation coefficient for *YFP-IAA1* overexpression (OX) transcript level dataset (see **Figure 2-16**, determined in T3 seedlings) and a dataset from testing for auxin-related phenotypes (experiment 1 to 17) was determined. Correlation coefficients are shown with green and red shades indicating correlation or no correlation, respectively. Note, that the absolute value for correlation coefficient rises above 0.5 for experiment 3 to 5, indicating a correlation between overexpression levels of the *YFP-IAA1* transgene and the auxin-dependent hypocotyl elongation in dark-grown seedlings. n signifies the number of lines analyzed for correlation. The lower part of the table shows, which lines were included in the analyzed datasets.

Experiment	<i>YFP-IAA1</i> OX transcript levels (T3) vs.	Pearson correlation coefficient	n
1	root elongation at low light (8-day seedlings) (Supplementary Figure 29)	-0.32	7
2	hypocotyl elongation at low light (8-day seedlings) (Supplementary Figure 30)	-0.36	7
3	hypocotyl elongation in the dark I (7-day seedlings) (Supplementary Figure 31)	-0.71	5
4	hypocotyl elongation in the dark II (5-day seedlings) (Supplementary Figure 32)	-0.79	9
5	hypocotyl elongation in the dark III (5-day seedlings) (Supplementary Figure 33)	-0.65	9
6	leaf areas (2-week rosettes)	-0.06	5
7	leaf areas (3.5-week rosettes, grown at high light)	-0.11	9
8	leaf areas (3.5-week rosettes, grown at low light)	0.15	9
9	root response to elevated temperature	-0.18	9
10	hypocotyl response to elevated temperature I	-0.10	9
11	hypocotyl response to elevated temperature II	-0.15	9
12	inhibition of root elongation on 25 nM IAA I		
13	inhibition of root elongation on 50 nM IAA I	-0.07	5
14	inhibition of root elongation on 100 nM IAA I	-0.08	5
12-14	(Supplementary Figure 27)		
15	inhibition of root elongation on 25 nM IAA II	-0.11	9
16	inhibition of root elongation on 50 nM IAA II	-0.20	9
17	inhibition of root elongation on 100 nM IAA II	0.07	9
15-17	(Supplementary Figure 28)		
Experiment	Set of 35S:: <i>YFP-IAA1</i> lines (T4) for correlation analysis		
1,2	<i>Col-0</i> <i>Col-0</i> #3.3 <i>Col-0</i> #7.9 <i>Col-0</i> #8.8 <i>tir1-1 afb2-3</i> #7.9 <i>tir1-1 afb3-4</i> #1.8 <i>tir1-1 afb3-4</i> #4.5		
3	<i>Col-0</i> <i>Col-0</i> #7.9 <i>tir1-1</i> #3.1 <i>tir1-1 afb2-3</i> #7.9 <i>tir1-1 afb3-4</i> #4.5		
6,13,14	<i>Col-0</i> <i>Col-0</i> #7.9 <i>tir1-1</i> #3.1 <i>tir1-1 afb2-3</i> #7.9 <i>tir1-1 afb3-4</i> #4.5		
4,5,7,8,9,10,11,15,16,17	<i>Col-0</i> <i>Col-0</i> #7.9 <i>Col-0</i> #8.8 <i>tir1-1</i> #1.10 <i>tir1-1</i> #3.1 <i>tir1-1 afb2-3</i> #4.6 <i>tir1-1 afb2-3</i> #7.9		

*tir1-1 afb3-4 #1.8**tir1-1 afb3-4 #4.5***Supplementary Table 10: Pearson correlation analysis for *YFP-IAA2* transgene expression level and selected phenotypic effects**

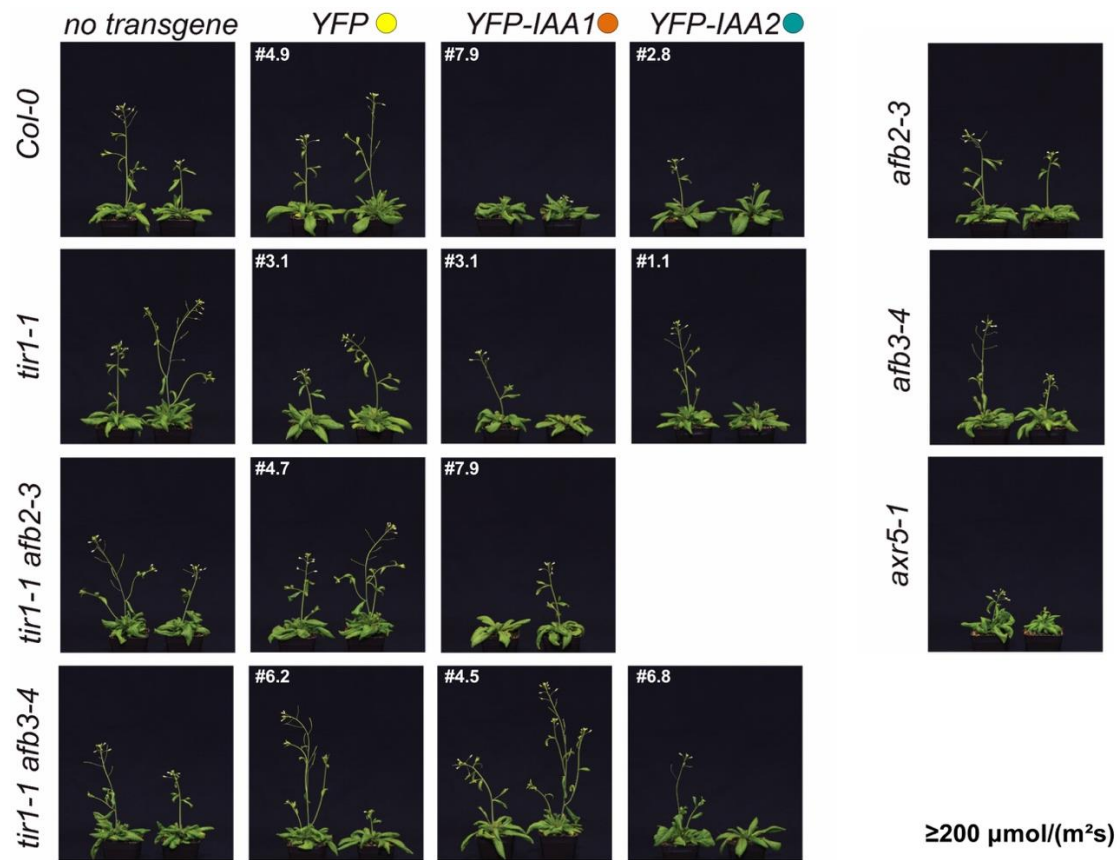
To test for correlation between transgene overexpression and phenotype, the correlation coefficient for *YFP-IAA1* overexpression (OX) transcript level dataset (see **Figure 2-16**, determined in T3 seedlings) and a dataset from testing for auxin-related phenotypes (experiment 1 to 17) was determined. Correlation coefficients are shown with green and red shades indicating correlation or no correlation, respectively. n signifies the number of lines analyzed for correlation. The lower part of the table shows, which lines were included in the analyzed datasets. Note that the experiments that show correlation with expression levels here, often have only small n underlying the correlation analysis.

Experiment	<i>YFP-IAA2</i> OX transcript levels (T3) vs.	Pearson correlation coefficient	n
1	root elongation at low light (8-day seedlings) (Supplementary Figure 29)	0.32	8
2	hypocotyl elongation at low light (8-day seedlings) (Supplementary Figure 30)	0.47	8
3	hypocotyl elongation in the dark I (7-day seedlings) (Supplementary Figure 31)	-0.96	4
4	hypocotyl elongation in the dark II (5-day seedlings) (Supplementary Figure 32)	-0.22	7
5	hypocotyl elongation in the dark III (5-day seedlings) (Supplementary Figure 33)	-0.37	7
6	leaf areas (2-week old rosettes)	-0.80	4
7	leaf areas (3.5-week rosettes, grown at high light)	0.23	7
8	leaf areas (3.5-week rosettes, grown at low light)	0.33	7
9	root response to elevated temperature	-0.42	7
10	hypocotyl response to elevated temperature I	-0.12	7
11	hypocotyl response to elevated temperature II	0.07	7
12	inhibition of root elongation on 25 nM IAA I	0.78	4
13	inhibition of root elongation on 50 nM IAA I	-0.40	4
14	inhibition of root elongation on 100 nM IAA I	-0.98	4
12-14	(Supplementary Figure 27)		
15	inhibition of root elongation on 25 nM IAA II	-0.18	7
16	inhibition of root elongation on 50 nM IAA II	-0.05	7
17	inhibition of root elongation on 100 nM IAA II	-0.45	7
15-17	(Supplementary Figure 28)		
Experiment	Set of 35S:: <i>YFP-IAA2</i> lines (T4) for correlation analysis		
1,2	<i>Col-0</i> <i>Col-0 #2.8</i> <i>Col-0 #3.4</i> <i>tir1-1 #1.1</i> <i>tir1-1 #6.1</i> <i>tir1-1 afb3-4 #2.4</i> <i>tir1-1 afb3-4 #5.8</i> <i>tir1-1 afb3-4 #6.8</i>		
6,3,12,13,14	<i>Col-0</i> <i>Col-0 #2.8</i> <i>tir1-1 #1.1</i> <i>tir1-1 afb3-4 #6.8</i>		
4,5,7,8,9,10,11,15,16,17	<i>Col-0</i> <i>Col-0 #2.8</i> <i>Col-0 #3.4</i> <i>tir1-1 #1.1</i> <i>tir1-1 #6.1</i> <i>tir1-1 afb3-4 #2.4</i> <i>tir1-1 afb3-4 #6.8</i>		



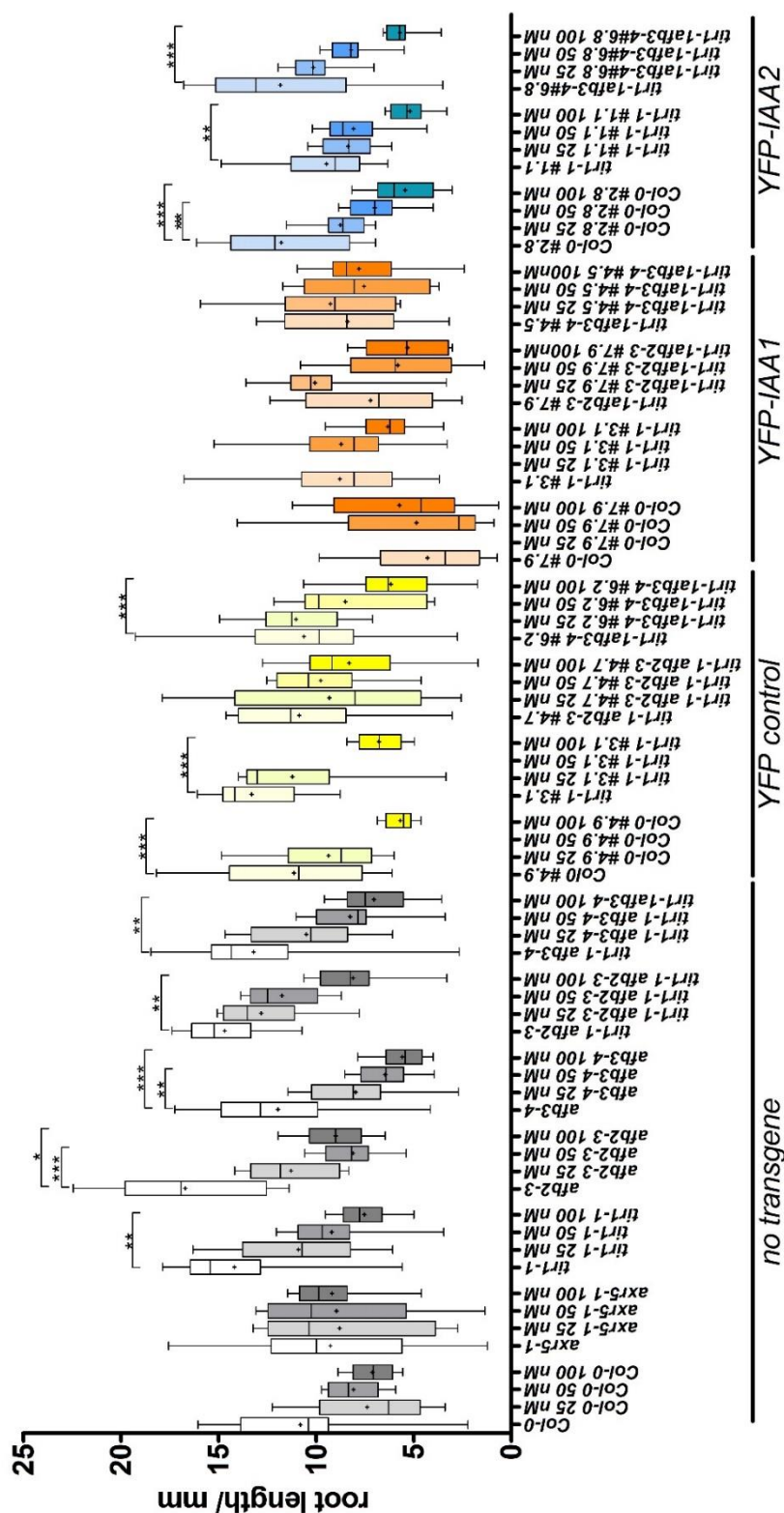
Supplementary Figure 25: Phenotypes of transgenic seedlings of 35S::YFP, 35S::YFP-IAA1 and 35S::YFP-IAA2 overexpressor lines

Seedlings were grown under conditions as indicated for 7 or 5 days as indicated at 22°C. Untransformed wild-type Col-0, *axr5-1*, and *tir1/afb* mutant seedlings are shown for reference. LD (16/8): Long-day (16 hours light/8 hours dark). Number indicates identity of the independent lines (compare **Table 2-2**).



Supplementary Figure 26: Phenotypes of 4-week old plants of 35S::YFP, 35S::YFP-IAA1 and 35S::YFP-IAA2 overexpressor lines

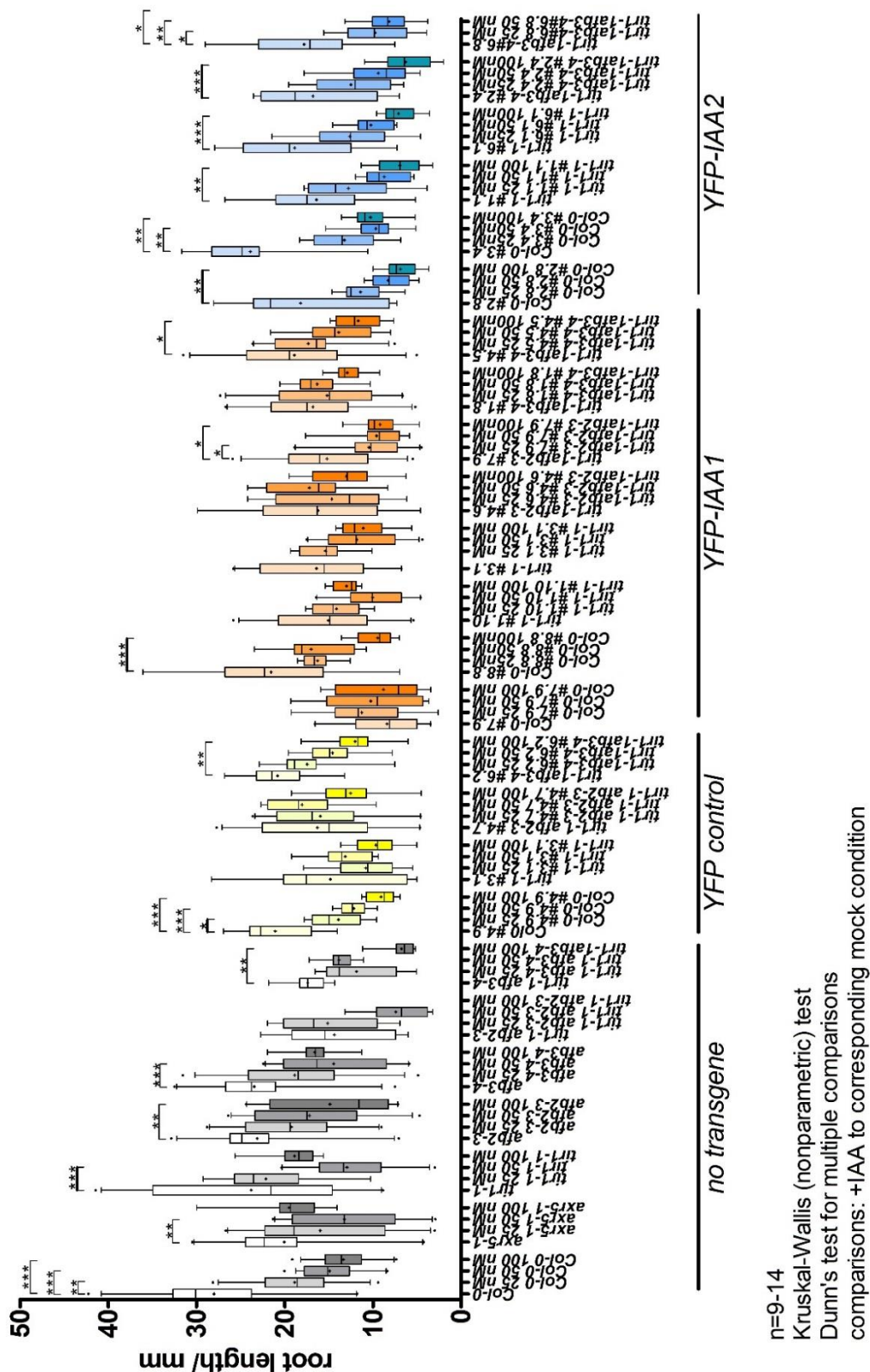
Plants were grown on 0.5x MS plates at $90 \mu\text{mol}/\text{m}^2\text{s}$ light fluency under long day conditions (16/8) at 22°C . After 8 days, plants were transferred to soil and grown at $\geq 200 \mu\text{mol}/\text{m}^2\text{s}$ light fluency under long day conditions (16/8) at 20°C for 3 more weeks. Untransformed wild-type Col-0, *axr5-1*, and *tir1/afb* mutant seedlings are shown for reference. Number indicates identity of the independent lines (compare **Table 2-2**).



n=9-14
 Kruskal-Wallis (nonparametric) test
 Dunn's test for multiple comparisons
 comparisons: +IAA to corresponding mock condition

Supplementary Figure 27: Root elongation assay with *35S::YFP*, *35S::YFP-IAA1* and *35S::YFP-IAA2* overexpressor lines

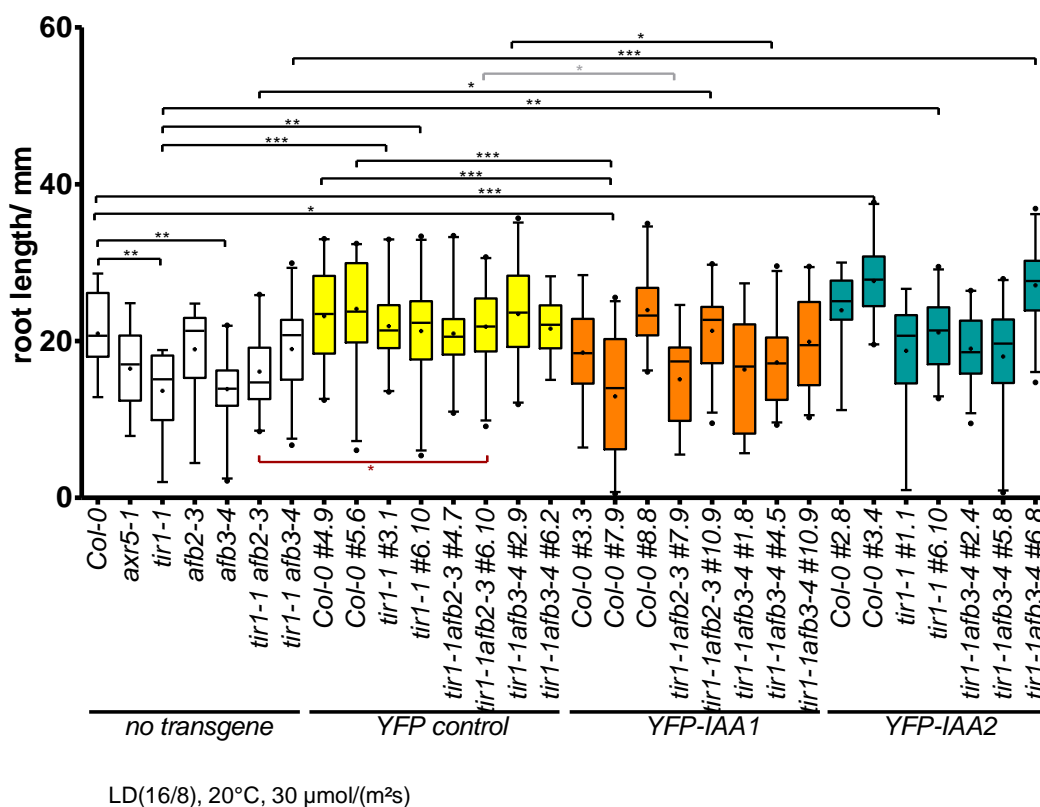
Seedlings were grown on 0.5x MS plates at long day conditions (16 hours day/ 8 hours night), 22° C, 90 μmol/(m²s) for 4 days. Seedlings were then transferred to plates containing indicated concentrations of auxin and further cultivated. Plates were scanned 3 days post transfer and root lengths measured. Box-plot depicts root length in mm of n=9-14 seedlings. Box extends from the 25th to 75th percentile, whiskers from the 5th to 95th percentile. Horizontal line denotes median. '+' denotes the mean. For statistical testing, Kruskal-Wallis (nonparametric) test was applied, followed by Dunn's Multiple comparison between IAA and corresponding mock treatments (* $p \leq 0.05$; ** $p \leq 0.01$; *** $p \leq 0.001$).



Supplementary Figure 28: Root elongation assay with 35S::YFP, 35S::YFP-IAA1 and 35S::YFP-IAA2 overexpressor lines

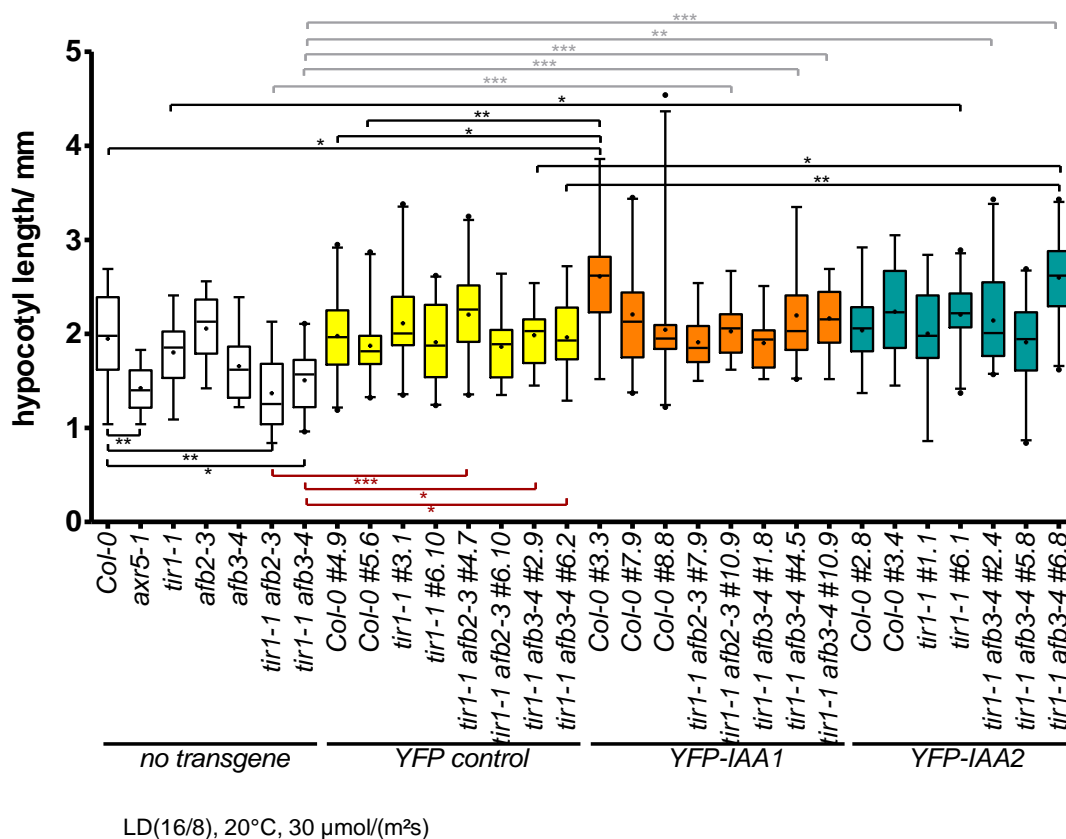
Seedlings were grown on 0.5x MS plates at long day conditions (16 hours day/ 8 hours night), 22° C, 90 μmol/(m²s) for 4 days. Seedlings were then transferred to plates containing indicated concentrations of auxin and further cultivated. Plates were scanned 3 days post transfer and root lengths measured. Box-plot depicts root length in mm of n=9-14 seedlings. Box extends from the 25th to 75th percentile, whiskers from the 5th to 95th percentile. Horizontal line denotes median. '+' denotes the mean. For statistical testing, Kruskal-Wallis (nonparametric) test

was applied, followed by Dunn's Multiple comparison between IAA and corresponding mock treatments (* $p \leq 0.05$; ** $p \leq 0.01$; *** $p \leq 0.001$).



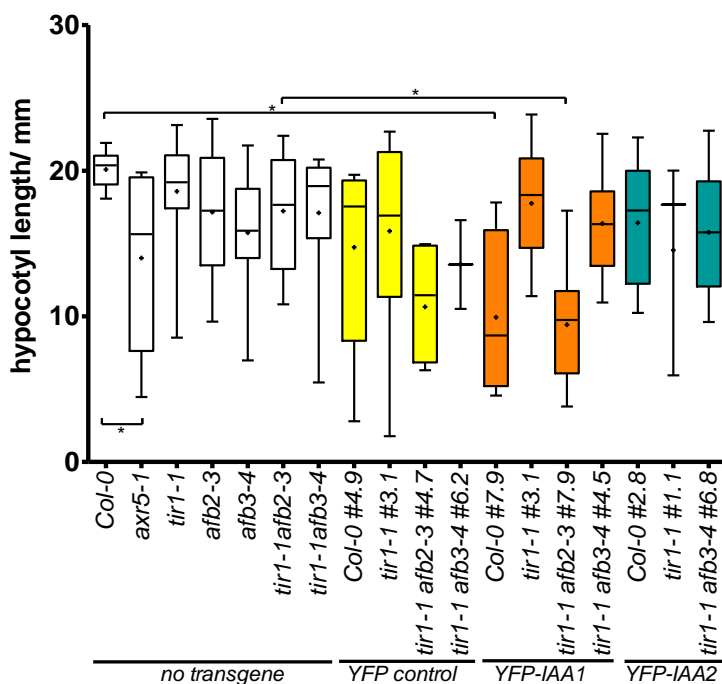
Supplementary Figure 29: Elongation of roots at low light in 8-day old seedlings of 35S::YFP, 35S::YFP-IAA1 and 35S::YFP-IAA2 overexpressor lines

Seedlings were grown on 0.5x MS plates at long day conditions (16 hours day/8 hours night), 20°C, and 30 $\mu\text{mol}/(\text{m}^2\text{s})$ for 8 days. Box-plot depicts root length in mm of $n=14-27$ seedlings. Box extends from the 25th to 75th percentile, whiskers from the 5th to 95th percentile. Horizontal line denotes median. Plus ('+') denotes the mean. For statistical testing, Kruskal-Wallis (nonparametric) test was applied, followed by Dunn's Multiple comparison between lines carrying no or the same transgene (* $p \leq 0.05$; ** $p \leq 0.01$; *** $p \leq 0.001$).



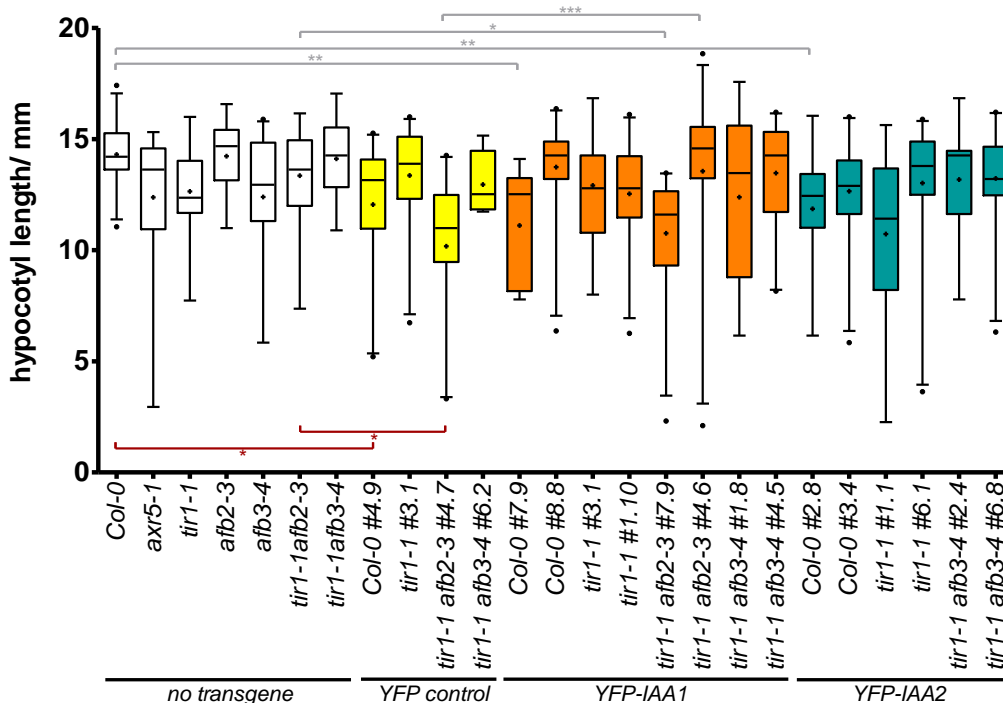
Supplementary Figure 30: Elongation of hypocotyls at low light in 8-day old seedlings of *35S::YFP*, *35S::YFP-IAA1* and *35S::YFP-IAA2* overexpressor lines

Seedlings were grown on 0.5x MS plates at long day conditions (16 hours day/8 hours night), 20°C, and 30 $\mu\text{mol}/(\text{m}^2\text{s})$ for 8 days. Box-plot depicts hypocotyl length in mm of n=13-23 seedlings. Box extends from the 25th to 75th percentile, whiskers from the 5th to 95th percentile. Horizontal line denotes median. '+' denotes the mean. For statistical testing, Kruskal-Wallis (nonparametric) test was applied, followed by Dunn's Multiple comparison between lines carrying no or the same transgene (* $p \leq 0.05$; ** $p \leq 0.01$; *** $p \leq 0.001$).



Supplementary Figure 31: Elongation of hypocotyls in dark-grown 7-day old seedlings of *35S::YFP*, *35S::YFP-IAA1* and *35S::YFP-IAA2* overexpressor lines

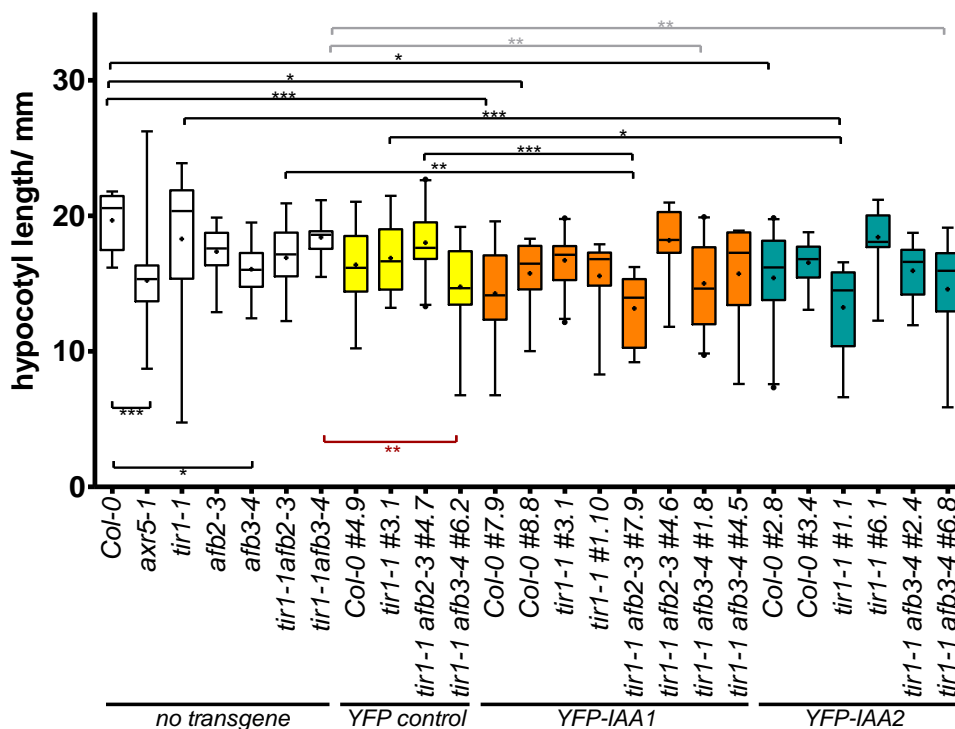
Seedlings were grown on 0.5x MS plates in the dark at 20°C for 8 days. Box-plot depicts hypocotyl length in mm of $n=7-14$ seedlings. Box extends from the 25th to 75th percentile, whiskers from the 5th to 95th percentile. Horizontal line denotes median. '+' denotes the mean. For statistical testing, Kruskal-Wallis (nonparametric) test was applied, followed by Dunn's Multiple comparison between lines carrying no or the same transgene ($* p \leq 0.05$).



Supplementary Figure 32: Elongation of hypocotyls in dark-grown 5-day old seedlings of *35S::YFP*, *35S::YFP-IAA1* and *35S::YFP-IAA2* overexpressor lines

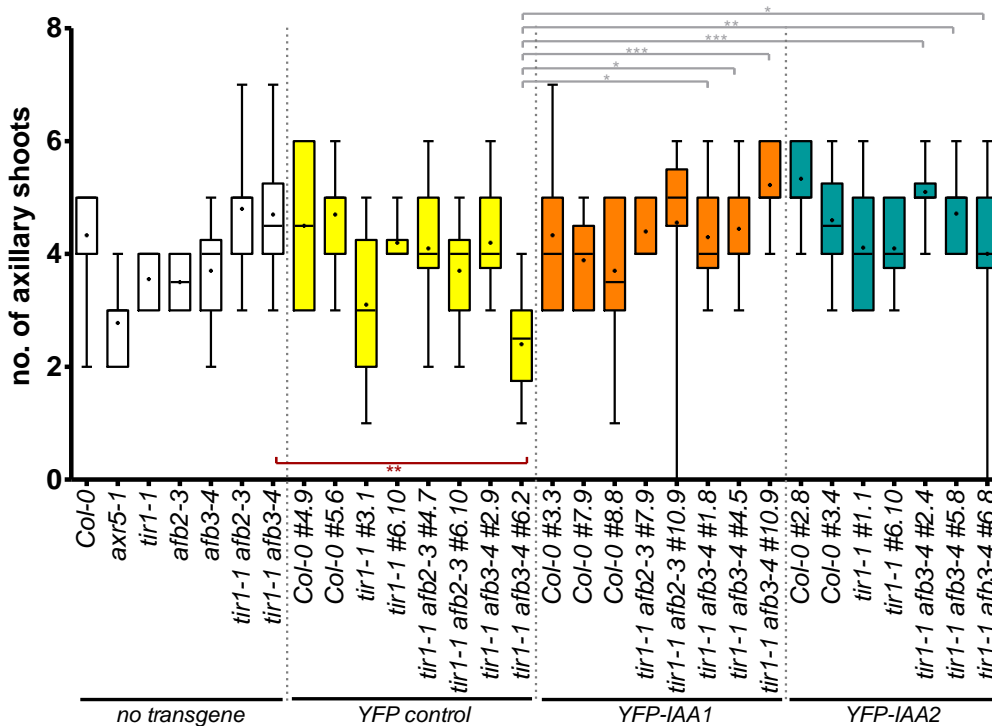
Seedlings were grown on 0.5x MS plates in the dark at 20°C for 5 days. Box-plot depicts hypocotyl length in mm of $n=7-27$ seedlings. Box extends from the 25th to 75th percentile, whiskers from the 5th to 95th percentile. Horizontal line denotes median. '+' denotes the mean. For statistical testing, Kruskal-Wallis (nonparametric) test was applied,

followed by Dunn’s Multiple comparison between lines carrying no or the same transgene (* $p \leq 0.05$; ** $p \leq 0.01$; *** $p \leq 0.001$).



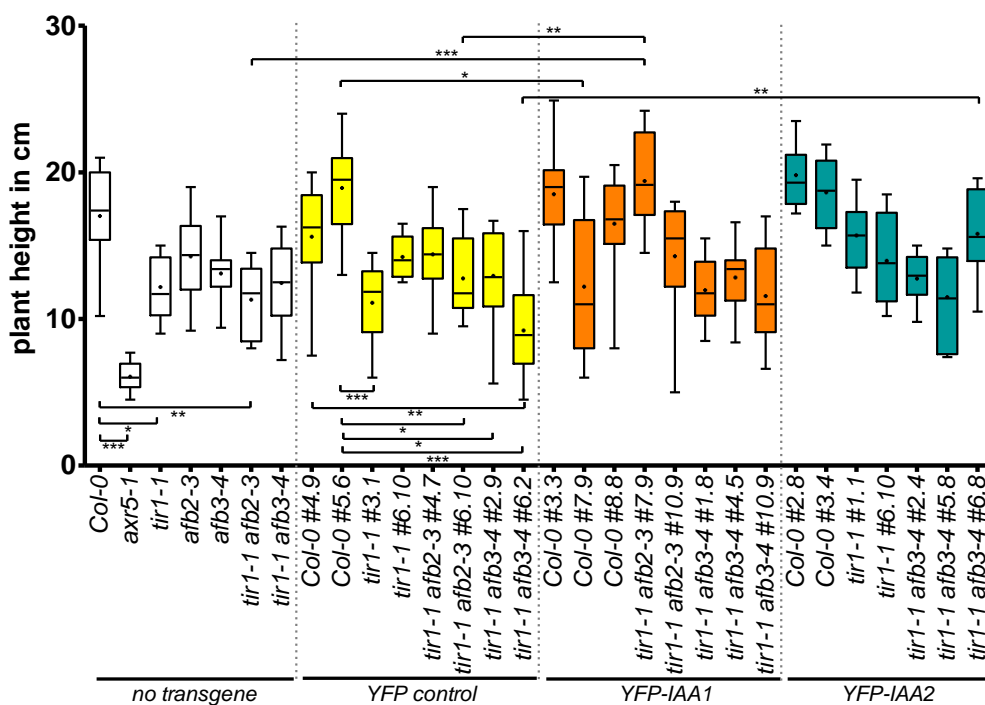
Supplementary Figure 33: Elongation of hypocotyls in dark-grown 5-day old seedlings of 35S::YFP, 35S::YFP-IAA1 and 35S::YFP-IAA2 overexpressor lines

Seedlings were grown on 0.5x MS plates in the dark at 20°C for 5 days. Box-plot depicts hypocotyl length in mm of n=7-27 seedlings. Box extends from the 25th to 75th percentile, whiskers from the 5th to 95th percentile. Horizontal line denotes median. Plus (+) denotes the mean. For statistical testing, Kruskal-Wallis (nonparametric) test was applied, followed by Dunn’s Multiple comparison between lines carrying no or the same transgene (* $p \leq 0.05$; ** $p \leq 0.01$; *** $p \leq 0.001$).



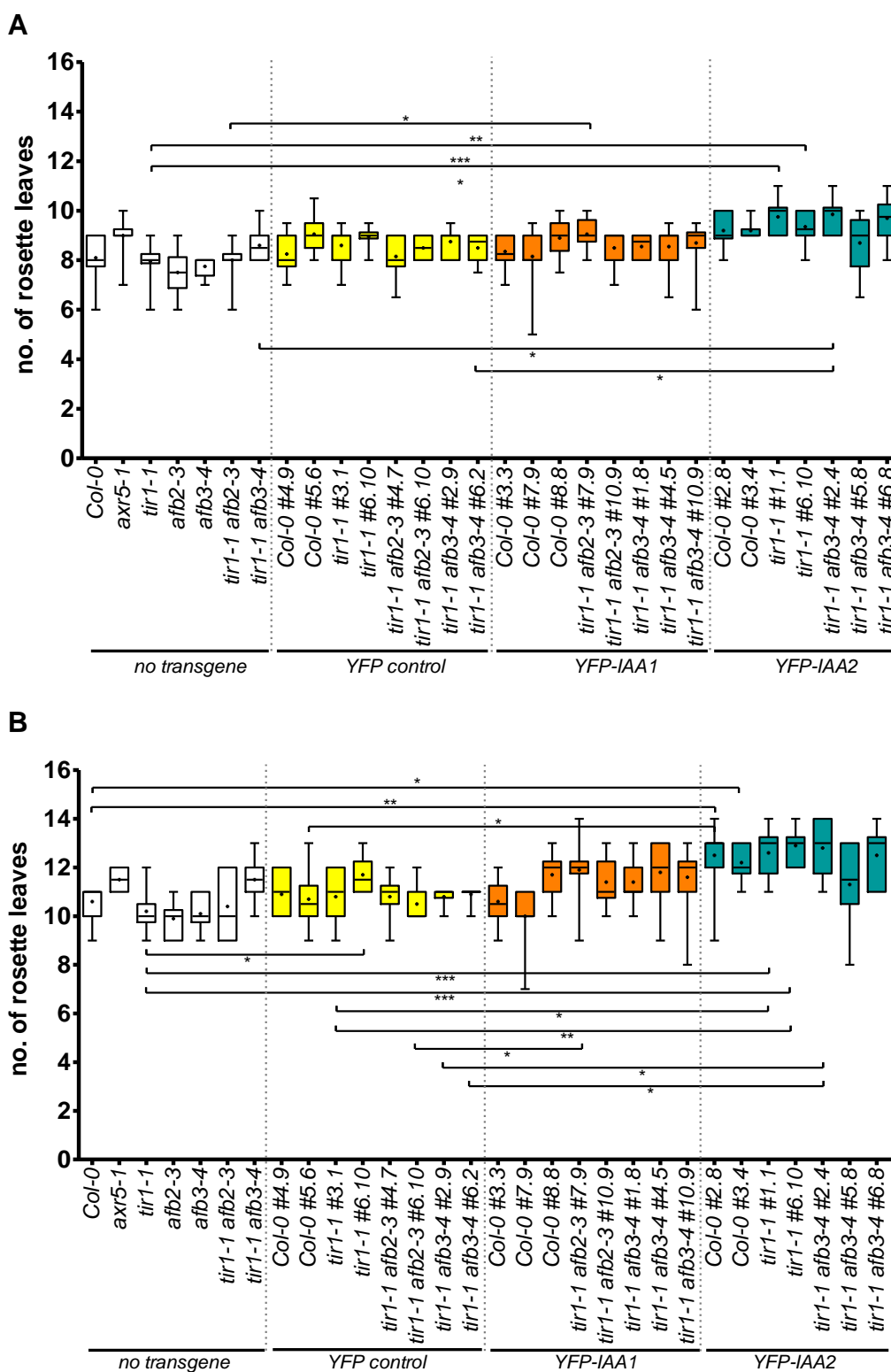
Supplementary Figure 34: Number of axillary shoots in 5-week old plants of *35S::YFP*, *35S::YFP-IAA1* and *35S::YFP-IAA2* overexpressor lines

Plants were grown on 0.5x MS plates for 8 days at long day conditions (16 hours day/8 hours night), 20° C, and 30 $\mu\text{mol}/(\text{m}^2\text{s})$, before being transferred to soil and grown at long day conditions, 21° C, and 100 $\mu\text{mol}/(\text{m}^2\text{s})$ for 27 more days. Box-plot depicts the number of axillary shoots per rosette for $n=9-10$ plants. Box extends from the 25th to 75th percentile, whiskers from the 5th to 95th percentile. Horizontal line denotes median. Plus ('+') denotes the mean. For statistical testing, Kruskal-Wallis (nonparametric) test was applied, followed by Dunn's Multiple comparison between lines carrying no or the same transgene (* $p \leq 0.05$; ** $p \leq 0.01$; *** $p \leq 0.001$).



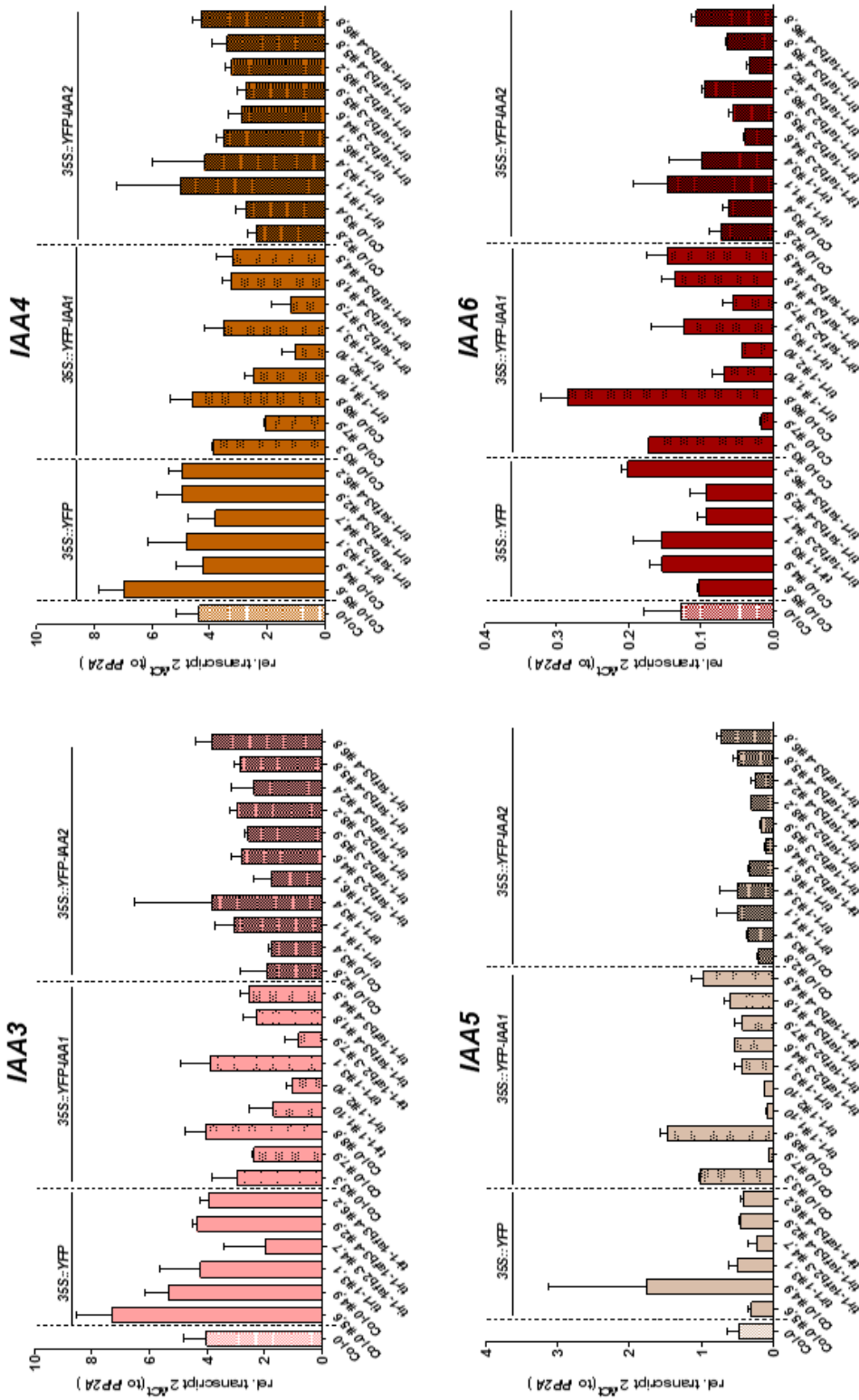
Supplementary Figure 35: Plant height of 5-week old plants of 35S::YFP, 35S::YFP-IAA1 and 35S::YFP-IAA2 overexpressor lines

Plants were grown on 0.5x MS plates for 8 days at long day conditions (16 hours day/8 hours night), 20° C, and 30 $\mu\text{mol}/(\text{m}^2\text{s})$, before being transferred to soil and grown at long day conditions, 21° C, and 100 $\mu\text{mol}/(\text{m}^2\text{s})$ for 27 more days. Total plant height was measured from rosette base to the tip of the longest shoot. Box-plot depicts the plant heights for n=9-10 plants. Box extends from the 25th to 75th percentile, whiskers from the 5th to 95th percentile. Horizontal line denotes median. Plus ('+') denotes the mean. For statistical testing, Kruskal-Wallis (nonparametric) test was applied, followed by Dunn's Multiple comparison between lines carrying no or the same transgene (* $p \leq 0.05$; ** $p \leq 0.01$; *** $p \leq 0.001$). n=10. Error bars denote standard deviation.



Supplementary Figure 36: Number of rosette leaves in 17-day old (A) and 20-day old (B) plants *35S::YFP*, *35S::YFP-IAA1* and *35S::YFP-IAA2* overexpressor lines

Plants were grown on 0.5x MS plates for 8 days at long day conditions (16 hours day/8 hours night), 20° C, and 30 $\mu\text{mol}/(\text{m}^2\text{s})$, before being transferred to soil and grown at long day conditions, 21° C, and 100 $\mu\text{mol}/(\text{m}^2\text{s})$. Rosette leaves were counted after plants were 17-days and 20-days old. Box-plot depicts the rosette leave number for $n=9-10$ plants. Box extends from the 25th to 75th percentile, whiskers from the 5th to 95th percentile. Horizontal line denotes median. Plus (+) denotes the mean. For statistical testing, Kruskal-Wallis (nonparametric) test was applied, followed by Dunn's Multiple comparison between lines carrying no or the same transgene (* $p \leq 0.05$; ** $p \leq 0.01$; *** $p \leq 0.001$).



Supplementary Figure 37: Transcript levels of *IAA3*, *IAA4*, *IAA5*, and *IAA6* in seedlings of *35S::YFP*, *35S::YFP-IAA1* and *35S::YFP-IAA2* overexpressor lines

Homozygous T3 lines overexpressing *YFP* (empty vector control; yellow), *YFP-IAA1* (orange) and *YFP-IAA2* (teal) in various genetic backgrounds were derived from independent lines. RNA from 5-day old seedlings was extracted, reverse-transcribed and analyzed for expression of auxin-responsive genes *IAA3*, *IAA4*, *IAA5* and *IAA6* through RT-qPCR. Transcript levels are displayed relative to the constitutively expressed reference gene *PP2A* (Czechowski *et al.*, 2005). Number of biological replicates analyzed for each as in **Figure 2-16** (n=2-3). Error bars denote standard error.

Supplementary Table 11: Exemplary crossing scheme for generating lines that carry the same *35S::YFP-IAA1* or *35S::YFP-IAA2* locus in different *tir1/afb* single or double mutant backgrounds

By crossing a homozygous transgenic YFP-overexpressor line (YY) in wild-type (++) background with a *tir1-1 afb2-3* or *tir1-1 afb3-4* double mutant (*tt aa*), and letting the resulting heterozygous F1 generation undergo selfing, a homogenous insertion of transgene will be achieved in all progeny. The F2 progeny (Punnett square) will yield ca. 1.6% of each desired genotype *YY ++ aa*, *YY tt ++*, and *YY tt aa* (framed genotypes in Punnett square).

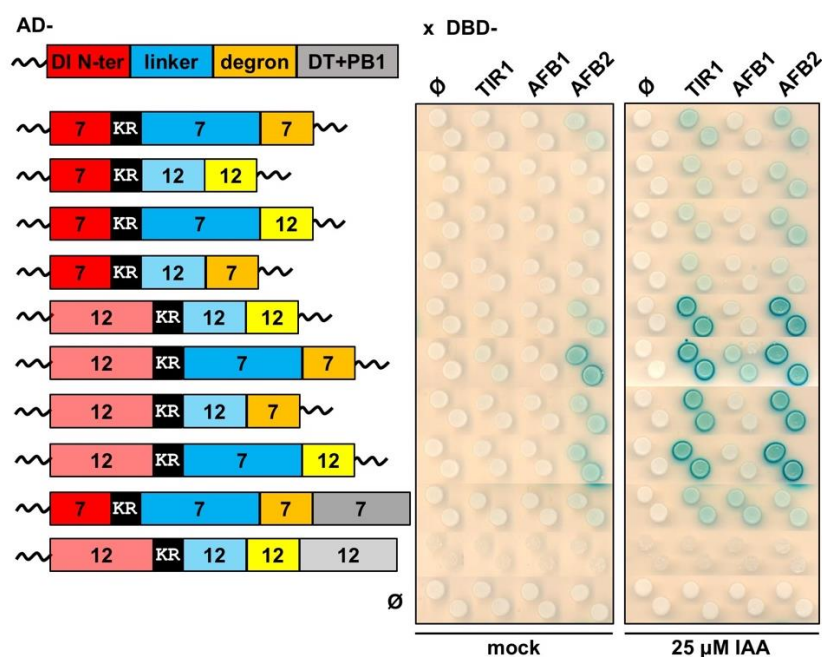
P	YY ++ ++ x ++ tt aa							
F1	Y+ +t +a							
F2	Y+ +t +a x Y+ +t +a							
	Y ++	Y +a	Y t+	+ t a	+++	++ a	+ t +	Y t a
Y ++	YY ++ ++	YY ++ +a	YY t+ ++	Y+ +t +a	Y+ ++ ++	Y+ ++ +a	Y+ +t ++	YY +t +a
Y +a	YY ++ a+	YY ++ aa	YY +t a+	Y+ +t aa	Y+ ++ a+	Y+ ++ aa	Y+ +t a+	YY +t aa
Y t+	YY t+ ++	YY t+ +a	YY tt ++	Y+ tt a+	Y+ t+ ++	Y+ t+ +a	Y+ tt ++	YY tt +a
+ t a	+Y t+ a+	+Y t+ aa	+Y tt a+	++ tt aa	++ t+ a+	++ t+ aa	++ tt a+	+Y tt aa
+++	+Y ++ ++	+Y ++ +a	+Y ++ ++	++ +t +a	++ ++ ++	++ ++ +a	++ ++ ++	+Y ++ +a
++ a	+Y ++ a+	+Y ++ aa	+Y ++ ++	++ +t aa	++ ++ a+	++ ++ aa	++ ++ ++	+Y ++ aa
+ t +	+Y t+ ++	+Y t+ +a	+Y t+ ++	++ t+ a+	++ t+ ++	++ t+ +a	++ tt ++	+Y t+ +a
Y t a	YY t+ a+	YY t+ aa	YY tt a+	Y+ tt aa	Y+ t+ a+	Y+ t+ aa	Y+ tt +a	YY tt aa

Allele	Symbol
<i>tir1-1</i>	<i>t</i>
<i>afb2-3</i>	<i>a</i>
<i>afb3-4</i>	<i>a</i>
<i>35S::YFP-IAA1</i>	<i>Y</i>
<i>35S::YFP-IAA2</i>	<i>Y</i>
<i>35S::YFP</i>	<i>Y</i>
+	wild-type

Supplementary Table 12: Overview of chimera modules nomenclature and sequences

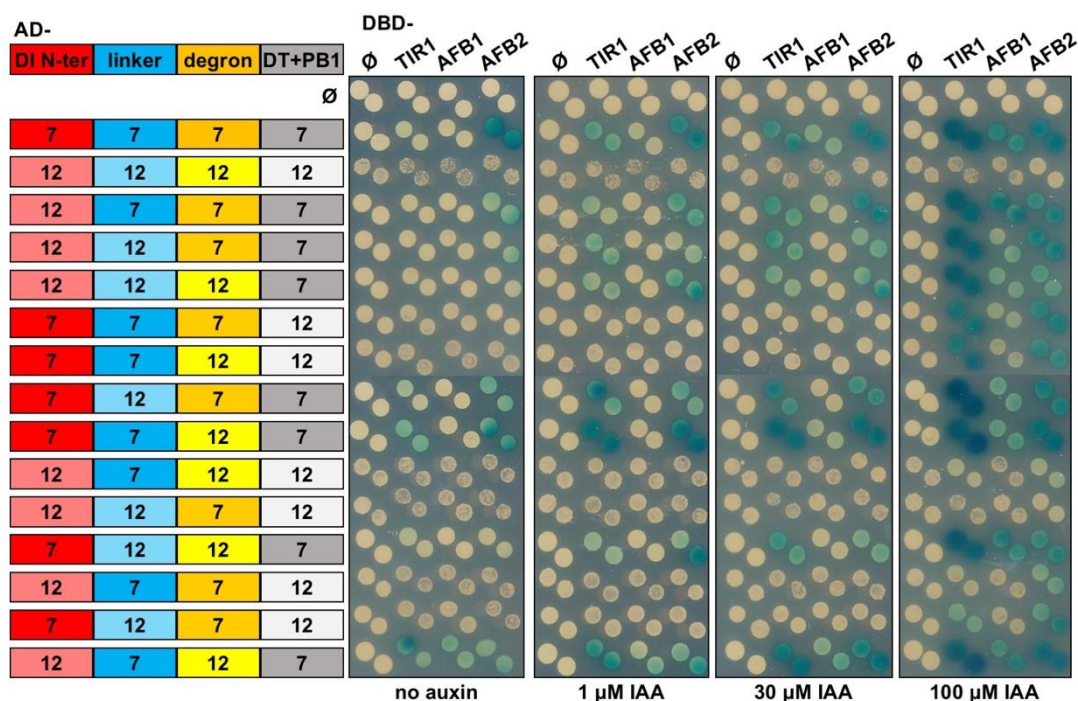
IAA7 and IAA12 modules are represented in darker and lighter shades, respectively. Domain I containing N-terminal module (DI N-ter; red), linker region between conserved KR duplet and degron (linker; blue), degron also known as domain II (degron; yellow), and PB1 domain (PB1; grey) are included in the 4 module chimeras. In 5 module chimeras, the variable part between degron and PB1 (formerly included in the PB1 module) is split into a separate module named the “degron tail” (DT; turquoise). Note, that the linker of IAA7 is significantly longer than that of IAA12. In contrast, the DI N-ter and DT of IAA12 is longer than that of IAA7. Conserved residues are bold and underlined. Only highly conserved residues were used as demarcations to split these AUX/IAAs into modules for the chimera approach.

IAA7	4 modules
DI N-ter	<u>MIGQLMNLKATELCLGL</u> PGGAEAVESPAKSAVGS K
linker	<u>RGFSETVDLMLNLQSNKEGSVDLKNVSAVPKEKTTLKDPSKPPAKAQV</u> V
degron	<u>VGWPPVRNYR</u>
PB1	<u>KNM</u> MTQQKTSSGAEAEASSEKAGNFGGGAAGAGL VKV SMDGAPYLKRVDLKMYK SYQDLSDALAKMFSSFTMGNYGAQGMIDFMNESKLMNLLNSSEYVPSYEDKDG DWMLVGDVPWEMFVESCRLRLIMKGSEAVGLAPRAMEKYCKNRS
IAA7	5 modules
DI N-ter	<u>MIGQLMNLKATELCLGL</u> PGGAEAVESPAKSAVGS K
linker	<u>RGFSETVDLMLNLQSNKEGSVDLKNVSAVPKEKTTLKDPSKPPAKAQV</u> V
degron	<u>VGWPPVRNYR</u>
DT	<u>KNM</u> MTQQKTSSGAEAEASSEKAGNFGGGAAGAGL V
PB1	<u>KV</u> SMDGAPYLKRVDLKMYKSYQDLSDALAKMFSSFTMGNYGAQGMIDFMNESK LMNLLNSSEYVPSYEDKDGDWMLVGDVPWEMFVESCRLRLIMKGSEAVGLAPR AMEKYCKNRS
IAA12	4 modules
DI N-ter	<u>MRGVSELEVGKSNLPAESELELGL</u> GLSLGGGAWKERGRILTAKDFPSVGS K
linker	<u>RSAESSSHQGASPPRSSQV</u>
degron	<u>VGWPPIGLHR</u>
PB1	<u>MN</u> SLVNNQAMKAARAEEGDGEKKVVKNDELKDVS MKVNPKVQGLGF VKV NMDG VGIGRKVDMRAHSSYENLAQTLEEMFFGMTGTTCREKVKPLRLLDGSSDFVLT YEDKEGDWMLVGDVPWRMFINSVKRLRIMGTSEASGLAPRRQE QKDRQRNNPV
IAA12	5 modules
DI N-ter	<u>MRGVSELEVGKSNLPAESELELGL</u> GLSLGGGAWKERGRILTAKDFPSVGS
linker	<u>KRSAESSSHQGASPPRSSQV</u>
degron	<u>VGWPPIGLHR</u>
DT	<u>MN</u> SLVNNQAMKAARAEEGDGEKKVVKNDELKDVS MKVNPKVQGLGF V
PB1	<u>KV</u> NMDGVGIGRKVDMRAHSSYENLAQTLEEMFFGMTGTTCREKVKPLRLLDGSSDFVLT YEDKEGDWMLVGDVPWRMFINSVKRLRIMGTSEASGLAPRRQE QKDRQRNNPV



Supplementary Figure 38: Preliminary assessment of TIR1/AFB:AUX/IAA-chimera interaction in yeast

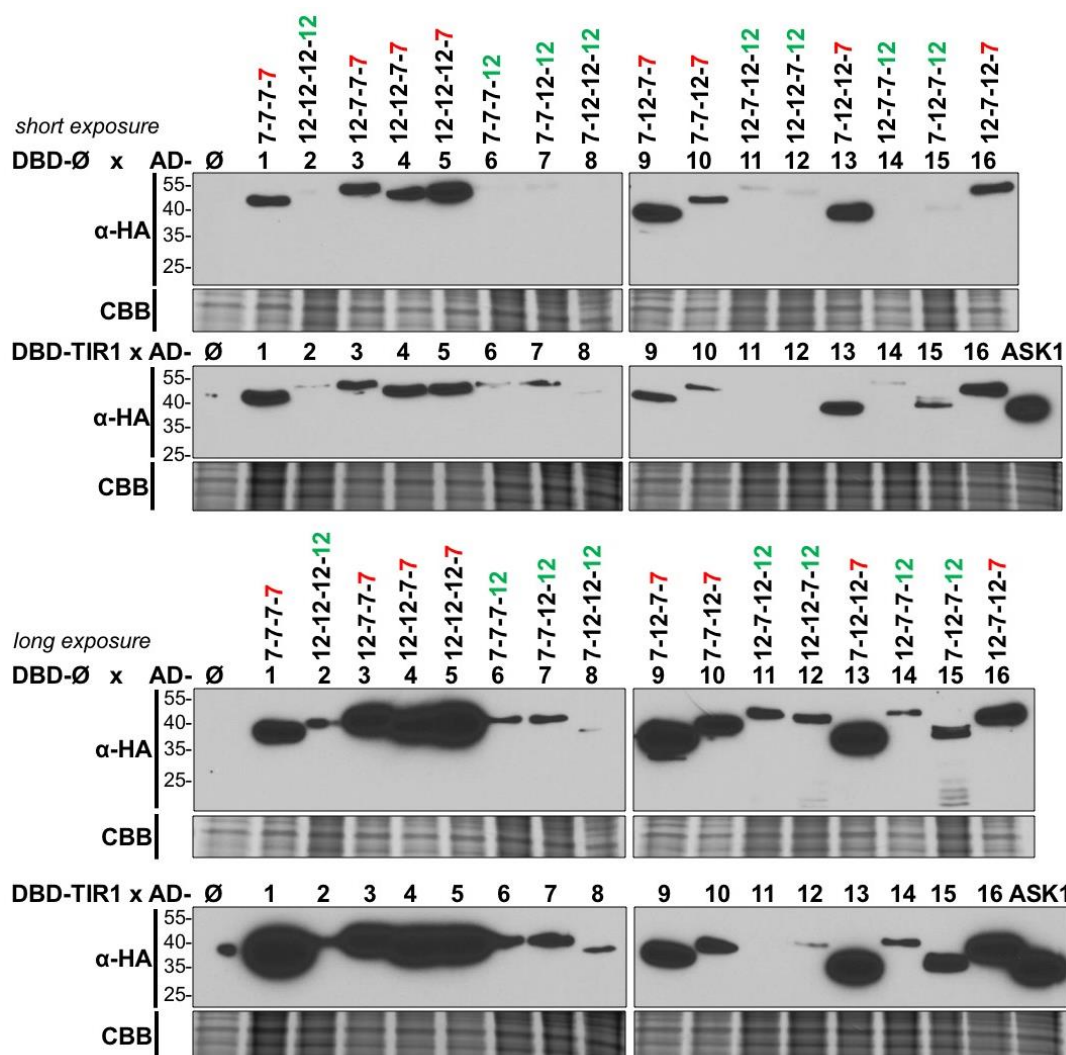
Overlap-PCR was initially applied to generate IAA7/IAA12-chimera fusions. These constructs were then Gateway-cloned to obtain AD fusions and therefore carry additional sequence stretches at the N- and C-terminus (wavy line). Diploid yeast co-expressing DBD-TIR1/-AFB1/-AFB2 and AD-chimera were tested for β -Gal reporter activity on selective induction medium with or without 25 μ M IAA. Yeast cell dispersions of the same OD₆₀₀ were spotted on selective induction medium plates and pictures taken after 3 days of growth at 30°C.



Supplementary Figure 39: Auxin-dependent interaction of chimeric IAA7/12 with TIR1/AFB1/AFB2 in yeast

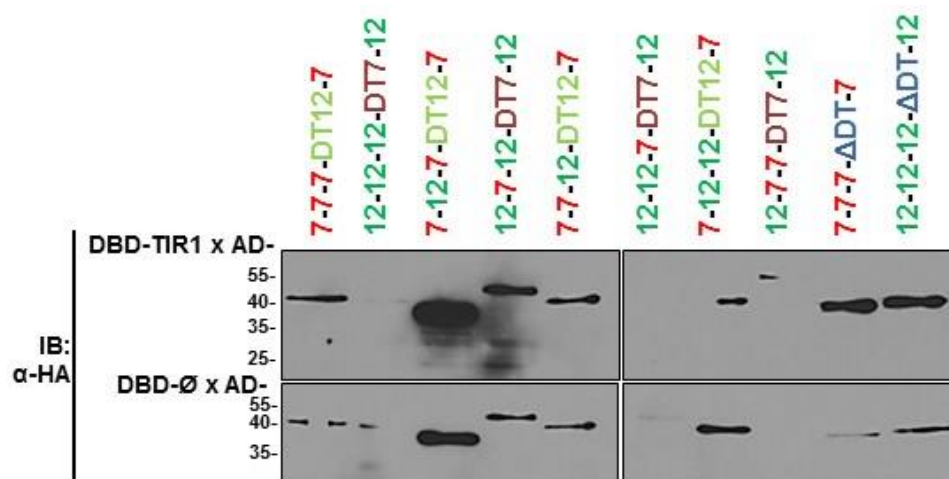
Diploid yeast expressing full-length AD-chimeras and DBD-TIR1/-AFB1/-AFB2 were tested for β -Gal reporter activity on selective induction medium with 0, 1, 30, or 100 μ M IAA. AD-chimeras contain 4 modules as depicted in the scheme on the left: 1) DI N-ter (red), 2) linker (blue), 3) degron (yellow), 4) degron-tail (DT) and PB1 (grey). Yeast cell dispersions of the same OD₆₀₀ were spotted on selective induction medium plates and pictures taken

after 3 days of growth at 30°C. This experiment and the one shown in **Figure 2-20 A** represent independent experiments.



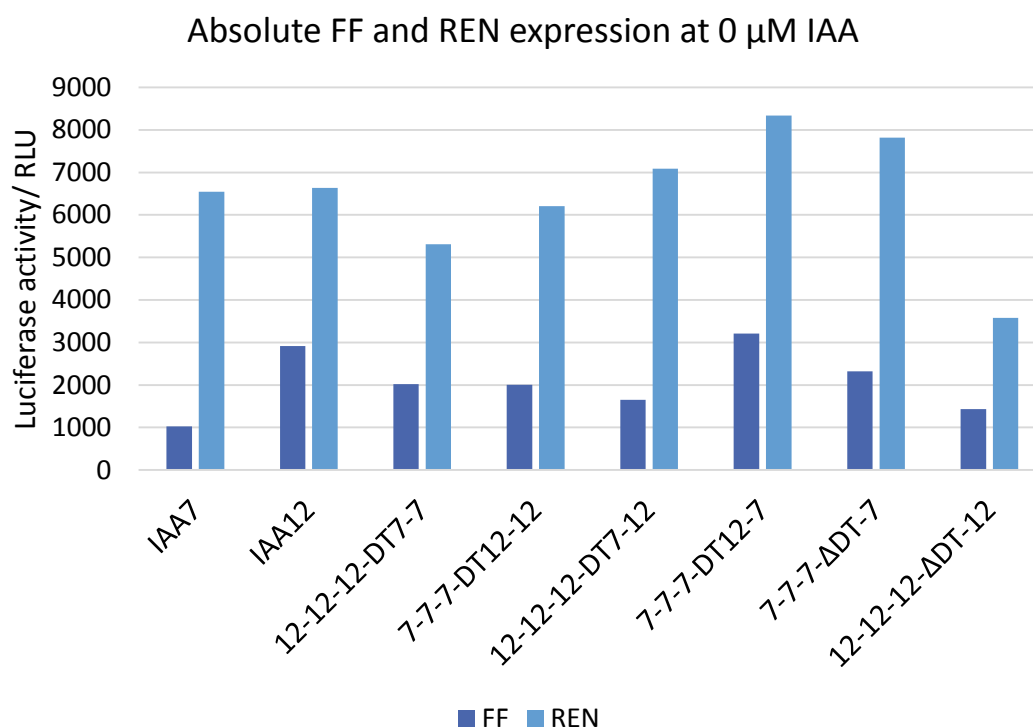
Supplementary Figure 40: Immunoblot analysis of AD-4-module-chimera protein expression from yeast strains used in Y2H assay (Figure 2-20 A)

Crude protein extracts were prepared from diploid yeasts expressing DBD-TIR1 and AD-AUX/IAA constructs. Yeast liquid cultures were grown in selective induction medium. Amount of starting material was adjusted to similar levels according to the culture OD_{600} . AD-fusion proteins carry an HA-tag between the AD and POI, and were therefore detected by immunoblotting with α -HA antibody (upper panels). Coomassie Brilliant Blue (CBB) staining of total protein is depicted as loading controls (lower panel).



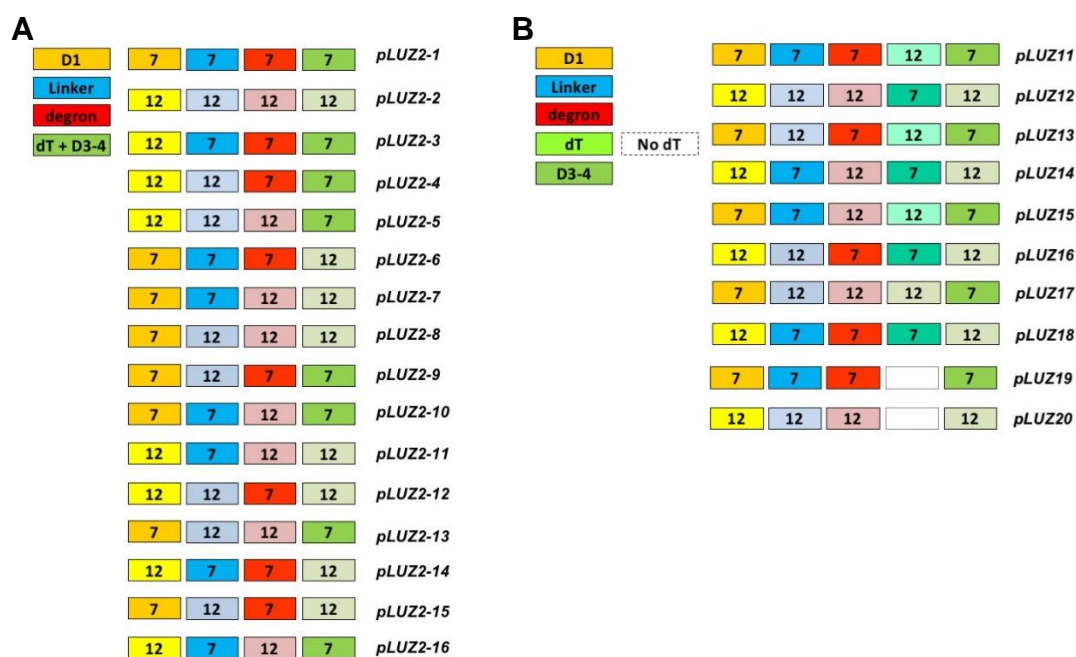
Supplementary Figure 41: Immunoblot analysis of AD-5-module-chimera protein expression from yeast strains used in Y2H assay (Figure 2-20 B)

Crude protein extracts were prepared from diploid yeasts expressing DBD-TIR1 and AD-chimera constructs. Yeast liquid cultures were grown in selective induction medium. Amount of starting material was adjusted to similar levels according to the culture OD_{600} . AD-fusion proteins carry an HA-tag between the AD and POI, and were therefore detected by immunoblotting with α -HA antibody.



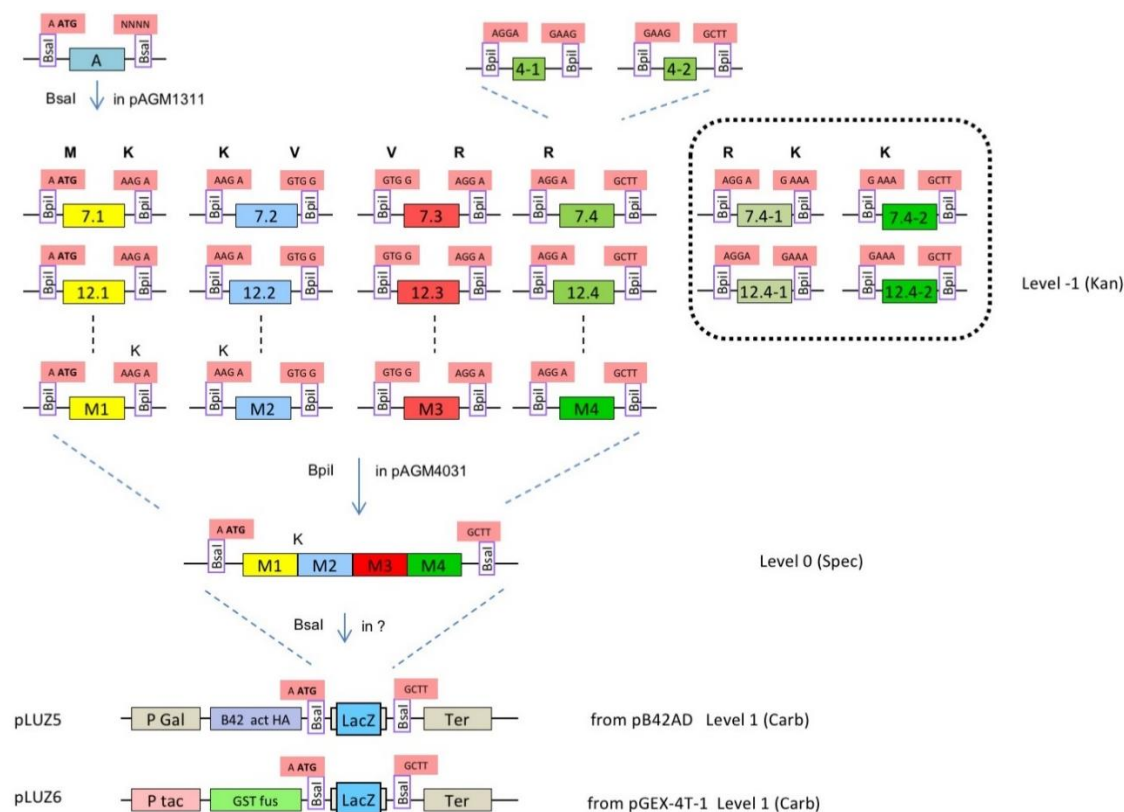
Supplementary Figure 42: Absolute Firefly Luciferase (FF) and Renilla Luciferase (REN) expression

IAA7/IAA12 chimeras (see schemes in Figure 2-19, Figure 2-20, and Supplementary Table 12) were fused as sensor modules to firefly luciferase (FF) in frame with a self-splicing renilla luciferase (REN) fusion for normalization of expression and expressed in *Arabidopsis mesophyll* protoplasts (Wend *et al.*, 2013). Here absolute values of FF and REN luciferase activity for untreated protoplasts (0 μ M IAA) are shown for indicated chimeric sensors in relative light units (RLU). Absolute Luciferase activity is indicative of basal expression of these luciferase fusions.



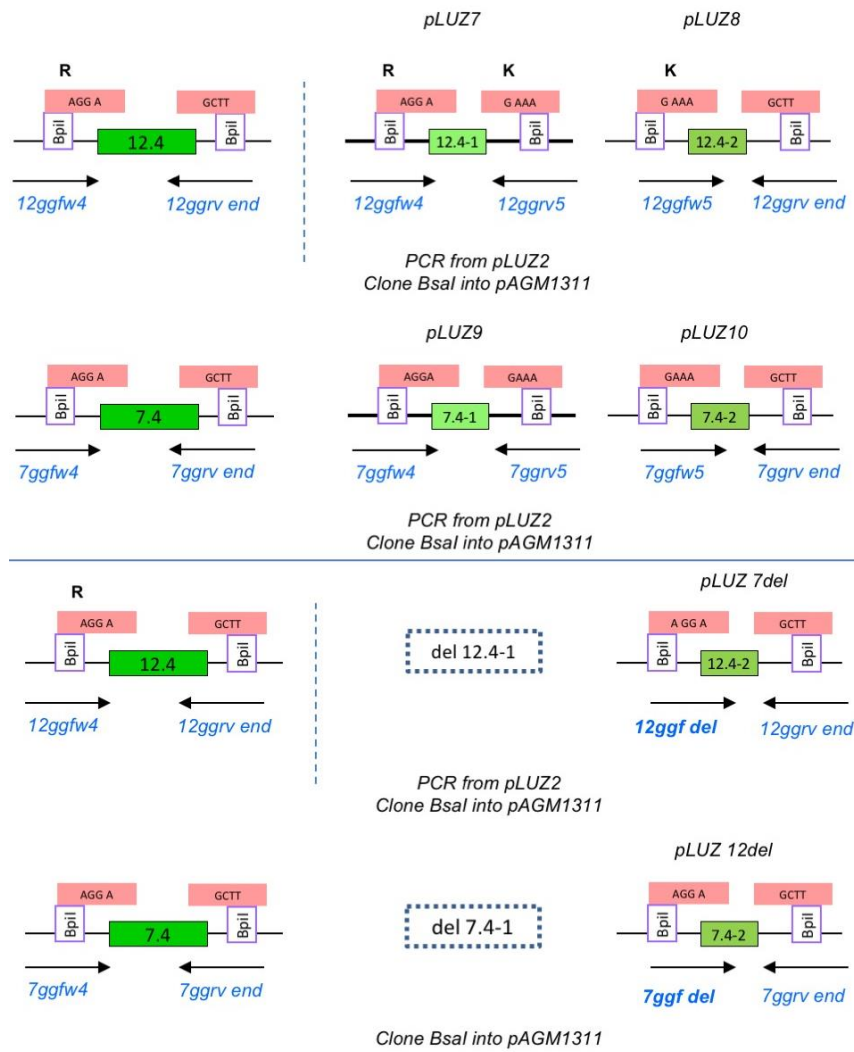
Supplementary Figure 43: Overview and nomenclature of 4-module (A) and 5-module (B) chimeric constructs

Module 1 corresponds to the domain I-containing N-terminal part N-ter DI (yellow box, "D1"). "Linker" is the variable sequence between conserved KR duplet and the conserved degron (blue box). "degron" denotes a conserved 10-residues degron sequence (red box). 4-module chimeras contain the fourth module consisting of the variable degron tail (dT) region and the highly conserved and folded PB1 domain (green box in A). 5-module chimeras contain a separate dT module (turquoise box) and a PB1 module (green box in B). Deletion of dT sequence is signified by a dashed white box. Numbers 7 and 12 indicate module is derived from IAA7 and IAA12, respectively. See **Supplementary Table 12** for module sequences. 4-module chimeras in Level 0 were named pLUZ2-1 to -16 as indicated in A. 5-module chimeras were named pLUZ11 to pLUZ20 in B.



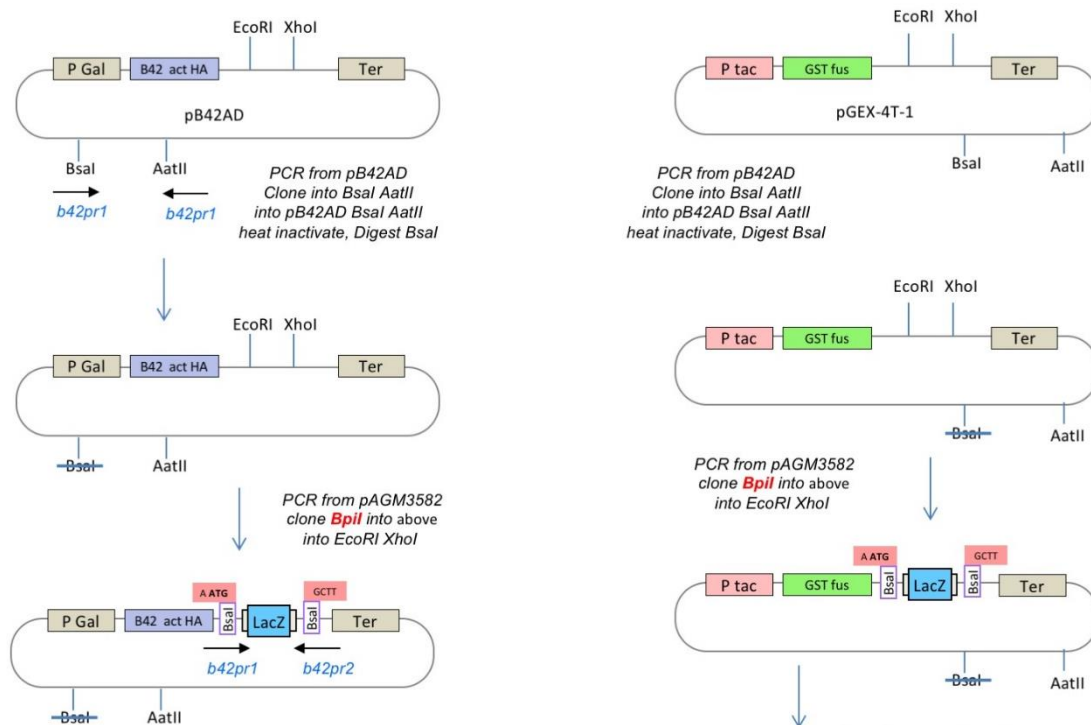
Supplementary Figure 44: Golden Gate Modular Cloning (MoClo) assembly strategy for 4-module and 5-module chimeras of *IAA7* and *IAA12*

PCR-amplified modules of *IAAn* (modules named n.1, n.2, n.3, n.4, n.4-1 and n.4-2 corresponding to N-ter DI, Linker, degenon, DT+PB1, DT and PB1, respectively) were *Bsal*-cloned into pAGM1311 Level -1 vector with kanamycin resistance (Kan). M, K, V and R denote the conserved amino acids in *IAA7* and *IAA12* sequence that were chosen as module borders for scarless assembly. Directional assembly of modules to a full length chimeric *AUX/IAA* was then performed by *Bpil*-cloning into pAGM4031 Level 0 vector (pLUZ2 constructs) with spectinomycin resistance (Spec). Expression vectors pLUZ5 and pLUZ6 for Level 1 cloning were generated by removing *Bsal* sites from the vector backbone of pB42AD and pGEX-4T-3, respectively, and inserting a *LacZa* cassette that can be replaced by *Bsal*-cloning (also see **Supplementary Figure 49** and **Supplementary Figure 50**). Dashed box shows later implemented splitting of module n.4 (degenon-tail+PB1) into n.4-1 (degenon-tail) and n.4-2 (PB1) for 5-module chimera strategy.

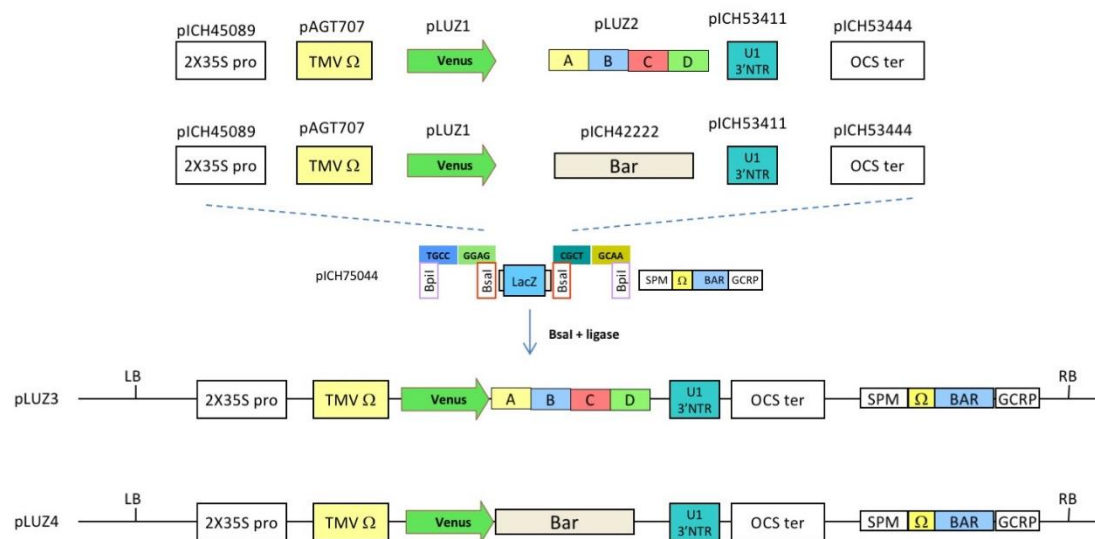


Supplementary Figure 45: Details of 5-module MoClo assembly

After pLUZ2 constructs were established, the 5-module chimeras were designed. From module 4 of a pLUZ2 template the new modules 4-1 and 4-2 corresponding to degron-tail and PB1 were amplified using the primers shown in blue with arrows, and fragments cloned into pAGM1311 Level -1 with Bsal



Supplementary Figure 46: pLUZ5 and pLUZ6 vector adaptation for Golden Gate cloning compatibility from pB42AD and pGEX-4T-3, respectively



Supplementary Figure 47: MoClo assembly scheme for Level 1 binary vector for plant overexpression of N-terminally VENUS-tagged chimeras

MoClo elements represented by colored boxes or arrow were *Bsal*-cloned from plasmids indicated above the boxes into the pICH75044 binary vector backbone. This yielded pLUZ3 plasmids where pLUZ2 chimera plasmids were used in the assembly. For an unspecific control plasmid, the phosphinothricin acetyltransferase gene (Bar) from pICH42222 was inserted instead of the chimeras, resulting in the pLUZ4 control plasmid.

Supplementary Table 13: Primers for amplification of AUX/IAA CDS blunt end fragments for Directional TOPO cloning (Thermo Fisher Scientific)

F and R denote forward and reverse primer, respectively.

primer	template gene	5'->3' sequence
IAA2-pENTR-F	<i>IAA2; At3g23030</i>	CACCATGGCGTACGAGA
IAA2-pENTR-R	<i>IAA2; At3g23030</i>	TCATAAGGAAGAGTCTAGAGC
IAA4-pENTR-F	<i>IAA4; At5g43700</i>	CACCATGGAAAAAGTTGATG
IAA4-pENTR-R	<i>IAA4; At5g43700</i>	TTAAAGACCACCACAACCTA
IAA5-pENTR-F	<i>IAA5; At1g15580</i>	CACCATGGCGAATGAGA
IAA5-pENTR-R	<i>IAA5; At1g15580</i>	TCATCCTCTGTTACATGATC
IAA6-pENTR-F	<i>IAA6; At1g52830</i>	CACCATGGCAAAGGAAGGTC
IAA6-pENTR-R	<i>IAA6; At1g52830</i>	TTAATCTTGCTGGAGACCAAAACC
IAA8-4-pENTR-F	<i>IAA8; At2g22670.4</i>	CACCATGAGTTCTGGGAAC
IAA8-pENTR-R	<i>IAA8; At2g22670</i>	TCAAACCCGCTCTTTGTTCT
IAA9-pENTR-F	<i>IAA9; At5g65670</i>	CACCATGTCCCCGGAAGA
IAA9-pENTR-R	<i>IAA9; At5g65670</i>	TTAAGCTCTCATCTTCGATTTCTC
IAA10-pENTR-F	<i>IAA10; At1g04100</i>	CACCATGAATGGTTTGCAAG
IAA10-pENTR-R	<i>IAA10; At1g04100</i>	CTACTTACCTACTCCAGCT
IAA11-pENTR-F	<i>IAA11; At4g28640</i>	CACCATGGAAGGCGGTT
IAA11-2-pENTR-R	<i>IAA11; At4g28640.2</i>	TTACAAAGAGAACATATAACTAATA
IAA13-pENTR-F	<i>IAA13; At2g33310</i>	CACCATGATTACTGAACTTGAG
IAA13-1-pENTR-R	<i>IAA13; At2g33310.1</i>	CTAAACCGGCTGCTTTTCG
IAA15-pENTR-F	<i>IAA15; At1g80390</i>	CACCATGTCACCGGAGGAA
IAA15-pENTR-R	<i>IAA15; At1g80390</i>	CTATAATCCAATAGCATCTCCGG
IAA16-pENTR-F	<i>IAA16; At3g04730</i>	CACCATGATTAATTTTGAGGC
IAA16-pENTR-R	<i>IAA16; At3g04730</i>	TCAACTTCTGTTCTTGCACCTT
IAA17_pENTR_F	<i>IAA17; At1g04250</i>	CACCATGATGGGCAGTGTGAGCTGA
IAA17_pENTR_R	<i>IAA17; At1g04250</i>	TCAAGCTCTGCTCTTGCACTTCTCCATCG
IAA18-pENTR-F	<i>IAA18; At1g51950</i>	CACCATGGAGGGTTATTCAA
IAA18-pENTR-R	<i>IAA18; At1g51950</i>	TCATCTTCTCATTTTCTCTTGC
IAA19-pENTR-F	<i>IAA19; At3g15540</i>	CACCATGGAGAAGGAAGGA
IAA19-pENTR-R	<i>IAA19; At3g15540</i>	TCACTCGTCTACTCCTCTAG
IAA2030-pENTR-F	<i>IAA20; At2g46990/ IAA30; At3g62100</i>	CACCATGGGAAGAGGGAGAAG
IAA20-pENTR-R	<i>IAA20; At2g46990</i>	TCAGTAGTGGTAATTAGCTCTTGAAATCTT
IAA26-pENTR-F	<i>IAA26; At3g16500</i>	CACCATGGAAGGTTGTCCAA
IAA26-pENTR-R	<i>IAA26; At3g16500</i>	TCAGTGCATCATCTTCTCTTGC
IAA27-pENTR-F	<i>IAA27; At4g29080</i>	CACCATGTCTGTATCTGTAGC
IAA27-pENTR-R	<i>IAA27; At4g29080</i>	CTAGTTCCCTGCTTCTGCACT
IAA29-pENTR-F	<i>IAA29; At4g32280</i>	CACCATGGAGTTGGATCT
IAA29-pENTR-R	<i>IAA29; At4g32280</i>	TTAAAACAAACATCTTGATATGCA
IAA30-pENTR-R	<i>IAA30; At3g62100</i>	TCAGTAGTGATAAGCTCTTGAGATCTTTA

IAA31-pENTR-F	<i>IAA31; At3g17600</i>	CACCATGGAGGTCTCTAACT
IAA31-pENTR-R	<i>IAA31; At3g17600</i>	TTAATACCTCTCCGGTCTCG
IAA32-pENTR-F	<i>IAA32; At2g01200</i>	CACCATGGACCCAAACACA
IAA32-2-pENTR-R	<i>IAA32; At2g01200.2</i>	TTAAAAGGGAAGAAGAGCATCG
IAA33-pENTR-F	<i>IAA33; At5g57420</i>	CACCATGAATAGTTTCGAGC
IAA33-pENTR-R	<i>IAA33; At5g57420</i>	TCACTCGTTTCTTTAACTTGTC
IAA34-pENTR-F	<i>IAA34; At1g15050</i>	CACCATGTATTGCAGCGAT
IAA34-pENTR-R	<i>IAA34; At1g15050</i>	TTAAAAGGGAAGTACAGCATC

Supplementary Table 14: Primers for amplification of AUX/IAA CDS attB site-containing fragments for Gateway cloning (Thermo Fisher Scientific)

attB1 and *attB2* denote forward and reverse primer, respectively.

primer	template gene	5'->3' sequence
attB1_IAA1	<i>IAA1 (At4g14560)</i>	GGGGACAAGTTTGTACAAAAAAGCAGGCTTCATGGAAGTCAC CAATGGGCTTAACC
attB2_STOP_IAA1	<i>IAA1 (At4g14560)</i>	GGGGACCACTTTGTACAAGAAAGCTGGGTCTCATAAGGCAGT AGGAGCTTCGGAT
attB1_IAA2	<i>IAA2 (At3g23030)</i>	GGGGACAAGTTTGTACAAAAAAGCAGGCTTCATGGCGTACGA GAAAGTCAACGAGC
attB2_IAA2_Stop	<i>IAA2 (At3g23030)</i>	GGGGACCACTTTGTACAAGAAAGCTGGGTCTCATAAGGAAGA GTCTAGAGCAGGA
attB1_IAA3	<i>IAA3 (At1g04240)</i>	GGGGACAAGTTTGTACAAAAAAGCAGGCTTCATGGATGAGTT TGTTAACCTCAAGG
attB1_IAA3_Stop	<i>IAA3 (At1g04240)</i>	GGGGACCACTTTGTACAAGAAAGCTGGGTCTCATAACCACA GCCTAACCTTTG
attB1_IAA6	<i>IAA6 (At1g52830)</i>	GGGGACAAGTTTGTACAAAAAAGCAGGCTTCATGGCAAAGGA AGGTCTAGCACTCG
attB2_IAA6_Stop	<i>IAA6 (At1g52830)</i>	GGGGACCACTTTGTACAAGAAAGCTGGGTCTTAATCTTGCTG GAGACCAAACCA
attB1_IAA7_F	<i>IAA7 (At3g23050.1)</i>	GGGGACAAGTTTGTACAAAAAAGCAGGCTTCATGATCGGCCA ACTTATGAACCTCA
IAA7 attB1 FW	<i>IAA7 (At3g23050.1)</i>	GGGGACAAGTTTGTACAAAAAAGCAGGCTTCATGATCGGCCA ACTTATGAAC
IAA7 attB2 RV	<i>IAA7 (At3g23050.1)</i>	GGGGACCACTTTGTACAAGAAAGCTGGGTCTCAAGATCTGTT CTTGCAGTACTTCT
attB1_IAA8	<i>IAA8 (At2g22670.4)</i>	GGGGACAAGTTTGTACAAAAAAGCAGGCTTCATGTCTTATCG ATTGCTAAGTGTGG
attB2_IAA8_Stop	<i>IAA8 (At2g22670.1)</i>	GGGGACCACTTTGTACAAGAAAGCTGGGTCTCAAACCCGCTC TTTGTCTTCGAT
attB1_IAA9	<i>IAA9 (At5g65670.2)</i>	GGGGACAAGTTTGTACAAAAAAGCAGGCTTCATGTCCCCGGA AGAGGAGCTACAGA
attB2_IAA9_Stop	<i>IAA9 (At5g65670.2)</i>	GGGGACCACTTTGTACAAGAAAGCTGGGTCTTAAGCTCTCAT CTTCGATTTCTCC
attB1_IAA10	<i>IAA10 (At1g04100)</i>	GGGGACAAGTTTGTACAAAAAAGCAGGCTTCATGAATGGTTT GCAAGAAGTTTGTT
attB2_IAA10_Stop	<i>IAA10 (At1g04100)</i>	GGGGACCACTTTGTACAAGAAAGCTGGGTCTACTTACCTAC TCCAGCTCCAATT

attB1_ IAA11	<i>IAA11 (At4g28640.1)</i>	GGGGACAAGTTTGTACAAAAAAGCAGGCTTCATGGAAGGCGG TTCCGCTAGTGGAT
attB2_ IAA11-1_ St	<i>IAA11 (At4g28640.1)</i>	GGGGACCACTTTGTACAAGAAAGCTGGGTCTCATAATATCAT CTGAGCTTTACCAGTA
attB1_ IAA12_ F	<i>IAA12 (At1g04550.2)</i>	GGGGACAAGTTTGTACAAAAAAGCAGGCTTCATGCGTGGTGT GTCAGAATTGGAGG
IAA12 attB1 FW	<i>IAA12 (At1g04550.2)</i>	GGGGACAAGTTTGTACAAAAAAGCAGGCTTCATGCGTGGTGT GTCAGAATT
IAA12 attB2 RV	<i>IAA12 (At1g04550.2)</i>	GGGGACCACTTTGTACAAGAAAGCTGGGTCTTAAACAGGGTT GTTTCTTTGTCTATC
attB1_ IAA13	<i>IAA13 (At2g33310)</i>	GGGGACAAGTTTGTACAAAAAAGCAGGCTTCATGATTACTGA ACTTGAGATGGGGA
attB2_ IAA13_ Stop	<i>IAA13 (At2g33310)</i>	GGGGACCACTTTGTACAAGAAAGCTGGGTCTTAAACCGGCTG CTTTCGCTGTCTC
attB1_ IAA14	<i>IAA14 (At4g14550)</i>	GGGGACAAGTTTGTACAAAAAAGCAGGCTTCATGAACCTTAA GGAGACGGAGCTTT
attB2_ IAA14_ Stop	<i>IAA14 (At4g14550)</i>	GGGGACCACTTTGTACAAGAAAGCTGGGTCTCATGATCTGTT CTTGAACCTTCTCC
attB1_ IAA16	<i>IAA16 (At3g04730)</i>	GGGGACAAGTTTGTACAAAAAAGCAGGCTTCATGATTAATTT TGAGGCCACGGAGC
attB2_ IAA16_ Stop	<i>IAA16 (At3g04730)</i>	GGGGACCACTTTGTACAAGAAAGCTGGGTCTCAACTTCTGTT CTTGCACTTTTCT
attB1_ IAA17	<i>IAA17 (At1g04250)</i>	GGGGACAAGTTTGTACAAAAAAGCAGGCTTCATGATGGGCAG TGTCGAGCTGAATC
attB2_ IAA17_ Stop	<i>IAA17 (At1g04250)</i>	GGGGACCACTTTGTACAAGAAAGCTGGGTCTCAAGCTCTGCT CTTGCACTTCTCC
attB1_ IAA19	<i>IAA19 (At3g15540)</i>	GGGGACAAGTTTGTACAAAAAAGCAGGCTTCATGGAGAAGGA AGGACTCGGGCTTG
attB2_ IAA19_ Stop	<i>IAA19 (At3g15540)</i>	GGGGACCACTTTGTACAAGAAAGCTGGGTCTCACTCGTCTAC TCCTCTAGGCTGC
attB1_ IAA26	<i>IAA26 (At3g16500)</i>	GGGGACAAGTTTGTACAAAAAAGCAGGCTTCATGGAAGGTTG TCCAAGAAACAGAG
attB2_ IAA26_ Stop	<i>IAA26 (At3g16500)</i>	GGGGACCACTTTGTACAAGAAAGCTGGGTCTCAGTGCATCAT CTTCTCTTGCTTA
attB1_ IAA28	<i>IAA28 (At5g25890)</i>	GGGGACAAGTTTGTACAAAAAAGCAGGCTTCATGGAAGAAGA AAAGAGATTGGAGC
attB1_ IAA28_ Stop	<i>IAA28 (At5g25890)</i>	GGGGACCACTTTGTACAAGAAAGCTGGGTCTTATTCCTTGCC ATGTTTTCTAGGT
attB1_ IAA33	<i>IAA33 (At5g57420)</i>	GGGGACAAGTTTGTACAAAAAAGCAGGCTTCATGAATAGTTT CGAGCCACAAAGCC
attB2_ IAA33_ Stop	<i>IAA33 (At5g57420)</i>	GGGGACCACTTTGTACAAGAAAGCTGGGTCTCACTCGTTTCT TTTAACTTGTCTT

Supplementary Table 15: Primers for site-directed mutagenesis (Agilent Technologies)

FW/F and RV/R denote forward and reverse primer, respectively.

primer	template gene	5'->3' sequence	description
SDM_ IAA1_ P61S _FW/ axr5-1_ FW	<i>IAA1 (At4g14560) CDS</i>	ATCGTTGGATGGCCTTCAGTGAGATC TAACCG	generating <i>axr5-1</i> mutation in <i>IAA1</i>
SDM_ IAA1_ P61S _RV/ axr5-1_ RV	<i>IAA1 (At4g14560) CDS</i>	CGGTTAGATCTCACTGAAGGCCATCC AACGAT	generating <i>axr5-1</i> mutation in <i>IAA1</i>

SDM_IIA2_P66S_FW	IIA2 (At3g23030) CDS	AATCGTTGGTTGGCCATCAGTGAGATCTTCCCCG	generating mutation in IAA2 corresponding to <i>axr5-1</i>
SDM_IIA2_P66S_R	IIA2 (At3g23030) CDS	CGGGAAGATCTCACTGATGGCCAACC AACGATT	generating mutation in IAA2 corresponding to <i>axr5-1</i>
SDM_IIA7_P87S / <i>axr2-1</i> _FW	IIA7 (At3g23050.1) CDS	CAAGTGGTGGGATGGTCACCTGTGAG GAACT	generating <i>axr2-1</i> mutation in IAA7
SDM_IIA7_P87S / <i>axr2-1</i> _RV	IIA7 (At3g23050.1) CDS	AGTTCCTCACAGGTGACCATCCCACC ACTTG	generating <i>axr2-1</i> mutation in IAA7
SDM_IIA12_P74 S/ <i>bdl</i> _FW	IIA12 (At1g04550.2) CDS	GTCAAGTGGTAGGATGGTCACCAATT GGGTTACAC	generating <i>bdl</i> mutation in IAA12
SDM_IIA12_P74 S/ <i>bdl</i> _RV	IIA12 (At1g04550.2) CDS	GTGTAACCCAATTGGTGACCATCCTA CCACTTGAC	generating <i>bdl</i> mutation in IAA12
R88_K89_FW	IIA1 (At4g14560) CDS	GAGTATGGACGGAGCTCCATATCTCG CTGCGATAGATCTCAAGATGTACAAA AAC	generating <i>basic patch</i> mutation in IAA1
R88_K89_RV	IIA1 (At4g14560) CDS	GTTTTTGTACATCTTGAGATCTATCG CAGCGAGATATGGAGCTCCGTCCATA CTC	generating <i>basic patch</i> mutation in IAA1
K78A_FW	IIA1 (At4g14560) CDS	ACAAAAACGTGAGTTATGTGGCAGTG AGTATGGACGGAGCTC	generating <i>basic patch</i> mutation in IAA1
K78A_RV	IIA1 (At4g14560) CDS	GAGCTCCGTCCATACTCACTGCCACA TAACTCACGTTTTTTG	generating <i>basic patch</i> mutation in IAA1
Venus S176G FW	EYFP	ATCGAGGACGGCGGCGTGCAGCTCG	generating VENUS from EYFP
Venus S176G RV	EYFP	CGAGCTGCACGCCCGCTCCTCGAT	generating VENUS from EYFP
Venus F47L FW	EYFP	CAAGCTGACCCTGAAGTTAATCTGCA CCACCGG	generating VENUS from EYFP
Venus F47L RV	EYFP	CCGGTGGTGCAGATTAACCTCAGGGT CAGCTTG	generating VENUS from EYFP
Venus V164A FW	EYFP	GAAGAACGGCATCAAGGCGAACTTCA AGATCCGCC	generating VENUS from EYFP
Venus V164A RV	EYFP	GGCGGATCTTGAAGTTCGCCTTGATG CCGTTCTTC	generating VENUS from EYFP
Venus F65L FW	EYFP	CCTCGTGACCACCTTAGGCTACGGCC T	generating VENUS from EYFP
Venus F65L RV	EYFP	AGGCCGTAGCCTAAGGTGGTCACGAG G	generating VENUS from EYFP
Venus M154T FW	EYFP	ACAGCCACAACGTCTATATCACGGCC GACAAGC	generating VENUS from EYFP
Venus M154T RV	EYFP	GCTTGTGCGCCGTGATATAGACGTTG TGGCTGT	generating VENUS from EYFP

Supplementary Table 16: General primers

These are mostly tag- or vector-specific primers, which were used for detection of specific fragments and to validate successful cloning or transformation in PCR reactions. FW/F/for and RV/R/rev denote forward and reverse primer, respectively.

primer	template	5'→3' sequence
35s FW	CaMV 35S promoter	TCCATTGCCAGCTATCTGTC
GST_F	Glutathione S-transferase (GST) tag in pGEX vectors	TGGTTCGCGTGGATCCCCG
pGEX 5' seq	Glutathione S-transferase (GST) tag in pGEX vectors	GGGCTGGCAAGCCACGTTTGGTG
pLexA FW	pLexA vector	CGTCAGCAGAGCTTACCATT
pLexA RV	pLexA vector	CGTTTTAAAACCTAAGAGTCA
pB42AD FW	pB42AD vector	CCAGCCTCTTGCTGAGTGGAGATG
pB42AD RV	pB42AD vector	TGTCAACAACGTATCTACCAACGA
YFP_FW	pB7WGY2 vector	GCGACGTAAACGGCCACAAG
YFP_RV	pB7WGY2 vector	CTTGTGGCCGTTTACGTCGC
YFPseq_for	pB7WGY2 vector	CAAAGACCCCAACGAGAAGC
YFPseq_rev	pB7WGY2 vector	GCTTCTCGTTGGGGTCTTTG
T7_FW		TAATACGACTCACTATAGGG
T7term_RV		GCTAGTTATTGCTCAGCGG
M13_for		GTA AACGACGGCCAG
M13_rev		CAGGAAACAGCTATGAC

Supplementary Table 17: Primers applied in Golden Gate cloning procedures to amplify fragments and to verify cloning and transformation success in PCR

FW and RV denote forward and reverse primer, respectively.

primer	template	5'→3' sequence	description
7GG_FW1	IAA7	TTGGTCTCAACATAATGATCG GCCAACTTATGAACCTCAAG	for amplification of module 1 IAA7 GoldenGate cloning
7GG_RV2_new	IAA7	TTGGTCTCAACAATCTTGCTT CCCACCGCGATTGGCAG	for amplification of module 1 IAA7 GoldenGate cloning
7GG_FW2	IAA7	TTGGTCTCAACATAAGAGAGG CTTCTCCGAAACCGTTGAT	for amplification of module 2 IAA7 GoldenGate cloning
7GG_RV3_new	IAA7	TTGGTCTCAACAACCACCT TGTGCTTTAGCAGGAGGC	for amplification of module 2 IAA7 GoldenGate cloning
7GG_FW3	IAA7	TTGGTCTCAACATGTGGGATG GCCACCTGTGAGGAACCTACAG GATTGTTGAGACC	for amplification of module 3 IAA7 GoldenGate cloning
7GG_RV4_new	IAA7	TTGGTCTCAACAATCCTGTAG TTCTCAGAGGTGGCCATCCC ACATGTTGAGACC	for amplification of module 3 IAA7 GoldenGate cloning
7GG_FW4	IAA7	TTGGTCTCAACATAGGAAGAA CATGATGACTCAGCAGAAG	for amplification of module 4 IAA7 GoldenGate cloning
7GG_Rvend_new	IAA7	TTGGTCTCAACAAAAGCTCAA GATCTGTTCTTGCACTAC	for amplification of module 4 IAA7 GoldenGate cloning

12GG_FW1	IAA12	TTGGTCTCAACATAATGCGTG GTGTGTCAGAATTGGAGG	for amplification of module 1 IAA12 GoldenGate cloning
12GG_RV2_new	IAA12	TTGGTCTCAACAATCTTAGAC CCAACGGAAGGAAAATCC	for amplification of module 1 IAA12 GoldenGate cloning
12GG_FW4	IAA12	TTGGTCTCAACATAGGATGAA CAGTTTGGTTAATAACC	for amplification of module 4 IAA12 GoldenGate cloning
12GG_Rvend_new	IAA12	TTGGTCTCAACAAAAGCCTAA ACAGGGTTGTTTCTTTGTCT	for amplification of module 4 IAA12 GoldenGate cloning
12GG_FW2	IAA12	TTGGTCTCAACATAAGAGATC TGCTGAATCTTCTCTCACCA AGGAGCTTCTCCTCCTCGTTC AAGTCAAGTGGTGGTTGTTGA GACC	for amplification of module 2 IAA12 GoldenGate cloning
12GG_RV3_new	IAA12	TTGGTCTCAACAACCACCACT TGACTTGAACGAGGAGAGAA GCTCCTTGGTGAGAGGAAGAT TCAGCAGATCTCTTATGTTGA GACC	for amplification of module 2 IAA12 GoldenGate cloning
12GG_FW3	IAA12	TTGGTCTCAACATGTGGGATG GCCACCAATTGGGTTACACAG GATTGTTGAGACC	for amplification of module 3 IAA12 GoldenGate cloning
12GG_RV4_new	IAA12	TTGGTCTCAACAATCCTGTGT AACCCAATTGGTGGCCATCCC ACATGTTGAGACC	for amplification of module 3 IAA12 GoldenGate cloning
12GGRV5	IAA12	TTGGTCTCAACAATTCACAA ACCCTAAGCCCTGAACTTTC	for Golden Gate to split the 4th modul into 2 seperate ones
12ggFW5	IAA12	TTGGTCTCAACATGAAAGTGA ATATGGATGGAGTTGG	for Golden Gate to split the 4th modul into 2 seperate ones
7GGRV5	IAA7	TTGGTCTCAACAATTCACCA AGCCGGCTCCGGCTG	for Golden Gate to split the 4th modul into 2 seperate ones
7GGFW5	IAA7	TTGGTCTCAACATGAAAGTCT CCATGGACGGTGC	for Golden Gate to split the 4th modul into 2 seperate ones
7ggfdel FW	IAA7 module 4	TTGGTCTCAACATAGGAAAGT CTCCATGGACGGTG	for Golden Gate to delete the degron tail in IAA7module 4
12ggfdel FW	IAA12 module 4	TTGGTCTCAACATAGGAAAGT GAATATGGATGGAG	for Golden Gate to delete the degron tail in IAA12module 4
G717c_GG_FW	pGEX4T-3 and pB42AD	CGGTGAGCGTGGCTCTCGCGG TATC	for SDM to remove Bsal site in the Amp cassette of pGEX4T-3 and pB42AD
G717c_GG_RV	pGEX4T-3 and pB42AD	GATACCGCGAGAGCCACGCTC ACCG	for SDM to remove Bsal site in the Amp cassette of pGEX4T-3 and pB42AD
b42pr1_GG	LacZ α	TTGAAGACAAAATTAATGTGA GACCGCAGCTGGC	to amplify and clone LacZ cassette in pGEX4T-3 and pB42AD
b42pr2_GG	LacZ α	TTGAAGACAATCGAAAGCTGA GACCGTCACAGC	to amplify and clone LacZ cassette in pGEX4T-3 and pB42AD
GEXpr1_GG	LacZ α	TTGAAGACAAAATTC AATGTG AGACCGCAGCTGGC	to amplify and clone LacZ cassette in pGEX4T-3 and pB42AD
7_g204a_FW	IAA7	CTGCTGTTCCCAAGGAGAAAA CTACCCTTAAAGATC	for SDM to eliminate Bsal or Bpi1 sites in IAA7
7_g204a_RV	IAA7	GATCTTTAAGGGTAGTTTTCT CCTTGGGAACAGCAG	for SDM to eliminate Bsal or Bpi1 sites in IAA7

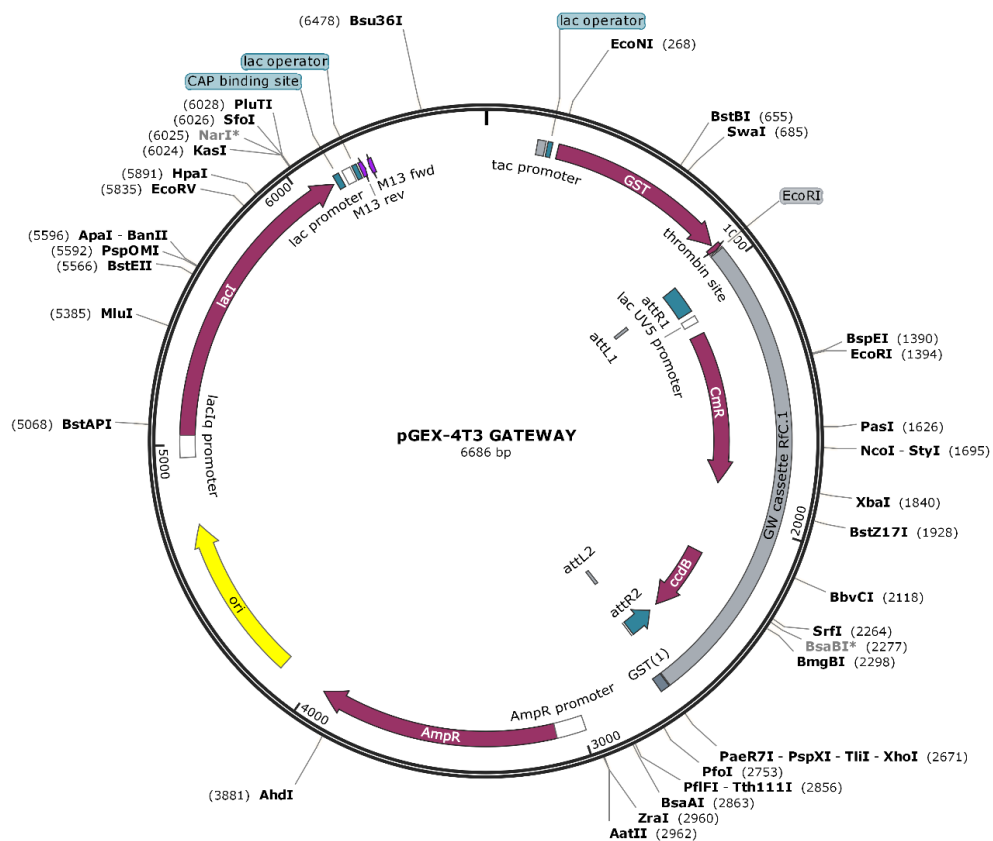
7_g303a_FW	IAA7	ACATGATGACTCAGCAGAAAA CCAGTAGTGGTGCG	for SDM to eliminate Bsal or Bpi1 sites in IAA7
7_g303a_RV	IAA7	CGCACCCTACTGGTTTTCTG CTGAGTCATCATGT	for SDM to eliminate Bsal or Bpi1 sites in IAA7
7_g384a_FW	IAA7	GGAGCCGGCTTGGTGAAGTC TCCATGGA	for SDM to eliminate Bsal or Bpi1 sites in IAA7
7_g384a_RV	IAA7	TCCATGGAGACTTTCACCAAG CCGGCTCC	for SDM to eliminate Bsal or Bpi1 sites in IAA7
AMP FW		ATGAGTATTCAACATTTCCGT GTCGCC	for SDM Lac cassette
pAGM1311 FW	pAGM1311	GGGCTGGCAAGCCACGTTTGG TG	For Golden Gate Cloning pAGM1311
pAGM1311 RV =MOCLOF	pAGM1311	AGCGAGGAAGCGGAAGAGCG	For Golden Gate Cloning pAGM1311
pAGM1311 FW1	pAGM1311	GAGTCAGTGAGCGAGGAAGC	
pAGM1311 FW4	pAGM1311	ATTACCGCCTTTGAGTGAGC	
7GG FW3 extension		TTGGTCTCAACATGTGGGATG GCCACCTGTGAGGAACACAG GATTGTTGAGACCGTCTTTCT ACATCGGTATGTACG	use to amplify IAA7 Modul 3 (Golden Gate)
45AFB3R2311RVextension		ACGGCTTAACGTAGAGATCAT CAACGAGAATGAGAATAATGG GATGGAACAGAATGAAGAAG TGAAAGA	use to amplify IAA7 Modul 4 (Golden Gate)
7GG FW3 Ext2	pICH31170	TTGGTCTCAACATGTGGGATG GCCACCTGTGAGGAACACAG GATTGTTGAGACCGTGGAAAC TTGGGACTTCAG	to amplify small IAA7 Module 3 (GG) using the pICH31170 (Marillonet) as frame template
pAGM1311 RV2 = MOCLOR		GCCACCTGACGTCTAAGAAAC C	
Venus GG FW	VENUS	TTGAAGACAACCATGGTGAGC AAGGGCGAGGAGC	Amplification Venus Casette
Venus_NS GG RV	VENUS	TTGAAGACAACATTTTGTACA GCTCGTCCATGCCGAG	Amplification Venus Casette
pAGM4031 FW2		AGGGGGAAACGCCTGGTA	for Golden Gate to sequence modules in pAGM4031
VENUS_GG_FWsequ		GCCACAACATCGAGGACG	for Golden Gate to sequence modules in Venus
7GG short FW	IAA7	TTGGTCTCAACATAAGAACAT GATGACTCAGCAGAAG	Golden Gate to generate a negative controle vector IAA7 (w/o any function)

Supplementary Table 18: Primers used in RT-qPCR

FW and RV denote forward and reverse primer, respectively.

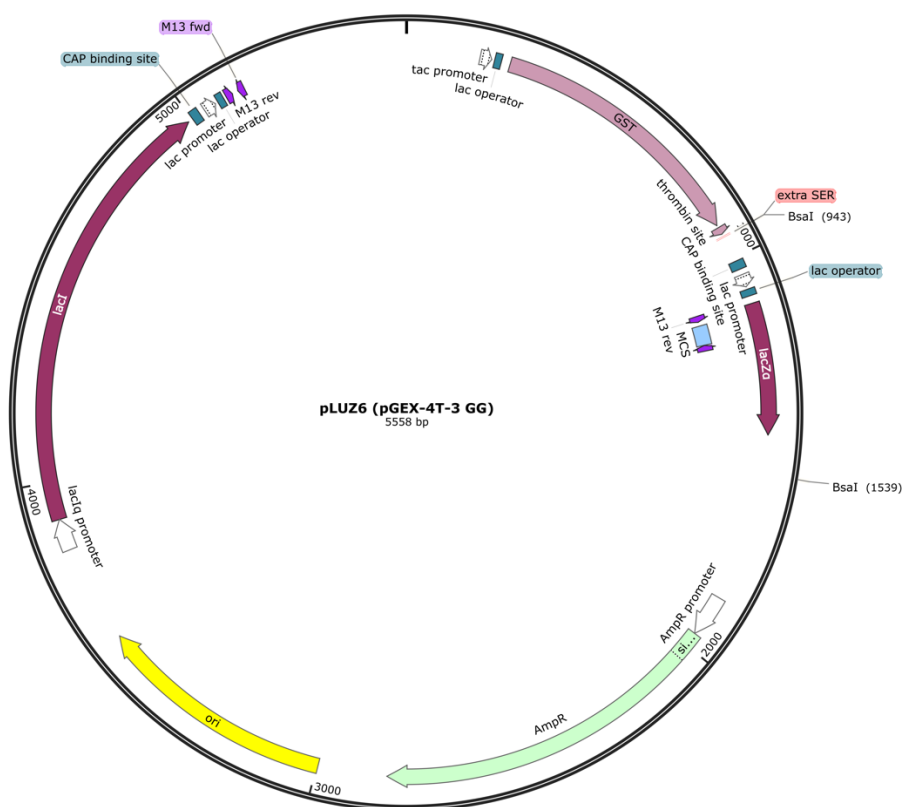
primer	template	5'→3' sequence	additional information
PP2A FW	AT1G13320	AGCCAACCTAGGACGGATCTGGT	reference gene
PP2A RV	AT1G13320	GCTATCCGAACCTTCTGCCTCAT TA	reference gene

YFP-qRT-FW	YFP from pB7WGY2	ACGTAAACGGCCACAAGTTC	for transgene-specific amplification
YFP-qRT-RV	YFP from pB7WGY2	AAGTCGTGCTGCTTCATGTG	for transgene-specific amplification
YFP-qRT-FW	YFP from pB7WGY2	ACATGGTCCTGCTGGAGTTC	for transgene-specific amplification
IAA1-qRT-RV	At4g14560	TTCTTGTGCTCCGGGTAATC	for transgene-specific amplification
IAA2-qRT-RV	At3g23030	CTTCCGGGTAATCCAAGACA	for transgene-specific amplification
qRT_IAA1#intr_FW	At4g14560	CGCAAGAACAACGACTCAAC	
qRT_IAA1#intr_RV	At4g14560	GAGATATGGAGCTCCGTCCA	
qRT_IAA2#intr_FW	At3g23030	AGCGTCTATTTGAGGAACTCG	
qRT_IAA2#intr_RV	At3g23030	AGGAGCTCCGTCCATACTCA	
qRT_IAA3_F	IAA3 (At1g04240)	GCATGAGGGTCAAGGAATCT	
qRT_IAA3_R	IAA3 (At1g04240)	ACATCACCAATGAGCATCCA	
qRT_IAA4#intr_F	IAA4 (At5g43700)	TGGATGCTTGTGGTGATGT	
qRT_IAA4#intr_R	IAA4 (At5g43700)	AGATCCTTTCATGATCCTTAGC C	
qRT_IAA5#intr_F	IAA5 (At1g15580)	AAGATCTTGCTTCCGCTCTG	
qRT_IAA5#intr_R	IAA5 (At1g15580)	GGAACATCTCCAGCAAGCAT	
qRT_IAA6#intr_F	At1g52830	ATGCTCGTCGGAGATGTACC	
qRT_IAA6#intr_R	At1g52830	TTCACGATCCTCAGCCTCTT	
IAA19 FW	At3g15540	AGTGAGCATGGATGGTGTGC	
IAA19 RV	At3g15540	CCGGTAGCATCCGATCTTTT	
GH3.1 FW	AT2G14960	ATGGCTTCGTTGGGACTTGT	
GH3.1 RV	AT2G14960	TCGTCGCCAGCTTCTTTACA	
qRT_SAUR9_F	AT4G36110	GACGTGCCAAAAGGTCACTT	
qRT_SAUR9_R	AT4G36110	AGTGAGACCCATCTCGTGCT	
qRT_TIR1#intr_F	At3g62980	TTTGTCAATGCCCTAAACTGC	
qRT_TIR1#intr_R	At3g62980	AATGCCACATTTGGTTCCAT	
qRT_AFB1#intr_F	At4g03190	GTCCGAATGCCTGATCTTGT	
qRT_AFB1#intr_R	At4g03190	ACACCCTCAGTTCTCGCAGT	
qRT_AFB2#intr_F	At3g26810	CGCAGCTGAGATTCATGGTA	
qRT_AFB2#intr_R	At3g26810	CTTCAAGCCCTTTGTACCT	
qRT_AFB3#intr_F	At1g12820	TCTCTTGCAAGTCCAGCTCA	
qRT_AFB3#intr_R	At1g12820	AGCTTGGACCTTCTTTCACG	



Supplementary Figure 48: pGEX-4T-3 Gateway-adapted vector map

Adaptation of pGEX-4T-3 (GE Healthcare Life Sciences) for Gateway cloning is described in **Section 6.6.7.3**.

**Supplementary Figure 49: pLUZ6 vector map**

Golden Gate-adapted pGEX-4T-3 vector as described in **Section 6.6.8.1** and **Supplementary Figure 46**.



Supplementary Figure 50: pLUZ5 vector map

Golden Gate-adapted pB42AD vector as described in Section 6.6.8.1 and Supplementary Figure 46.

Acknowledgements

Diese Arbeit wäre so nicht möglich gewesen ohne die unschätzbare wertvolle Hilfe und Unterstützung vieler Menschen, denen ich an dieser Stellen meinen herzlichen Dank aussprechen möchte.

First, I would like to thank Luz Irina, who has supervised my work with much commitment and has taught me so much. Luz Irina, not only am I indebted to you for invaluable input and guidance with regard to my research, I am also thankful for your relentless encouragement and for pushing me towards excellence. My time in your lab and under your supervision formed me as a scientist and as a person. I tremendously appreciate that. It has always been immensely encouraging to know you are earnestly interested in the success of my project. Not least, thank you for your patience and support with my writing.

Further, I am grateful to Prof. Steffen Abel for hosting me as a PhD student in the Molecular Signal Processing Department, for his support and for reviewing my thesis. I also thank my reviewers Prof. Ingo Heilmann and Prof. Claus Schwechheimer. I appreciate the time and effort you readily invested to review my thesis. I also would like to thank my PhD committee, Prof. Steffen Abel, Prof. Marcel Quint, and Prof. Sacha Baginsky, who with their comments and constructive criticism helped in steering my doctoral research into a fruitful direction.

This work has benefited from a number of collaborative efforts. I thank Richard Bartelt and Wolfgang Brandt for homology modeling of AFBs, and Sophia Samodelov and Matias Zurbriggen for stability assays with AUX/IAA chimeras. My thanks to all for fruitful discussions on interpretation of the results. Philipp and Marcel (and in the very beginning, also Kristian), thank you for analyses of AUX/IAA sister pair expression and sequence divergence, and for never becoming tired of explaining molecular evolution to a biochemist.

Des Weiteren danke ich allen, die mit helfenden Händen und klugen Ratschlägen zu dieser Arbeit beigetragen haben.

Many thanks go to Carolin Delker, who helped on a number of experiments with data analysis and statistics. Thank you, Carolin, for your always enlightening explanations and suggestions regarding heatmaps, clustering, statistical testing, correlation analyses and what not! I also would like to thank every colleague at the MSV department who provided helpful advice on my project.

Verona, danke vor allem, dass du meine zahllosen Chimeren GoldenGate-kloniert hast, und obendrein für all deine Hilfe hier und da. Esme, muchas gracias für endlose Propagation und Selektion transgener Pflanzenlinien und arbeitsintensive Phänotypisierungen und vieles mehr. Ich bin mir des Vorrechts bewusst, dich als meine HiWi gehabt zu haben! Annabell, danke für deine Hilfe mit all den Pflanzen und Hefen. Ohne euch hätte ich das niemals alles geschafft.

Danke an meine ganze Labor-Gang, und alle, die ein und ausgegangen sind. Martin, you genius, ich hab unsere Diskussionen genossen. Thanks for taking over IAA6 and IAA19, and making it a neat Master's thesis. And thanks for pushing the lab's experimental repertoire a leap forward with *in vitro* binding assays. My project truly benefitted from that! Micha, thanks for taking over. Own it! I know you already do, and I rest assured :). Verona, Nora, Katrin, ich hab so gern mit euch gelacht und Unfug getrieben! Verona, du hattest immer ein offenes Ohr, wenn ich Dampf ablassen musste und hast nebenbei auch noch dafür gesorgt, dass das Labor um mich herum nicht komplett verwahrlost. Danke! Ihr alle habt die Arbeit zu was gemacht, wo man gerne hingehet und auch mal Durststrecken übersteht. Auch wenn unsere Universen sich im „normalen Leben“ vielleicht nie überschritten hätten, war es mir ein Vergnügen und Vorrecht euch alle kennenzulernen und mit euch zusammenzuarbeiten.

Mein Dank gilt auch den Mitarbeitern des IPB, die stets eine hervorragende Infrastruktur für die wissenschaftliche Arbeit zur Verfügung stellten. Insbesondere möchte ich Thomas Vogt danken, dass er immer Wege gefunden hat, dass ich nicht auf meinem Tritium-Müll sitzenbleibe. Den Gärtnern möchte ich danken für ihre unschätzbare Hilfe vom Pflanztopf bis zur Samentüte.

Meine Mensa-Gang (Jana, Anja, Nadine, Philipp, Romina, Carla, Wenke, Julia) und Theresa, ich vermisse euch! Danke für eure Kollegialität, danke, dass ihr – im positiven Sinne! – so normal seid, für alle mittägliche Ablenkung, and for sharing in the highs and lows of PhD life.

Nicht zuletzt möchte ich auch meiner Familie und meinen Freunden danken. Iyke, Maureen, Pastor, Damaris, Sabine, Timmi – throughout all this time you have been friends and friends indeed. Thanks for your prayers, your encouragement, for pulling me into the presence of God, for helping me stay focused on what really counts. Mama, Papa, Suse, Razu – danke für eure Liebe und eure Unterstützung an allen Enden, vor allem moralisch, und für euer Verständnis, dass ich mich in den letzten Jahren oft so rar gemacht hab.

Danke!

Curriculum vitae

Name: Antje Hellmuth

Nationality: German

Day of birth: 28.02.1986

Place of birth: Havelberg, Germany

Education and research experience

- 01/2011 – present **PhD candidate**
Faculty I of Natural Science – Biological Sciences
Martin-Luther University of Halle-Wittenberg
Dissertation thesis “Biochemical characterization of auxin co-receptors in *Arabidopsis thaliana*”
Research Group “Signal Integration”
Supervisor: Dr. Luz Irina A. Calderón Villalobos
Leibniz Institute of Plant Biochemistry, Halle (Saale)
- 10/2010 – 12/2010 **Student assistant/ research assistant**
Department of Stress- and Developmental Biology
Supervisor: Dr. Lore Westphal
Leibniz Institute of Plant Biochemistry, Halle (Saale)
- 04/2009 – 09/2010 **Research trainee and Master student**
Thesis “Functional characterization of F-Box proteins in *Arabidopsis thaliana*”
Independent Junior Research Group “Auxin Signaling”
Supervisor: Dr. Marcel Quint
Leibniz Institute of Plant Biochemistry, Halle (Saale)
- 10/2005 – 09/2010 **Studies in biochemistry**
Martin-Luther-University of Halle-Wittenberg
Graduation: Diplom-Biochemikerin, final grade 2.0
- 09/1996 – 07/2005 **High-School education** at Diesterweg-Gymnasium Tangermünde
Graduation: Abitur, final grade 1.0

Conference attendances

- 16th EMBO/EMBL Science and Society conference “Emerging biotechnologies: Hype, hope and hard reality” 2015, Heidelberg (Germany)
- 4th & 5th Halle Conference on Recombinant Proteins, 2011 und 2015, Halle (Saale)
- EMBO-Workshop “Advances in protein–protein interaction analysis and modulation” 2014, Hyères (France)
- Botanikertagung 2013, Tübingen (Germany)
- Black Forest Retreat 2012 on Molecular Plant Science, Herzogenhorn (Germany) – *Best Poster Award*

Halle (Saale), January 2016

Antje Hellmuth

Statutory declaration

Hiermit erkläre ich an Eides statt, dass ich mich mit der vorliegenden wissenschaftlichen Arbeit erstmals um die Erlangung des Doktorgrades bewerbe, die Arbeit selbständig und ohne fremde Hilfe verfasst, nur die angegebenen Quellen und Hilfsmittel genutzt und die den benutzten Werken wörtlich oder inhaltlich entnommenen Stellen als solche kenntlich gemacht habe.

Halle (Saale), den _____

Antje Hellmuth